

**The high energy behavior of QCD:
The effective action
and the triple-Pomeron-vertex**

Dissertation
zur Erlangung des Doktorgrades
des Departments Physik
der Universität Hamburg

vorgelegt von
Martin Hentschinski
aus Deggendorf

Hamburg 2009

Erstgutachter der Dissertation:	Prof. Dr. J. Bartels
Zweitgutachter der Dissertation:	Prof. Dr. V. Schomerus
Erstgutachter der Disputation:	Prof. Dr. J. Bartels
Zweitgutachter der Disputation:	Prof. Dr. B. A. Kniehl
Datum der Disputation:	13. Juli 2009
Vorsitzender des Prüfungsausschusses:	Prof. Dr. G. Sigl
Vorsitzender des Promotionsausschusses:	Prof. Dr. R. Klanner
Departmentleiter:	Prof. Dr. J. Bartels
Dekan der Fakultät für Mathematik, Informatik und Naturwissenschaften:	Prof. Dr. H. Graener

Abstract

We study integrations over light-cone momenta in the high energy effective action of QCD. After a brief review of the effective action, we arrive on a regularization mechanism from matching of effective action diagrams with QCD diagrams, which we apply to a re-derivation of the reggeized gluon and of the BFKL-equation. We study consequences of the proposed regularization on the analytic structure of $2 \rightarrow 3$ and $2 \rightarrow 4$ production amplitudes in the Multi-Regge-Kinematics. We derive a certain part of the 1-loop corrections to the production vertex and demonstrate that they yield the on-set of corrections demanded by the Steinmann-relations. The Reggeon-Particle-2-Reggeon vertex is determined and applied to the construction of various signature configurations of the production amplitudes. We extend the proposed regularization method to states of three and four reggeized gluons and propose a supplement to the effective Lagrangian. We derive vertices for the $1 - 3$ and $2 - 4$ reggeized-gluon-transition inside the elastic amplitude and verify that signature conservation is obeyed. Integral equations for the state of three and four reggeized gluons are formulated and shown to be in accordance with a result by Bartels and Wüsthoff. In a second part we investigate the high-energy behavior of QCD for different surface topologies of color graphs. After a brief review of the planar limit (bootstrap and gluon reggeization) and of the cylinder topology (BFKL) we investigate the $3 \rightarrow 3$ scattering in the triple Regge limit which belongs to the pair-of-pants topology. We re-derive the triple Pomeron vertex function and show that it belongs to a specific set of graphs in color space which we identify as the analog of the Mandelstam diagram. We then extend the study to the high-energy behavior of $\mathcal{N} = 4$ SYM where we find a new class of color graphs not present in QCD.

Zusammenfassung

Wir untersuchen Integrationen über Lichtkegelimpulse in der effektiven Wirkung der Hochenergie-QCD. Nach einem kurzem Überblick über die effektive Wirkung erhalten wir durch Abgleich von Diagrammen der effektiven Wirkung und der QCD einen Regularisierungsmechanismus, den wir zu einer erneuten Ableitung des reggeisierten Gluons und der BFKL-Gleichung benutzen. Wir untersuchen die Auswirkungen des vorgeschlagenen Regularisierungsmechanismus' auf die analytische Struktur von $2 \rightarrow 3$ und $2 \rightarrow 4$ Produktionsamplituden in der Multi-Regge-Kinematik. Wir bestimmen einen Teil der 1-Schleifen-Korrekturen zur Produktionsvertex und zeigen, dass sie Anzeichen für die aufgrund der Steinmann-Beziehungen benötigten Korrekturen liefern. Die Reggeon-Teilchen-2 Reggeon-Vertex wird bestimmt und zur Konstruktion verschiedener Signatur-Konfigurationen von Produktionsamplituden benutzt. Wir erweitern den vorgeschlagenen Regularisierungsmechanismus zur Beschreibung von Zuständen bestehend aus drei bzw. vier reggeisierten Gluonen und schlagen eine Ergänzung zum effektiven Lagrangian vor. Vertizes die den Übergang von $1 - 3$ und $2 - 4$ reggeisierten Gluonen beschreiben werden für die elastische Streuamplitude abgeleitet und wir zeigen, dass Signaturerhaltung in der effektive Wirkung erfüllt ist. Wir formulieren Integralgleichungen für den Zustand aus drei bzw. vier reggeisierten Gluonen und zeigen, dass diese im Farbsinglet in Übereinstimmung mit einem früherem Ergebnis von Bartels und Wüsthoff sind. In einem zweiten Teil untersuchen wir das Hochenergieverhalten der QCD für verschiedene Oberflächentopologien von Farbgraphen. Nach einem kurzem Überblick über den planaren Limes (Bootstrap und Reggesierung des Gluons) und der Zylindertopologie (BFKL) untersuchen wir die Hosentopologie. Wir reproduzieren die Triple-Pomeron-Vertex-Funktion und zeigen, dass sie zu einer bestimmten Gruppe von Farbgraphen gehört, die wir als das Analog zum Mandelstam-Diagramm identifizieren. Wir erweitern die Untersuchung auf $\mathcal{N} = 4$ SYM und finden eine neue Klasse von Farbgraphen, die in der QCD nicht vorhanden ist.

Contents

1	Introduction	1
2	The gauge invariant effective action of high energy QCD	7
2.1	High-energy-QCD amplitudes within the LLA	7
2.2	Gluon production within the (Quasi-) Multi-Regge-Kinematics	10
2.3	The effective action of high energy QCD	12
2.4	Virtual corrections from the effective action	14
3	The elastic amplitude	16
3.1	The reggeized gluon in the effective action	17
3.1.1	Central rapidity diagrams and the gluon trajectory function	18
3.1.2	Reggeization of the gluon	23
3.1.3	Quasi-elastic corrections	25
3.2	Exchange of two reggeized gluons	28
3.2.1	The Born-diagrams	28
3.2.2	Higher order corrections: the BFKL-equation	31
3.3	Conclusion	37
4	Loop corrections to production processes from the effective action	38
4.1	Analytical representation of production amplitudes	38
4.2	The production amplitude with negative signature in all t -channels	41
4.2.1	The production amplitude at Leading Logarithmic Accuracy	41
4.2.2	The Reggeon-Reggeon-particle vertex at 1-loop	42
4.3	Positive and mixed signed production amplitudes	49
4.3.1	The Reggeon-Particle-2Reggeon (RP2R)-vertex	50
4.3.2	Mixed and positive signature for the $2 \rightarrow 3$ amplitude	53
4.3.3	Mixed and positive signature for the $2 \rightarrow 4$ amplitude	56
4.4	Conclusion	58

5	Exchanges of $n > 2$ reggeized gluons in the elastic amplitude	60
5.1	The pole prescription of induced vertices	60
5.1.1	The induced vertex of the first order	61
5.1.2	The induced vertex of the second order	63
5.1.3	The induced vertex of the third order	66
5.2	Quark-impact factors and subtraction terms	67
5.2.1	The quark-impact factor with three gluons	68
5.2.2	The quark-impact factor with four gluons	71
5.3	Number changing Reggeon transition kernels	72
5.3.1	The transition of 1-2 and 1-3 reggeized gluons	73
5.3.2	The transition of 2-3 and 2-4 reggeized gluons	76
5.4	The state of three and four reggeized gluons	79
5.4.1	Integral equations	79
5.4.2	The four reggeized gluon state in the color singlet	80
5.4.3	The Born-result	81
5.4.4	The four reggeized gluons and the triple Pomeron vertex	82
5.5	Conclusion	83
6	The triple Pomeron vertex and the pair-of-pants topology	86
6.1	Introduction	86
6.2	Elastic amplitudes	87
6.2.1	The large N_c expansion	88
6.2.2	Planar amplitudes: Reggeization of the gluon	89
6.2.3	Cylinder topology: The BFKL-Pomeron	93
6.3	Six-point amplitudes and the pair-of-pants -topology	95
6.4	Color factors with pair-of-pants topology	98
6.4.1	Color factors at Born-level	98
6.4.2	Gluon production on the pair-of-pants surface	98
6.4.3	Two-to-two Reggeon transitions	99
6.4.4	Two-to-four Reggeon transition	101
6.4.5	Two-to-three Reggeon transition	102
6.4.6	Planar and non-planar partial waves	104
6.5	Integral equations: gluon amplitudes with planar color structure	105
6.5.1	Integral equations for the three gluon amplitude	106
6.5.2	Reggeization of the three-gluon amplitude	106
6.5.3	The integral equations for the four gluon amplitude with planar color structure	107
6.5.4	Reggeization of four-gluon-amplitudes with planar color structure	109
6.6	The triple Pomeron vertex on the pair-of-pants	110
6.7	The six-point amplitude on the pair-of-pants surface	112
6.8	Conclusion	114

7	The topology of the triple Pomeron vertex in $\mathcal{N} = 4$ SYM	116
7.1	Topology of graphs in $\mathcal{N} = 4$ SYM	117
7.2	Selection of diagrams	119
7.3	Analytic expressions	122
7.4	Conclusions	125
8	Summary and outlook	126
A	The Rapidity scheme	129
B	Integrals	131
B.1	The integral I_1	131
B.2	The integral I_2	135
	Acknowledgements	143

Chapter 1

Introduction

Quantum Chromodynamics (QCD) is nowadays well established as the microscopic theory of strong interactions. It is stated in terms of a non-abelian gauge theory with the gauge group $SU(N_c)$ with $N_c = 3$ the number of colors and with quarks and gluons as its elementary degrees of freedom. Due to its complicated mathematical structure, an exact analytic determination of its correlation functions is currently out of reach and one needs to apply approximative methods to arrive on predictions from the theory. Generally, the strong coupling constant α_s is large and cannot be used as a small parameter to expand correlation functions in a perturbative series. In that case one mainly relies on lattice models, using simulations on a computer, and QCD sum rules. Fortunately, there exists a class of processes where the strong coupling is small and a perturbative treatment can be given meaning: Due to asymptotic freedom [1, 2], the strong-coupling constant α_s turns out to be small in presence of a hard scale and consequently hard scattering processes allow for a perturbative description.

Before the advent of QCD, Regge-theory [3] was used to describe the high-energy limit of scattering amplitudes of strong interactions. The analysis was mainly based on fundamental principles such as analyticity, unitarity and Lorentz-invariance of scattering amplitudes. In the high-energy- or Regge-limit, where the squared center-of-mass energy s is considerably larger than the momentum transfer t and all other mass scales, scattering amplitudes were shown to be determined by the position of singularities of their partial wave amplitude in the complex angular momentum plane. Starting from the assumption that the leading singularities in the complex angular momentum plane were pole-singularities only, so-called Regge-poles, phenomenological successful models could be constructed, which were used to describe scattering processes at high energies. In particular, apart from Regge-poles with the quantum numbers of physical particles, the Pomeron, a Regge-pole with the quantum numbers of the vacuum and even parity, was introduced to explain the experimentally observed asymptotic rise of the total cross-section with center of mass energy. By analytical continuation, Regge-poles could be furthermore related to the spectrum of hadronic states in the crossed channel: All strongly interacting particles turned out to lie on remarkably straight Regge-trajectories, passing for the mass of particles through their physical spin and it was one of the triumphs of Regge-theory, to relate experimental results in different physical channels by crossing [4].

However it was soon realized that in a relativistic theory Regge-poles require the simultaneous presence of branch-cuts, so-called Regge-cuts, in the complex angular momentum plane, which could be understood to arise from the exchange of two or more Regge-poles. Starting with the pioneering work of Gribov [5], a Reggeon-field-theory was developed [4–6], which describes the interactions between the various Reggeons and physical particles. Reggeon-field-theory is formulated in two space dimensions, transverse to the scattering axis, and one time-like dimension, given by the rapidity variable.

As soon as QCD was identified as the correct description of strong interactions, it was natural to ask, whether the findings of Regge-theory could be derived directly from the new, fundamental theory of the strong interactions. Unfortunately, physics described by Regge-theory is typically soft

and there is not a hard scale which would justify a perturbative treatment. There exists, however, a class of processes, like scattering of two highly virtual photons at high center-of-mass energies, where the virtuality of the photon provides a hard scale Q^2 which allows for a perturbative study of the Regge-limit. Nevertheless, large logarithms in the center-of-mass-energy \sqrt{s} can compensate for the smallness of the coupling and therefore spoil the validity of any finite order correction; a resummation of terms enhanced by large logarithms becomes necessary. The resulting Leading Logarithmic Approximation (LLA) resums maximally enhanced perturbative terms of the order $(\alpha_s \ln s)^n$ to all orders in the strong coupling constant, which is achieved by the Balitsky-Fadin-Kuraev-Lipatov (BFKL)-equation [7–11]. For the scattering of colored objects one finds as a result of the LLA-resummation reggeization of QCD-scattering amplitudes: The interaction between scattering particles is mediated through the exchange of a single Regge-pole. This Regge-pole carries the quantum numbers of the gluon and its trajectory $j(t)$ passes for $t = 0$ (corresponding to the vanishing mass of the gluon) through one (corresponding to the gluon’s physical spin). Consequently this Regge pole is naturally identified as the reggeized gluon. With the BFKL-equation nowadays also known within the Next-to-Leading-Logarithmic-Approximation (NLLA) [12, 13], reggeization of QCD-amplitudes is now confirmed also if sub-leading corrections are taken into account [14]. For scattering of colorless objects the interaction is mediated at LLA and NLLA by the famous BFKL-Pomeron. It is given as a state of two reggeized gluons and yields a cut rather than a pole in the complex angular momentum plane.

The BFKL-Pomeron predicts for the total cross-section a power-like rise with s , which ultimately would violate unitarity. It is therefore believed that at some value of s so-called unitarity corrections will become sizable that will restore unitarity. In the last 15 years a number of alternative approaches have been developed, which are meant to supplement the BFKL-equation. Among the most popular ones are the dipole model [15–18], the BK-equation [19–21], the Balitsky-hierarchy [19, 22, 23] and the JIMWLK-equation [24–32]. They are all based on the idea of saturation of gluon densities at high energies. While the power-like rise of the total-cross-section predicted by the BFKL-equation can be attributed to an infinite rise of gluon densities, these are believed to saturate at a certain value of s , which tames the growth of cross-sections.

Seen from the point of view of Regge-theory, the existence of moving Regge-poles allows to conclude that the high energy behavior of QCD can be reformulated in terms of a 2+1 dimensional Reggeon field theory. Such a reformulation seems to be the most comprehensive description of the high-energy behavior of QCD, in particular to address the issue of unitarity corrections. Both t -channel and s -channel unitarity can be regarded to be fulfilled automatically in such a reformulation. Elements of this field theory are at first given by generalizations of the BFKL-equation to the exchange of $n > 2$ reggeized gluons, which is described by the BKP-equation [33, 34]. Furthermore vertices describing transitions from two to four [35–37] and two to six reggeized gluons [38] have been derived so far.

A number of remarkable properties have been found at LLA for the known elements of Reggeon-field-theory: They are invariant under Möbius transformation in two-dimensional transverse coordinate space and states of arbitrary many reggeized gluons are integrable in the large N_c limit [39–41]. These properties are generally believed for QCD to be inherited from its maximal supersymmetric extension, $\mathcal{N} = 4$ Super-Yang-Mills-Theorie (SYM): Both theories coincide with each other within the LLA. $\mathcal{N} = 4$ SYM is on the other hand known to be conformal invariant in 3 + 1 dimensions and believed to be integrable with an enormous amount of activity in this direction in recent years [42–51]. The above mentioned properties of Reggeon-field-theory gained further interest with the advance of the AdS/CFT correspondence, which relates $\mathcal{N} = 4$ SYM, to supergravity on five-dimensional AdS space [52–54]. In particular the question arises whether a gravity dual of Reggeon-field theory in string theory exists.

In spite of all these progresses and impressive results, understanding of Reggeon-field-theory is still limited and a complete description of the high energy behavior for QCD and its supersymmetric extensions is not yet achieved. A systematic approach to derive for non-abelian gauge theories the elements of Reggeon field theory promises to be the effective action proposed by Lipatov in [55, 56]. The reformulation of quantum-field-theories such as QCD as effective field theories has nowadays become a popular and powerful method for the analysis of multi-scale problems. In particular the use of effective field theories generally simplifies practical calculations and allows to derive

results which are only very hard or even impossible to be obtained directly from QCD, due to the sheer complexity of the underlying expressions¹. Popular examples of such effective theories range nowadays from Chiral-Perturbation-Theory [59], over Soft-Collinear-Effective Field [60–65] and Heavy-Quark-Effective-Theory [66] up to Non-Relativistic QCD [67,68] .

A first proposal for an effective field theory for QCD in the Regge-limit has then been given in [69] which later could be explicitly re-derived directly from the QCD-action [70,71]. A more general effective action, which implicitly includes the first effective action, was then proposed in [55,56]. It is thought to provide a systematic approach to the unitarization of the BFKL-Pomeron and for the determination of sub-leading corrections beyond the LLA.

In the high-energy limit, scattering particles are close to opposite parts of the light-cone and therefore separated by a large relative difference in rapidity. The interaction between individual parts of the amplitude is highly non-local in rapidity, which complicates the analysis in terms of Feynman-diagrams considerably. The effective action then aims on a local description, where the interaction between QCD-particles, quarks, gluons and ghosts is restricted to a small interval in rapidity. Interaction between regions significantly separated in rapidity is on the other hand mediated by reggeized gluons. To arrive at such a description, it is needed to integrate out the modes of highly virtual particles, which spoil for usual QCD such a factorization. In the case of the effective action this is not done in a literal sense within the QCD-path-integral, but the effective description is obtained from the study of QCD tree-amplitudes in the high energy limit. As a result of such an analysis one obtains apart from the reggeized gluon fields an infinite number of new, induced vertices, which supplement the QCD-Lagrangian.

In contrast to $2 + 1$ dimensional Reggeon-field-theory, the effective action [55,56] is stated in usual $3 + 1$ dimensional space-time. For real production processes at three-level, the conversion into a $2 + 1$ dimensional description takes place automatically: The kinematics of produced particles is fixed and the mass-shell condition of produced particles reduces amplitudes of the effective action immediately into the required $2 + 1$ dimensional form. However for the determination of virtual corrections, an integration over longitudinal momenta is needed. While corresponding integrations over transverse momenta can be performed by using standard techniques, longitudinal integrations take a special role in the effective action. They contain an implicit integration over rapidity and are therefore in potential conflict with the desired locality in rapidity. Attempting a naive unrestricted integration, one makes the unpleasant observation that some integrals turn out to be divergent and even worse some contributions seem to be counted twice. The emergence of new divergences in effective theories, which have not been present in the underlying theory is natural and occurs also for other effective field theories: Effective theories provide simplifications in the description of amplitudes compared to the underlying full theory, which sometimes spoils convergences of integrals due neglecting certain parts. For the effective action [55,56] this requires to find a regularization that ensures locality in rapidity and absence of over-counting. Apart from that, another point requires clarification, if one attempts to carry out integrals over longitudinal momenta within the effective action: The induced vertices that supplement for the effective action the QCD-Lagrangian yield poles in the longitudinal momenta. Whenever those induced vertices appear as a part of an integral, a suitable prescription how to circumvent these singularities needs to be given.

The first part of this thesis is dedicated to the study of the following points: We propose a regularization mechanism that ensure locality of effective amplitudes in rapidity in accordance with the underlying principles of the effective action. To arrive on such a prescription we match the elastic scattering amplitude of the effective action at low orders in the strong coupling with the corresponding QCD- expression, which further allows to find the correct pole prescription for the relevant induced vertex. The obtained prescription is then used for a re-derivation of the reggeized gluon and of the BFKL-equation from the effective action within leading logarithmic accuracy.

A suitable testing ground for the found prescription and the LLA-resummations within the effective action is given by the determination of loop-corrections to production amplitudes: Due to the Steinmann-relations [72], these amplitudes have a non-trivial structure with respect to their energy discontinuities. The latter arise from logarithms and resumming them within the LLA in the

¹For a pedagogical introduction to effective field theories in particle physics see [57,58]

effective action, the question arises in which sense production amplitudes from the effective action are in agreement with the Steinmann-relations [72].

To arrive from the effective action on a description in terms of a field theory of reggeized gluons, a description for states of $n > 2$ reggeized gluons is further needed. In particular the regularization method needs to be extended and the pole structure of higher induced vertices is to be determined. As a reference process we consider elastic quark-quark scattering with exchange of up to four reggeized gluons. The description of the state of three and four reggeized gluons requires apart from pairwise interaction between reggeized gluons, also vertices that describe transitions from one-to-three and two-to-four reggeized gluons. For the state of four reggeized gluons the obtained result is then shown to agree with the two-to-four Reggeon transition vertex derived in [35].

Another route for a deeper understanding of Reggeon-field-theory is given by a systematic study of its large N_c limit: In the classical paper by 't Hooft [73] it has been shown that an expansion in the rank of the gauge group N_c organizes the color structure of Feynman diagrams in terms of topologies of two-dimensional surfaces which resemble the loop expansion of a closed string theory. In particular with the advance of the AdS/CFT correspondence where the string coupling on the gravity side could be shown to be proportional to N_c^{-1} , this observation has gained new attention.

From the point of view of Reggeon-field-theory, it is at first the integrability of states of $n > 2$ of reggeized gluons which trigger the interest in the large N_c expansion. They belong, like the BFKL-Pomeron, to the class of color factors with the topology of a cylinder. The leading term of the large N_c expansion is on the other hand given by color factors that have the topology of a plane, and one usually refers to these leading contributions as 'planar' diagrams. As it is the leading term in the expansion, the 'large N_c limit' and the 'planar' limit are often used interchangeable for each other. Planar diagrams contribute, for example, to gluon-gluon scattering amplitudes or to multi-gluon production amplitudes.

The integrable BKP-states belong then together with the BFKL-Pomeron to the class of processes in which the N_c leading color factors do not fit onto the plane, and the whole expansion starts with a formally sub-leading term. An example of such a physical process is given by the scattering of two electromagnetic currents or virtual photons in the Regge-limit, where the N_c -leading color factor has the topology of a cylinder.

In the second part of this thesis we go then one step further and consider color factors with the topology of a pair-of-pants, Fig.1.1a. As a suitable process for its study we consider scattering of a highly virtual photon on two virtual photons in the so-called triple Regge limit, Fig.1.1b. This process has been considered before in [35] for $N_c = 3$ and has been shown to yield the transition from two to four reggeized gluons.

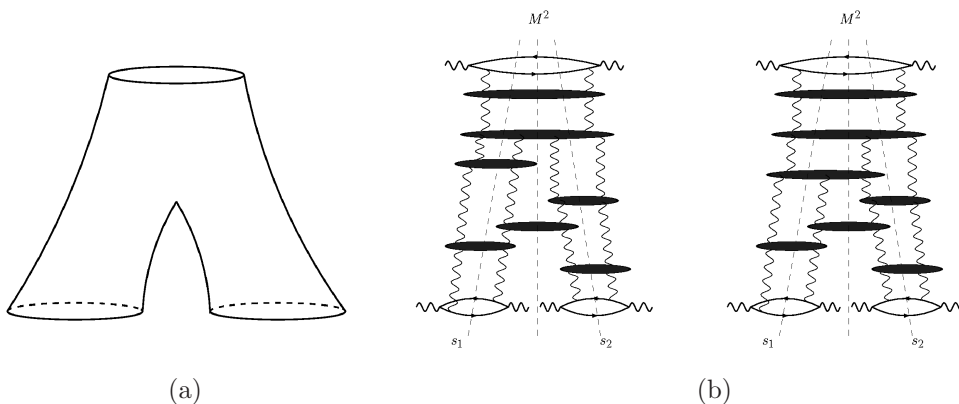


Figure 1.1: (a) The 'pair of pants' topology. (b) Typical contributions to the triple energy discontinuity for scattering of three virtual photons. For $\mathcal{N} = 4$ SYM, the virtual photons are replaced by R -currents.

In principal it is straight forward to determine the large N_c limit of the yet existing result [74–76], but the connection with the expansion in terms of topologies is not apparent: Instead of the 'pants'

it rather seems to belong to three disconnected cylinders. We therefore re-derive the result of the large- N_c limit of [35] by summing only those diagrams which belong to the topology of Fig.6.1 and demonstrate that 'reggeizing' and 'irreducible' terms of [35] can be attributed to distinct classes of diagrams on the surface of the pair-of-pants. The study of these color diagrams allows especially for a new view on the reggeization of the gluon and on the triple-Pomeron-vertex: whereas reggeization can be understood as a feature of planar QCD, the triple-Pomeron-vertex requires a non-planar structure, which reminds of the non-planar Mandelstam cross diagram [77].

Especially due to the advance of the AdS/CFT correspondence with string coupling $g_s \sim 1/N_c$ on the gravity side, it seems natural to use this topological approach for studying the Regge-limit of $\mathcal{N} = 4$ SYM. A program to study the high-energy limit on both sides of the correspondence has been initiated in [78]. It was found that it is convenient to use R -currents which result from the global $SU_R(4)$ symmetry of $\mathcal{N} = 4$ SYM to formulate correlators which are well-defined both on the gauge theory side and on the string side of the correspondence. For the elastic scattering of two R -currents, both sides of the correspondence have been investigated: On the string side, the leading contribution in the zero slope limit is given by Witten diagrams with graviton exchange. For the gauge theory side, the impact factor of the R -current consists of the sum of a fermion and a scalar loop in the adjoint representation of the gauge group, while the interaction is mediated in the high energy limit by the BFKL-Pomeron.

The study has then been extended on the gauge theory side to the six-point function of R -currents in the triple-Regge-limit in [79]. For finite N_c one finds apart from the triple-Pomeron-vertex and the reggeizing terms, a new contribution which appears due to the adjoint representation of all particles in $\mathcal{N} = 4$ SYM and has no counterpart in QCD. We then consider also this process with the topological expansion of color factors and suggest a possible interpretation of the result on the gravity side of the AdS/CFT-correspondence.

This thesis is organized as follows: Chapter 2 gives an introduction to the effective action. We summarize the ideas that underlie its derivation, discuss the building blocks of the effective action and outline the points that need clarification for a determination of virtual corrections from the effective action. Chapter 3 is dedicated to the discussion of the elastic quark-quark scattering amplitude. We match effective theory amplitudes at low orders in the coupling with QCD amplitudes and propose a regularization method for longitudinal integrations. The proposed method is then applied to the derivation of the reggeized gluon for the negative signatured part of the elastic scattering amplitude. Rules for longitudinal integrations of loops with 2 reggeized gluons are derived and applied to a derivation of the BFKL-equation. In Chapter 4 we extend our study to the $2 \rightarrow 3$ and $2 \rightarrow 4$ production amplitude. We derive a certain part of the one-loop corrections to the production vertex and show that they provide the onset of corrections needed for a fulfillment of the Steinmann-relations. Furthermore we derive the Reggeon-Particle-2 Reggeons vertex from the effective and apply it to the various parts of the $2 \rightarrow 3$ and $2 \rightarrow 4$ production amplitude with positive and mixed signature. In Chapter 5 we extend our results to exchanges with $n > 2$ reggeized gluons. As a reference process we use again elastic scattering of two quarks. We present a recipe for the derivation of the pole-prescription of higher induced vertices and explicitly determine the pole structure up to the third order in the Yang-Mills-coupling. We formulate a scheme that allows to carry out longitudinal loop integrals for loops containing $n > 2$ reggeized gluons and determine the quark-impact factors for coupling of three and four reggeized gluons. We further derive vertices that describe in the elastic amplitude transitions from one-to-three and two-to-four reggeized gluons. We demonstrate that these vertices are for the state of four reggeized gluons, together with pairwise interactions of reggeized gluons, in accordance with the $2 \rightarrow 4$ Reggeon transition vertex of [35]. In Chapter 6 we discuss the $2 \rightarrow 4$ Reggeon transition vertex or triple-Pomeron-vertex from the point of view of the large N_c expansion. After a brief review of the planar limit (bootstrap and reggeization) and of the cylinder topology (BFKL) we investigate the 6-point amplitude in the triple-Regge-limit, which belongs to the pair of pants topology. We identify the triple-Pomeron-vertex function and show that it belongs to a specific set of graphs in color space which we identify as the analogue of the Mandelstam diagram. In Chapter 7 we extend this study to the high energy behavior of a six-point correlator of R -currents in $\mathcal{N} = 4$ SYM. We find three distinct classes, where one of them yields the triple-Pomeron-vertex. The final Chapter 8 contains our conclusions. In Appendix A we present an alternative regularization scheme for the effective

action. Appendix B contains details about the evaluation of integrals.

Chapter 2

The gauge invariant effective action of high energy QCD

In this chapter we give a short but comprehensive introduction to the principles that underlie the effective action. In Sec.2.1 we recall general facts about QCD scattering amplitudes at high energies and we motivate the formulation of an effective action. In Sec.2.2 we consider tree-amplitudes in the so-called Quasi-Multi-Regge-Kinematics which lay the basis for the derivation of the effective action. In Sec.2.3 we present the effective action and its field content and give the (unregularized) Feynman-rules. In Sec.2.4 we formulate the points which require clarification and which will be studied in the following chapters.

2.1 High-energy-QCD amplitudes within the LLA

The formulation of the effective action is based on the fact that scattering amplitudes reggeize in the high-energy-limit of QCD. In particular, the reggeized gluon is to be understood as the effective degree-of-freedom in the t -channel of high-energy-QCD amplitudes.

This observation arises at first from the analysis of the elastic scattering amplitude within the Leading Logarithmic Approximation (LLA). There, perturbative terms of the order $\sim (\alpha_s \ln s)^n$ are resummed to all orders, as the smallness of the strong coupling constant α_s is compensated by the large logarithm $\ln s$. As a result of such an analysis it has been found [7–11] that the elastic scattering amplitude, Fig.2.1a, factorizes within the LLA into the exchange of a single reggeized gluon and its couplings to external particles. The elastic scattering amplitude of particles with color indices A, B and helicities λ_A, λ_B , takes the following Regge-form,

$$\mathcal{M}_{2 \rightarrow 2}(s, t) = 2g \delta_{\lambda_A \lambda_{A'}} T_{AA'}^c \frac{s^{1+\beta(t)}}{t} g \delta_{\lambda_B \lambda_{B'}} T_{BB'}^c, \quad (2.1)$$

with $j(t) = 1 + \beta(t)$ the gluon Regge trajectory. As usually, the Mandelstam variable $s = (p_A + p_B)^2$ yields the squared center-of-mass energy of the elastic amplitude while $t = (p_A - p'_A)^2$ gives the squared momentum transfer. The $T_{AA'}^c$ are generators of the $SU(N_c)$ gauge group in the representation corresponding to the scattering particles and g is the Yang-Mills coupling constant. Remarkably, the complete elastic scattering amplitude, Eq. (2.1), is within the LLA given by the Born-amplitude times the Reggeon-factor $s^{\beta(t)}$, which gathers all higher order corrections. Moreover, reggeization of the gluon occurs not only for the elastic scattering amplitude, but also for the high energy limit of a general QCD-amplitude, where additionally n gluons are produced, Fig.2.1b. Within the LLA, production of the $2 + n$ real particles takes place in the Multi-Regge-Kinematics (MRK) where the squared pair-energy of two neighboring produced gluons, $s_r = (k_r + k_{r-1})^2$, is significantly larger than the momentum transfers in the various t -channels, which are all of the same order of magnitude:

$$s = (p_A + p_B)^2 \gg s_r = (k_r + k_{r-1})^2 \gg \mathbf{q}_r^2 = -t_r, \quad k_r = q_{r+1} - q_r, \quad (2.2)$$

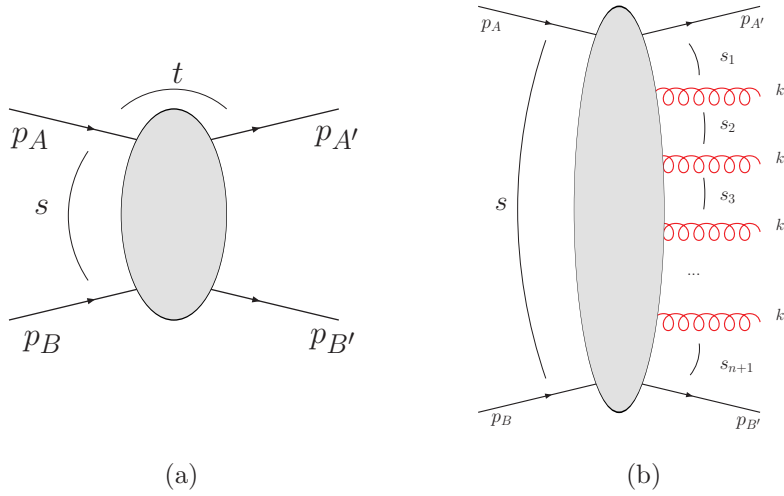


Figure 2.1: The elastic (a) and the n -particle production amplitude (b) in the Regge-limit and in the Multi-Regge-Kinematics respectively.

and we refer to Fig.2.1b for the nomenclature. As the elastic scattering amplitude, Eq.(2.1), the amplitude for the production of n gluons takes within the LLA the following factorizing Regge-form:

$$\mathcal{M}_{2 \rightarrow 2+n} = 2sg\delta_{\lambda_A \lambda_{A'}} T_{AA'}^{c_1} \frac{s_1^{\beta(q_1^2)}}{t_1} [gT_{c_1 c_2}^{d_1} C^\mu(q_1, q_2) \epsilon_\mu^*(k_1)] \frac{s_2^{\beta(q_2^2)}}{t_2} \dots \frac{s_{n+1}^{\beta(q_{n+1}^2)}}{t_{n+1}} g\delta_{\lambda_B \lambda_{B'}} T_{BB'}^{c_{n+1}}, \quad (2.3)$$

with $T_{ab}^c = -if_{abc}$ are $SU(N_c)$ generators in the adjoint representation. Similar to the elastic amplitude, the n -particle production amplitude has the remarkable feature that the all order resummed expression is within the LLA given by the Born-amplitude, times a Reggeon-factor $s_r^{\beta(-q_r^2)}$, for every squared sub-center-of-mass energy s_r . One therefore observes that within the LLA the complete interaction between s -channel produced particles in the (Multi-) Regge-Kinematics can be reduced to the exchange of a single reggeized gluon. It is then this observation which leads to the statement that the reggeized gluon is the relevant degree of freedom in the t -channel of any QCD-amplitudes at high energies. In Eq.(2.3), $C_\mu(q_1, q_2)$ is the effective Reggeon-Reggeon-Particle vertex, which describes the production of a gluon by a reggeized gluon, and $\epsilon_\mu(k_r)$, the polarization vector of the produced gluon. This production vertex is an effective vertex, which contains apart from the three-gluon-vertex also so-called induced parts:

$$2C^\mu(q_1, q_2) = \gamma^{\mu-+} - 2\frac{q_1^2}{q_2}(n^-)^\mu - 2\frac{q_2^2}{q_1}(n^+)^\mu \quad (2.4)$$

where

$$\gamma^{\mu-+} = q_1^+(n^-)^\mu + q_2^-(n^+)^\mu - 2(q_1 + q_2)^\mu, \quad (2.5)$$

is the light-cone projection of the three-gluon-vertex. The above light-cone basis is defined as

$$n^- = \frac{p_A}{E}, \quad n^+ = \frac{p_B}{E}, \quad E = \sqrt{s}/2, \quad n^+ \cdot n^- = 2. \quad (2.6)$$

Light-cone vectors are therefore proportional to momenta p_A and p_B of the scattering particles¹. With

$$k^\pm = (n^\pm)_\mu k^\mu, \quad (2.7)$$

¹In case of massive scattering particles, one should first construct a suitable Sudakov-basis of light-like momenta and then use those for the above definition.

the Sudakov-decomposition of an arbitrary four-momentum is given by

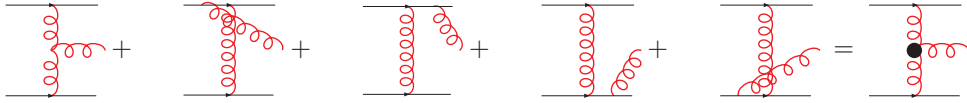
$$k = k^+ \frac{n^-}{2} + k^- \frac{n^+}{2} + k_\perp. \quad (2.8)$$

For the description of high-energy-QCD amplitudes it is further useful to introduce rapidity, which is defined as

$$Y_k = \frac{1}{2} \ln \frac{k^+}{k^-}. \quad (2.9)$$

In terms of rapidity, the MRK, Eq. (2.2), translates for instance into strong ordering of the produced particles in rapidity i.e. produced particles are separated significantly in their relative rapidity. The projections of the three-gluon-vertex in Eq.(2.4) on light-cone directions results from the polarization tensor of t -channel gluons in the high-energy limit: Connecting s -channel particles widely separated in rapidity, its polarization tensor reduces in a covariant gauge to its longitudinal part $n_\mu^+ n_\nu^- / 2$, while all other polarizations are suppressed by powers of s .

To illustrate the origin of the induced terms in Eq. (2.4), we recall that scattering of two quarks in the Regge-limit with production of one additional gluon at central rapidities is obtained by the following set of Feynman diagrams:



$$(2.10)$$

In the above sum, the vertex to the right is then to be associated with the production vertex, Eq. (2.4), which gathers all contributions to the production of a particle at central rapidities. The induced terms of Eq.(2.4) arise from the diagrams in Eq.(6.18), where the produced gluon couples directly to the upper and lower quark respectively. Supplementing the three-gluon vertex with these induced contributions, the production vertex turns out to be gauge invariant,

$$C_\mu(q_1, q_2)k^\mu = 0, \quad k = q_1 - q_2, \quad (2.11)$$

which makes it possible to chose an arbitrary gauge for each of the produced gluons. Similarly to the production vertex, effective vertices can be formulated for the coupling of scattering particles to reggeized gluons. In the case where the particle A in Fig.2.1 is given by a gluon, we have for the coupling of the reggeized gluon in the t -channel to the s -channel gluons

$$2p_A^+ g \delta_{\lambda_A \lambda_{A'}} = \epsilon_{\lambda_A} (p_A)^\mu \epsilon_{\lambda_{A'}}^\nu (p_A')^\nu \Gamma_{GGR}^{\mu\nu}(p_A, q), \quad (2.12)$$

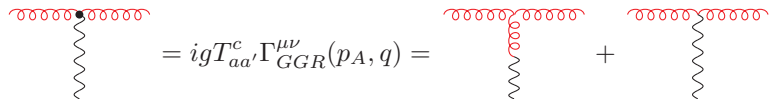
where $\Gamma_{GGR}^{\mu\nu}$ is the effective Gluon-Gluon-Reggeon (GGR) vertex. Similar to the production vertex it is given as the sum of the three-gluon-vertex and an induced contribution [69–71]:

$$\Gamma_{GGR}^{\mu\nu}(p_A, q) = \gamma^{\mu\nu+} - \frac{q^2}{p_A^+} (n^+)^\mu (n^+)^\nu, \quad (2.13)$$

with

$$\gamma^{\mu\nu+} = g^{\mu\nu} 2p_A^+ - (n^+)^\mu (p_A + q)^\nu - (p_A - 2q)^\mu (n^+)^\nu. \quad (2.14)$$

To illustrate the different contributions to the effective vertices, it proves useful to introduce a diagrammatic language which describes the various interactions between the reggeized gluon (denoted by wavy lines) and the standard QCD-gluon (curly lines). The effective GGR-vertex appears then as the following sum



$$= ig T_{aa'}^c \Gamma_{GGR}^{\mu\nu}(p_A, q) = \quad (2.15)$$

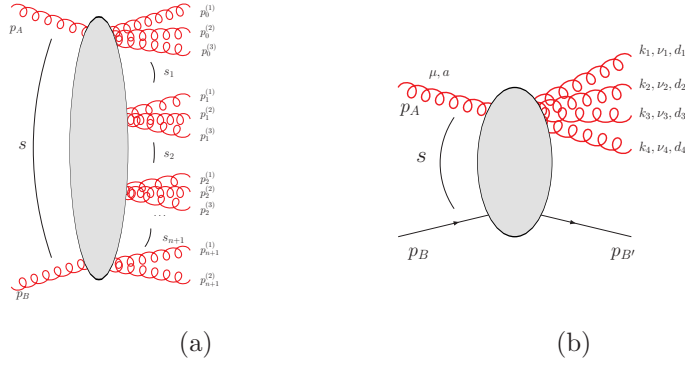


Figure 2.2: a: The Quasi-Multi-Regge-Kinematics b: Quasi-elastic scattering of the quark B on the gluon A, where the gluon fragments into a cluster of gluons, nearby in rapidity.

where the first diagram on the right hand side denotes coupling of the reggeized gluon to the three-gluon-vertex, and the second diagram denotes the new induced contribution,

$$\begin{array}{c} \text{red wavy line} \\ \text{zigzag line} \end{array} = \Delta_{aa'c}^{\mu\nu+}(p_A^+) = -igq^2 \frac{T_{aa'}^c}{p_A^+} (n^+)^{\mu} (n^+)^{\nu}. \quad (2.16)$$

The vertex has the property

$$\Gamma_{RGG}^{\mu\nu}(p_A, q) \cdot p_{A'}^{\nu} = p_A^+ p_A^{\mu} - p_A^2 (n^+)^{\mu}. \quad (2.17)$$

If the initial gluon A is on the mass-shell ($p_A^2 = 0$) and its polarization vector satisfies the Lorentz-condition $\epsilon_{\lambda A}(p_A) \cdot p_A = 0$, this vertex is gauge invariant. It is therefore possible to use arbitrary gauges also for this vertex. The following picture arises: In the Regge-limit, interaction between s -channel particles that are significantly separated in rapidity is mediated by a reggeized gluon, which couples to the s -channel particles by gauge invariant Reggeon-particle vertices. This implies that the reggeized gluon itself is invariant under local gauge transformations, apart from the fact that it carries color indices and transforms globally in the adjoint representation of $SU(N_c)$.

2.2 Gluon production within the (Quasi-) Multi-Regge-Kinematics

The above results suggest to reformulate QCD at high energies as an effective field theory, that describes the interaction of QCD particles with the reggeized gluon. The idea to formulate a calculus that describes the interaction of Reggeons and usual particles goes back to the work of Gribov [5]. For QCD, a first effective action for the Multi-Regge-Kinematics has been derived in [69–71]. In the following we consider the more general effective action [55,56], which allows to go beyond the LLA and permits to derive loop corrections to the above presented LLA-amplitudes. In following we shortly sketch the derivation of this action in presented in [55]: To this end one uses that an action and its Lagrangian are classical objects and therefore all information it contains about the interaction of its fields is already present in tree-amplitudes. To obtain the relevant tree-amplitudes of high-energy QCD beyond the LLA, it is needed to extend the previously discussed MRK to the Quasi-Multi-Regge-Kinematics (QMRK) [80], where the final state particles are separated into several groups of an arbitrary number of particles with fixed invariant mass. Each of these groups of particles is produced in the Multi-Regge-Kinematics with respect to each other and Eq.(2.2) holds now for groups rather than single particles. In particular (see Fig.2.2a for the nomenclature).

$$k_r = \sum_j p_r^{(j)} \quad k_r^2 = \text{fixed}, \quad r = 0, \dots, n+1, \quad (2.18)$$

with

$$s = (p_A + p_B)^2 \gg s_r = (k_r + k_{r-1})^2 \gg \mathbf{q}_r^2 = -t_r, \quad k_r = q_{r+1} - q_r. \quad (2.19)$$

In terms of rapidity, produced particles are grouped into rapidity clusters where particles inside of each cluster are close in rapidity with respect to each other, whereas each cluster is separated significantly in rapidity from the other clusters.

Similar to the amplitudes of the LLA, we attempt to arrive in the following at a description, where the interaction between the different clusters is mediated by the exchange of a single reggeized gluons, which couples to the produced particles by means of gauge invariant effective vertices.

For simplicity, one starts with the quasi-elastic process where the gluon A fragments into a number of gluons, Fig.2.2b. Omitting polarization vectors of external gluons, we start with the following ansatz for the quasi-elastic amplitude (following closely [55]) with production of n gluons in the fragmentation region of the gluon A :

$$\mathcal{M}_{ad_1\dots d_n}^{\mu\nu_1\dots\nu_n} = \Gamma_{ad_1\dots d_n c}^{\mu\nu_1\dots\nu_n+} \frac{1}{q^2} p_B^- g T_{BB'}^c \delta_{\lambda_B \lambda_{B'}}. \quad (2.20)$$

In the above formula, ν_i and d_i , with $i = 1, \dots, n$, denote Lorentz and color indices of the produced gluons, whereas μ and a belongs to the initial gluon A . We begin with the case where two gluons are produced in the fragmentation region and attempt to construct the effective 3-Gluon-Reggeon vertex building all possible combinations of the usual three- and four gluon vertices and the induced vertex Eq. (2.16). However it turns out that the set of these diagrams is not sufficient to build a gauge invariant vertex and it is necessary to introduce a further induced vertex,

$$\Delta_{ad_1 d_2 c}^{\mu\nu_1 \nu_2+}(p_A^+, k_1^+, k_2^+) = \begin{array}{c} \text{Diagram: A wavy line from the bottom labeled } q_+, c \text{ splits into two wavy lines going up and to the right. The top-left wavy line is labeled } p_A, \mu, a \text{ and } k_1, \nu_1, d_1. \text{ The top-right wavy line is labeled } k_2, \nu_2, d_2. \end{array} = ig^2 q^2 \left(\frac{T_{d_2 d_1}^d T_{ad}^c}{k_2^+ p_A^+} + \frac{T_{d_2 a}^d T_{d_1 d}^c}{k_2^+ k_1^+} \right) (n^+)^{\mu} (n^+)^{\nu_1} (n^+)^{\nu_2}, \quad (2.21)$$

which we call in the following the induced vertex of the second order, in contrast to the induced vertex of the first order Eq. (2.16). The vertex Eq. (2.21) can be shown to be Bose-symmetric making use of the Jacobi-identity

$$T_{d_2 a}^d T_{d_1 d}^c - T_{d_2 d_1}^d T_{ad}^c = T_{d_1 a}^d T_{d_2 d}^c, \quad (2.22)$$

and conservation of 'plus'- momenta in the quasi-elastic regime:

$$p_A^+ + k_1^+ + k_2^+ = 0. \quad (2.23)$$

The complete 3-Gluon-Reggeon vertex arises as the sum of the following contributions

$$\Gamma_{ad_1 d_2 c}^{\mu\nu_1 \nu_2+} = \begin{array}{c} \text{Diagram 1: } \text{Diagram 2: } \text{Diagram 3: } \text{Diagram 4: } \text{Diagram 5: } \end{array}, \quad (2.24)$$

where we used the vertex Eq. (2.15) to keep the expression compact. This 3-Gluon-Reggeon vertex can be verified to be gauge invariant [55, 81]

$$(p_A)_\mu \Gamma_{ad_1 d_2 c}^{\mu\nu_1 \nu_2+} = (k_i)_{\nu_i} \Gamma_{ad_1 d_2 c}^{\mu\nu_1 \nu_2+} = 0, \quad i = 1, 2. \quad (2.25)$$

For the general case $n > 2$ it can be shown that gauge invariance requires to introduce an infinite set of induced vertices which satisfy the following recurrence relation

$$\begin{aligned} \Delta_{d_0 d_1 \dots d_n c}^{\nu_0 \nu_1 \dots \nu_r+}(k_0^+, k_1^+, \dots, k_r^+) &= \\ &= \frac{(n^+)^{\nu_r}}{k_r^+} \sum_{i=0}^{r-1} T_{a_r a_i}^a \Delta_{d_0 d_1 \dots d_{i-1} d_{i+1} \dots d_n c}^{\nu_0 \nu_1 \dots \nu_{r-1}+}(k_0^+, \dots, k_{i-1}^+, k_i^+ + k_r^+, k_{i+1}^+, \dots, k_{r-1}^+). \end{aligned} \quad (2.26)$$

These vertices can be shown to be invariant under simultaneous exchange of color, momenta and polarization of the gluons making use of the Jacobi-identity Eq.(2.22) and the constraint

$$\sum_{i=0}^r k_i^+ = 0. \quad (2.27)$$

We therefore arrive at a set of diagrammatic rules that allow to construct production amplitudes in the quasi-elastic region, corresponding to Fig. 2.2b. As far as the origin of the newly introduced induced vertices is concerned, one should think of them, similar to Eq. (6.18), as radiative corrections that originate from particles close in rapidity to the particle B.

Furthermore, using symmetry arguments, fragmentation in the region of the particle B , is described by a similar set of diagrams, with 'plus'-indices interchanged by the corresponding 'minus'-indices. To describe then production of gluons at central rapidities within the Quasi-Multi-Regge-Kinematics, Fig. 2.2, the usual QCD-vertices need to be combined with induced vertices with both 'plus' and 'minus' indices. That these combinations lead indeed to gauge invariant production vertices has been verified explicitly for up to three produced gluons in [55,81]. We therefore arrived at a set of diagrammatic rules which allows to build all tree-amplitudes within the QRMK. In particular, these rules yield gauge invariant vertices, which describe the production of s -channel gluons, whereas the interaction between clusters of these gluons is mediated by the (bare) reggeized gluon, which is invariant under local gauge transformations.

2.3 The effective action of high energy QCD

It is then possible to derive an effective action which reproduces the above set of rules. It has been formulated in [55] and is given by

$$S_{\text{eff}} = \int d^4x (\mathcal{L}_{\text{QCD}}(v_\mu, \psi) + \mathcal{L}_{\text{ind}}(v_\pm, A_\pm)). \quad (2.28)$$

It contains apart from the fields $v_\mu(x)$ and $\psi(x)$ corresponding to gluons and quarks respectively the reggeized gluon field $A_\pm(x)$. As reggeized gluons connect clusters with significantly different rapidities, these fields obey the constraint

$$\partial_\mp A_\pm = 0. \quad (2.29)$$

Furthermore they are invariant, $\delta A_\pm = 0$, under infinitesimal, local gauge transformations

$$\delta v_\mu = [D_\mu, \chi], \quad \delta \Psi = -\chi \Psi, \quad (2.30)$$

where D_μ denotes the covariant derivative and χ the parameter of the gauge transformations which decreases at $x \rightarrow \infty$. On the other hand, the fields A_\pm belong globally to the adjoint representation of $SU(N_c)$ and transform for constant χ as

$$\delta A_\pm = g[A_\pm, \chi]. \quad (2.31)$$

The Lagrangian of the effective action consists besides of the usual QCD -Lagrangian of an additional induced term which contains the kinetic term for the reggeized gluon field and its coupling to gluons.

$$\mathcal{L}_{\text{ind}}(v_\pm, A_\pm) = \text{tr} [(A_-(v) - A_-) \partial_\sigma^2 A_+] + \text{tr} [(A_-(v) - A_-) \partial_\sigma^2 A_+] \quad (2.32)$$

where the induced Reggeon-gluon vertices take the following form

$$\begin{aligned} A_\pm(v) &= -\frac{1}{g} \partial_\pm U(v_\pm) = -\text{tr} \frac{1}{g} \partial_\pm \mathcal{P} \exp \left(-\frac{1}{2} g \int_{-\infty}^{x^\pm} dx'^\pm v_\pm(x') \right) \\ &= v_\pm - g v_\pm (1/\partial_\pm) v_\pm + g^2 v_\pm (1/\partial_\pm) v_\pm (1/\partial_\pm) v_\pm - \dots \end{aligned} \quad (2.33)$$

In the above expression, $v_\mu(x)$ and $A_\pm(x)$ are anti-Hermitian matrices in the fundamental representation of $SU(N_c)$ -Lie algebra:


$$v_\mu(x) = -it^a v_\mu^a(x), \quad A_\pm(x) = -it^a A_\pm^a(x), \quad [t^a, t^b] = if^{abc}t^c, \quad \text{tr}(t^a t^b) = \frac{1}{2}. \quad (2.34)$$

The above effective action describes the interaction of reggeized gluons with quarks and gluons, local in rapidity. In terms of the amplitudes Fig. 2.2 locality in rapidity means that the interactions between particles and reggeized gluons is always restricted to a single rapidity cluster, whereas the interaction between clusters is mediated by reggeized gluons alone. To make this statement more quantitative, one further introduces a parameter η which can be numerically big, but which is always significantly smaller than the rapidity-interval over which the complete amplitude extends $\Delta Y = \ln s \gg \eta$. Interactions between particles and reggeized gluons are then restricted to a rapidity interval $(Y_0 - \eta, Y_0 + \eta)$. Reggeized gluon fields mediate the interaction over rapidity intervals larger than η and never occur within any rapidity cluster; their propagator connects only parts of the amplitude which differ in their relative rapidity more than the parameter η . For the interaction of particles inside of a cluster, η takes therefore the role of an ultra-violet cut-off in the relative longitudinal momenta, while it occurs as an infra-red cut-off for the interaction between neighboring clusters. For physical observables, the dependence on η has to cancel in analogy to the dependence on a factorization scale in hard processes.

Due to the presence of a term linear in v_\pm , the Euler-Lagrange equations for the effective action have even in perturbation theory a non-trivial classical solution $v_\pm = A_\pm + \mathcal{O}(g)$. The complete classical solution is so far only known as a perturbative series in g [56]. In the following take the perspective of [81] and include into the Feynman-rules a vertex that describes the direct transition between reggeized gluons and gluons. We therefore do not subtract the gluon field v_\pm from the reggeized gluon A_\pm , but solve the equations of motions perturbatively.

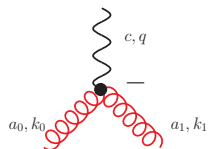
Feynman rules of the effective action

The Feynman rules of the effective action were initially given in [81]. However as there occurred a mixing of different conventions, we find it useful to state the relevant expressions her explicitly another time. Our Feynman-rules have been derived from the Lagrangian according to the conventions of [82] and all momenta are taken to be in-going. The Feynman-rules of the QCD-part of the effective Lagrangian can be obtained for instance from [82]. There are an infinite number of induced vertices. In the following we state them explicitly up to $\mathcal{O}(g^3)$, which covers all induced vertices that will be needed in this thesis. With $\mathbf{q}^2 = -q_\perp^2$ denoting the Euclidean, two-dimensional squared momentum of the reggeized gluon, the induced vertex of the zeroth order, which describes the direct transition of a QCD-gluon into a reggeized gluon, is given by:



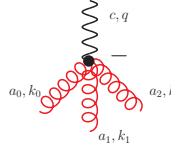
$$- = \Delta_{a_0 c}^{\nu_0 +} = -i\mathbf{q}^2 \delta^{a_0 c} (n^-)^{\nu_0}, \quad k_0^- = 0, \quad (2.35)$$

where ν_0 is the polarization of the gluon. For the induced vertex of the first order we obtain:



$$- = \Delta_{a_0 a_1 c}^{\nu_0 \nu_1 +} = g\mathbf{q}^2 f^{a_0 a_1 c} \frac{1}{k_0^-} (n^-)^{\nu_0} (n^-)^{\nu_1}, \quad k_0^- + k_1^- = 0, \quad (2.36)$$

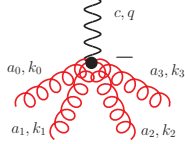
and for the induced vertex of the second order,



$$= \Delta_{a_0 a_1 a_2 c}^{\nu_0 \nu_1 \nu_2 +} = ig^2 \mathbf{q}^2 \left(\frac{f a_2 a_1 a f a_0 a c}{k_2^- k_0^-} + \frac{f a_2 a_0 a f a_1 a c}{k_2^- k_1^-} \right) (n^-)^{\nu_0} (n^-)^{\nu_1} (n^-)^{\nu_2},$$

$$k_0^- + k_1^- + k_2^- = 0. \quad (2.37)$$

For the induced vertex of the third order one finds



$$= \Delta_{a_0 a_1 a_2 a_3 c}^{\nu_0 \nu_1 \nu_2 \nu_3 +}, \quad (2.38)$$

with

$$\Delta_{a_0 a_1 a_2 a_3 c}^{\nu_0 \nu_1 \nu_2 \nu_3 +} = g^3 \mathbf{q}^2 \left[\frac{f a_3 a_2 c_2}{k_3^-} \left(\frac{f c_2 a_0 c_1 f a_1 c_1 c}{(k_0^- + k_1^-) k_1^-} + \frac{f c_2 a_1 c_1 f a_0 c_1 c}{(k_0^- + k_1^-) k_0^-} \right) \right. \\ \left. + \frac{f a_3 a_0 c_2}{k_3^-} \left(\frac{f c_2 a_1 c_1 f a_2 c_1 c}{(k_2^- + k_1^-) k_2^-} + \frac{f c_2 a_2 c_1 f a_1 c_1 c}{(k_2^- + k_1^-) k_1^-} \right) \right. \\ \left. + \frac{f a_3 a_1 c_2}{k_3^-} \left(\frac{f c_2 a_0 c_1 f a_2 c_1 c}{(k_2^- + k_0^-) k_2^-} + \frac{f c_2 a_1 c_1 f a_0 c_1 c}{(k_2^- + k_0^-) k_0^-} \right) \right] (n^-)^{\nu_0} (n^-)^{\nu_1} (n^-)^{\nu_2} (n^-)^{\nu_3}, \quad (2.39)$$

and

$$k_0^- + k_1^- + k_2^- + k_3^- = 0. \quad (2.40)$$

Note that in [81] a general formula for the induced vertex of the n-th order has been given. Above we stated only the induced vertices for the Reggeon-field $A_-(x)$. There exists also the same type of vertices for the field $A_+(x)$. They are obtained by replacing all minus- by plus-labels. Besides the induced vertices, we also obtain from the effective action as a new element the propagator of the bare reggeized gluon



$$= \frac{i/2}{\mathbf{q}^2} \quad (2.41)$$

where the longitudinal part $q^+ q^-$ vanishes due to the constraint $\partial_{\pm} A_{\mp} = 0$. As mentioned before, the propagator of the reggeized gluon connects only parts of the amplitude which are significantly separated in rapidity. With the factorization parameter η this constraint can be formulated by supplementing the propagator of the reggeized gluon with $\theta(Y_1 - Y_2 - \eta)$ where $Y_{1,2}$ are the rapidities of the clusters which are connected by the reggeized gluon.

2.4 Virtual corrections from the effective action

The above effective action can be used to determine tree amplitudes with Quasi-Multi-Regge-Kinematics to arbitrary accuracy. In particular the production vertices needed for the derivation of the BFKL-equation at NNLA have been derived in [81] and they have been used for the construction of real corrections in [83]. However the potential region of applicability of the effective action should be clearly beyond the derivation of tree-amplitudes. Indeed it promises to be a powerful tool that allows for the determination of the Regge-limit of complete amplitudes, including virtual corrections. In particular the effective action should enable us to determine loop corrections to the Regge-trajectory and to the vertices describing coupling of the reggeized gluons to QCD-particles,

which are required for the determination of higher order corrections to the BFKL-equation. Furthermore it should be possible to determine directly from the effective action amplitudes where two and more reggeized gluons are exchanged in the t -channel. In particular, the effective action seems to provide a self-consistent approach for unitarization of the BFKL-Pomeron.

Attempting such calculations starting from the Feynman rules of the effective action one soon encounters a number of complications which allow not for a straight forward determination of the desired quantities. All these complications are connected with the determination of loop-corrections and therefore do not occur for tree-amplitudes. The following points require clarification, in order to be able to use the effective action for the determination of virtual corrections:

- First, one needs an adequate regularization that ensures locality in rapidity of the amplitudes of the effective action: For real particle production, the QMRK fixes the rapidity of the produced particles, which allows to organize produced particles into local rapidity clusters. Loop integrals extend on the other hand over the full range of rapidities, which can lead to a violation of the locality constraint.
- Second, the operators that yield the induced vertices are singular and a suitable prescription for the occuring poles is needed: As far as the production of real particles in the QMRK is concerned, these poles are fixed to non-zero values by the QMRK, while integrating over longitudinal momenta, one enters naturally also the region, where the operators become singular.
- Third, amplitudes in the Regge-limit are known to have a certain analytical structure. This particularly concerns the occurrence of discontinuities in Mandelstam-variables. This point is closely connected to the ones mentioned above. Starting from a too simple prescription it turns out that certain discontinuities are missed and one obtains incorrect results for more complicated quantities [84].
- Fourth, attempting to determine integrations of loops that contain reggeized gluons, one finds integrals over light-cone momenta which are not convergent. It turns out that at one-loop a simple cut-off can be applied, corresponding to a principal values description [84], while for the exchange of more than two reggeized gluons this procedure fails.
- Fifth, the determination of NLLA-corrections requires to consider renormalization of the effective theory. This implies to supplement the effective action by suitable counter-terms.

In the following we address all of these points besides the last one, which is left for future studies.

Chapter 3

The elastic amplitude

As a start of our studies of longitudinal integrations within the effective action, we discuss the Regge limit $s \gg -t$ of the elastic scattering amplitude, Fig.3.1. In QCD, within the Leading and

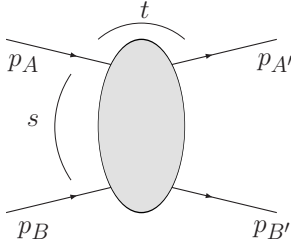


Figure 3.1: The elastic quark-quark scattering amplitude.

Next-to-Leading Logarithmic Approximation (LLA) and (NLLA), the elastic amplitude or 4-point amplitude is known to reggeize in the Regge-limit i.e. the interaction between the scattering quarks A and B (and similarly for gluons) is mediated by a single reggeized gluon. For elastic-scattering amplitudes with quantum numbers that do not allow for the exchange of a single reggeized gluon, the interactions is mediated by two or more reggeized gluons. In all these processes, the reggeized gluon is always associated with the 'Regge-limit' of a certain sub-4-point-amplitude. The elastic scattering amplitude is therefore not only an interesting object to be studied within the effective theory, but it constitutes also one of the basic building blocks of the effective theory, as only the associated 4-point amplitude allows a proper definition of the reggeized gluon.

The outline of this chapter is the following: In Sec.3.1 we study reggeization of the gluon within the effective action. We will derive a prescription for (longitudinal) loop integrals of gluon-loops, to which at least one reggeized gluon couples and demonstrate reggeization of the gluon in the effective theory by resumming a certain class of diagrams. In Sec.3.2 we consider the state of two reggeized gluons as a first example for interactions between reggeized gluons, which will lead us to the BFKL-equation.

The kinematics of the process that is studied here is the following:

As depicted in Fig.3.1, we consider scattering of two highly energetic quarks, with almost light-like momenta p_A and p_B which are close to the minus and the plus light-cone. In particular $p_A^+ \gg p_A^-$ and $p_B^- \gg p_B^+$. The two quarks have therefore mass $m_A^2 = p_A^+ p_A^-$ and $m_B^2 = p_B^+ p_B^-$ which within the LLA can be taken to be of similar size of the absolute value of the momentum transfer $\sqrt{|t|}$. In particular, to a good approximation we have $s = (p_A + p_B)^2 \simeq p_A^+ p_B^-$. The error of this approximation is of the order m^2/s and as the general accuracy of the effective action is not higher than $1/s$, those corrections will be frequently neglected, whenever it facilitates the calculations. The difference in rapidity of quark A, $Y_A = 1/2 \ln(p_A^+/p_A^-)$, and quark B, $Y_B = -1/2 \ln(p_B^-/p_B^+)$,

is given by

$$Y_{AB} = \frac{1}{2} \ln \left(\frac{p_A^+ p_B^-}{p_A^- p_B^+} \right) = \ln \left(\frac{s}{m_A m_B} \right), \quad (3.1)$$

where the last identity holds with power accuracy and is therefore exact within the effective action. In the Regge-limit $s \gg -t, m_A^2, m_B^2$ the two quarks are therefore separated by a large difference in rapidity. Furthermore we introduce a four-momentum $q = p_A - p'_A = p'_B - p_B$ with $t = q^2$ which yields the momentum transfer. In the Regge-limit, $q^2 = q_\perp^2 = -\mathbf{q}^2$, where we indicate with bold letters two-dimensional, Euclidean momenta. If not indicated otherwise, we always use the Feynman-gauge in our calculations.

3.1 The reggeized gluon in the effective action

In QCD, the scattering quarks interact at tree-level by exchange of a single gluon, Fig.3.2a. As the Lagrangian of the effective action contains the complete QCD-Lagrangian, this graph exists also in the effective theory. However in the effective theory, this graph comes with the restriction that the scattering quarks are close in rapidity. More accurate, introducing a factorization parameter η which separates interactions local in rapidity from non-local ones, this graph describes only the scattering process, if the difference of the scattering quarks' rapidities, Y_{AB} , is smaller than η . In the Regge-limit, however, $Y_{AB} > \eta$ (for any meaningful value of η): The quarks are non-local in rapidity and they interact within the effective action not by a QCD-gluon, but by a reggeized gluon, Fig.3.2b. This case is of course highly trivial, but it illustrates in a simple way the



Figure 3.2: Tree-level diagrams in QCD and in the effective theory. For the effective theory we will take from now on the convention that the reggeized gluon couples directly to the quark in an apparent way.

underlying principle of the effective theory: Interactions local in rapidity are described by standard QCD-degree-of-freedom, whereas non-local interactions by reggeized gluons alone.

For later reference, and as the coupling of one gluon to one reggeized gluon has no kinematical meaning, it is useful to define the effective quark-reggeized gluon-quark vertex:

$$\begin{array}{c} \text{---} p, i \\ \bullet \\ \text{---} p', j \\ \text{---} k, a \end{array} = \begin{array}{c} \text{---} p, i \\ \text{---} k, a \\ \text{---} p', j \end{array} =igt_{ij}^a \eta^\pm, \quad k^- = 0. \quad (3.2)$$

For on-shell quarks, the Quark-Quark-Reggeon vertex is in the Regge-limit given by

$$\Gamma_{QR}^{\pm, a\lambda\lambda'} = p_\pm \tilde{\Gamma}_{QR}^{a\lambda\lambda'} = \bar{u}_{\lambda'}(p')igt_{ij}^a \eta^\pm u_\lambda(p) \simeq t_{ij}^a ig2p^\pm \delta_{\lambda\lambda'}. \quad (3.3)$$

which yields for the tree-level amplitude in the Regge-limit

$$\begin{aligned} \mathcal{M}_{2 \rightarrow 2}^{\text{tree}}(s, t) &= -i\bar{u}_Aigt^a\gamma \cdot n^+u_A \frac{-i/2}{q_\perp^2} \bar{u}_Bigt^a\gamma \cdot n^-u_B \\ &= 2p_A^+p_B^-gt_{AA'}^c \frac{1}{-q^2}gt_{BB'}^c. \end{aligned} \quad (3.4)$$

In the following we shall discuss corrections to the tree-level-diagram Eq.(3.4). In doing so, we focus on corrections that yield large logarithms in the center of mass energy s and make use of

simplifications due to the LLA. In principle this allows to neglect any dependence on a transverse scale and similarly on the factorization parameter η . On the other hand a consistent formulation of the effective theory requires cancellation of any arbitrarily introduced scale and we will therefore also demonstrate how such a cancellation can be achieved.

3.1.1 Central rapidity diagrams and the gluon trajectory function

In this paragraph we focus on the central rapidity diagram CR in Fig.3.3, where both reggeized gluons couple to the gluon loop by an induced vertex. As we will see, this diagram yields the gluon-trajectory-function, together with a large logarithm in s . That this type of diagram yields

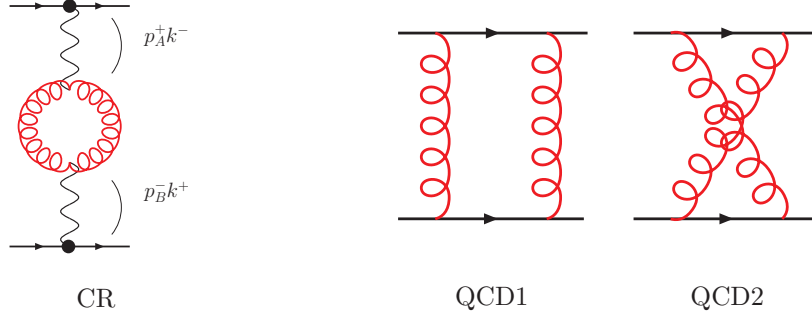


Figure 3.3: The central rapidity diagram of the effective action, where both reggeized gluons couple to gluon by an induced vertex. It arises for a particular kinematical limit out of the two QCD-diagrams to the right

the gluon-trajectory and that their resummation leads to reggeization of the gluon, has been already noted in [55]. Apart from the diagram CR, Fig. 3.3, there are also central rapidity diagrams, where the reggeized gluons couples to the gluon-loop by a three- or four-gluon vertex, see Fig.3.6. Their loop integral does not contribute within the LLA. They will be shortly addressed at the end of this paragraph. Using the unregulated Feynman rules of the effective action, see Sec. 2.3, the diagram CR of Fig.3.3 yields the following expression:

$$i\mathcal{M}^{\text{CR}}(s, t) = s \tilde{\Gamma}_{QQR}^c \int \frac{dk^+ dk^-}{2\pi} \int \frac{d^2 \mathbf{k}}{(2\pi)^3} \frac{i/2}{\mathbf{q}^2} \left(\frac{g\mathbf{q}^2 f^{abc}}{-k^-} \frac{-i}{k^2 + i\epsilon} \frac{-i}{(q-k)^2 + i\epsilon} \frac{g\mathbf{q}^2 f^{abc'}}{k^+} \right) \frac{i/2}{\mathbf{q}^2} \tilde{\Gamma}_{QQR}^{c'}. \quad (3.5)$$

The term within the big bracket represents together with the integral the gluon loop, to which the reggeized gluons couple. Note that the loop-integral in Eq.(3.5) contains implicitly an integration over the rapidity $Y_k = \ln(k^+/k^-)/2$ of the gluons inside the loop, which extends from minus to plus infinity. Furthermore, any rapidity-dependence inside of the integrand of Eq.(3.5) cancels and the expression is not restricted to central rapidities, but highly non-local in rapidity. The derivation of the effective action on the other hand requires that interactions of usual QCD-degrees-of-freedom, quarks and gluons, are restricted to rapidity intervals $\Delta Y < \eta$, while any interactions, that extends over rapidity intervals $\Delta Y > \eta$ is mediated by reggeized gluons alone. For real particle production, from which the effective action has been originally derived, the rapidities of the produced particles are fixed and they are either close or not. For the loop integrals of virtual corrections on the other hand, we integrate at first over all rapidities which requires to implement a restriction to central rapidity values. In principle this can be done by applying straight forward cut-offs to the rapidity/light-cone-momenta of the longitudinal loop integral. However this method has some drawbacks as it does not allow to include correctly phases: The imaginary part of the reggeized gluon is lost and therefore also its signature.

To provide an appropriate prescription and regularization of the integrals over longitudinal momenta k^+ and k^- , it is instructive to compare the above effective action diagram with the underlying QCD-amplitude, from which the effective action diagram arises. In the Regge-limit, at one

loop, the relevant QCD-diagrams are given by diagrams QCD1 and QCD2, Fig. 3.3, with exchange of two t -channel gluons. Their sum is given by

$$\begin{aligned}
i\mathcal{M}_{\text{QCD}} &= \\
&= \frac{1}{2} \int \frac{d^4k}{(2\pi)^4} \bar{u}_{A'}(p'_A) \left(\frac{igt^{c_1}\gamma^{\mu_1}i(p'_A - \not{k})igt^{c_2}\gamma^{\mu_2}}{(p_A - k)^2 + i\epsilon} + \frac{igt^{c_2}\gamma^{\mu_2}i(p'_A - \not{q} + \not{k})igt^{c_1}\gamma^{\mu_1}}{(p_A - q + k)^2 + i\epsilon} \right) u_A(p_A) \\
&\quad \times \frac{-ig_{\mu_1\nu_1}}{k^2 + i\epsilon} \frac{-ig_{\mu_2\nu_2}}{(q - k)^2 + i\epsilon} \times \\
&\quad \bar{u}_{B'}(p'_B) \left(\frac{igt^{c_1}\gamma^{\nu_1}i(p'_B + \not{k})igt^{c_2}\gamma^{\nu_2}}{(p_B + k)^2 + i\epsilon} + \frac{igt^{c_2}\gamma^{\nu_2}i(p'_B + \not{q} - \not{k})igt^{c_1}\gamma^{\nu_1}}{(p_B + q - k)^2 + i\epsilon} \right) u_B(p_B). \tag{3.6}
\end{aligned}$$

Making use of simplifications that apply due to the Regge-limit such as neglecting small longitudinal components of external particles and restricting to longitudinal polarization of the t -channel gluons, which amounts to replace the polarization tensor $g_{\mu\nu}$ by its longitudinal components $n_\mu^+ n_\nu^- / 2$, we arrive at

$$\begin{aligned}
i\mathcal{M}_{\text{QCD}} &= g^4 (p_A^+ p_B^-) \int \frac{dk^+ dk^-}{2\pi} \int \frac{d^2\mathbf{k}}{(2\pi)^3} \left(\frac{(t^{c_1} t^{c_2})_{AA'}}{-k^- - \frac{\mathbf{k}^2 + m_A^2 + i\epsilon}{p_A^+ - k^+}} + \frac{(t^{c_2} t^{c_1})_{AA'}}{k^- - \frac{(\mathbf{q} - \mathbf{k})^2 + m_A^2 + i\epsilon}{p_A^+ + k^+}} \right) \\
&\quad \frac{1}{k^+ k^- - \mathbf{k}^2 + i\epsilon} \frac{1}{k^+ k^- - (\mathbf{q} - \mathbf{k})^2 + i\epsilon} \left(\frac{(t^{c_1} t^{c_2})_{BB'}}{k^+ - \frac{(\mathbf{q} - \mathbf{k})^2 + m_B^2 - i\epsilon}{p_B^- + k^-}} + \frac{(t^{c_2} t^{c_1})_{BB'}}{-k^+ - \frac{\mathbf{k}^2 + m_B^2 - i\epsilon}{p_B^- - k^-}} \right). \tag{3.7}
\end{aligned}$$

To re-obtain the effective theory diagram CR, Eq.(3.5), we further need to expand the terms inside the big brackets in Eq.(3.7), in $p_A^+ k^-$ and $p_B^- k^+$, which correspond to the squared center-of-mass-energies of the quark-gluon-sub-amplitudes. We obtain

$$\begin{aligned}
\frac{t^{c_1} t^{c_2}}{-k^- - \frac{\mathbf{k}^2 + m_A^2 - i\epsilon}{p_A^+ - k^+}} + \frac{(t^{c_2} t^{c_1})}{k^- - \frac{(\mathbf{q} - \mathbf{k})^2 + m_A^2 - i\epsilon}{p_A^+ + k^+}} &= t^{c_1} t^{c_2} \frac{p_A^+}{-p_A^+ k^- + i\epsilon} + t^{c_2} t^{c_1} \frac{p_A^+}{p_A^+ k^- + i\epsilon} + \mathcal{O}\left(\frac{1}{p_A^+ k^-}\right), \\
\frac{t^{c_1} t^{c_2}}{k^+ - \frac{(\mathbf{q} - \mathbf{k})^2 + m_B^2 + i\epsilon}{p_B^- + k^-}} + \frac{t^{c_2} t^{c_1}}{-k^+ - \frac{\mathbf{k}^2 + m_B^2 + i\epsilon}{p_B^- - k^-}} &= t^{c_1} t^{c_2} \frac{p_B^-}{p_B^- k^+ + i\epsilon} + t^{c_2} t^{c_1} \frac{p_B^-}{-p_B^- k^+ + i\epsilon} + \mathcal{O}\left(\frac{1}{p_B^- k^+}\right). \tag{3.8}
\end{aligned}$$

Building symmetric combinations of the $SU(N_c)$ generators, $t^{c_1} t^{c_2} \rightarrow \{t^{c_1}, t^{c_2}\}/2$ the poles in k^- and k^+ cancel and we obtain no logarithm in s from Eq.(3.7). In the effective action, this contribution is contained in a different diagram (see Sec.3.2) and appears as a state of two reggeized gluons. For the antisymmetric color combination $t^{c_1} t^{c_2} \rightarrow [t^{c_1} t^{c_2}]/2 = if^{c_1 c_2 c} t^c / 2$, the QCD diagram coincides with Eq. (3.5), as long as we take into account only the most leading term of the expansion Eq.(3.8). This is however only meaningful, if the squared center of mass energies of the quark-gluon-sub-amplitudes $p_A^+ k^-$ and $p_B^- k^+$, are larger than all other scales inside the denominators on the left hand side of Eq.(3.8). To give meaning to Eq.(3.5), it is therefore necessary to implement a certain lower cut-off on $p_A^+ k^-$ and $p_B^- k^+$. This can be achieved by making use of a property of the following Mellin-integral:

$$\lim_{\nu \rightarrow 0} \int_{0-i\infty}^{0+i\infty} \frac{d\omega}{2\pi i} \frac{1}{\omega + \nu} \left(\pm \frac{p_A^+ k^-}{\Lambda_a} \right)^\omega = \begin{cases} 1 & |p_A^+ k^-| > \Lambda_a \\ 0 & \text{otherwise} \end{cases}, \tag{3.9}$$

where the contour of integration runs along the imaginary axis, to the right of the pole at $-\nu$. The above method has compared to the the cut-off regularization the advantage, that it allows to give already the bare reggeized gluon the analytical properties of the reggeized gluon. In particular, the parameter $-\nu$ acquires in the above the interpretation of an infinitesimal small Regge-trajectory and Eq.(3.9) allows to specify the phase of $p_A^+ k^-$. This allows to introduce signature also for the bare reggeized gluon. Depending on the choice of sign inside the bracket, Eq.(3.9), has a branch

cut along the negative (+) or positive (-) $p_A^+ k^-$ axis. These branch cuts should be associated with production thresholds of the underlying QCD-amplitude and they should therefore coincide with imaginary parts of the QCD-amplitude, Eq.(3.8). Restricting to antisymmetric color exchange and neglecting terms of the order k^+/p_A^+ , the combination of quark-propagators in the first line of Eq.(3.8) takes the following form:

$$\frac{1}{2} \left[\frac{-p_A^+}{p_A^+ k^- + \mathbf{k}^2 + m_A^2 - i\epsilon} - \frac{-p_A^+}{-p_A^+ k^- + (\mathbf{q} - \mathbf{k})^2 + m_A^2 - i\epsilon} \right]. \quad (3.10)$$

The first term acquires an imaginary part or rather a discontinuity only for negative values of $p_A^+ k^-$, while for the second term, the discontinuity is present for positive values of $p_A^+ k^-$. In Eq.(3.10) only pole-discontinuities occur. However including higher order corrections to the quark-gluon sub-amplitudes, these poles turn into branch cuts. It is therefore natural to identify the imaginary parts of Eq.(3.10) with the branch-cuts of Eq.(3.9) which yields

$$-\frac{p_A^+}{\Lambda_a} \lim_{\nu \rightarrow 0} \int \frac{d\omega}{4\pi i} \frac{1}{\omega + \nu} \left[\left(\frac{p_A^+ k^- - i\epsilon}{\Lambda_a} \right)^{\omega-1} - \left(\frac{-p_A^+ k^- - i\epsilon}{\Lambda_a} \right)^{\omega-1} \right]. \quad (3.11)$$

Note that the above prescription found for the branch cuts coincides with the Feynman rules for bypassing singularities [85]: singularities on the real axis are circumvented by leading the contour below the negative real axis and above the positive real axis. Together with the requirement that reggeized gluons carry negative signature, this rule allows to derive the right $i\epsilon$ -prescription without referring to the underlying QCD-Feynman diagram. We shall make use of this during later parts of this thesis. From a diagrammatic point of view, the regularization Eq.(3.9) belongs to the propagator of the reggeized gluon as this is the only non-local part of the effective theory. In this sense, Eq.(3.9) gives a particular realization of the constraint that all interaction that is non-local in rapidity, is mediated by a reggeized gluon.

To evaluate the loop integral in Eq.(3.5), we replace the pole $1/k^-$ by Eq.(3.11) and further perform a similar replacement for the pole $1/k^+$. As Eq.(3.11) yields a Reggeon with negative signature and trajectory $-\nu$ and as signature is generally conserved for the elastic amplitude [5, 86], we expect that also the complete reggeized gluon has negative signature. This is indeed the case. Performing the afore-mentioned replacements, we start with the following expression for the central-rapidity diagram CR:

$$\begin{aligned} i\mathcal{M}^{\text{CR}}(s, t) &= s \tilde{\Gamma}_{QR}^c \int \frac{dk^+ dk^-}{2\pi} \\ &\frac{i/2}{\mathbf{q}^2} \int \frac{d\omega_1}{4\pi i} \frac{1}{\omega_1 + \nu} \left[\frac{p_A^+}{p_A^+ k^- + i\epsilon} \left(\frac{-p_A^+ k^- - i\epsilon}{\Lambda_a} \right)^{\omega_1} + \frac{p_A^+}{p_A^+ k^- - i\epsilon} \left(\frac{p_A^+ k^- - i\epsilon}{\Lambda_a} \right)^{\omega_1} \right] \\ &\frac{(-g^2 N_c)}{2} \int \frac{d^2 \mathbf{k}}{(2\pi)^3} \frac{-i}{k^2 + i\epsilon} \frac{-i}{(q - k)^2 + i\epsilon} 2\mathbf{q}^4 \\ &\frac{i/2}{\mathbf{q}^2} \int \frac{d\omega_2}{4\pi i} \frac{1}{\omega_2 + \nu} \left[\frac{p_B^-}{p_B^- k^+ + i\epsilon} \left(\frac{-p_B^+ k^+ - i\epsilon}{\Lambda_b} \right)^{\omega_2} + \frac{p_B^-}{p_B^- k^+ - i\epsilon} \left(\frac{p_B^+ k^+ - i\epsilon}{\Lambda_b} \right)^{\omega_2} \right] \tilde{\Gamma}_{QR}^c \\ &= i\mathcal{M}_{2 \rightarrow 2}^{\text{tree}}(s, t) \int \frac{d\omega_1}{2\pi i} \int \frac{d\omega_2}{2\pi i} \frac{1}{\omega_1 + \nu} \left| \frac{p_A^+}{\Lambda_a} \right|^{\omega_1} A(\omega_1, \omega_2) \frac{1}{\omega_2 + \nu} \left| \frac{p_B^-}{\Lambda_b} \right|^{\omega_2}, \end{aligned} \quad (3.12)$$

with

$$\begin{aligned} A(\omega_1, \omega_2) &= \frac{(ig^2 N_c \mathbf{q}^2)}{2} \int \frac{dk^+ dk^-}{2\pi} \int \frac{d^2 \mathbf{k}}{(2\pi)^3} \frac{1}{k^2 + i\epsilon} \frac{1}{(q - k)^2 + i\epsilon} \\ &\frac{1}{2} [(k^- - i\epsilon)^{\omega_1-1} - (-k^- - i\epsilon)^{\omega_1-1}] \frac{1}{2} [(k^+ - i\epsilon)^{\omega_2-1} - (-k^+ - i\epsilon)^{\omega_2-1}]. \end{aligned} \quad (3.13)$$

In our notation we suppressed the dependence of $A(\omega_1, \omega_2)$ on $t = \mathbf{q}^2$. To evaluate the longitudinal integrals we start with the integration in k^- and restrict ourselves first to the case $k^+ < 0$. Then only the cut $(-k^-)^{\omega_1}$ along the positive axis contributes, while for the cut along the negative axis

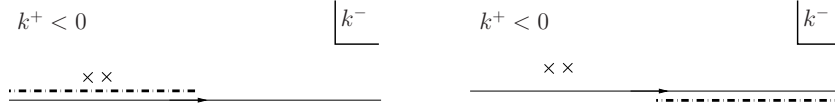


Figure 3.4: The complex k^- -plane for $k^+ < 0$ for the left and the right hand cut respectively. The crosses indicate the position of the poles from the gluon-propagators $1/(k^2 + i\epsilon)$ and $1/((q - k)^2 + i\epsilon)$.

the contour of integration can be enclosed without encircling any pole or branch-cut. For $k^+ > 0$, on the other hand, it is the branch cut along the negative axis that contributes. In both cases the k^- -integral can be evaluated by taking residues of the poles of the gluon-propagators and we obtain

$$A(\omega_1, \omega_2) = \frac{(-g^2 N_c \mathbf{q}^2)}{2} \int \frac{d^2 \mathbf{k}}{(2\pi)^3} \left[\frac{(\mathbf{k}^2)^{\omega_1}}{\mathbf{k}^2 [(\mathbf{q} - \mathbf{k})^2 - \mathbf{k}^2]} - \frac{((\mathbf{q} - \mathbf{k})^2)^{\omega_1}}{(\mathbf{q} - \mathbf{k})^2 [(\mathbf{q} - \mathbf{k})^2 - \mathbf{k}^2]} \right] \frac{e^{-i\pi\omega_2} + 1}{4} \left(\int_0^\infty \frac{dk^+}{k^+} (k^+)^{\omega_2 - \omega_1} + \int_{-\infty}^0 \frac{dk^+}{-k^+} (-k^+)^{\omega_2 - \omega_1} \right). \quad (3.14)$$

Within the LLA, we further replace¹ $(\mathbf{k}^2)^{\omega_1}$ and $(\mathbf{q} - \mathbf{k})^2)^{\omega_1}$ by $(\mathbf{q}^2)^{\omega_1}$, and we find:

$$A(\omega_1, \omega_2) = \frac{g^2 N_c}{2} \int \frac{d^2 \mathbf{k}}{(2\pi)^3} \frac{-\mathbf{q}^2}{\mathbf{k}^2 (\mathbf{q} - \mathbf{k})^2} \frac{e^{-i\pi\omega_2} + 1}{2} (\mathbf{q}^2)^{\omega_2} \int_0^\infty \frac{dk^+}{k^+} (k^+)^{\omega_2 - \omega_1}. \quad (3.15)$$

To evaluate the integral over k^+ , we first need to specify, which of the two ω_i -contours, $i = 1, 2$ is to the right of the other. As there is no singularity to the left of the ω_1 and ω_2 contours, we are free to chose $\Re\omega_2 > \Re\omega_1$. With such a choice, we obtain for the integral over k^+

$$\int_0^\infty \frac{dk^+}{k^+} (k^+)^{\omega_2 - \omega_1} = \frac{1}{\omega_2 - \omega_1} \lim_{\rho \rightarrow \infty} (\rho)^{\omega_2 - \omega_1}. \quad (3.16)$$

To give sense to this result, we need to move the ω_2 contour to left of the singularity at $\omega_2 = \omega_1$, i.e. we pick up the residue at $\omega_2 = \omega_1$ while the remaining part vanishes as now $\omega_2 < \omega_1$. Of course we could have been equally well started with $\Re\omega_2 < \Re\omega_1$, and one can verify that this leads to the identical result. In short, the above k^+ -integral yields nothing but a delta-function $2\pi i \delta(\omega_1 - \omega_2)$ and we obtain

$$A(\omega_1, \omega_2) = \beta(\mathbf{q}^2) \frac{[(-\mathbf{q}^2 - i\epsilon)^{\omega_2} + (\mathbf{q}^2 - i\epsilon)^{\omega_2}]}{2} 2\pi i \delta(\omega_2 - \omega_1), \quad (3.17)$$

with

$$\beta(\mathbf{q}^2) = \frac{g^2 N_c}{2} \int \frac{d^2 \mathbf{k}}{(2\pi)^3} \frac{-\mathbf{q}^2}{\mathbf{k}^2 (\mathbf{q} - \mathbf{k})^2}, \quad (3.18)$$

the gluon trajectory function. For the complete diagram we obtain

$$\begin{aligned} i\mathcal{M}^{\text{CR}}(s, t) &= i\mathcal{M}_{2 \rightarrow 2}^{\text{tree}}(s, t) \beta(\mathbf{q}) \int \frac{d\omega_1}{2\pi i} \frac{1}{(\omega_1 + \nu)^2} \frac{1}{2} \left[\left(-\frac{p_A^+ p_B^- \mathbf{q}^2}{\Lambda_a \Lambda_b} \right)^{\omega_1} + \left(\frac{p_A^+ p_B^- \mathbf{q}^2}{\Lambda_a \Lambda_b} \right)^{\omega_1} \right] \\ &= i\mathcal{M}_{2 \rightarrow 2}^{\text{tree}}(s, t) \beta(\mathbf{q}) \frac{1}{2} \left[\ln \left(-\frac{p_A^+ p_B^- \mathbf{q}^2}{\Lambda_a \Lambda_b} \right) + \ln \left(\frac{p_A^+ p_B^- \mathbf{q}^2}{\Lambda_a \Lambda_b} \right) \right]. \end{aligned} \quad (3.19)$$

One can define now parameters

$$\lambda_{a,b} = \frac{\Lambda_{a,b}}{m_{A,B} \sqrt{\mathbf{q}^2}}, \quad (3.20)$$

which allow to write the above result as

$$\text{CR} = i\mathcal{M}_{2 \rightarrow 2}^{\text{tree}}(s, t) \beta(\mathbf{q}) \frac{1}{2} \left[\ln \left(-\frac{p_A^+ p_B^-}{m_A m_B} \right) + \ln \left(\frac{p_A^+ p_B^-}{m_A m_B} \right) - \ln(\lambda_a \lambda_b) \right]. \quad (3.21)$$



Figure 3.5: Diagrams in the quasi-elastic regions of quark A and B resp., that cancel the cut-off dependence of the central rapidity diagram CR.

Within the LLA, all transverse scale are of the same order of magnitude and we can set $\lambda_{a,b} = 1$. In general, the parameters $\lambda_{a,b}$ are supposed to cancel with quasi-elastic diagrams, Fig.3.5. How this can occur in detail, will be addressed in Sec.3.1.3.

In the above calculation, a certain regularization scheme has been used, that imposed certain lower cut-offs, Λ_a and Λ_b , on the squared center-of-mass energies of the corresponding quark-gluon sub-amplitudes. This regularization scheme is very plausible, as it exactly imposes the requirements that are needed to obtain the effective theory diagram from the underlying QCD-diagram. Furthermore, taking residues of the gluon propagators during the above calculation, we explicitly set $k^+k^- = (\mathbf{q} - \mathbf{k})^2$ and $k^+k^- = \mathbf{k}^2$. Together with the bounds $p_A^+k^- > \Lambda_a$ and $p_B^-k^+ > \Lambda_b$ and with $\mathbf{k}^2 \simeq (\mathbf{q} - \mathbf{k})^2 \simeq \mathbf{q}^2$ in the LLA, the rapidity of the gluon $Y_k = \ln(k^+/k^-)/2$ is then restricted to central values, $Y_k \in [-\ln(\Lambda_a/\sqrt{\mathbf{q}^2}p_A^+), \ln(\Lambda_b/\sqrt{\mathbf{q}^2}p_B^-)]$ as expected and required for the central rapidity diagram. Also the imaginary part and therefore negative signature of the reggeized gluon are mapped obtained correctly. Nevertheless the method has some drawbacks: To obtain the correct gluon trajectory function, it has been necessary to neglect a dependence of the Reggeon-factors on transverse scales. This dependence is irrelevant within the LLA, but has to be included if one goes beyond the LLA. At the present stage it is not clear, whether such a contribution is meaningful or not within the NLLA. In the recent literature [87] it has been reported that difficulties arise with certain LLA-regularization schemes if used for NLLA-calculations. The whole setup of [87] differs from the present one. Particularly our method of regularization is at first not related to the one to which [87] refers. Nevertheless we want to note that it is also possible to introduce a scheme which imposes the lower bound directly on the rapidity of the gluon loop, rather than on (sub)-center-of-mass-energies. Some details about this scheme are presented in App.A and we refer there for details. Within the LLA, both schemes yield identical results and none of the schemes can be ruled out.

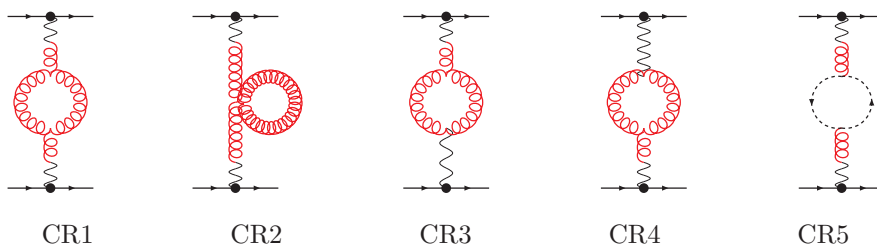


Figure 3.6: Further diagrams that occur from the effective action for the central rapidities. Their sum yields zero result.

Besides the diagram CR, which we discussed so far, there are also diagrams, in which one or both reggeized gluons couple to the gluon-loop by a three or a four-gluon vertex and there is furthermore a diagram that contains a ghost-loop. These diagrams are shown in Fig.3.6. In their sum, these

¹Note that this only applies within the LLA, where all transverse scales are of the same order of magnitude. For higher accuracy, a further non-zero contribution is obtained from the above calculation.

diagrams yield the following expression

$$\begin{aligned} \text{CR1} + \text{CR2} + \text{CR3} + \text{CR4} = s\tilde{\Gamma}_{QQR}^c g^2 \frac{N_c}{2} \int \frac{dk^+ dk^-}{2\pi} \int \frac{d^2\mathbf{k}}{(2\pi)^3} \frac{i/2}{\mathbf{q}^2} \frac{1}{k^2 + i\epsilon} \frac{1}{(q-k)^2 + i\epsilon} \\ (2\mathbf{k}^2 + 2(\mathbf{q} - \mathbf{k})^2 - 8\mathbf{q}^2) \frac{i/2}{\mathbf{q}^2} \tilde{\Gamma}_{QQR}^c. \end{aligned} \quad (3.22)$$

Unlike the diagram CR, Eq. (3.22), contains no pole in a light-cone momentum. It is therefore possible to evaluate the integrals over k^+ and k^- without introducing any regularization: The integrals are convergent, all singularities lie on the same side of the integration contour and the integral gives zero result.

On the other hand, the momentum structure of the above denominators is simplified due to the coupling of the reggeized gluons. This is only justified, if the squared sub-center-of mass energies $p_A^+ k^-$ and $p_B^- k^+$ are large. Furthermore, introducing a regularization allows also to take explicitly into account negative signature of the reggeized gluon. It seems therefore plausible to introduce an analogous regularization by a Mellin-integral also for these contributions.

Within the LLA, the question cannot be answered whether one should include a regularization for these diagrams or not: In any case the integral does not contribute within the LLA. The answer to this question lies at the NLLA: In that case, the integral still vanishes if no regularization is included, while it is non-zero with regularization. For the following discussion we take the convention that the Mellin-integral should be also used for those diagram that do not come with an explicit pole in k^+ and k^- . The definite answer however can be only given if corrections beyond the LLA are considered.

3.1.2 Reggeization of the gluon

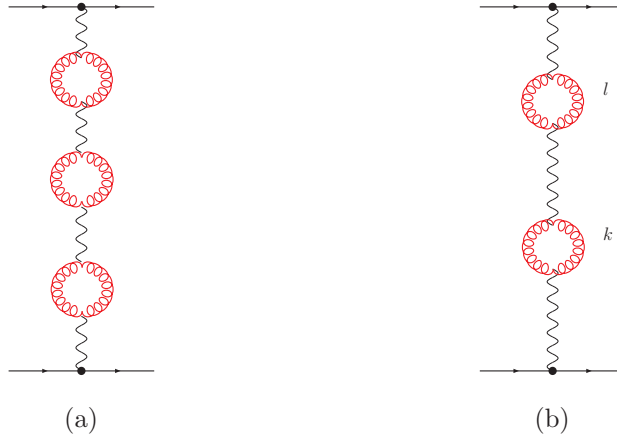
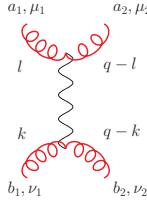


Figure 3.7: (a): Type of diagram that need to be resummed to obtain reggeization of the gluon. (b): The two-loop example

With the leading non-trivial order of the reggeized gluon derived, we demonstrate in the following that reggeization of the gluon arises within the effective action by resumming diagrams like Fig. 3.7a, which contain an arbitrary number of gluon loops. We start with the diagram containing two gluon loops, Fig.3.7b: Every reggeized gluon couples to the gluon loops by an induced vertex of the first order which yield poles in the light cone momenta l^+, l^- and k^+, k^- respectively. While at one-loop, both poles could be identified with the most leading term of the expansion of the regarding quark-propagators, in the two-loop case the poles in l^+ and k^- arise due to a gluon propagator inside a QCD-ladder graph, as illustrated in Fig.3.8a. Without going into details about the structure of the underlying QCD-graph, it is clear that these poles arise from an expansion of a QCD 4-point amplitude, similar to the one-loop case. This requires to impose again a lower

bound Λ_c on the squared sub-center-of-mass energy l^+k^- . We therefore insert for the combination 'induced vertex' times 'reggeized gluon propagator' times 'induced vertex' the following expression into the diagram



$$= f^{a_1 a_2 c} (n^+)^{\mu_1} (n^+)^{\mu_2} f^{b_1 b_2 c} (n^-)^{\nu_1} (n^-)^{\nu_2} \frac{i\mathbf{q}^2}{2} \quad (3.23)$$

$$\times \int \frac{d\omega_3}{4\pi i} \frac{\Lambda_c^{\omega_3}}{\omega_3 + \nu} \left[(-l^+k^+ - i\epsilon)^{\omega_3 - 1} - (l^+k^+ - i\epsilon)^{\omega_3 - 1} \right].$$

Again the cut-off Λ_c needs to be canceled by a similar contribution in a different diagram. While the cut-offs Λ_a and Λ_b are canceled by diagrams in the quasi-elastic region of the scattering quarks (see Sec.3.1.3), we expect 'intermediate' cut-offs like Λ_c to cancel with the corresponding part in higher order corrections to the trajectory function, see Fig.3.8b. Making repeatedly use of our

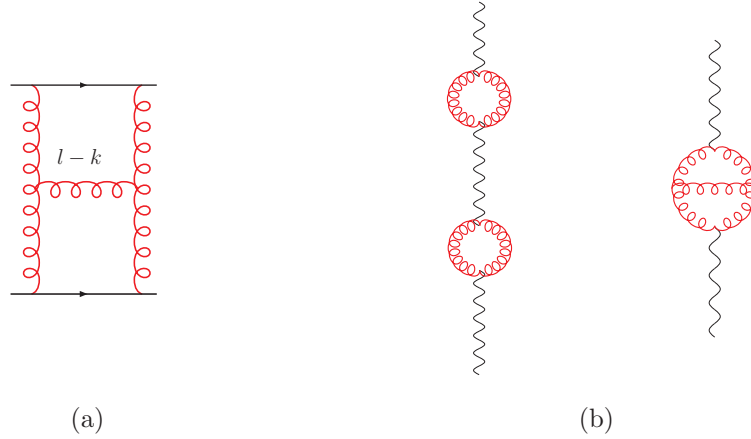


Figure 3.8: (a): QCD-ladder graph where the vertical gluon propagator leads to the poles in l^+ and k^- . (b):Summing NLLA-diagrams, like the one to the left one expects to obtain a contribution that is proportional to the product of two gluon trajectories functions. The cut-off Λ_c separates this local (rapidity) contributions from the non-local contribution at the rhs.

result for the function $A(\omega_1, \omega_2)$, Eq. (3.17), we obtain at two-loop the following result

$$\mathcal{M}_{2 \rightarrow 2}^{2\text{loop}} = \mathcal{M}_{2 \rightarrow 2}^{\text{tree}}(s, t) \times \int \frac{d\omega}{2\pi i} \frac{\beta^2(\mathbf{q}^2)}{(\omega + \nu)^3} \frac{1}{2} \left[\left(-\frac{p_A^+ p_B^- \mathbf{q}^4}{\Lambda_a \Lambda_b \Lambda_c} \right)^\omega + \left(\frac{p_A^+ p_B^- \mathbf{q}^4}{\Lambda_a \Lambda_b \Lambda_c} \right)^\omega \right]. \quad (3.24)$$

Within the LLA we replace the cut-offs by a typical transverse scale of the process, $\Lambda_a \Lambda_b \Lambda_c = m_A m_B \mathbf{q}^2$, for instance, and with this choice, one obtains similarly for the diagram with n -loops

$$i\mathcal{M}_{2 \rightarrow 2}^{\text{LLA, } n\text{-loop}}(s, t) = i\mathcal{M}_{2 \rightarrow 2}^{\text{tree}}(s, t) \times \int \frac{d\omega}{2\pi i} \frac{\beta^n(\mathbf{q}^2)}{(\omega + \nu)^{n+1}} \frac{1}{2} \left[\left(-\frac{p_A^+ p_B^-}{m_A m_B} \right)^\omega + \left(\frac{p_A^+ p_B^-}{m_A m_B} \right)^\omega \right], \quad (3.25)$$

Summing over the number n of gluon loops, we obtain with

$$\sum_{n=0}^{\infty} \frac{\beta^n(\mathbf{q}^2)}{(\omega + \nu)^{n+1}} = \frac{1}{\omega + \nu - \beta(\mathbf{q})} \quad (3.26)$$

reggeization of the gluon:

$$\mathcal{M}_{2 \rightarrow 2}^{\text{LLA}}(s, t) = \mathcal{M}_{2 \rightarrow 2}^{\text{tree}}(s, t) \times \int \frac{d\omega}{2\pi i} \frac{1}{\omega - \beta(\mathbf{q}^2)} \frac{1}{2} \left[\left(-\frac{p_A^+ p_B^-}{m_A m_B} \right)^\omega + \left(\frac{p_A^+ p_B^-}{m_A m_B} \right)^\omega \right]. \quad (3.27)$$

Inserting Eq. (3.4) for the tree-level amplitude, the result can be written in a form that makes negative signature of the reggeized gluon apparent

$$\mathcal{M}_{2 \rightarrow 2}^{\text{LLA}}(s, t) = 2g^2 \frac{s}{t} \int \frac{d\omega}{2\pi i} \frac{1}{\omega - \beta(\mathbf{q}^2)} \left| \frac{s}{m_A m_B} \right|^\omega \frac{\xi^{(-)}(\omega)}{2}, \quad \xi^{(-)}(\omega) = e^{-i\pi\omega} + 1. \quad (3.28)$$

From the point of view of the effective action, the following representation is however more adequate:

$$i\mathcal{M}_{2 \rightarrow 2}^{\text{LLA}}(s, t) = \int \frac{d\omega}{4\pi i} \Gamma_{PPR}(p_A, q) \frac{i/2}{\mathbf{q}^2} \frac{\xi^{(-)}(\omega)}{\omega - \beta(\mathbf{q}^2)} \left| \frac{p_A^+ p_B^-}{s_R} \right|^\omega \Gamma_{PPR}(p_B, q). \quad (3.29)$$

Here $\Gamma_{PPR}(p_A, q)$ are the Particle-Particle-Reggeon vertices which describe the coupling of a particle, a quark (P=Q) or a gluon (P=G), to the reggeized gluon in the t -channel. Corrections due to resummation of central rapidity-diagrams as illustrated above, are then taken into account, by replacing every bare by the resummed reggeized gluon. Due to the non-local nature of the reggeized gluon, it is needed to consider a reggeized gluon always as an object embedded into a minimal elastic amplitude which yields a well-defined dependence of the reggeized gluon on the squared center-of-mass energy of the sub-amplitude, $s = p_A^+ p_B^-$, and its momentum transfer, $t = -\mathbf{q}^2$. We note that for the reggeized gluons s should be always defined as the product of p_A^+ and p_B^- , also if transverse components and other light-cone momenta of the particles A and B are non-zero. For the description of reggeized gluons it is furthermore advisable to keep explicitly the Mellin-integral. Due to Eq. (3.9), it provides a natural implementation of the non-locality constraint in rapidity of the reggeized gluon.

3.1.3 Quasi-elastic corrections

Before finishing the discussion of the single reggeized-gluon-exchange, we demonstrate how a cancellation of the previously introduced cut-offs can occur if one goes beyond the strict LLA. The quasi-elastic diagrams QEA and QEB, Fig.3.9, do not contribute within the LLA, but only at NLLA. Also we do not attempt to determine the full quasi-elastic-corrections to the quark-reggeized-gluon coupling, but are merely interested in the logarithmic part that should allow a cancellation of the above introduced parameter λ_a and λ_b . It is further natural to expect, that this contribution oc-

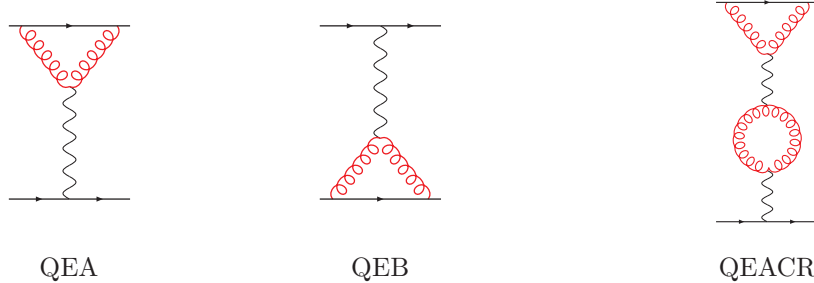


Figure 3.9: Diagrams in the quasi-elastic regions of quark A and B resp., where the reggeized gluon couples to the loop by an induced vertex. To the left a higher order example

curs inside the diagrams QEA and QEB which contain an induced vertex. Like the central rapidity diagram CR, these diagrams arise from the QCD-diagrams QCD1 and QCD2, Fig.3.3, in a certain kinematical limit. Diagrams where the reggeized gluon couple to the gluon-loop by a three-gluon vertex, are expected to lead to usual QCD-vertex corrections and are not of interest to us in the present context. Also for the diagram QEA we attempt in the following to extract only its leading logarithmic part, needed for the cancellation, while we discard all other contributions. For the diagram QEA in Fig.3.3, un-regularized Feynman-rules of the effective action lead to the following

expression

$$i\mathcal{M}^{\text{QEA}}(s, t) = \int \frac{d^4k}{(2\pi)^4} \bar{u}(p_A - q) i g t^a \not{x}^+ \frac{i(\not{p}_A - \not{k} + m_A)}{(p_A - k)^2 - m_A^2 + i\epsilon} i g t^b \not{x}^+ u(p_A) \\ \frac{-i}{k^2 + i\epsilon} \frac{-i}{(q - k)^2 + i\epsilon} \frac{f^{abc}}{k^+} \frac{i/2}{q^2 2} \bar{u}(p_B + q) i g t^c \not{\eta}^+ u(p_B). \quad (3.30)$$

Due to on-shellness of the quark A and A', $q^- = (\mathbf{q}^2 + m_A^2)/p_A^+$ and $p_A^- = m_A^2/p_A^+$ are small and neglected in the following. For quasi-elastic corrections, the requirements imposed by locality in rapidity are more involved than in the previously discussed case of central-rapidity diagrams: Namely it is needed to combine two constraints in that case: From the point of view of the loop build from the quark and the gluons in Fig.3.9, diagram QEA, rapidity of the gluon-loop Y_k is restricted to the $[Y_A - \eta, Y_A + \eta]$, with Y_A the rapidity of the quark. While Y_k is bounded from above by the sheer structure of the integrand in Eq.(3.30), a regularization for the lower end is required that ensures that this bound is fulfilled. Anticipating that integral over longitudinal momenta will be performed by taking residues of the gluon-propagator, the gluon can at least with LLA accuracy be regarded as being close to the mass-shell also in the present case. Imposing therefore a lower bound $p_B^- k^+ > p_A^+ p_B^- / \lambda_a$ will result in a constraint $Y_K > Y_A - \ln \lambda_a$ which sets the rapidity of the gluon inside the loop close to the one of the quark A. From the point of view of the reggeized gluon, on the other hand, the requirement arises that the rapidities of the gluon loop and the quark B respectively are significantly separated. For the leading order diagram QEA, Fig.3.9, this is fulfilled automatically as long as scattering of the two quarks takes place in the Regge-limit. Including however higher order corrections in the central-rapidity region as diagram QEACR, Fig.3.9, it is needed to make this constraint explicit.

Making use of Eq.(3.9) and Eq.(3.11) we propose to use the following regulated expression:

$$i\mathcal{M}^{\text{QEA}}(s, t) = \int \frac{d\omega}{2\pi i} \Gamma_{QQR}(\omega, \lambda_a; p_A, q) \frac{i/2}{q^2} \frac{1}{\omega + \nu} \left| \frac{p_A^+ p_B^-}{m_A m_B} \right|^\omega \Gamma_{QQR}(p_B, q), \quad (3.31)$$

with

$$\Gamma_{QQR}(\omega, \lambda_a; p_A, q) = \Gamma_{QQR}(p_A, q) \gamma_+(\omega, \lambda_a), \quad (3.32)$$

and

$$\gamma(\omega, \lambda_a) = \frac{-g^2 N_c \mathbf{q}^2}{2} \int \frac{dk^+ dk^-}{2\pi} \int \frac{d^2\mathbf{k}}{(2\pi)^3} \frac{p_A^+ - k^+}{(p_A - k)^2 - m_A^2 + i\epsilon} \frac{1}{k^2 + i\epsilon} \frac{1}{(q - k)^2 + i\epsilon} \\ \int \frac{d\omega'}{4\pi i} \frac{p_B^-}{\omega' - \omega} \left(\frac{\lambda_a}{p_A^+ p_B^-} \right)^{\omega'} \left[(p_B^- k^+ - i\epsilon)^{\omega' - 1} - (-p_B^- k^+ - i\epsilon)^{\omega' - 1} \right]. \quad (3.33)$$

In the above expression we therefore use a combination of two Mellin-integrals to impose the required bounds. Furthermore they allow to write the complete expression in a factorized form, which allows to include in a simple and straight forward way corrections from the central rapidities or the quasi-elastic region of the quark B. The Mellin-integral in ω' in Eq.(3.33) ensures then that the gluon loop is close in rapidity to the quark A. Carrying out this integral one picks up to pole at $\omega' = \omega$ and the ω' -factors in Eq.(3.33) combine with the ω -factors in Eq.(3.31). Together the lead to the constraint $p_B^- k^+ > \frac{m_A m_B}{\lambda_a}$ i.e. the product $p_B^- k^+$ is required to be bigger than the typical transverse scale, which seems to be a reasonable constraint, taking into account the discussion of the previous paragraphs.

In Eq. (3.33) the integral over k^- is only non-zero if $p_A^+ > k^+ > 0$, and taking residues of the gluon propagators we obtain

$$\gamma_+(\omega, \lambda_a) = \frac{-g^2 N_c \mathbf{q}^2}{2} \int \frac{d\omega'}{4\pi i} \frac{1}{\omega' - \omega} \int_0^{p_A^+} \frac{dk^+}{k^+} [(-k^+)^{\omega'} + (k^+)^{\omega'}] \left(\frac{\lambda_a}{p_A^+} \right)^{\omega'} \\ \int \frac{d^2\mathbf{k}}{(2\pi)^3} \frac{1}{(\mathbf{q} - \mathbf{k})^2 - \frac{k^+}{k^+ - p_A^+} (\mathbf{k}^2 + m_A^2)} \frac{1}{\mathbf{k}^2 - \frac{k^+}{k^+ - p_A^+} (\mathbf{k}^2 + m_A^2)}. \quad (3.34)$$

We are only interested in the leading logarithmic part of the integral, which is proportional to $1/\omega$. It arises from the region of integration with strong ordering of momenta, $p_A^+ \gg k^+$. We obtain

$$\gamma_+(\omega, \lambda_a) = \int \frac{d\omega'}{4\pi i} \frac{1}{\omega' - \omega} [(-\lambda_a)^{\omega'} + (\lambda_a)^{\omega'}] \frac{\beta(\mathbf{q})}{\omega'} = \frac{\beta(\mathbf{q})}{\omega} \left[\frac{(-\lambda_a)^\omega + (\lambda_a)^\omega}{2} - 1 \right], \quad (3.35)$$

where we set $\Re\omega' > 0$. We obtain for Eq.(3.31)

$$i\mathcal{M}^{\text{QEA}}(s, t) = i\mathcal{M}^{\text{tree}}(s, t) \int \frac{d\omega}{2\pi i} \frac{1}{\omega + \nu} \left| \frac{p_A^+ p_B^-}{m_A m_B} \right|^\omega \frac{\beta(\mathbf{q})}{\omega} \left[\frac{(-\lambda_a)^\omega + (\lambda_a)^\omega}{2} - 1 \right], \quad (3.36)$$

and with $\nu \rightarrow 0$ we find

$$\mathcal{M}^{\text{QEA}} = \mathcal{M}_{2 \rightarrow 2}^{\text{tree}}(s, t) \beta(\mathbf{q}) \frac{\ln(-\lambda_a) + \ln(\lambda_a)}{2} \quad (3.37)$$

and similarly for the diagram QEB

$$\mathcal{M}^{\text{QEB}} = \mathcal{M}_{2 \rightarrow 2}^{\text{tree}}(s, t) \beta(\mathbf{q}) \frac{\ln(-\lambda_b) + \ln(\lambda_b)}{2}. \quad (3.38)$$

As a consequence, in the sum of central rapidity and quasi-elastic diagrams, the dependence on the parameters λ_a and λ_b cancels as required

$$\mathcal{M}^{\text{QEA}} + \mathcal{M}^{\text{CR}} + \mathcal{M}^{\text{QEB}} = \mathcal{M}_{2 \rightarrow 2}^{\text{tree}}(s, t) \beta(\mathbf{q}) \frac{1}{2} \left[\ln \left(-\frac{p_A^+ p_B^-}{m_A m_B} \right) + \ln \left(\frac{p_A^+ p_B^-}{m_A m_B} \right) \right]. \quad (3.39)$$

It is also straight-forward, to verify with Eq.(3.36) cancellation of the parameter λ_a , if corrections that lead to reggeization of the gluon like diagram QEACR in Fig.3.9, are additionally included. With central-rapidity diagrams resummed to all orders (and treating those within the LLA) Eq.(3.36) turns into

$$\begin{aligned} i\mathcal{M}^{\text{QEA}}(s, t) &= i\mathcal{M}^{\text{tree}}(s, t) \int \frac{d\omega}{2\pi i} \frac{1}{\omega - \beta(\mathbf{q})} \left| \frac{p_A^+ p_B^-}{m_A m_B} \right|^\omega \frac{\beta(\mathbf{q})}{\omega} \left[\frac{(-\lambda_a)^\omega + (\lambda_a)^\omega}{2} - 1 \right] \\ &= i\mathcal{M}^{\text{tree}}(s, t) \int \frac{d\omega}{2\pi i} \frac{1}{\omega - \beta(\mathbf{q})} \left| \frac{p_A^+ p_B^-}{m_A m_B} \right|^\omega \xi^{(-)}(\omega) \frac{\beta(\mathbf{q})}{\omega} \left[|\lambda_a|^\omega - \frac{1}{\xi^{(-)}(\omega)} \right]. \end{aligned} \quad (3.40)$$

In the second line of Eq. (3.40), all corrections that formally belong to the Quark-Quark-Reggeon vertex at NLLA are contained in the squared bracket to the left. As all of parameters inside the bracket are small in comparison with the difference in rapidity Y_{AB} , we therefore expand this bracket up to order g^2 , which corresponds to the order of the additional correction of the additionally included quasi-elastic diagram. We expand up to order ω and arrive at

$$i\mathcal{M}^{\text{QEA}}(s, t) = i\mathcal{M}^{\text{tree}}(s, t) \int \frac{d\omega}{2\pi i} \frac{1}{\omega - \beta(\mathbf{q})} \left| \frac{p_A^+ p_B^-}{m_A m_B} \right|^\omega \xi^{(-)}(\omega) \frac{\beta(\mathbf{q})}{\omega} \frac{\ln(-\lambda_a) + \ln(\lambda_a)}{2}. \quad (3.41)$$

The above expression has now to cancel the corresponding factor λ_a in the diagrams of Sec.3.1.2, where this dependence is kept explicitly. From Eq.(3.24) and Eq.(3.27) we find, converting Λ_A into λ_a according to Eq.(3.20) and dropping all other cut-off factors, the following expression:

$$\begin{aligned} &i\mathcal{M}^{\text{tree}}(s, t) \int \frac{d\omega}{4\pi i} \frac{1}{\omega - \beta(\mathbf{q})} \left[\left(\frac{-p_A^+ p_B^-}{m_A m_B \lambda_a} \right)^\omega + \left(\frac{p_A^+ p_B^-}{m_A m_B \lambda_a} \right)^\omega \right] \\ &= i\mathcal{M}^{\text{tree}}(s, t) \int \frac{d\omega}{4\pi i} \left[\left(\frac{-p_A^+ p_B^-}{m_A m_B} \right)^\omega + \left(\frac{p_A^+ p_B^-}{m_A m_B} \right)^\omega \right] \left[\frac{1}{\omega - \beta(\mathbf{q})} - \frac{\omega}{\omega - \beta(\mathbf{q})} \frac{\ln(-\lambda_a) + \ln(\lambda_a)}{2} \right]. \end{aligned} \quad (3.42)$$

In the second line corrections beyond the LLA have been expanded up to order ω . Adding Eq.(3.42) and Eq. (3.40), the pole $1/(\omega - \beta(\mathbf{q}))$ cancels for the part proportional to $\ln(\lambda_a)$, in accordance with the present accuracy of our calculations, and the integral over ω yields zero result for the λ_a -dependent part.

We therefore conclude this section on the exchange of a single reggeized gluon with the observation that a cancellation of the factorization parameter can be achieved, if corrections beyond the LLA are included.

3.2 Exchange of two reggeized gluons

In the following we consider the first example of an amplitude in the effective theory, with interaction of reggeized gluons. From a technical view-point this means, that we turn to loop-integrations with at least two reggeized gluons inside the loop. As a particular process we consider the elastic amplitude with exchange of two reggeized gluons. In the Reggeon-calculus [5, 6], this kind of diagrams are known as *Regge-cuts* as they lead to branch cuts in the complex angular momentum. In the present study they are of two-fold interest: At first they allow to determine the Regge-limit of elastic amplitudes, where external quantum numbers do not allow for the exchange of a single reggeized gluon. This is for instance the case if we project the external quark-states on the color singlet or if we explicitly require the amplitude to have positive signature. Furthermore it is principally possible that those diagrams provide sub-leading corrections to the reggeized gluon.

3.2.1 The Born-diagrams

To leading order in g^2 , the relevant diagrams are given by 2R1 and 2R2, as depicted in Fig.3.10. Another set of diagrams that occurs in principal as well is given by the graphs in Fig.3.11. These

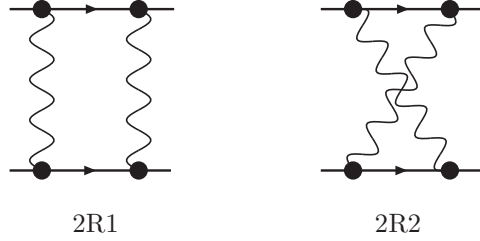


Figure 3.10: Diagrams with exchange of two reggeized gluons. Coupling of the reggeized gluon to the quark is described by the effective vertex Eq.(3.2).

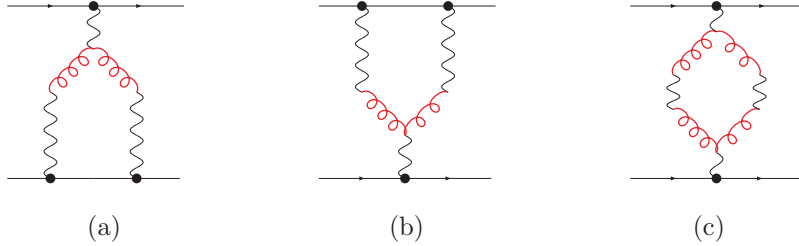


Figure 3.11: Feynman diagrams of the effective action provide besides diagrams 2R1 and 2R1 also the following set of diagrams, where one reggeized gluon splits up into two by an induced vertex. Diagrams where the induced vertex is replaced by a three-gluon-vertex exist as well, but there immediate zero due to the general properties of the reggeized gluon fields $A_{\pm}(x)$.

diagrams take a special role in the discussion of the two-Reggeon exchange and will be addressed further down in this paragraph. For the sum of the diagrams 2R1 and 2R2 un-regularized Feynman rules of the effective action yield the following expression:

$$\begin{aligned}
 & \mathcal{M}_{2 \rightarrow 2}^{\text{B|2R}}(s, t) \\
 &= i |p_A^+| |p_B^-| \int \frac{d^2 k_{\perp}}{(2\pi)^2} \left[(ig)^2 \int \frac{d\mu_A}{(-2\pi i)} \left(\frac{(t^{a_1 t^{a_2}})_{AA'}}{\mu_A - \mathbf{k}^2 - m_A^2 + i\epsilon} + \frac{(t^{a_2 t^{a_1}})_{AA'}}{-\mu_A - (\mathbf{q} - \mathbf{k})^2 - m_A^2 + i\epsilon} \right) \right] \\
 & \times \frac{1}{\mathbf{k}^2 (\mathbf{q} - \mathbf{k})^2} \left[(ig)^2 \int \frac{d\mu_B}{2\pi} \left(\frac{(t^{a_1 t^{a_2}})_{BB'}}{\mu_B - \mathbf{k}^2 - m_B^2 + i\epsilon} + \frac{(t^{a_2 t^{a_1}})_{BB'}}{-\mu_B - (\mathbf{q} - \mathbf{k})^2 - m_B^2 + i\epsilon} \right) \right], \quad (3.43)
 \end{aligned}$$

where we defined $\mu_A = -p_A^+ k^-$ and $\mu_B = p_B^- k^+$. The longitudinal loop integral factorizes and the integration can be carried out separately for each of the quark impact factors, which are given by the big squared brackets in the first and second line of Eq.(3.43). This kind of factorization is typical for loop-integrations of reggeized gluons. We therefore obtain

$$\mathcal{M}_{2 \rightarrow 2}^{\text{B|2R}} = 2\pi i |p_A^+| |p_B^-| \int \frac{d^2 k_\perp}{(2\pi)^3} \frac{1}{\mathbf{k}^2 (\mathbf{q} - \mathbf{k})^2} A_{AA'}^{a_1 a_2}(\mathbf{k}, \mathbf{q} - \mathbf{k}) A_{BB'}^{a_1 a_2}(\mathbf{k}, \mathbf{q} - \mathbf{k}), \quad (3.44)$$

with the quark-impact factor for two reggeized gluons given by

$$A_{AA'}^{a_1 a_2}(\mathbf{k}, \mathbf{q} - \mathbf{k}) = -g^2 \int \frac{d\mu_A}{(-2\pi i)} \left(\frac{(t^{a_1} t^{a_2})_{AA'}}{\mu_A - \mathbf{k}^2 - m_A^2 + i\epsilon} + \frac{(t^{a_2} t^{a_1})_{AA'}}{-\mu_A - (\mathbf{q} - \mathbf{k})^2 - m_A^2 + i\epsilon} \right), \quad (3.45)$$

$$A_{BB'}^{a_1 a_2}(\mathbf{k}, \mathbf{q} - \mathbf{k}) = -g^2 \int \frac{d\mu_B}{(-2\pi i)} \left(\frac{(t^{a_1} t^{a_2})_{BB'}}{\mu_B - \mathbf{k}^2 - m_B^2 + i\epsilon} + \frac{(t^{a_2} t^{a_1})_{BB'}}{-\mu_B - (\mathbf{q} - \mathbf{k})^2 - m_B^2 + i\epsilon} \right). \quad (3.46)$$

As the impact factors do neither depend on p_A^+ nor on p_B^- , it is immediately clear, that the two reggeized gluon exchange amplitude, Eq.(3.44), is symmetric under $s \rightarrow -s$ and therefore allows only for positive signature exchange in the t -channel. From now on we restrict to the impact factor of the upper quark A, while the result for the quark B follows by symmetry. We then decompose color into a symmetric and an anti-symmetric part and obtain

$$A_{AA'}^{a_1 a_2}(\mathbf{k}, \mathbf{q} - \mathbf{k}) = \frac{1}{2} \{t^{a_1}, t^{a_2}\}_{AA'} A_{(2;0)}^{(+)}(\mathbf{k}, \mathbf{q} - \mathbf{k}) + \frac{1}{2} [t^{a_1}, t^{a_2}]_{AA'} A_{(2;0)}^{(-)}(\mathbf{k}, \mathbf{q} - \mathbf{k}), \quad (3.47)$$

with

$$A_{(2;0)}^{(+)}(\mathbf{k}, \mathbf{q} - \mathbf{k}) = -g^2 \int \frac{d\mu_A}{(-2\pi i)} \left(\frac{1}{\mu_A - \mathbf{k}^2 - m_A^2 + i\epsilon} + \frac{1}{-\mu_A - (\mathbf{q} - \mathbf{k})^2 - m_A^2 + i\epsilon} \right), \quad (3.48)$$

and

$$A_{(2;0)}^{(-)}(\mathbf{k}, \mathbf{q} - \mathbf{k}) = -g^2 \int \frac{d\mu_A}{(-2\pi i)} \left(\frac{1}{\mu_A - \mathbf{k}^2 - m_A^2 + i\epsilon} - \frac{1}{-\mu_A - (\mathbf{q} - \mathbf{k})^2 - m_A^2 + i\epsilon} \right). \quad (3.49)$$

We start with the symmetric case: In the sum of the two denominators, the singularity in μ_A cancels and the integral over μ_A is convergent. Enclosing therefore for the *sum* of the two terms the contour of integration at infinity, we obtain

$$A_{(2;0)}^{(+)}(\mathbf{k}, \mathbf{q} - \mathbf{k}) = -g^2, \quad (3.50)$$

and

$$\mathcal{M}_{2 \rightarrow 2}^{\text{B|2R}} = \frac{i\pi}{2} \{t^{a_1}, t^{a_2}\}_{AA'} \{t^{a_1}, t^{a_2}\}_{BB'} g^4 |p_A^+ p_B^-| \int \frac{d^2 \mathbf{k}}{(2\pi)^3} \frac{1}{\mathbf{k}^2 (\mathbf{q} - \mathbf{k})^2}. \quad (3.51)$$

The discussion in the anti-symmetric case requires more care. The logarithmic singularity in μ_A does not cancel and the integral over the two terms appears to be ill-defined. To understand the origin of this singularity, we return once again to the QCD-diagrams QCD1 and QCD2 in Fig.3.3. Taking into account simplifications due to the Regge-limit, their sum is given by Eq.(3.7), which we state here once again:

$$\mathcal{M}_{\text{QCD}} = g^4 (p_A^+ p_B^-) \int \frac{dk^+ dk^-}{2\pi i} \int \frac{d^2 \mathbf{k}}{(2\pi)^3} \left(\frac{(t^{c_1} t^{c_2})_{AA'}}{-k^- - \frac{\mathbf{k}^2 + m_A^2 + i\epsilon}{p_A^+ - k^+}} + \frac{(t^{c_2} t^{c_1})_{AA'}}{k^- - \frac{(\mathbf{q} - \mathbf{k})^2 + m_A^2 + i\epsilon}{p_A^+ + k^+}} \right) \frac{1}{k^+ k^- - \mathbf{k}^2 + i\epsilon} \frac{1}{k^+ k^- - (\mathbf{q} - \mathbf{k})^2 + i\epsilon} \left(\frac{(t^{c_1} t^{c_2})_{BB'}}{k^+ - \frac{(\mathbf{q} - \mathbf{k})^2 + m_B^2 - i\epsilon}{p_B^- + k^-}} + \frac{(t^{c_2} t^{c_1})_{BB'}}{-k^+ - \frac{\mathbf{k}^2 + m_B^2 - i\epsilon}{p_B^- - k^-}} \right)$$

For the symmetric color combination, k^- and k^+ are in the integral fixed by the poles of the quark-propagators, inside the big brackets. Consequently $k^+ k^- \ll \mathbf{k}^2, (\mathbf{q} - \mathbf{k})^2$ and we find the expressions

corresponding to the symmetric projection of the diagrams 2R1 and 2R2. For antisymmetric t -channel color on the other hand, the leading pole in the expansion of the big brackets in $\mu_A = -p_A^+ k^-$ and $\mu_B = -p_B^- k^+$ does not cancel. It was shown in Sec.3.1.1 that it rather leads to the induced vertex which enters for $\mu_A, \mu_B > \Lambda_a, \Lambda_b$ the central rapidity and quasi-elastic diagrams. In particular, integrating in Eq.(3.49) this pole-part over the full range of μ_A and μ_B , we would count this contribution twice, due to its presence in quasi-elastic and central-rapidity diagrams. To avoid this unjustified double-counting, this pole needs to be subtracted from Eq.(3.49) for large values of μ_A and μ_B respectively and doing so, integrals over μ_A and μ_B turn out to be convergent.

The particular form of the term we should subtract is given by the graphs in Fig.3.11 or for the impact alone by Fig.3.12, which describes the splitting of a single reggeized gluon into two reggeized gluons by an induced vertex. Applying the same factorization as for the impact factor, the diagram

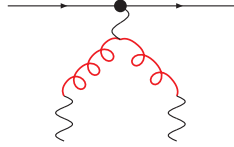


Figure 3.12: Coupling of a reggeized gluon to two reggeized gluons by an induced vertices. These diagrams do not contribute to physical amplitudes, however they provide the diagrammatic form of the subtraction terms in the antisymmetric color sector.

Fig.3.12 yields, including a lower bound on μ_A due to the presence of the reggeized gluon,

$$A_{AA'}^{S a_1 a_2} = \frac{-g^2}{2} [t^{a_1}, t^{a_2}]_{AA'} \int \frac{d\mu_A}{(-2\pi i)} \int_{0-i\infty}^{0+i\infty} \frac{d\omega}{2\pi i} \frac{\Lambda_a^{-\omega}}{\omega + \nu} \left[(\mu_A - i\epsilon)^{\omega-1} - (-\mu_A - i\epsilon)^{\omega-1} \right]. \quad (3.52)$$

Making use of

$$\int_{0-i\infty}^{0+i\infty} \frac{d\omega}{2\pi i} \frac{1}{\omega + \nu} \left(\frac{\mu_A}{\Lambda_a} \right)^\omega = 1 - \int_{0-i\infty}^{0+i\infty} \frac{d\omega}{2\pi i} \frac{-1}{\omega - \nu} \left(\frac{\mu_A}{\Lambda_a} \right)^\omega \quad (3.53)$$

where on the right-hand-side, the pole in ω is now to the left of the contour, we find, subtracting Eq.(3.52) from Eq.(3.49)

$$\begin{aligned} & A_{AA'}^{a_1 a_2, (-)}(\mathbf{k}, \mathbf{q} - \mathbf{k}) - A_{AA'}^{S a_1 a_2}(\mathbf{k}, \mathbf{q} - \mathbf{k}) = \\ & = \frac{ig^2}{2} [t^{a_1}, t^{a_2}]_{AA'} \int \frac{d\mu_A}{2\pi} \left\{ \int_{0-i\infty}^{0+i\infty} \frac{d\omega}{2\pi i} \frac{-\Lambda_a^\omega}{\omega - \nu} \left[(\mu_A - i\epsilon)^{\omega-1} - (-\mu_A - i\epsilon)^{\omega-1} \right] \right. \\ & \left. + \left(\frac{1}{\mu_A - \mathbf{k}^2 - m_A^2 + i\epsilon} - \frac{1}{\mu_A + i\epsilon} \right) - \left(\frac{1}{-\mu_A - (\mathbf{q} - \mathbf{k})^2 - m_A^2 + i\epsilon} - \frac{1}{\mu_A + i\epsilon} \right) \right\}. \quad (3.54) \end{aligned}$$

In the last line all integrals are now convergent. Taking residues, the result of the two brackets cancels. In the first line, there is no singularity in the ω -plane to the left of the ω -contour which allows to move the ω -contour to the left until ω acquires a negative real part and the integral over μ_A gets convergent. As there is no further singularity in the μ_A -plane, we close the μ_A -contour without encircling any singularity at infinity and Eq.(3.54) vanishes.

This is the expected result as at high center of mass energies s , the QCD amplitude with anti-symmetric color exchange reggeizes and is described by the exchange of a single reggeized gluon. In particular the amplitude with antisymmetric color in the t -channel is given by the sum of quasi-elastic and central-rapidity diagrams alone.

The method developed here for longitudinal integrations in the context of loops containing two or more reggeized gluons, turns out to be a rather general one: The part of the amplitudes that can be constructed from direct coupling the reggeized gluons by induced vertices is already contained in the corresponding central-rapidity diagrams.

A comment is in order concerning diagrams like Fig.3.11: With our subtraction-mechanism, those diagrams are subtracted by themselves and do not contribute. This subtraction mechanism can

be further automatized by adding a subtraction term to the Lagrangian, that subtracts these contributions automatically. Details about the subtraction term will be presented in Sec.5.2.

Another comment is in order concerning the decoupling of the anti-symmetric two Reggeon state of the quark: To study reggeization of the gluon, one usually makes use of s -channel dispersion relations (see for instance [88] for a pedagogical introduction). This requires to determine the s -discontinuity of the elastic amplitude (i.e. its imaginary part). Applying a bootstrap, the discontinuity is expressed as a bound state of two reggeized gluons. However, after resumming corrections within the LLA by the BFKL-equation to all orders, the two Reggeon state drops out and one is left with the exchange of a single reggeized gluon, for details see [88–90]. As a consequence, also in the dispersion-relation based approach, the anti-symmetric two Reggeon state decouples from the quark. In the effective action the reggeized gluon comes explicitly with negative signature and therefore contains also the s -discontinuity of the elastic amplitude.

3.2.2 Higher order corrections: the BFKL-equation

Higher order corrections to the diagrams in Fig.3.10 are two-fold: On the one hand they involve corrections due to reggeization of the gluon, which are taken into account by replacing bare reggeized gluons by their resummed counterparts Eq.(3.27). On the other hand there are corrections due to interactions between reggeized gluons. In particular, every interaction between two reggeized gluons yields a logarithm in s and must be taken into account with the LLA. Interactions between the two reggeized gluons are then resummed by the BFKL-equation, which we will derive in the following. Furthermore, there exist also corrections due to exchange of more than two reggeized gluons. For the elastic amplitude, these corrections are formally sub-leading within in the LLA. They are addressed in Cha.5. Within the LLA interactions between two reggeized gluons is given by the diagrams in Fig.3.13. There we use the gauge invariant production or Lipatov vertex

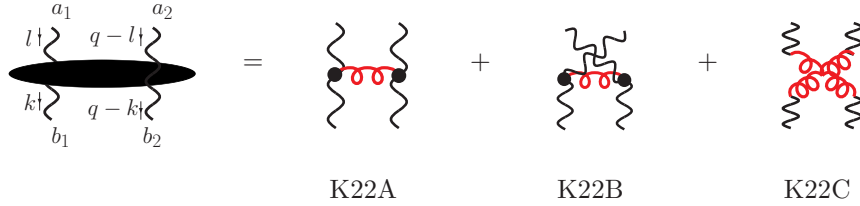


Figure 3.13: Interaction of two reggeized gluons which yields to 2-to-2 reggeized gluons transition kernel.

$$\text{Diagram} = 2gf^{acb}C_\mu(l, k), \quad (3.55)$$

which is an effective vertex. Within the effective action it arises as a combination of the diagrams in Fig.3.14 which yields

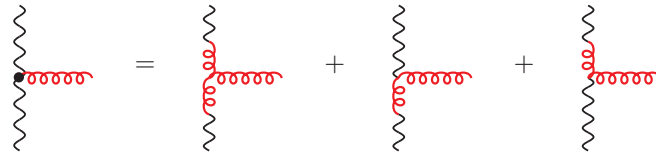


Figure 3.14: The effective particle production or Lipatov vertex in the effective action formalism.

$$C_\mu(l, k) = \left(\frac{l^+}{2} + \frac{l_1^2}{k^-}\right) (n^-)^\mu + \left(\frac{k^-}{2} + \frac{k_2^2}{l^+}\right) (n^-)^\mu - (l+k)_\perp^\mu. \quad (3.56)$$

The production vertex is gauge invariant; especially the relation

$$C_\mu(l, k) \cdot (l - k)^\mu = 0, \quad (3.57)$$

holds also if the gluon is off-shell. For the individual diagrams in Fig.3.13 one obtains the following expressions

$$\text{K22A} = -i8g^2 T_{a_1 c}^{b_1} T_{c a_2}^{b_2} \left[\frac{1}{2} + \left(-\mathbf{q}^2 + \frac{(\mathbf{l} - \mathbf{q})^2 \mathbf{k}^2}{-l^+ k^-} + \frac{(\mathbf{k} - \mathbf{q})^2 \mathbf{l}^2}{-l^+ k^-} \right) \frac{1}{-l^+ k^- - (\mathbf{l} - \mathbf{k})^2 + i\epsilon} \right], \quad (3.58)$$

$$\text{K22B} = -i8g^2 T_{a_1 c}^{b_2} T_{c a_2}^{b_1} \left[\frac{1}{2} + \left(-\mathbf{q}^2 + \frac{\mathbf{l}^2 \mathbf{k}^2}{l^+ k^-} + \frac{(\mathbf{k} - \mathbf{q})^2 (\mathbf{l} - \mathbf{q})^2}{l^+ k^-} \right) \frac{1}{l^+ k^- - (\mathbf{l} - \mathbf{q} + \mathbf{k})^2 + i\epsilon} \right], \quad (3.59)$$

$$\text{K22C} = i4g^2 (T_{a_1 c}^{b_1} T_{c a_2}^{b_2} + T_{a_1 c}^{b_2} T_{c a_2}^{b_1}), \quad (3.60)$$

where $T_{ac}^b = if^{abc}$ are generators in the adjoint representation of $SU(N_c)$. In the sum of the three diagrams, K22C cancels the constant term in K22A and K22B and we obtain

$$\begin{aligned} \text{K22A} + \text{K22B} + \text{K22C} = & -i8g^2 \left[-\mathbf{q}^2 \left(\frac{T_{a_1 c}^{b_1} T_{c a_2}^{b_2}}{-l^+ k^- - (\mathbf{l} - \mathbf{k})^2 + i\epsilon} + \frac{T_{a_1 c}^{b_2} T_{c a_2}^{b_1}}{l^+ k^- - (\mathbf{l} - \mathbf{q} + \mathbf{k})^2 + i\epsilon} \right) \right. \\ & + T_{a_1 c}^{b_1} T_{c a_2}^{b_2} \left(\frac{(\mathbf{l} - \mathbf{q})^2 \mathbf{k}^2}{-l^+ k^-} + \frac{(\mathbf{k} - \mathbf{q})^2 \mathbf{l}^2}{-l^+ k^-} \right) \frac{1}{-l^+ k^- - (\mathbf{l} - \mathbf{k})^2 + i\epsilon} \\ & \left. + T_{a_1 c}^{b_2} T_{c a_2}^{b_1} \left(\frac{\mathbf{l}^2 \mathbf{k}^2}{l^+ k^-} + \frac{(\mathbf{k} - \mathbf{q})^2 (\mathbf{l} - \mathbf{q})^2}{l^+ k^-} \right) \frac{1}{l^+ k^- - (\mathbf{l} - \mathbf{q} + \mathbf{k})^2 + i\epsilon} \right]. \end{aligned} \quad (3.61)$$

Similar to the two-gluon quark-impact-factor in Sec.3.2, if we project on the antisymmetric color



K22S

Figure 3.15: Subtraction term for the interaction of two-reggeized gluons. It takes into account the contributions of the two-Reggeon-interaction with anti-symmetric t -channel color that are already contained in the reggeized gluon.

channel, we find in the first line, once we integrate over light-cone momenta, a logarithmic singularity in $l^+ k^-$. For values of $l^+ k^-$ larger than Λ_c , this pole is already included in the 2-loop reggeized gluon, Sec.3.1.2 and particularly Eq.(3.23). The corresponding contribution needs therefore to be subtracted, and the precise form of the subtraction term is obtained from the graph K22S in Fig.3.15, which yields the following expression:

$$\text{K22S} = -i8g^2 \mathbf{q}^2 [T^{b_1}, T^{b_2}]_{a_1 a_2} \int \frac{d\omega}{4\pi i} \frac{1}{\omega + \nu} \left[\left(\frac{l^+ k^- - i\epsilon}{\Lambda_c} \right)^{\omega-1} - \left(\frac{-l^+ k^- - i\epsilon}{\Lambda_c} \right)^{\omega-1} \right]. \quad (3.62)$$

Making use of Eq.(3.53), we obtain altogether for the interaction kernel

$$\begin{aligned} \text{K22A} + \text{K22B} + \text{K22C} - \text{K22S} = & -i8g^2 \left[T_{a_1 c}^{b_1} T_{c a_2}^{b_2} \frac{-\mathbf{q}^2 (\mathbf{l} - \mathbf{k})^2 + (\mathbf{l} - \mathbf{q})^2 \mathbf{k}^2 + (\mathbf{k} - \mathbf{q})^2 \mathbf{l}^2}{(-l^+ k^-) (-l^+ k^- - (\mathbf{l} - \mathbf{k})^2 + i\epsilon)} \right. \\ & + T_{a_1 c}^{b_2} T_{c a_2}^{b_1} \frac{-\mathbf{q}^2 (\mathbf{l} - \mathbf{q} + \mathbf{k}) + \mathbf{l}^2 \mathbf{k}^2 + (\mathbf{k} - \mathbf{q})^2 (\mathbf{l} - \mathbf{q})^2}{(l^+ k^-) (l^+ k^- - (\mathbf{l} - \mathbf{q} + \mathbf{k})^2 + i\epsilon)} \\ & \left. + \mathbf{q}^2 [T^{b_1}, T^{b_2}]_{a_1 a_2} \int \frac{d\omega}{4\pi i} \frac{\Lambda_c}{\omega - \nu} \left[(l^+ k^- - i\epsilon)^{\omega-1} - (-l^+ k^- - i\epsilon)^{\omega-1} \right] \right] \end{aligned} \quad (3.63)$$

where in the last line the ω -contour is to the left of the pole at $\omega = \nu$ and the $i\epsilon$ -prescription of the poles is given by

$$\frac{1}{l^+k^-} = \left(\frac{1/2}{l^+k^- + i\epsilon} + \frac{1/2}{l^+k^- - i\epsilon} \right) = \frac{1}{4} \left(\frac{p_B^-}{p_B^- l^+ + i\epsilon} + \frac{p_B^-}{p_B^- l^+ - i\epsilon} \right) \left(\frac{p_A^+}{p_A^+ k^- + i\epsilon} + \frac{p_A^+}{p_A^+ k^- - i\epsilon} \right). \quad (3.64)$$

To obtain the one-loop correction to the quark-quark-scattering amplitude with exchange of two reggeized gluons within the LLA, we insert the reggeized gluon interaction vertex Fig.3.13 into the Born diagram Fig.3.16a, which leads to the graph of Fig.3.16b. To evaluate the integration over

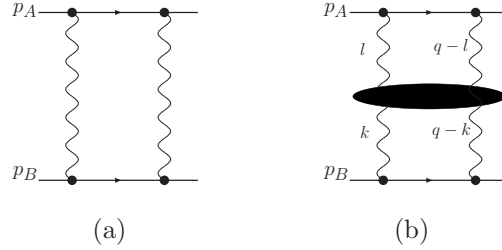


Figure 3.16: Quark-quark-scattering at Born-level and with insertion of one interaction kernel between the reggeized gluons.

longitudinal loop momenta l and k , the following peculiarity of a theory of reggeized gluons has to be taken into account: Every single reggeized gluon belongs to a certain 4-point sub-amplitude inside the complete amplitude and presence of the reggeized gluons requires, that the center of mass energy of the sub-amplitude is significantly larger than all other scales that occur for this particular sub-amplitude. Example of such sub-amplitudes are shown in Fig.3.17. Imposing these

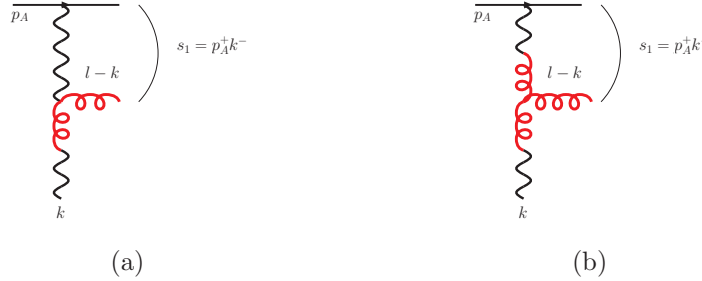


Figure 3.17: 4-point sub-amplitudes with a Regge-pole i.e. the interaction is mediated by the reggeized gluon, involving an induced vertex of the first order (a) and the three-gluon vertex (b).

lower bounds is not only demanded due to the presence of the reggeized gluons, but they also appear naturally if one attempts to derive the graphs of the effective theory from the underlying QCD-graphs, similar to Sec.3.1. For graphs that contain combinations of induced vertices, as Fig.3.18a, this occurs in the same way as for the reggeized gluon in Sec.3.1.1. There, the induced vertices could be shown to arise as the leading term of the expansion of the corresponding quark-propagators, Eq.(3.11). To give meaning to the expansion, we need to introduce lower bounds on the center-of-mass energies of the sub-amplitudes.

Apart from diagrams with induced vertices, the interaction kernel Fig.3.13 contains also contributions due to the three-gluon-vertices, of which the QCD counter-part is shown in Fig.3.18b. Also in that case, the effective action graphs imply simplification that only apply if the sub-energies $s_1 = p_A^+ k^-$ and $s_2 = p_B^- l^+$ are large. In the effective theory diagram at the right hand side of Fig.3.18b, the propagator of the gluon with momentum $l - k$ is considerably simplified compared to the corresponding gluon propagator in full QCD to the left: Within the effective theory, 'small' longitudinal momenta l^- and k^+ are neglected against the corresponding 'large' momenta k^- and l^+ respectively. From Sec.3.2.1 we know, that products $p_A^+ l^-$ and $p_B^- k^+$ are of the order of

the transverse scale and consequently neglecting l^- and k^+ in the propagator is only justified if $s_1 = p_A^+ k^-$ and $s_2 = p_B^- l^+$ are considerably larger than the transverse scale.

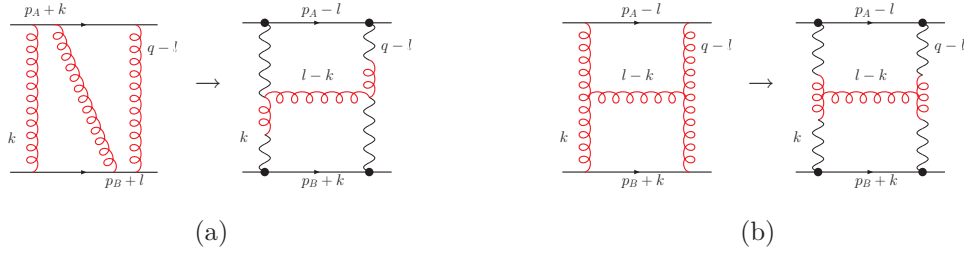


Figure 3.18: Emergence of effective action graphs out of usual QCD-diagrams. (a): Combination of two induced vertices, which arise out of the quark-propagators $(p_A^- \mathcal{L})^{-1}$ and $(p_B^- + k)^{-1}$. (b): Combination of two three-gluon vertices. In both cases the gluon propagator in the effective theory is simplified due to the particular kinematics, compared to the full QCD diagram.

In the case of the 2-2 reggeized gluon transition we are now in the comfortable situation that the constraint due to both reggeized gluons can be gathered into one single constraint for the sub-amplitudes depicted in Fig.3.19. As in Sec.3.1.1, the (inverse) Mellin-integrals, Eq.(3.9), can be used to impose the lower cut-offs. As explained in Sec.3.1.1 this factors lead to branch cuts in the complex plane along the real axis, and both their phase and a prescription how to lead the contour of integration around these branch-cuts has to be given. For the diagrams containing

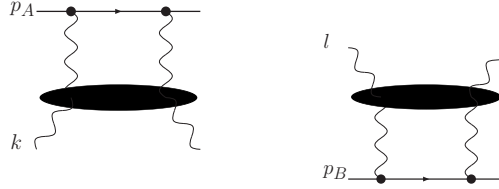


Figure 3.19: Sub-amplitudes of the second diagram of Fig.3.16: For each of the two sub-amplitudes, presence of the two reggeized gluons requires that the corresponding squared sub-center-of-mass energies, $s_1 = (p_A - k)^2$ and $s_2 = (p_B + l)^2$ are significantly larger than a lower cut-off Λ .

induced vertices, the result of Sec.3.1.1 applies immediately. They contain a pole with a certain $i\epsilon$ -prescription, and poles slightly below the real axis are associated with a branch-cut along the positive semi-axis, while poles slightly above the real axis come with a branch cut along the negative semi-axis. At first the interaction vertex that come at first with no pole. However, such a pole appears after the subtraction of the diagram K2S in Eq.(3.63). Furthermore, this pole comes with the same pole-prescription as the poles of the induced vertices. We will treat these poles in the following like poles arising from induced vertices and particularly require that their $i\epsilon$ -prescription coincides with the $i\epsilon$ -prescription of the branch-cuts of the Mellin integral, Eq.(3.9). Poles coming with a $+i\epsilon$ will be associated with a branch cut along the positive semi-axis. Poles with a $-i\epsilon$ with a branch cut along the negative semi-axis, in accordance with the Feynman-prescription for bypassing singularities on the real-axis. For every sub-amplitude of Fig.3.19, the poles in l^+ and k^- are therefore replaced by the following expressions

$$\begin{aligned} \frac{1}{l^+} &\rightarrow p_B^- \int \frac{d\omega_2}{4\pi i} \frac{\Lambda_b^{\omega_2}}{\omega_2 + \nu} \left[(p_B^- l^+ - i\epsilon)^{\omega_2 - 1} - (-p_B^- l^+ - i\epsilon)^{\omega_2 - 1} \right], \\ \frac{1}{k^-} &\rightarrow p_A^+ \int \frac{d\omega_1}{4\pi i} \frac{\Lambda_a^{\omega_1}}{\omega_1 + \nu} \left[(p_A^+ k^- - i\epsilon)^{\omega_1 - 1} - (-p_A^+ k^- - i\epsilon)^{\omega_1 - 1} \right]. \end{aligned} \quad (3.65)$$

This result can be also obtained by simply inserting the resummed reggeized gluon from Eq.(3.29) into our expression. From Eq.(3.29), every reggeized gluon carries a phase factor $\sim (e^{-i\pi\omega} + 1)$, with ω the Mellin variable/the trajectory function of the regarding reggeized gluon. The overall

phase is therefore given by the product of the two phase factors which can be rewritten (following closely [5, 6]) as

$$\frac{e^{-i\pi\omega} + 1}{2} \frac{e^{-i\pi\omega'} + 1}{2} = \frac{e^{-i\pi(\omega+\omega')} + 1}{2} \gamma_{\omega;\omega'}^{(-,-)}, \quad (3.66)$$

with

$$\gamma_{\omega;\omega'}^{(-,-)} = \frac{\cos(\pi\omega/2) \cos(\pi\omega'/2)}{\cos(\pi(\omega+\omega')/2)}. \quad (3.67)$$

To low orders in g^2 , and within the LLA, $\gamma_{\omega_1;\omega_2}^{(-,-)} = 1$ and our above choice for the phases, Eq. (3.65) is indeed in accordance with the phase structure of the reggeized gluons. Only starting from the NNLLA, corrections due the real factor $\gamma_{\omega_1;\omega_2}^{(-,-)}$ need to be included. In the following, it will be convenient for us to introduce the abbreviations

$$\begin{aligned} \mathbf{l}_1 &= \mathbf{l}, & \mathbf{l}_2 &= (\mathbf{q} - \mathbf{l}), \\ \mathbf{k}_1 &= \mathbf{k}, & \mathbf{k}_2 &= (\mathbf{q} - \mathbf{k}). \end{aligned} \quad (3.68)$$

The one-loop correction to the elastic quark-quark-scattering amplitude with exchange of two reggeized gluons is then given by:

$$\begin{aligned} \mathcal{M}_{2 \rightarrow 2}^{\text{1L}(+)} &= 2\pi i |p_A^+| |p_B^-| \int \frac{d\omega_1}{2\pi i} \int \frac{d\omega_2}{2\pi i} A_{(2;0)}^{a_1 a_2} \otimes_{\mathbf{l}} \frac{1}{\omega_1 - \beta(\mathbf{l}_1) - \beta(\mathbf{l}_2)} \left| \frac{p_A^+}{\Lambda_a} \right|^{\omega_1} \\ &B^{a_1 a_2; b_1 b_2}(\omega_1, \omega_2) \otimes_{\mathbf{k}} \frac{1}{\omega_2 - \beta(\mathbf{k}_1) - \beta(\mathbf{k}_2)} \left| \frac{p_B^-}{\Lambda_b} \right|^{\omega_2} A_{(2;0)}^{b_1 b_2}. \end{aligned} \quad (3.69)$$

In analogy to the function $A(\omega_1, \omega_2)$ in the case of the reggeized gluon, Eq. (3.13), we define a function $B(\omega_1, \omega_2)$. As for the reggeized gluon, this function can be defined within different schemes. Generally it can be written as the sum of the following three terms

$$\begin{aligned} B^{a_1 a_2; b_1 b_2}(\omega_1, \omega_2) &= T_{a_1 c}^{b_1} T_{c a_2}^{b_2} B^{(12)}(\omega_1, \omega_2) + T_{a_1 c}^{b_2} T_{c a_2}^{b_1} B^{(21)}(\omega_1, \omega_2) \\ &[T^{b_1}, T^{b_2}]_{a_1 a_2} B^{(R)}(\omega_1, \omega_2), \end{aligned} \quad (3.70)$$

where we suppressed in our notation the dependence on momenta and cut-offs. A convolution symbol which includes the propagators of the reggeized gluons is defined as follows:

$$\otimes_{\mathbf{k}} = \int \frac{d^2 \mathbf{k}}{(2\pi)^3} \frac{1}{\mathbf{k}_1^2 \mathbf{k}_2^2}, \quad (3.71)$$

with $\mathbf{k}_1 + \mathbf{k}_2 = \mathbf{q}$. We obtain

$$\begin{aligned} B^{(ij)}(\omega_1, \omega_2) &= \frac{i}{4} \mathcal{K}_{2 \rightarrow 2}(\mathbf{l}_1, \mathbf{l}_2, \mathbf{k}_i, \mathbf{k}_j) \int \frac{dl^+ k^-}{2\pi} \frac{(\mathbf{l}_1 - \mathbf{k}_i)^2}{-l^+ k^- - (\mathbf{l}_1 - \mathbf{k}_i)^2 + i\epsilon} \\ &[(k^- - i\epsilon)^{\omega_1 - 1} - (-k^- - i\epsilon)^{\omega_1 - 1}] [(l^+ - i\epsilon)^{\omega_2 - 1} - (-l^+ - i\epsilon)^{\omega_2 - 1}], \end{aligned} \quad (3.72)$$

with

$$\mathcal{K}_{2 \rightarrow 2}(\mathbf{l}_1, \mathbf{l}_2, \mathbf{k}_1, \mathbf{k}_2) = \frac{g^2}{2} \left(\mathbf{q}^2 - \frac{\mathbf{l}_2^2 \mathbf{k}_1^2}{(\mathbf{l}_1 - \mathbf{k}_1)^2} + \frac{\mathbf{k}_2^2 \mathbf{l}_1^2}{(\mathbf{l}_1 - \mathbf{k}_1)^2} \right). \quad (3.73)$$

$B^{(R)}$ contains the contribution due to the last line of Eq.(3.63) and can be shown to vanish. The longitudinal integrals of Eq.(3.72) are evaluated similar to Sec.3.1.1 and yield:

$$B^{(ij)}(\omega_1, \omega_2) = -2\pi i \delta(\omega_1 - \omega_2) \frac{[-(\mathbf{l}_1 - \mathbf{k}_i)^2]^{\omega_1} + [(\mathbf{l}_1 - \mathbf{k}_i)^2]^{\omega_1}}{2} \mathcal{K}_{2 \rightarrow 2}(\mathbf{l}_1, \mathbf{l}_2, \mathbf{k}_i, \mathbf{k}_j). \quad (3.74)$$

Making use of simplifications due to the LLA, we set $\Lambda_a \Lambda_b / (\mathbf{l}_1 - \mathbf{k}_i)^2 = m_A m_B$. Introducing further

$$B^{(\pm)}(\omega_1, \omega_2, p_A^+, p_B^-) = B^{(12)}(\omega_1, \omega_2, p_A^+, p_B^-) \pm B^{(21)}(\omega_1, \omega_2, p_A^+, p_B^-), \quad (3.75)$$

we find

$$B^{a_1 a_2; b_1 b_2}(\omega_1, \omega_2, p_A^+, p_B^-) = \{T^{b_1}, T^{b_2}\}_{a_1 a_2} B^{(+)}(\omega_1, \omega_2, p_A^+, p_B^-) + [T^{b_2}, T^{b_1}]_{a_1 a_2} B^{(-)}(\omega_1, \omega_2, p_A^+, p_B^-). \quad (3.76)$$

From the previous paragraph we know, that the quark impact factor for two reggeized gluons couples only to the symmetric color configuration in the t -channel. However there exists also the case of a non-zero coupling of a two reggeized gluon-state with antisymmetric color (we will encounter an example in Sec.4.2.2). Generalizing our results in analogy to the reggeized gluon Sec. 3.1.2 to the elastic quark-quark-scattering amplitude with exchange of two reggeized gluons, with n interactions we obtain for the every inserted interaction between two reggeized gluons, a factor

$$\otimes_{\mathbf{k}} \mathcal{K}_{2 \rightarrow 2}^{\{a\} \rightarrow \{b\}} \frac{1}{\omega - \beta(\mathbf{k}_1) - \beta(\mathbf{k}_2)}, \quad (3.77)$$

with

$$\mathcal{K}_{2 \rightarrow 2}^{\{a\} \rightarrow \{b\}} = f^{a_1 b_1 c} f^{c b_2 a_2} \mathcal{K}_{2 \rightarrow 2}(\mathbf{l}_1, \mathbf{l}_2; \mathbf{k}_1, \mathbf{k}_2) + f^{a_1 b_2 c} f^{c b_1 a_2} \mathcal{K}_{2 \rightarrow 2}(\mathbf{l}_1, \mathbf{l}_2; \mathbf{k}_2, \mathbf{k}_1). \quad (3.78)$$

The all order amplitude is therefore within the LLA given by

$$\mathcal{M}_{2 \rightarrow 2}^{\text{LLA}|2\text{R}} = i\pi |p_A^+| |p_B^-| \int \frac{d\omega}{2\pi i} \left[\left(\frac{-p_A^+ p_B^-}{m_A^+ m_B^-} \right)^\omega + \left(\frac{p_A^+ p_B^-}{m_A^+ m_B^-} \right)^\omega \right] \phi(\omega, t), \quad (3.79)$$

where the partial wave $\phi(\omega, t)$ is a convolution of the upper and the lower quark-impact factors and the BFKL-Green's function:

$$\phi(\omega, t) = A_{(2;0)}^{a_1 a_2}(\mathbf{l}_1, \mathbf{l}_2) \otimes_{\mathbf{l}} G_{\text{BFKL}}^{a_1 a_2; b_1 b_2}(\mathbf{l}_1, \mathbf{l}_2; \mathbf{k}_1, \mathbf{k}_2) \otimes_{\mathbf{k}} A_{(2;0)}^{a_1 a_2}(\mathbf{k}_1, \mathbf{k}_2), \quad (3.80)$$

where the BFKL-Green's function $G_{\text{BFKL}}^{a_1 a_2; b_1 b_2}$ is given as the solution of the BFKL-equation

$$(\omega - \beta(\mathbf{l}_1^2) - \beta(\mathbf{l}_2^2)) G_{\text{BFKL}}^{a_1 a_2; b_1 b_2}(\mathbf{l}_1, \mathbf{l}_2; \mathbf{k}_1, \mathbf{k}_2) = \delta^{a_1 b_1} \delta^{a_2 b_2} (2\pi)^3 \delta^{(2)}(\mathbf{l} - \mathbf{k}) + \left(\mathcal{K}_{2 \rightarrow 2}^{\{c\} \rightarrow \{b\}} \otimes G_{\text{BFKL}}^{c_1 c_2; b_1 b_2} \right)(\mathbf{l}_1, \mathbf{l}_2; \mathbf{k}_1, \mathbf{k}_2). \quad (3.81)$$

As can be easily verified, $\mathcal{M}_{2 \rightarrow 2}^{\text{LLA}|2\text{R}}$ is invariant under substitutions $p_A, p_B \rightarrow -p_A, -p_B$ and has therefore positive signature, as expected. Furthermore, with

$$e^{-i\pi\omega} + 1 = 2i \frac{e^{-i\pi\omega} - 1}{\sin \pi\omega} \cos^2(\omega\pi/2), \quad (3.82)$$

and using that $\cos^2(\omega\pi/2) \rightarrow 1$ for the LLA the amplitude can brought into the form, usually stated for the Sommerfeld-Watson representation, of an amplitude with positive signature:

$$\mathcal{M}_{2 \rightarrow 2}^{\text{LLA}(+)} = -2\pi \int \frac{d\omega}{2\pi i} |s|^{1+\omega} \frac{\xi^{(+)}(\omega)}{\sin \pi\omega} \phi(\omega, t) \quad \xi^{(+)}(\omega) = e^{-i\pi\omega} - 1 \quad (3.83)$$

with $\xi^{(+)}$ the signature factor for positive signature exchange. The negative signature part of the quark-quark scattering amplitude is completely contained in the reggeized gluon: Decomposing the quark-impact factor $A_{(2;0)}^{a_1 a_2}$ into a color singlet part $A_{(2;0)}^{(\mathbf{1})}$ and a color octet part $A_{(2;0)}^{(\mathbf{8})}$ and convoluting them with the BFKL-Green's function, one obtains in the octet-case from the BFKL-equation a pole-solution, which inserted into Eq. (3.83) exhibits the reggeized gluon. Within the effective action the antisymmetric octet $\mathbf{8}_A$ state of two reggeized gluons decouples from the quark, while the antisymmetric resummed reggeized gluon arises due to resummation of corrections to the bare reggeized gluon, as illustrated in Sec.3.1. It is in the effective theory a elementary degree of freedom. In particular its derivation does not make use of the bootstrap relations [7–10], [89, 90]. The state of two reggeized gluons in the symmetric octet $\mathbf{8}_S$ on the other hand couples to the quark and correspondingly there exists a pole solution to the BFKL-equation, the so-called 'd'-Reggeon. Unlike the antisymmetric 'f'-Reggeon, it is not a fundamental degree of freedom in the effective theory, but arises as a state of two reggeized gluons.

3.3 Conclusion

In the present chapter, the elastic scattering amplitude has been studied from the point of view of the effective action and rules for the occurring longitudinal integrations have been given. In short, interaction between two particles is only described by a reggeized gluon if the center-of-mass energy of the minimal elastic (sub-)amplitude that can be associated with its exchange is larger than a certain lower bound; otherwise the interaction is mediated by a usual QCD-gluon. The propagator of the reggeized gluon depends therefore not only on the momenta of the reggeized gluon (as usual), but furthermore also on the momenta of the particle it couples to. In order to incorporate that lower bound, it turned out that the Mellin-integral Eq. (3.9) provides a suitable regularization method. It has the nice properties that it both allows to include negative signature of the reggeized gluon and higher order loop correction in an easy and straight-forward way. In particular, imposing this bound turned out to be sufficient to keep the interactions of QCD-particles in the effective action local in rapidity. Using this rules, we showed within the LLA that the leading part of the elastic amplitude is within the effective action completely summarized in the exchange of a single (resummed) reggeized gluon with negative signature. Due to the introduced cut-off, the reggeized gluon carries a dependence on an arbitrary mass-scale. Within the LLA, this mass-scale can be chosen to be of the size of the typical transverse scale and this dependence is not of interest. Beyond the LLA however, it is essential that this scale cancels for physical amplitudes. It was demonstrated that such a cancellation can be achieved for the elastic amplitude by taking into account quasi-elastic corrections to the quark-reggeized gluon couplings, which are formally beyond the LLA.

For the part of the elastic amplitude with positive signature, on the other hand, interaction between the scattering quarks is mediated by the state of two reggeized gluon and interaction between the two reggeized gluons is resummed by the famous BFKL-equation. For the longitudinal integrals occurring due to loops containing reggeized gluons, two points are worth to be noted:

At first, integrals over longitudinal components show generally a logarithmic divergence which at first does not allow for an evaluation of the integrals. The occurrence of this divergence can be traced back to a part in these integrals which is already contained in the induced vertices. This part therefore needs to be subtracted in order to avoid to count this contribution twice. This subtraction term can be obtained from graphs which contain induced vertices to which *only* reggeized gluons couple.

For loop-corrections to the exchange of reggeized gluons one further has to take into account the following: Defining for every single reggeized gluon a 4-point-sub-amplitude inside the complete amplitude, presence of the reggeized gluon requires that the center-of-mass energy of the sub-amplitude is significantly larger than all other scales. To implement this lower bound we used again the Mellin-integral. It allows to include signature of the reggeized gluon and to include corrections due to reggeization of the gluon. In particular the position of the resulting branch-cut is determined by the signature factor of the reggeized gluon. For loop integrations as in the above it is convenient to combine the two signature factors into a single one, making use of Eq.(3.66). If additional poles in light-cone momenta occur, either from induced vertices or due to a subtraction by a subtraction-diagram, it turns out to be mandatory that the $i\epsilon$ prescription of the branch-cut coincides with the one of the poles.

Chapter 4

Loop corrections to production processes from the effective action

In the foregoing chapter, from the study of the elastic amplitude within the LLA, a set of rules has been derived, that can be used to determine the interaction of reggeized gluons within the effective action. A non-trivial testing-ground for these rules is given by loop-corrections to production amplitudes in the Multi-Regge-Kinematics. As for the elastic amplitudes, loop corrections lead within the LLA to logarithms in the various center-of-mass-energies of the initial and final state particles. These logarithms yield in the physical region discontinuities, which can be associated with production thresholds of produced particles. There exists a non-trivial constraint on the occurrence of these discontinuities, the Steinmann-relations [72]. The proposed regularization by the Mellin-integral on the other hand introduces automatically discontinuities and it is a priori not clear, to which extend this is in accordance with the Steinmann-relations or not.

The outline of this chapter is the following: In Sec. 4.1 we explain the constraints due to the Steinmann-relations and introduce the analytic representations of the $2 \rightarrow 3$ and $2 \rightarrow 4$ amplitude. In Sec. 4.2 we discuss corrections to the production amplitude with negative signature in all t -channels, while in the Sec. 4.3 the various production amplitudes with positive and mixed signature are presented.

4.1 Analytical representation of production amplitudes

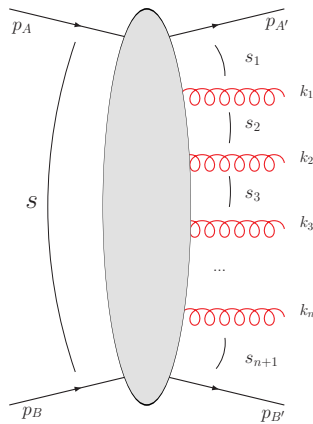


Figure 4.1: The Multi-Regge-Kinematics of the $n + 2$ -particle production amplitude.

In the following section we give a summary of the analytical representations of the $2 \rightarrow 3$ and the

$2 \rightarrow 4$ production amplitude in the high energy limit, which generalizes the representation of the elastic amplitude. In general, we consider in the following the n -particle production amplitude in the Multi-Regge-Kinematics (see also Fig.4.1) which is defined as

$$s, s_r \rightarrow \infty, \quad s_r/s \rightarrow 0, \quad (4.1)$$

$$t_r, \kappa_r = k_r^+ k_r^- = \mathbf{k}_r^2 = \text{fixed}, \quad (4.2)$$

with

$$\begin{aligned} s &= (p_A + p_B)^2, & s_r &= (k_r + k_{r-1})^2, \\ k_r &= q_r - q_{r-1}. & t_r &= q_r^2. \end{aligned} \quad (4.3)$$

A key element in the study of production amplitudes are the Steinmann-relations [72] which forbid the existence of simultaneous energy discontinuities in overlapping channels. As an example, we

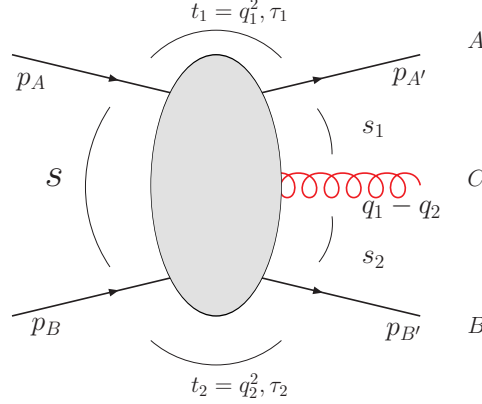


Figure 4.2: The $2 \rightarrow 3$ production amplitude

consider the $2 \rightarrow 3$ production amplitude in Fig. 4.2: The produced particle C can either build a resonance or bound state with the particle A' or the particle B' , but never with both of them. In more technical terms this means, that in the physical region, the production amplitude can either have a discontinuity in s_1 - corresponding to a bound state of particles A' and C - or in s_2 , which corresponds to a bound state of particles C and B' , but never in both of them at a time. On the other hand the particles A' , B' and C can form a single resonance state, which corresponds to the discontinuity in s . The discontinuity structure of the $2 \rightarrow 3$ amplitude in the high energy limit is further illustrated in Fig. 4.3. In the double-Regge-kinematics an analytic representation can be

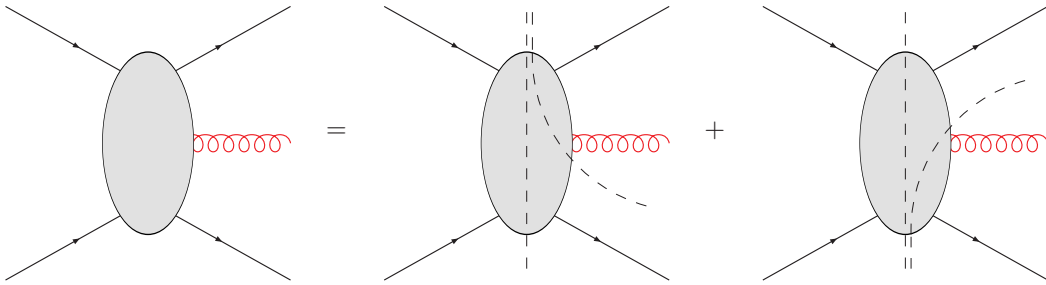


Figure 4.3: Analytic structure of the $2 \rightarrow 3$ production amplitude. It is given as a sum of two terms which have either allow for cuts in s and s_1 or in s and s_2

formulated, which respects the Steinmann-rules. In the case of the elastic scattering amplitude, such a representation is given by

$$\mathcal{M}_{2 \rightarrow 2}^{(\tau)} = s \int \frac{d\omega}{2\pi i} |s|^\omega \xi^{(\tau)}(\omega) \frac{F(\omega; t)}{\sin(\pi\omega)}, \quad (4.4)$$

with

$$\xi^{(\tau)}(\omega) = e^{-i\pi\omega} - \tau, \quad \tau = \pm 1, \quad (4.5)$$

with τ the signature of the amplitude. As there is just one direct channel, the Steinmann relations provide no further constraint on the discontinuities in s . For $2 \rightarrow 3$ production amplitude, an analogous analytic representation is given as the sum of two terms, which allow either for a discontinuity in s and s_1 or in s and s_2 ,

$$\begin{aligned} \mathcal{M}_{2 \rightarrow 3} = s \int \frac{d\omega_1}{2\pi i} \int \frac{d\omega_2}{2\pi i} \left(|s|^{\omega_2} |s_1|^{\omega_1 - \omega_2} \xi_{(\omega_2)}^{(\tau_2)} \xi_{(\omega_1, \omega_2)}^{(\tau_1, \tau_2)} \frac{V_1(\omega_1, \omega_2; t_1, t_2, \kappa_1)}{\sin \pi \omega_{12}} \right. \\ \left. + |s|^{\omega_1} |s_2|^{\omega_2 - \omega_1} \xi_{(\omega_1)}^{(\tau_1)} \xi_{(\omega_2, \omega_1)}^{(\tau_2, \tau_1)} \frac{V_2(\omega_1, \omega_2; t_1, t_2, \kappa_1)}{\sin \pi \omega_{21}} \right), \end{aligned} \quad (4.6)$$

where we defined

$$\omega_{ij} = \omega_i - \omega_j, \quad (4.7)$$

and $\tau_{1,2} = \pm 1$ is the signature of the t_1 and t_2 -channel respectively. Furthermore a generalized signature factor is defined as

$$\xi_{(\omega_1, \omega_2)}^{(\tau_1, \tau_2)} = e^{-i\pi(\omega_1 - \omega_2)} + \tau_1 \tau_2 \quad (4.8)$$

while the partial waves V_1 and V_2 are real. Representations like Eq. (4.6) have been first derived from models which contain only Regge-poles like massive ϕ^3 -theory [91, 92], the dual Veneziano 6-point amplitude [93] and from generalized Froissart-Gribov partial wave representations [94]. As for the elastic amplitude, the above representation can be used to determine the $2 \rightarrow 3$ production amplitude within the LLA by taking discontinuities in s , s_1 and/or s_2 . This allows for the determination of V_1 and V_2 from on-shell, tree-level production amplitudes, making use of unitarity in all sub-channels. Such a program has been carried out in [89] and [33] and also recently in [83], where the analytical properties of Bern-Dixon-Smirnov (BDS)-amplitudes [95] in the high-energy limit have been examined.

In the case of the $2 \rightarrow 4$ amplitude, the analytic representation in the triple-Regge-limit requires already five terms. It is given by

$$\begin{aligned} \mathcal{M}_{2 \rightarrow 4} = s \int \frac{d\omega_1}{2\pi i} \int \frac{d\omega_2}{2\pi i} \int \frac{d\omega_3}{2\pi i} \\ \left(|s_1|^{\omega_1 - \omega_2} |s_{012}|^{\omega_2 - \omega_3} |s|^{\omega_3} \xi_{(\omega_1, \omega_2)}^{(\tau_1, \tau_2)} \xi_{(\omega_2, \omega_3)}^{(\tau_2, \tau_3)} \xi_{(\omega_3)}^{(\tau_3)} \frac{W_1(\omega_1, \omega_2, \omega_3; t_1, t_2, t_3, \kappa_1, \kappa_2)}{\sin \pi \omega_{12} \sin \pi \omega_{23}} \right. \\ + |s_3|^{\omega_3 - \omega_2} |s_{123}|^{\omega_2 - \omega_1} |s|^{\omega_1} \xi_{(\omega_3, \omega_2)}^{(\tau_3, \tau_2)} \xi_{(\omega_2, \omega_1)}^{(\tau_2, \tau_1)} \xi_{(\omega_1)}^{(\tau_1)} \frac{W_2(\omega_1, \omega_2, \omega_3; t_1, t_2, t_3, \kappa_1, \kappa_2)}{\sin \pi \omega_{32} \sin \pi \omega_{21}} \\ + |s_2|^{\omega_2 - \omega_1} |s_{012}|^{\omega_1 - \omega_3} |s|^{\omega_3} \xi_{(\omega_2, \omega_1)}^{(\tau_2, \tau_1)} \xi_{(\omega_1, \omega_3)}^{(\tau_1, \tau_3)} \xi_{(\omega_3)}^{(\tau_3)} \frac{W_3(\omega_1, \omega_2, \omega_3; t_1, t_2, t_3, \kappa_1, \kappa_2, \kappa_{123})}{\sin \pi \omega_{21} \sin \pi \omega_{13}} \\ + |s_2|^{\omega_2 - \omega_3} |s_{123}|^{\omega_3 - \omega_1} |s|^{\omega_1} \xi_{(\omega_2, \omega_3)}^{(\tau_2, \tau_3)} \xi_{(\omega_3, \omega_1)}^{(\tau_3, \tau_1)} \xi_{(\omega_1)}^{(\tau_1)} \frac{W_4(\omega_1, \omega_2, \omega_3; t_1, t_2, t_3, \kappa_1, \kappa_2, \kappa_{123})}{\sin \pi \omega_{23} \sin \pi \omega_{31}} \\ \left. + |s_3|^{\omega_3 - \omega_2} |s_1|^{\omega_1 - \omega_2} |s|^{\omega_2} \xi_{(\omega_3, \omega_2)}^{(\tau_3, \tau_2)} \xi_{(\omega_1, \omega_2)}^{(\tau_1, \tau_2)} \xi_{(\omega_2)}^{(\tau_2)} \frac{W_5(\omega_1, \omega_2, \omega_3; t_1, t_2, t_3, \kappa_1, \kappa_2)}{\sin \pi \omega_{32} \sin \pi \omega_{12}} \right). \end{aligned} \quad (4.9)$$

where we defined

$$\begin{aligned} s_{012} &= (p_A + k_2)^2 = -p_A^+ q_3^- & s_{123} &= (p_B + k_1)^2 = p_B^- q_1^+ \\ \kappa_{123} &= (\mathbf{k}_1 + \mathbf{k}_2)^2 = (\mathbf{q}_1 - \mathbf{q}_3)^2 \end{aligned} \quad (4.10)$$

Taking discontinuities in s_1 , s_2 , s_3 , s_{012} and s_{123} , the partial waves W_i can be determined from unitarity as outlined in [33, 83, 89]. In the following we attempt a derivation of the LLA $2 \rightarrow 3$ and $2 \rightarrow 4$ production amplitude from the effective action. Particular focus will be given on the analytic structure of the results and too which extend the Steinmann-relations can be regarded to be fulfilled, if logarithms are resummed within the effective action, employing the LLA.

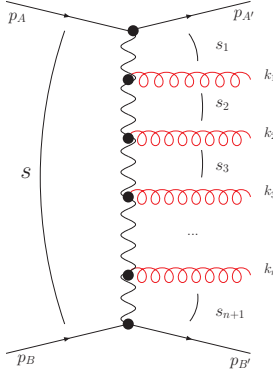


Figure 4.4: Production amplitude in the MRK to leading order. All t -channel exchanges are reggeized and contain the maximal number of possible logarithms

4.2 The production amplitude with negative signature in all t -channels

We start with the case where the signature in all t -channels is negative. From the discussion in the previous chapter and from general reasoning we know, that this includes the part that is leading in the Leading Logarithmic Approximation.

4.2.1 The production amplitude at Leading Logarithmic Accuracy

With the produced particles in the Multi-Regge-Kinematics separated by a large difference in rapidity, it is immediately clear that the interaction between s -channel produced particles is mediated by reggeized gluons alone, while the leading contribution is given by the exchange of a single reggeized gluon with negative signature. Production of the real particles is on the other hand described by the production vertex, which has been introduced already in the context of the BFKL-equation in Eq.(3.55):

$$\begin{array}{c} \text{wavy line} \\ \bullet \\ \text{wavy line} \end{array} \text{---} \text{red curly line} = 2igT_{ba}^c C_\mu(q_1, q_2), \quad (4.11)$$

with

$$C_\mu(q_1, q_2) = \left(\frac{q_1^+}{2} + \frac{q_1^-}{q_2^-} \right) (n^-)^\mu + \left(\frac{q_2^-}{2} + \frac{q_2^+}{q_1^+} \right) (n^-)^\mu - (q_1 + q_2)_\perp^\mu, \quad (4.12)$$

where we take q_1 incoming and q_2 outgoing from the vertex. We note here, that if contracted with a physical polarization vector, the production amplitude can be shown to depend only on transverse momenta, and the dependence on q_1^+ and q_2^- can be eliminated. The production amplitude in the Multi-Regge-Kinematics, Fig.4.1 is therefore at Leading-Logarithmic-Accuracy given by diagrams like Fig.4.4. Using our result from Sec.3.1, we would at first insert in Fig.4.4 for every reggeized gluon that connects two s -channel gluons with momentum k_{r-1} and momentum k_r , the following expression:

$$\frac{i/2}{\mathbf{q}_r^2} \int \frac{d\omega_r}{2\pi i} \frac{1}{\omega_r - \beta(\mathbf{q}_r^2)} \frac{1}{2} \left[\left(\frac{-s_r}{(\kappa_{r1}\kappa_r)^{1/2}} \right)^{\omega_r} + \left(\frac{s_r}{(\kappa_{r1}\kappa_r)^{1/2}} \right)^{\omega_r} \right] \quad (4.13)$$

The above expression however has a non-zero discontinuity in s_r . Correspondingly, Fig. 4.4 has for every squared sub-energy s_r , $r = 1, \dots, n$ a non-zero discontinuity in contradiction to the Steinmann-relations which forbid simultaneous singularities in over-lapping channels. At first it seems that the effective action is in conflict with the Steinmann-relations. This problem can only be

solved if the complete all order production vertex has an internal phase structure, which balances the phase structure of the reggeized gluon. Within the LLA only the leading part of the complete production vertex is taken into account, which is completely real. We therefore conclude that as long we take into account only the leading part of the production vertex, we should simultaneously only include the most leading, real part of Eq.(4.13). This requires to suppress for the production amplitude at LLA the imaginary parts of the reggeized gluons, which is of the same order as higher order correction to the production vertex. As a consequence, within the LLA, we should in Fig.4.4 insert instead of Eq.(4.13)

$$\frac{i/2}{\mathbf{q}_r^2} \int \frac{d\omega_r}{2\pi i} \frac{1}{\omega_r - \beta(\mathbf{q}_r)} \left| \frac{s_r}{(\kappa_{r1}\kappa_r)^{1/2}} \right|^{\omega_r}, \quad (4.14)$$

which means to take into account for every single reggeized gluon only the leading real part.

4.2.2 The Reggeon-Reggeon-particle vertex at 1-loop

In this paragraph we attempt to determine the one-loop corrections to the production vertex and verify, whether it shows the on-set of corrections needed for the complete production amplitude to satisfy the Steinmann-relations.

From a technical point of view, the 1-loop-correction to the production vertex shares many features with the 1-loop correction to the quark-reggeized gluon coupling of Sec.3.1.3. As there, the 1-loop correction to the production-vertex belongs formally to the NLLA, while all large logarithms in s_1 and s_2 are already resummed by central-rapidity diagrams of the adjacent reggeized gluons. Furthermore, in analogy to Sec.3.1.3, we are in the following only interested in a certain part of the complete 1-loop corrections. Whereas in Sec.3.1.3 we mainly focused on the cancellation of the factorization parameter that separates the central-rapidity diagrams from the quasi-elastic diagrams, we are in the following especially interested in the part that carries the internal phase structure of the vertex.

It turns out that this phase structure is particularly connected with a certain set of diagrams, to which we will restrict in the following. In particular, presence of the non-trivial phase structure is immediately connected to the presence of discontinuities of the complete production amplitude: In the physical region of the different s -channels (for the $2 \rightarrow 3$ amplitude these are s , s_1 and s_2), these discontinuities occur only in diagrams which can be 'cut' in the corresponding s -channel energy variables, which requires in the underlying QCD-diagram the presence of at least two t -channel gluons. In the effective theory those states are for negative signature gathered in induced vertices¹ and we therefore restrict in the following to diagrams that involve at least one induced vertex of the first or higher order.

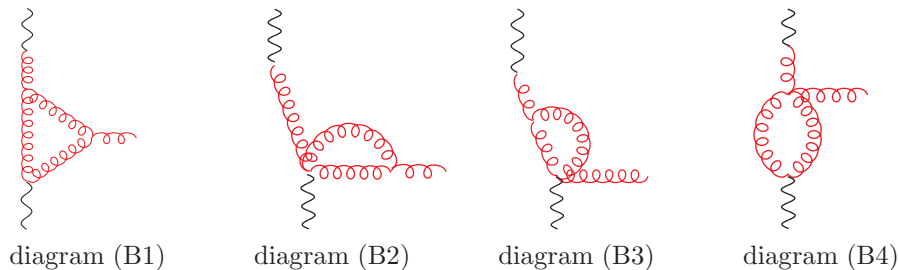


Figure 4.5: Feynman-diagrams contributing to the 1-loop corrections to the Reggeon-Reggeon-Particle vertex, which contain one induced vertex, occurring in the coupling to the lower reggeized gluon. The corresponding diagrams where the upper, minus reggeon couples by a induced vertex to the gluon loop, are not shown explicitly and can be obtained from the former ones by corresponding replacements

Relevant examples of diagrams are listed in Fig.4.5 and Fig.4.6. In all these diagrams, a reggeized gluon couples from above and below to a gluon-loop. In the following we concentrate on the $2 \rightarrow 3$

¹This is certainly true at this level of accuracy. We however note that also the exchange of three, five, etc reggeized gluons turns out to carry negative signature, which however constitutes in this case a higher order effect.

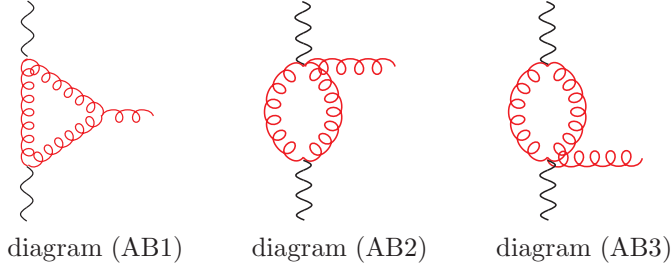


Figure 4.6: Feynman-diagrams contributing to the 1-loop corrections to the Reggeon-Reggeon-Particle vertex where the reggeized gluons couple from below and from above by induced vertices to the gluon loop.

production amplitude. The corrections obtained for the production vertex can similarly be used for amplitudes with more produced particles, like the $2 \rightarrow 4$ production amplitude, and we will return to this particular case at the end of this paragraph.

As in Sec. 3.1.3, loop-corrections to Particle-Reggeon vertices require to impose certain restrictions on the center-of-mass energy of the quark-gluon sub-amplitude. In order to do so, we factorize the production amplitude, similar to the treatment of the quasi-elastic corrections in Sec. 3.1.3, in the following way:

$$\begin{aligned}
i\mathcal{M}_{2 \rightarrow 3} = & s \int \frac{d\omega_1}{2\pi i} \int \frac{d\omega_2}{2\pi i} \tilde{\Gamma}_{QQR}^a(\omega_1; q_1; \lambda_{11}) \times \frac{i/2}{\mathbf{q}_1^2} \frac{1}{\omega_1 - \beta(\mathbf{q}_1^2)} \left| \frac{s_1}{s_{R_1} \lambda_{11} \lambda_{12}} \right|^{\omega_1} \\
& \times \Gamma_{RRG}^{acb, \mu}(\omega_1, \omega_2; q_1, q_2; \lambda_{12}, \lambda_{21}) \times \frac{i/2}{\mathbf{q}_2^2} \frac{1}{\omega_2 - \beta(\mathbf{q}_2^2)} \left| \frac{s_2}{s_{R_2} \lambda_{21} \lambda_{22}} \right|^{\omega_2} \times \tilde{\Gamma}_{QQR}^b(\omega_2; q_2; \lambda_{22}). \quad (4.15)
\end{aligned}$$

s_{R_1} and s_{R_2} are the regarding transverse scales of the reggeized gluons, which can be set to be $s_{R_1} = m_A \kappa_1^{1/2}$ and $s_{R_2} = m_B \kappa_1^{1/2}$ in accordance with our previous conventions. The precise choice does indeed not matter here and we only require a certain fixed scale, of the order of the transverse scales of the process. λ_{ij} $i, j = 1, 2$ are factorization parameters of the reggeized gluon and of the particle-reggeized gluon vertices respectively.

From Sec. 3.1.3 we have the following expression for the sum of Born and one-loop contributions of the quark-reggeized gluon vertex (while as far one-loop corrections are concerned, only the leading logarithmic part of diagrams like Fig. 3.9 is included)

$$\Gamma_{QQR}^a(\omega_1; q_1; \lambda_{11}) = \Gamma_{QQR}^a(q_1) \left(\frac{\omega_1 - \beta(\mathbf{q}_1^2)}{\omega_1} + \frac{\beta(\mathbf{q}_1^2)}{\omega_1} \left[(-\lambda_{11})^{\omega_1} + (\lambda_{11})^{\omega_1} \right] \right), \quad (4.16)$$

where the first term leads to a vanishing expression, once inserted into the final result. For the diagrams like Fig. 4.5 and Fig. 4.6 that yield the one-loop correction to the production vertex we make an ansatz in analogy to Eq. (3.32) of Sec. 3.1.3: The situation is most straight forward for diagrams which involve only couplings of a reggeized gluon to two QCD-gluons, like diagram B1 in Fig. 4.5. In that case we start with the following expression

$$\begin{aligned}
\Gamma_{B1}^{acb, \mu}(\omega_1, \omega_2; q_1, q_2; \lambda_{12}, \lambda_{21}) = & \int \frac{d^4 k}{(2\pi)^4} \bar{\gamma}_{3G, \nu_1 - \nu_2}^{e_1 a e_2}(\omega_1; -k, q_1, k - q_1) \frac{-i}{(q_1 - k)^2} \\
& \gamma_{3G, \nu_1 \mu \nu_2}^{e_2 b e_3}(q_1 - k, q_2 - q_1, k - q_2) \frac{-i}{(q_2 - k)^2} \bar{\Delta}_{+, \nu_1 \nu_2}^{e_1 a e_2}(\omega_2; q_2 - k, -q_2, k) \frac{-i}{k^2}, \quad (4.17)
\end{aligned}$$

where γ_{3G} is the usual three-gluon-vertex, while the three-gluon-vertex $\bar{\gamma}_{3G}(\omega_1)$ and the induced vertex $\bar{\Delta}_+(\omega_2)$ are modified due to their coupling to the reggeized gluons. They require negative signature and a lower bound in their corresponding squared center-of-mass energy. For the modified three-gluon-vertex, the sub-amplitude that belongs to the reggeized gluon is depicted in Fig. 4.7a, which has a center-of-mass energy $p_A^+ k^-$. As for the quasi-elastic region in Sec. 3.1.3 we impose for vertex corrections the lower bound $p_A^+ k^- > s_1/\lambda_{12}$, which we implement as usual by the Mellin-

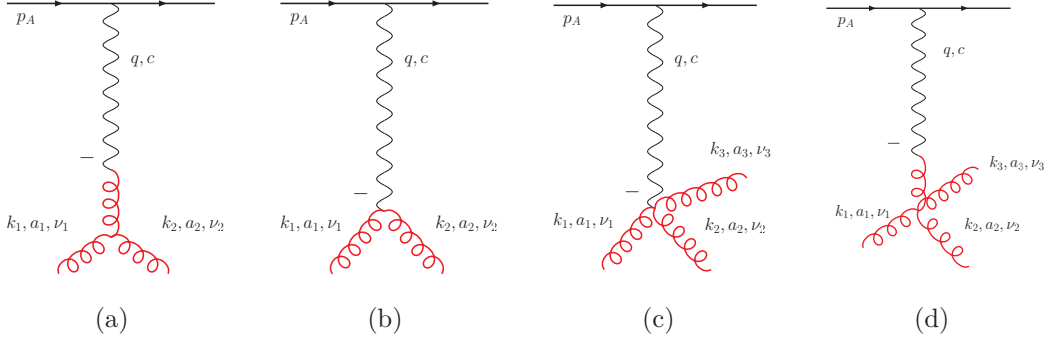


Figure 4.7: Quark-gluon sub-amplitudes of the various couplings of reggeized gluons to the gluon loop in Fig.4.5 and Fig.4.6.

integral:

$$\bar{\gamma}_{3G, \nu_1 - \nu_2}^{e_1 a e_2}(\omega_1; -k, q_1, k - q_1) = \int \frac{d\omega'_1}{4\pi i} \frac{1}{\omega'_1 - \omega_1} \left[\left(\frac{-p_A^+ k^- - i\epsilon}{s_1/\lambda_{12}} \right)^{\omega'_1} + \left(\frac{p_A^+ k^- - i\epsilon}{s_1/\lambda_{12}} \right)^{\omega'_1} \right] \gamma_{3G, \nu_1 - \nu_2}^{e_1 a e_2}(-k, q_1, k - q_1) \quad (4.18)$$

Similarly one has the following expression for the induced vertex of the first order, Fig. 4.7b

$$\bar{\Delta}_{+, \nu_1 \nu_2}^{e_1 a e_2}(\omega_1; -k, q_1, k - q_1) = \int \frac{d\omega'_1}{4\pi i} \frac{1}{\omega'_1 - \omega_1} \left[\left(\frac{-p_A^+ k^- - i\epsilon}{s_1/\lambda_{12}} \right)^{\omega'_1} + \left(\frac{p_A^+ k^- - i\epsilon}{s_1/\lambda_{12}} \right)^{\omega'_1} \right] g \mathbf{q}_1^2 f^{e_1 a e_2} \frac{1}{-k^-} n_{\nu_1}^- n_{\nu_2}^-, \quad (4.19)$$

where the $i\epsilon$ -prescription of the pole in k^- has to coincide as usually with the $i\epsilon$ -prescription of the branch-cuts due to the Mellin-integral. For the sub-amplitudes Fig. 4.7c and Fig. 4.7d which contain more than three gluons on their lower end, the definition of the center-of-mass energy on which the lower bound is to be imposed is less apparent: Choosing at random one of the three external gluon momenta to define the center-of-mass energy of the reggeized gluon, breaks Bose-symmetry of both the induced vertex of the second order and the four-gluon-vertex. While the momentum of the produced gluon is special, as it is fixed already by the Multi-/Double-Regge-Kinematics and as it only indirectly contributes to the loop integral, keeping such a symmetry is particularly desirable for the two gluons that enter the gluon-loop. For the induced vertex of the second order, the right choice can be deduced from the pole-structure, which can be always stated in a form, that it contains only one pole, with the loop-momentum k^- : With the unregularized vertex given by

$$\Delta_{\mu\nu_1\nu_2}^{ce_1e_2a} = -i\mathbf{q}_1^2 \left[\frac{f^{ce_1e} f_{e_2ea}}{q_2^-(-k^-)} + \frac{f^{ce_1e} f_{e_2ea}}{q_2^-(k^- - q_2^-)} \right] n_{\mu}^- n_{\nu_1}^- n_{\nu_2}^-, \quad (4.20)$$

we shall use in the following

$$\bar{\Delta}_{-, \nu_1 \nu_2 \mu}^{e_1 a e_2}(\omega_1) = \frac{-i\mathbf{q}_1^2}{q_2^-} n_{\mu}^- \int \frac{d\omega'_1}{4\pi i} \frac{1}{\omega'_1 - \omega_1} \left[\frac{f^{ce_1e} f_{e_2ea}}{(-k^-)} \left(\left(\frac{-p_A^+ k^- - i\epsilon}{s_1/\lambda_{12}} \right)^{\omega'_1} + \left(\frac{p_A^+ k^- - i\epsilon}{s_1/\lambda_{12}} \right)^{\omega'_1} \right) + \frac{f^{ce_1e} f_{e_2ea}}{(k^- - q_2^-)} \left(\left(\frac{-p_A^+(k^- - q_2^-) - i\epsilon}{s_1/\lambda_{12}} \right)^{\omega'_1} + \left(\frac{p_A^+(k^- - q_2^-) - i\epsilon}{s_1/\lambda_{12}} \right)^{\omega'_1} \right) \right] n_{\nu_1}^- n_{\nu_2}^-, \quad (4.21)$$

for our calculations. We note here, that in general it is non-trivial that the $i\epsilon$ prescription of the pole due to the second induced vertex coincides with the $i\epsilon$ prescription of the pole of the first

induced vertex. We will address the $i\epsilon$ -prescription of the higher induced vertices in Sec. 5.1 and anticipating the result obtained there, it can be confirmed that this is indeed true, if one of the three gluons that couple to the induced vertex is real.

For the reggeized gluon coupling to the four-gluon-vertex, Fig. 4.7d, we propose a similar modification. As for the induced vertex of the second order, we propose for every occurring color structure a different regularization, such that the complete vertex has the desired symmetry. With the (unmodified) four-gluon vertex in Fig. 4.7d given by

$$\begin{aligned} \gamma_{4G,-\mu\nu_1\nu_2}^{ace_1e_2} = & -ig^2 [f^{ace} f^{e_1e_2e} (n_{\nu_1}^- g_{\mu\nu_2} - n_{\nu_2}^- g_{\mu\nu_1}) + f^{ae_1e} f^{ce_2e} (n_{\nu_2}^- g_{\mu\nu_1} - n_{\mu}^- g_{\nu_1\nu_2}) \\ & + f^{ae_2e} f^{ce_1e} (n_{\nu_1}^- g_{\mu\nu_2} - n_{\mu}^- g_{\nu_1\nu_2})], \end{aligned} \quad (4.22)$$

we use the following modified version in our calculations

$$\begin{aligned} \tilde{\gamma}_{4G,-\mu\nu_1\nu_2}^{ace_1e_2}(\omega_1) = & -ig^2 \int \frac{d\omega'_1}{2\pi i} \frac{1}{\omega'_1 - \omega_1} \\ & \left[f^{ace} f^{e_1e_2e} (n_{\nu_1}^- g_{\mu\nu_2} - n_{\nu_2}^- g_{\mu\nu_1}) \left(\left(\frac{-p_A^+ q_2^- - i\epsilon}{s_1/\lambda_{12}} \right)^{\omega'_1} + \left(\frac{p_A^+ q_2^- - i\epsilon}{s_1/\lambda_{12}} \right)^{\omega'_1} \right) \right. \\ & + f^{ae_1e} f^{ce_2e} (n_{\nu_2}^- g_{\mu\nu_1} - n_{\mu}^- g_{\nu_1\nu_2}) \left(\left(\frac{-p_A^+ k_1^- - i\epsilon}{s_1/\lambda_{12}} \right)^{\omega'_1} + \left(\frac{p_A^+ k_1^- - i\epsilon}{s_1/\lambda_{12}} \right)^{\omega'_1} \right) \\ & \left. + f^{ae_2e} f^{ce_1e} (n_{\nu_1}^- g_{\mu\nu_2} - n_{\mu}^- g_{\nu_1\nu_2}) \left(\left(\frac{-p_A^+ k_2^- - i\epsilon}{s_1/\lambda_{12}} \right)^{\omega'_1} + \left(\frac{p_A^+ k_2^- - i\epsilon}{s_1/\lambda_{12}} \right)^{\omega'_1} \right) \right], \end{aligned} \quad (4.23)$$

with $k_1 = k$ and $k_2 = q_2 - k$. The above expression is symmetric under simultaneous exchange of momenta, polarization and color of the three gluons as needed. In the evaluation of the longitudinal integrations we then restrict to the leading logarithmic part of the integrals, similar to Sec. 3.1.3. We note that in principle also the sub-leading part can show some sort of divergence, which however only occurs if the different transverse momenta are not of the same order of magnitude. Those kind of divergences is thus related to transverse logarithms which are not taken into account within the LLA.

For the evaluation of the leading part, knowledge of two integrals I_1 and I_2 is sufficient. Integral I_1 can be found in slightly different form already in the analysis of massive ϕ^3 -theory of [91]. It is given by

$$\begin{aligned} I_1 = & \frac{1}{2} \int \frac{dk^+ k^-}{2\pi} \int \frac{d^2\mathbf{k}}{(2\pi)^3} \frac{-i}{k^2 + i\epsilon} \frac{-i}{(q_1 - k)^2 + i\epsilon} \frac{-i}{(q_2 - k)^2 + i\epsilon} \frac{1}{k^+ k^-} \\ & \left[\left(\frac{-p_A^+ k^- - i\epsilon}{s_1/\lambda_{12}} \right)^{\omega'_1} + \left(\frac{p_A^+ k^- - i\epsilon}{s_1/\lambda_{12}} \right)^{\omega'_1} \right] \left[\left(\frac{-p_B^- k^+ - i\epsilon}{s_2/\lambda_{21}} \right)^{\omega'_2} + \left(\frac{p_B^- k^+ - i\epsilon}{s_2/\lambda_{21}} \right)^{\omega'_2} \right] \\ = & \lambda_{12}^{\omega'_1} \lambda_{21}^{\omega'_2} \left[\kappa_1^{-\omega_1} \xi_{\omega'_1}^{(-)} \xi_{\omega'_2 \omega'_1}^{(-,-)} \frac{F_1(\omega'_1, \omega'_2, t_1, t_2, \kappa_1)}{\sin \pi(\omega'_2 - \omega'_1)} + \kappa_1^{-\omega'_2} \xi_{\omega'_2}^{(-)} \xi_{\omega'_1 \omega'_2}^{(-,-)} \frac{F_1(\omega'_2, \omega'_1, t_1, t_2, \kappa_1)}{\sin \pi(\omega'_1 - \omega'_2)} \right], \end{aligned} \quad (4.24)$$

with signature factors defined as in Eqs. (4.5) and (4.8) and

$$\begin{aligned} F_1(\omega'_1, \omega'_2, t_1, t_2, \kappa) = & \frac{-i\pi}{2} \int \frac{d^2\mathbf{k}}{(2\pi)^3} \int_0^\infty d\lambda \lambda^{2-\omega'_1} e^{-i\pi\omega'_1/2} \int \prod_{i=1}^3 dx_i \delta(1 - \sum_{i=1}^3 x_i) x_2^{\omega'_2 - \omega'_1} \\ & e^{-i\lambda(x_1 \mathbf{k}^2 + x_2(\mathbf{q}_1 - \mathbf{k})^2 + x_3(\mathbf{q}_2 - \mathbf{k})^2)} \frac{M(\omega'_2 | \omega'_2 - \omega'_1 + 1 | i\kappa_1 \lambda x_2 x_3)}{\Gamma(\omega'_2 - \omega'_1 + 1) \Gamma(1 - \omega'_2)}, \end{aligned} \quad (4.25)$$

where $M(a|b|z) = {}_1F_1(a|b|z)$ is a confluent hypergeometric function (Kummer's function [96]). The LLA corresponds to the limit $\omega'_1, \omega'_2 \rightarrow 0$ which can be taken safely as $M(a|b|z)/\Gamma(b)$ is an entire function of all its variables. We find

$$F_1(\omega'_1, \omega'_2, t_1, t_2, \kappa) = \frac{-\pi}{2} \int \frac{d^2\mathbf{k}}{(2\pi)^3} \frac{(\mathbf{k}^2)^{\omega'_1}}{\mathbf{k}^2 (\mathbf{q}_1 - \mathbf{k})^2 (\mathbf{q}_2 - \mathbf{k})^2}, \quad (4.26)$$

where $(\mathbf{k}^2)^{\omega_1}$ represents a typical transverse scale of the production amplitude such as \mathbf{q}_1^2 , \mathbf{q}_2^2 or κ_1 which is not specified in the LLA. The second integral is very similar to Eq. (B.31), but has a slightly simpler structure

$$\begin{aligned}
I_2 &= \frac{-i}{2} \int \frac{dk^+ k^-}{2\pi} \int \frac{d^2 \mathbf{k}}{(2\pi)^3} \frac{-i}{k^2 + i\epsilon} \frac{-i}{(q_2 - \mathbf{k})^2 + i\epsilon} \frac{1}{k^+ k^-} \\
&\quad \left[\left(\frac{-p_A^+ k^- - i\epsilon}{s_1/\lambda_{12}} \right)^{\omega_1'} + \left(\frac{p_A^+ k^- - i\epsilon}{s_1/\lambda_{12}} \right)^{\omega_1'} \right] \left[\left(\frac{-p_B^- k^+ - i\epsilon}{s_2/\lambda_{21}} \right)^{\omega_2'} + \left(\frac{p_B^- k^+ - i\epsilon}{s_2/\lambda_{21}} \right)^{\omega_2'} \right] \\
&= \lambda_{12}^{\omega_1'} \lambda_{21}^{\omega_2'} \kappa_1^{-\omega_2'} \xi_{\omega_2'}^{(-)} \xi_{\omega_1' \omega_2'}^{(-,-)} \frac{F_2(\omega_2', \omega_1', t_2, \kappa_1)}{\sin \pi(\omega_1' - \omega_2')} \Big|_{\Re \omega_2' > \Re \omega_1'} .
\end{aligned} \tag{4.27}$$

Note that the evaluation of I_2 requires the ω_2' -contour to be to the right of the ω_1' contour. F_2 is given by

$$\begin{aligned}
F_2(\omega_1', \omega_2', t_2, \kappa) &= \frac{-\pi}{2} \int \frac{d^2 \mathbf{k}}{(2\pi)^3} \int_0^\infty d\lambda \lambda^{1-\omega_1'} e^{-i\pi\omega_2'/2} \int \prod_{i=1}^2 dx_i \delta(1 - \sum_{i=1}^2 x_i) x_2^{\omega_1' - \omega_2'} \\
&\quad e^{-i\lambda(x_1 \mathbf{k}^2 + x_2 (\mathbf{q}_2 - \mathbf{k})^2)} \frac{1}{\Gamma(\omega_2' - \omega_1' + 1) \Gamma(1 - \omega_2')},
\end{aligned} \tag{4.28}$$

which reduces in the limit $\omega_1', \omega_2' \rightarrow 0$ to

$$F_2(\omega_1', \omega_2', t_1, t_2, \kappa) = \frac{\pi}{2} \int \frac{d^2 \mathbf{k}}{(2\pi)^3} \frac{(\mathbf{k}^2)^{\omega_1'}}{\mathbf{k}^2 (\mathbf{q}_2 - \mathbf{k})^2}. \tag{4.29}$$

We then write the production vertex as the sum of its Born and 1-loop corrections $\delta\Gamma_{RRG}^\mu$

$$\begin{aligned}
\Gamma_{RRG}^{acb, \mu}(\omega_1, \omega_2; q_1, q_2; \lambda_{12}, \lambda_{21}) &= 2gf^{acb} C^\mu(q_1, q_2) \frac{\xi^-(\omega_1)}{2} \frac{\xi^-(\omega_2)}{2} \\
&\quad + \delta\Gamma_{RRG}^{acb, \mu}(\omega_1, \omega_2; q_1, q_2; \lambda_{12}, \lambda_{21}),
\end{aligned} \tag{4.30}$$

where signature factors of the adjacent reggeized gluons are absorbed in the production vertex, in accordance with our decomposition Eq. (4.15). For the 1-loop corrections we find within our accuracy

$$\begin{aligned}
\delta\Gamma_{RRG}^{acb, \mu}(\omega_1, \omega_2; q_1, q_2; \lambda_{12}, \lambda_{21}) &= \int \frac{d\omega_1'}{4\pi i} \int \frac{d\omega_2'}{4\pi i} \frac{1}{\omega_1' - \omega_1} \frac{1}{\omega_2' - \omega_2} \lambda_{12}^{\omega_1'} \lambda_{21}^{\omega_2'} \\
&\quad \left[\kappa_1^{-\omega_2'} \xi_{\omega_2'}^{(-)} \xi_{\omega_1' \omega_2'}^{(-,-)} \frac{V_a(q_1, q_2)}{\omega_1' - \omega_2'} \Big|_{\Re \omega_1' > \Re \omega_2'} + \kappa_1^{-\omega_1'} \xi_{\omega_1'}^{(-)} \xi_{\omega_2' \omega_1'}^{(-,-)} \frac{V_a(q_2, q_1)}{\omega_2' - \omega_1'} \Big|_{\Re \omega_2' > \Re \omega_1'} \right. \\
&\quad \left. \left(\kappa_1^{-\omega_1'} \xi_{\omega_1'}^{(-)} \xi_{\omega_2' \omega_1'}^{(-,-)} \frac{1}{\omega_2' - \omega_1'} + \kappa_1^{-\omega_2'} \xi_{\omega_2'}^{(-)} \xi_{\omega_1' \omega_2'}^{(-,-)} \frac{1}{\omega_1' - \omega_2'} \right) V_b(q_1, q_2) \right],
\end{aligned} \tag{4.31}$$

where

$$V_a(q_1, q_2) = \beta(\mathbf{q}_1) 2gf^{acb} C^\mu(q_1, q_2) \tag{4.32}$$

$$V_b(q_1, q_2) = \frac{N_c g^2}{2} \int \frac{d^2 \mathbf{k}}{(2\pi)^3} \frac{\mathbf{q}_2^2 \mathbf{q}_1^2}{\mathbf{k}^2 (\mathbf{q}_1 - \mathbf{k})^2 (\mathbf{q}_2 - \mathbf{k})^2} 2gf^{acb} C^\mu(q_1 - \mathbf{k}, q_2 - \mathbf{k}) \tag{4.33}$$

and we approximated

$$\frac{\pi}{\sin \pi(\omega_1' - \omega_2')} \simeq \frac{1}{\omega_1' - \omega_2'},$$

in accordance with the LLA. Note that Eq. (4.31) resembles closely the analytic representation of the $2 \rightarrow 3$ production amplitude Eq. (4.38). However, whereas Eq. (4.38) represents the analytic structure of the $2 \rightarrow 3$ production *amplitude*, Eq.(4.31) constitutes merely the 1-loop correction to the production *vertex* (with the Born-term not yet included) and is only exact up to $\mathcal{O}(g^3)$.

Eq. (4.38) can only be obtained from the effective action, if corrections concerning the phase structure of the production vertex are resummed to all orders in perturbation theory. Nevertheless the strong coincidence in the structure of Eq. (4.38) and Eq.(4.31) is encouraging as it suggests that the effective action indeed yields the correct analytic structure of the production amplitude. Evaluating the integrals over ω'_1, ω'_2 in Eq.(4.31) and expanding in 'small' logarithms $\ln \lambda_{1,2}$ and $\ln \kappa_1$, we obtain

$$\begin{aligned} \delta\Gamma_{RRG}^{acb,\mu}(\omega_1, \omega_2; q_1, q_2; \lambda_{12}, \lambda_{21}) &= \frac{\xi^-(\omega_1)}{2} \frac{\xi^-(\omega_2)}{2} \left[\frac{\ln -\lambda_{12} + \ln \lambda_{12}}{2} V_a(q_1, q_2) \right. \\ &\quad \left. + \frac{\ln -\lambda_{21} + \ln \lambda_{21}}{2} V_a(q_2, q_1) + \frac{\ln -\kappa_1 + \ln \kappa_1}{2} V_b(q_2, q_1) \right], \end{aligned} \quad (4.34)$$

where we extracted the complete signature factors of the reggeized gluons that couple to the production vertex, whereas all other factors have been expanded up to $\mathcal{O}(\omega_i)$. Together with the Born term we obtain

$$\begin{aligned} \Gamma_{RRG}^{acb,\mu}(\omega_1, \omega_2; q_1, q_2; \lambda_{12}, \lambda_{21}) &= 2gf^{acb} \times \\ &\quad \frac{\xi^-(\omega_1)}{2} \frac{\xi^-(\omega_2)}{2} \left[\left(1 + \frac{\ln -\lambda_{12} + \ln \lambda_{12}}{2} \beta(\mathbf{q}_1) + \frac{\ln -\lambda_{21} + \ln \lambda_{21}}{2} \beta(\mathbf{q}_2) \right) C^\mu(q_1, q_2) \right. \\ &\quad \left. + \frac{\ln -\kappa_1 + \ln \kappa_1}{2} \frac{N_c g^2}{2} \int \frac{d^2 \mathbf{k}}{(2\pi)^3} \frac{\mathbf{q}_2^2 \mathbf{q}_1^2}{\mathbf{k}^2 (\mathbf{q}_1 - \mathbf{k})^2 (\mathbf{q}_2 - \mathbf{k})^2} C^\mu(q_1 - \mathbf{k}, q_2 - \mathbf{k}) \right]. \end{aligned} \quad (4.35)$$

Inserting the result into Eq. (4.15) and expanding there the Regge-factors and the quark-reggeized gluon vertex, Eq. (4.16), in $\lambda_{11}, \lambda_{12}, \lambda_{21}$ and λ_{22} we find that to the desired accuracy the dependence on these parameters vanishes for the complete amplitude:

$$\begin{aligned} \mathcal{M}_{2 \rightarrow 3} &= 2s \int \frac{d\omega_1}{2\pi i} \int \frac{d\omega_2}{2\pi i} g t^a \times \frac{1}{t_1} \frac{1}{\omega_1 - \beta(\mathbf{q}_1^2)} \left| \frac{s_1}{s_{R_1}} \right|^{\omega_1} \frac{\xi^-(\omega_1)}{2} \\ &\quad \times g T_{ba}^c \tilde{\Gamma}_{RRG}^\mu(q_1, q_2) \times \frac{1}{t_2} \frac{1}{\omega_2 - \beta(\mathbf{q}_2^2)} \left| \frac{s_2}{s_{R_2}} \right|^{\omega_2} \frac{\xi^-(\omega_2)}{2} \times g t^b, \end{aligned} \quad (4.36)$$

with

$$\tilde{\Gamma}_{RRG}^\mu(q_1, q_2) = C^\mu(q_1, q_2) + \frac{\ln -\kappa_1 + \ln \kappa_1}{2} \frac{N_c g^2}{2} \int \frac{d^2 \mathbf{k}}{(2\pi)^3} \frac{\mathbf{q}_2^2 \mathbf{q}_1^2 C^\mu(q_1 - \mathbf{k}, q_2 - \mathbf{k})}{\mathbf{k}^2 (\mathbf{q}_1 - \mathbf{k})^2 (\mathbf{q}_2 - \mathbf{k})^2}, \quad (4.37)$$

and $t_{1,2} = -\mathbf{q}_{1,2}^2$. We shall confront this result at first with the analytic representation of the $2 \rightarrow 3$ amplitude Eq. (4.6), which we rewrite as

$$\begin{aligned} \mathcal{M}_{2 \rightarrow 3} &= s \int \frac{d\omega_1}{2\pi i} \int \frac{d\omega_2}{2\pi i} |s_1|^{\omega_1} |s_2|^{\omega_2} \\ &\quad \left(\kappa_1^{-\omega_2} \xi_{(\omega_2)}^{(\tau_2)} \xi_{(\omega_1, \omega_2)}^{(\tau_1, \tau_2)} \frac{V_1(\omega_1, \omega_2; t_1, t_2, \kappa_1)}{\sin \pi \omega_{12}} + \kappa_1^{-\omega_1} \xi_{(\omega_1)}^{(\tau_1)} \xi_{(\omega_2, \omega_1)}^{(\tau_2, \tau_1)} \frac{V_2(\omega_1, \omega_2; t_1, t_2, \kappa_1)}{\sin \pi \omega_{21}} \right). \end{aligned} \quad (4.38)$$

Following closely [97], we introduce for Eq. (4.38) factors

$$\phi_{\omega_1 \omega_2}^{\omega_1} = \frac{1}{\xi_{\omega_1}^{(-)} \xi_{\omega_2}^{(-)}} \xi_{\omega_1}^{(-)} \xi_{\omega_2 \omega_1}^{(-,-)} \quad \text{and} \quad \phi_{\omega_1 \omega_2}^{\omega_2} = \frac{1}{\xi_{\omega_1}^{(-)} \xi_{\omega_2}^{(-)}} \xi_{\omega_2}^{(-)} \xi_{\omega_1 \omega_2}^{(-,-)} \quad (4.39)$$

and rewrite them as

$$\phi_{\omega_1 \omega_2}^{\omega_i} = e^{i\pi \omega_i} - \frac{1}{\xi_{\omega_1}^{(-)} \xi_{\omega_2}^{(-)}} (e^{-i\pi \omega_i} - e^{i\pi \omega_i}). \quad (4.40)$$

Eq. (4.38) takes then the form

$$\begin{aligned} \mathcal{M}_{2 \rightarrow 3} &= s \int \frac{d\omega_1}{2\pi i} \int \frac{d\omega_2}{2\pi i} |s_1|^{\omega_1} \frac{\xi_{\omega_1}^{(-)}}{2} |s_2|^{\omega_2} \frac{\xi_{\omega_2}^{(-)}}{2} \\ &\quad \frac{\kappa_1^{-\omega_2} \phi_{\omega_1 \omega_2}^{\omega_2} V_1(\omega_1, \omega_2; t_1, t_2, \kappa_1) - \kappa_1^{-\omega_1} \phi_{\omega_1 \omega_2}^{\omega_1} V_2(\omega_1, \omega_2; t_1, t_2, \kappa_1)}{\sin \pi \omega_{12}}. \end{aligned} \quad (4.41)$$

Assuming from now on to have to this accuracy for negative signature only exchange of Regge-poles in both t -channels, we define functions $\tilde{V}_i(t_1, t_2, \kappa_1)$ by

$$V_i(\omega_1, \omega_2; t_1, t_2, \kappa_1) = g t^a \frac{1}{\omega_1 - \beta(\mathbf{q}_1^2)} \frac{1}{t_1} \times T_{ba}^c \pi \tilde{V}_i(t_1, t_2, \kappa_1) \times \frac{1}{\omega_2 - \beta(\mathbf{q}_2^2)} \frac{1}{t_2} g t^b. \quad (4.42)$$

The functions \tilde{V}_i can be determined within the LLA [83, 89] from taking discontinuities in Eq. (4.6) and making use of unitarity²:

$$\tilde{V}_1(t_1, t_2, \kappa_1) = \beta(\mathbf{q}_1^2) C^\mu(q_1, q_2) + \frac{N_c g^2}{2} \int \frac{d^2 \mathbf{k}}{(2\pi)^3} \frac{\mathbf{q}_2^2 \mathbf{q}_1^2}{\mathbf{k}^2 (\mathbf{q}_1 - \mathbf{k})^2 (\mathbf{q}_2 - \mathbf{k})^2} C^\mu(q_1 - \mathbf{k}, q_2 - \mathbf{k}) \quad (4.43)$$

$$\tilde{V}_2(t_1, t_2, \kappa_1) = \beta(\mathbf{q}_2^2) C^\mu(q_1, q_2) + \frac{N_c g^2}{2} \int \frac{d^2 \mathbf{k}}{(2\pi)^3} \frac{\mathbf{q}_2^2 \mathbf{q}_1^2}{\mathbf{k}^2 (\mathbf{q}_1 - \mathbf{k})^2 (\mathbf{q}_2 - \mathbf{k})^2} C^\mu(q_1 - \mathbf{k}, q_2 - \mathbf{k}). \quad (4.44)$$

Taking into account that κ_1 =fixed in the Double-Regge-Kinematics, we expand

$$\kappa_1^{\omega_i} \phi_{\omega_1 \omega_2}^{\omega_i} = 1 + \omega_i \frac{\ln -\kappa_1 + \ln \kappa_1}{2} + \dots \quad (4.45)$$

where the dots indicate terms of higher order in ω_1, ω_2 which is equivalent to terms of higher order in g^2 . With $\sin \pi \omega_{12} \simeq \pi \omega_{12}$ due to the LLA, one can then verify that Eq. (4.41) and Eq. (4.36) agree with each other at the desired accuracy. Eq. (4.36) also satisfies the Steinmann-relations in this sense. Whereas Eq. (4.41)/Eq. (4.6) satisfy the Steinmann-relations by construction, Eq. (4.36) does so only within the achieved accuracy. The complete inner analytic structure of the production vertex that is needed in a field theory of Reggeons in order to satisfy the Steinmann-relations, is only obtained to the level of accuracy the phase structure of the production vertex has been determined. This should not be understood as a failure of the effective theory or its prescription of longitudinal integrations, but is natural for an analysis bases on the LLA, as the logarithms inside the production vertex which yield the analytic structure are small and not included at LLA. On the other hand this tells us that care is needed when dealing with the phase structure of reggeized gluons within the effective action: It can be only trusted up to the level of accuracy one goes beyond the LLA, in particular when reggeized gluon - particle vertices have a inner phase structure, as it is the case for the production amplitude.

Similar observations hold for the $2 \rightarrow 4$ production amplitude. This case is generally more involved than the $2 \rightarrow 3$ production amplitude: Apart from the Regge-pole exchange in all three t -channels, the further exchange of a state of two or more reggeized gluons in the t_2 -channel is required by unitarity. For negative signature, on the other hand, this contribution can be shown to be of higher order in g^2 from the analysis of the analytic representation Eq. (4.9), which is confirmed by the results from the effective action. For the present level of accuracy, the interaction is for negative signature mediated by Regge-pole-exchange alone. Recent interest in the analytical structure of LLA-production amplitudes in the planar limit is triggered by the study of BDS-amplitudes. In that case the Regge-cut contribution is already relevant at the present level of accuracy [83].

For the effective action, we start with the following expression, which generalizes Eq. (4.15):

$$\begin{aligned} i\mathcal{M}_{2 \rightarrow 4} &= s \int \frac{d\omega_1}{2\pi i} \int \frac{d\omega_2}{2\pi i} \int \frac{d\omega_3}{2\pi i} \tilde{\Gamma}_{QQR}^a(\omega_1; q_1; \lambda_{11}) \times \frac{i/2}{\mathbf{q}_1^2} \frac{1}{\omega_1 - \beta(\mathbf{q}_1)} \left| \frac{s_1}{s_{R_1} \lambda_{11} \lambda_{12}} \right|^{\omega_1} \\ &\times \Gamma_{RRG}^{ac_1 e, \mu_1}(\omega_1, \omega_2; q_1, q_2; \lambda_{12}, \lambda_{21}) \times \frac{i/2}{\mathbf{q}_2^2} \frac{1}{\omega_2 - \beta(\mathbf{q}_2)} \left| \frac{s_2}{s_{R_2} \lambda_{21} \lambda_{23}} \right|^{\omega_2} \times \left(\xi_{\omega_2}^{(-)} \right)^{-1} \\ &\times \Gamma_{RRG}^{ec_2 b, \mu_2}(\omega_2, \omega_3; q_2, q_3; \lambda_{23}, \lambda_{32}) \times \frac{i/2}{\mathbf{q}_3^2} \frac{1}{\omega_3 - \beta(\mathbf{q}_3)} \left| \frac{s_3}{s_{R_3} \lambda_{32} \lambda_{33}} \right|^{\omega_2} \times \tilde{\Gamma}_{QQR}^b(\omega_2; q_2; \lambda_{33}). \quad (4.46) \end{aligned}$$

According to our conventions, the signature factors of the reggeized gluons are absorbed into the production vertices which requires introduction of the factor $(\xi_{\omega_2}^{(-)})^{-1}$. We further note, that within our achieved accuracy the above obtained loop-correction to the production amplitude can only be

²The following choice coincides with the one of [83] for the functions V_1 and V_2 up to a factor π which has been extracted in the present case

inserted for one of the production amplitudes, while for the other one should simply use the Born result. Making use of the results Eq. (4.16) and Eq. (4.35) we obtain

$$\begin{aligned}
\mathcal{M}_{2 \rightarrow 4} = & 2s \int \frac{d\omega_1}{2\pi i} \int \frac{d\omega_2}{2\pi i} \int \frac{d\omega_3}{2\pi i} g t^a \times \frac{1}{t_1} \frac{1}{\omega_1 - \beta(\mathbf{q}_1^2)} \left| \frac{s_1}{s_{R_1}} \right|^{\omega_1} \frac{\xi^-(\omega_1)}{2} \\
& \left[\times g T_{eq}^{c_1} C^{\mu_1}(q_1, q_2) \times \frac{1}{t_2} \frac{1}{\omega_2 - \beta(\mathbf{q}_2^2)} \left| \frac{s_2}{s_{R_2}} \right|^{\omega_2} \frac{\xi^-(\omega_2)}{2} \times g T_{be}^{c_2} C^{\mu_2}(q_2, q_3) \right. \\
& + \times g T_{ea}^{c_1} \delta \tilde{\Gamma}_{RRG}^{\mu_1}(q_1, q_2) \times \frac{1}{t_2} \frac{1}{\omega_2 - \beta(\mathbf{q}_2^2)} \left| \frac{s_2}{s_{R_2}} \right|^{\omega_2} \frac{\xi^-(\omega_2)}{2} \times g T_{be}^{c_2} C^{\mu_2}(q_2, q_3) \\
& \left. + \times g T_{ea}^{c_1} C^{\mu_1}(q_1, q_2) \times \frac{1}{t_2} \frac{1}{\omega_2 - \beta(\mathbf{q}_2^2)} \left| \frac{s_2}{s_{R_2}} \right|^{\omega_2} \frac{\xi^-(\omega_2)}{2} \times g T_{be}^{c_2} \delta \tilde{\Gamma}_{RRG}^{\mu_2}(q_2, q_3) \right] \\
& \times \frac{1}{t_3} \frac{1}{\omega_3 - \beta(\mathbf{q}_3^2)} \left| \frac{s_3}{s_{R_3}} \right|^{\omega_3} \frac{\xi^-(\omega_3)}{2} \times g t^b
\end{aligned} \tag{4.47}$$

where

$$\delta \tilde{\Gamma}_{RRG}^{\mu}(q_1, q_2) = \frac{\ln -\kappa_1 + \ln \kappa_1}{2} \frac{N_c g^2}{2} \int \frac{d^2 \mathbf{k}}{(2\pi)^3} \frac{\mathbf{q}_2^2 \mathbf{q}_1^2}{\mathbf{k}^2 (\mathbf{q}_1 - \mathbf{k})^2 (\mathbf{q}_2 - \mathbf{k})^2} C^{\mu}(q_1 - k, q_2 - k) \tag{4.48}$$

is the one-loop contribution of Eq. (4.37). This result needs then to be confronted with the analytical representation of the $2 \rightarrow 4$ production amplitude, Eq. (4.9). As for the $2 \rightarrow 3$ amplitude, the partial waves W_i , $i = 1, \dots, 5$ can be determined at LLA by taking discontinuities of Eq. (4.9) and making use of unitarity in the (sub-)channels (see [83,89]). Extracting furthermore in Eq. (4.9) signature factors for each t -channel and expanding the remainder up to the above level of accuracy, we find agreement of both expressions. In particular, Regge-cut contributions cancel for negative signature at this level of accuracy and Eq. (4.47) yields the correct result.

4.3 Positive and mixed signatred production amplitudes

So far we concentrated our analysis on production amplitudes in which all t -channels carry negative signature. From a technical point of view, the analysis of production amplitudes with positive and mixed signature is slightly simpler: We don't need to extract the analytic structure from NLLA-calculations. It is sufficient to consider the interaction of reggeized gluons instead, which is similar to the derivation of the BFKL-equation in Sec.3.2.

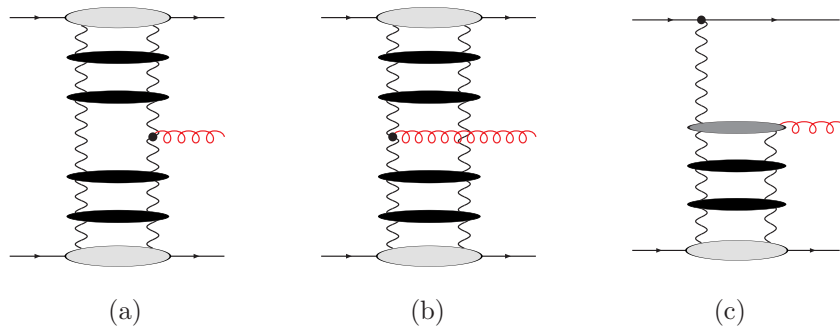


Figure 4.8: $2 \rightarrow 3$ production amplitude with positive ($\tau_1 = \tau_2 = +1$) and mixed ($\tau_1 = -1, \tau_2 = +1$). The grey blobs on the top on the bottom of the diagram denote the quark-impact factors, whereas interaction between reggeized gluons is described by the BFKL-Kernel. In (c) a new vertex appears: The Reggeon-Particle-Reggeon-Reggeon (RP2R) vertex.

The different contributions that can occur for the $2 \rightarrow 3$ production amplitude are summarized in Fig.4.8. In the case where both t -channels carry positive signature, ($\tau_1 = \tau_2 = +1$), Fig.4.8a and Fig.4.8b, interaction in both t -channels is mediated by a state of two reggeized gluons, which is

described by the BFKL-equation. The production of the gluon at central rapidities is described on the other hand by the leading order production vertex Eq.(4.11). The third graph in Fig.4.8c corresponds to mixed signature, where the t_1 channel carries negative signature ($\tau_1 = -1$) and the t_2 -channel positive signature ($\tau_2 = +1$). The case where $\tau_1 = +1$ and $\tau_2 = -1$ exists as well and follows from the above case by symmetry. For mixed symmetry, a new element occurs, the Reggeon-Particle-2 Reggeon vertex ((RP2R)-vertex), which we will derive from the effective action in Sec.4.3.1. Knowledge of this vertex is then also sufficient to build all positive and mixed

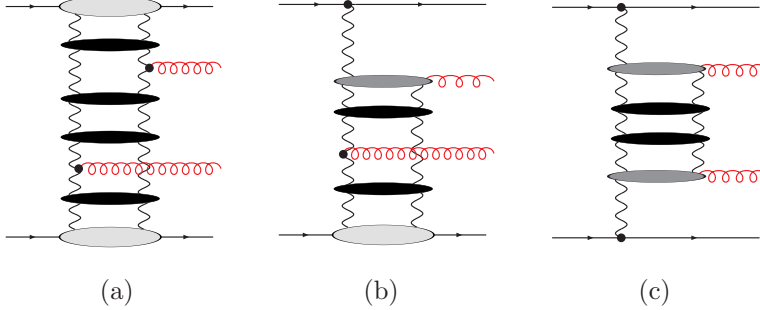


Figure 4.9: Contributions to the $2 \rightarrow 4$ production amplitude with positive (a) and mixed (b,c,d) signature. Explicitly we have the following signature configurations a: $(+, +, +)$, b: $(-, +, +)$, c: $(-, +, -)$

signed $2 \rightarrow 4$ production amplitudes, Fig.4.9, apart from the combination $(+, -, +)$, which explicitly requires the exchange of three reggeized gluons, which has not been addressed so far. Apart from that it is sub-leading compared to the other signature configurations and we will not include it in our present analysis.

4.3.1 The Reggeon-Particle-2Reggeon (RP2R)-vertex

In the following we will discuss the derivation of the Reggeon-Particle-2Reggeon (RP2R)-vertex from the effective action. To do so, we will apply the rules for the interactions of reggeized gluons of Sec.3.2.

We further that the derivation of the RP2R-vertex from the effective action was also addressed in [98]. During their derivation, the authors of [98] find a certain ambiguity concerning the evaluation of longitudinal integrals. In the following we demonstrate that such an ambiguity does not occur, if one applies the rules derived in Sec.3.2. In contrast to our general analysis, which is based on covariant Feynman gauge, the authors of [98] use in their analysis the light-cone gauge, $V_+ = 0$, which makes it difficult to compare directly between the two calculations. Nevertheless we believe that the problem of [98] arises due to a misinterpretation of the Feynman-rules of the effective action and due to the absence of subtraction terms, as introduced in Sec.3.2 and not due to a peculiarity of the light-cone gauge.

As for the correction to the production amplitude in Sec.4.2.2, we will use in the following the $2 \rightarrow 3$ production amplitude, Fig.4.8c, as a reference process. There all corrections above the RP2R-vertex are resummed within the LLA by the upper reggeized gluon, whereas below such resummation is performed by the BFKL-Green's function. We factorize this amplitude in the following way

$$i\mathcal{M}_{2 \rightarrow 3}^{(-,+)} = p_A^+ |p_B^-| \int \frac{d\omega_1}{2\pi i} \int \frac{d\omega_2}{2\pi i} \frac{1}{2} [(-s_2)^{\omega_2} + s_2^{\omega_2}] \Gamma_{QR}^a(q_1) \times \frac{1}{\omega_1 - \beta(q_1^2)} \frac{i/2}{q_1^2} \\ \times \int \frac{d^2 \mathbf{k}}{(2\pi)^2} \Gamma_{RP2R}^{acb_1 b_2, \mu}(\omega_1; p_A^+, q_1^+, \mathbf{k}, \mathbf{q}_2 - \mathbf{k}) \times \frac{1}{k^2 (q_2 - \mathbf{k})^2} \times A^{b_1 b_2}(\omega_2; \mathbf{k}, \mathbf{q}_2 - \mathbf{k}), \quad (4.49)$$

with

$$A_2^{b_1 b_2}(\omega_2; \mathbf{k}, \mathbf{q}_2 - \mathbf{k}) = G_{\text{BFKL}}^{b_1 b_2; b'_1 b'_2}(\omega_2; \mathbf{k}, \mathbf{q}_2 - \mathbf{k}; \mathbf{l}, \mathbf{q}_2 - \mathbf{l}) \otimes_l A_{(2,0)}^{b'_1 b'_2}(\mathbf{l}, \mathbf{q}_2 - \mathbf{k}) \quad (4.50)$$

where G_{BFKL} is the BFKL-Green's function Eq. (3.81).

As usually for loops containing two or more reggeized gluons, the longitudinal integration factorizes and it is sufficient to consider the diagrams of Fig.4.10. Apart from the diagrams that are depicted

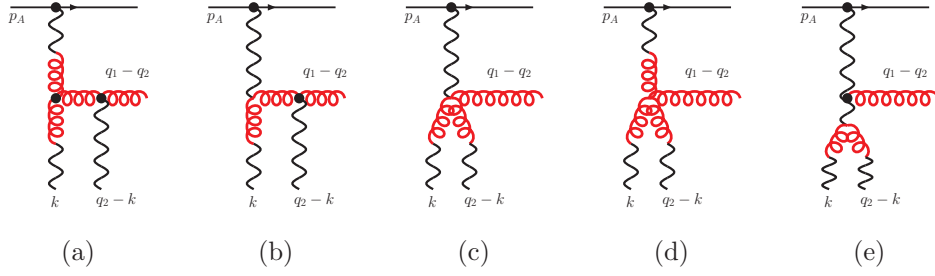


Figure 4.10: Different kinds of effective Feynman-graphs, that contribute to the RP2R-vertex. The last graph is a subtraction graph, that subtracts the logarithmic singularity of the first graph.

in Fig.4.10, there occurs also the combination where in Fig.4.10a and Fig.4.10b the lower two reggeized gluons are interchanged. Fig.4.10e is a subtraction graph and comes with a relative minus sign. The necessity of including such a subtraction graph is motivated similar to Sec.3.2: There, for both the quark-impact factor and the BFKL-interaction-kernel a subtraction graph has been introduced to resolve a counting problem with the reggeized gluon and to make the integral over light-cone momenta finite. For exactly the same reason, one also requires a subtraction graph for the RP2R-vertex.

To evaluate the integration over longitudinal momenta it turns out to be advisable not to consider individual diagrams, but to group the sum of all diagrams first according to their color- and then according to their transverse momentum structure. In this way, already some of the singularities cancel by themselves. Furthermore the transverse momentum structure can be classified according to their dependence on transverse reggeized gluon momenta. Generally one finds that terms that depend only on the sum of the two momenta are less convergent. This is to be expected, as it is this class of contributions that initially gave rise to the induced vertices. As a consequence, we expect these divergences to be removed by a subtraction term, like Fig. 4.10e.

In the present case, we also drop all terms that vanish for production of a real particle i.e. that are either proportional to $(q_1 - q_2)^2 = 0$ or to $(q_1 - q_2)^\mu$ and therefore orthogonal to physical polarizations. The transverse momentum structure reduces for the unintegrated RP2R-vertex to two classes of terms: For the first class the numerator depends only on the sum of the transverse momenta of both reggeized gluons,

$$(T^{b_1} T^{b_2})_{ac} G_{(A)}^\mu = ig^2 (T^{b_1} T^{b_2})_{ac} \frac{q_1^+}{-q_1^+ k^- - (\mathbf{q}_1 - \mathbf{k})^2 + i\epsilon} C_\mu(q_1, q_2). \quad (4.51)$$

For the second class, the numerator explicitly depends on the momenta of the individual reggeized gluons, \mathbf{k} and $\mathbf{q}_2 - \mathbf{k}$,

$$(T^{b_1} T^{b_2})_{ac} G_{(B)}^\mu = ig^2 (T^{b_1} T^{b_2})_{ac} \frac{q_1^2}{-k^- - q_1^+ k^- - (\mathbf{q}_1 - \mathbf{k})^2 + i\epsilon} C_\mu(q_1 - k, q_2 - k), \quad (4.52)$$

with

$$C_\mu(q_1 - k, q_2 - k) = \left(\frac{q_1^+}{2} + \frac{(\mathbf{q}_1 - \mathbf{k})^2}{q_2^-}\right)(n^-)^\mu + \left(\frac{q_2^-}{2} + \frac{(\mathbf{q}_2 - \mathbf{k})^2}{q_1^+}\right)(n^+)^\mu - (q_1 + q_2 - 2k)_\perp^\mu, \quad (4.53)$$

not dependent on k^- . For each of the above terms there exists also a corresponding 'crossed' term which is obtained by simultaneously interchanging momenta and color labels of the two lower reggeized gluons.

Attempting to integrate both classes over k^- , we find that the second class, Eq. (4.52), yields a convergent integrand, where the first class does not. Concentrating at first on the second class, one realizes that it comes with an additional pole in k^- , compared to the first class. Even though by grouping sums of diagrams, the relation to individual diagrams is less pronounced, it is nevertheless clear, that this pole is due to an induced vertex and needs to be treated with the corresponding prescription.

To evaluate the k^- -integral over Eq. (4.52), we further add the Reggeon factor of the upper reggeized gluon and obtain the following integral

$$(T^{b_1}T^{b_2})_{ac}\Gamma_{(B)}^\mu = ig^2(T^{b_1}T^{b_2})_{ac} \int \frac{dk^-}{2\pi} \left[\frac{1}{2} \left[\left(\frac{p_A^+ k^- - i\epsilon}{\Lambda_a} \right)^{\omega_1} + \left(\frac{-p_A^+ k^- - i\epsilon}{\Lambda_a} \right)^{\omega_1} \right] \frac{q_1^2}{-k^- - q_1^+ k^- - (\mathbf{q}_1 - \mathbf{k})^2 + i\epsilon} C_\mu(q_1 - k, q_2 - k) \right], \quad (4.54)$$

where the $i\epsilon$ -prescription of the pole in k^- is meant to coincide with the $i\epsilon$ -prescription of the branch-cut it is multiplied with. The integral is easily evaluated and we find

$$(T^{b_1}T^{b_2})_{ac}\Gamma_{(B)}^\mu = \frac{g^2}{2}(T^{b_1}T^{b_2})_{ac} \frac{q_1^+}{|q_1^+|} \left| \frac{p_A^+}{q_1^+} \right|^{\omega_1} \left(\frac{(\mathbf{q}_1 - \mathbf{k})^2}{\Lambda_a} \right)^\omega \frac{q_1^2}{(\mathbf{q}_1 - \mathbf{k})^2} C_\mu(q_1 - k, q_2 - k), \quad (4.55)$$

with $\Lambda_a \simeq (\mathbf{q}_1 - \mathbf{k})^2$ due to the LLA. Next we turn to the symmetric term, Eq.(4.51). Unlike Eq.(4.52) it provides at first not a convergent integrand. On the other hand, this term has the same numerator as the subtraction term and we can expect that after subtraction of Fig. 4.10e we will obtain a convergent integrand. To this end we add and subtract a term with the same pole structure as the subtraction graph and obtain for Eq. (4.51)

$$(T^{b_1}T^{b_2})_{ac}G_{(A)}^\mu = ig^2(T^{b_1}T^{b_2})_{ac} \left[\frac{C_\mu(q_1, q_2)}{2} \left(\frac{q_1^+}{-q_1^+ k^- + i\epsilon} - \frac{q_1^+}{q_1^+ k^- + i\epsilon} \right) + \frac{(\mathbf{q}_1 - \mathbf{k})^2 C_\mu(q_1, q_2)}{-q_1^+ k^- - (\mathbf{q}_1 - \mathbf{k})^2 + i\epsilon} \frac{1}{2} \left(\frac{q_1^+}{-q_1^+ k^- + i\epsilon} - \frac{q_1^+}{q_1^+ k^- + i\epsilon} \right) \right]. \quad (4.56)$$

Apart from the above contribution, we also have the contribution, where the two lower reggeized gluons are interchanged and which takes the following form:

$$(T^{b_2}T^{b_1})_{ac}G_{(AX)}^\mu = ig^2(T^{b_2}T^{b_1})_{ac} \left[\frac{C_\mu(q_1, q_2)}{2} \left(\frac{q_1^+}{q_1^+(k^- - q_2^-) + i\epsilon} - \frac{q_1^+}{q_1^+(q_2^- - k^-) + i\epsilon} \right) + \frac{(\mathbf{q}_1 - \mathbf{k})^2 C_\mu(q_1, q_2)}{q_1^+(k^- - q_2^-) - (\mathbf{q}_1 - \mathbf{q})^2 + i\epsilon} \frac{1}{2} \left(\frac{q_1^+}{q_1^+(k^- - q_2^-) + i\epsilon} - \frac{q_1^+}{q_1^+(q_2^- - k^-) + i\epsilon} \right) \right]. \quad (4.57)$$

The two terms in the first line of Eq. (4.56) and Eq. (4.57) agree with each other in their momentum part, up to the factor q_2^- in the denominator. For the integral over k^- this factor can be removed by a corresponding shift in the integration variable or, alternatively, by adding and subtracting a corresponding term which does *not* contain this factor q_2^- . One can then verify that the difference between the terms with and without q_2^- is convergent and vanishes, once it is integrated over k^- . After those manipulations, the momentum factors in the first lines of Eq. (4.56) and Eq. (4.57) agree exactly, while they come with a relative minus sign and different ordering of color factors. For their sum, the color factor reduces to the commutator and the sum agrees in both color- and in momentum- structure with the subtraction graph, Fig. 4.10e. As a consequence, the sum of the first lines of the rhs of Eq. (4.56) and Eq. (4.57) is canceled by the subtraction graph and we are left with the contributions in the second line of Eq. (4.56) and Eq. (4.57) respectively,

For their integral over k^- , we then restrict to Eq. (4.56) alone. Together with the Reggeon-factor of the upper reggeized gluon we find:

$$(T^{b_1}T^{b_2})_{ac}\Gamma_{(A)}^\mu = ig^2(T^{b_1}T^{b_2})_{ac} \int \frac{dk^-}{2\pi} \frac{1}{2} \left[\left(\frac{p_A^+ k^- - i\epsilon}{\Lambda_a} \right)^{\omega_1} + \left(\frac{-p_A^+ k^- - i\epsilon}{\Lambda_a} \right)^{\omega_1} \right] \frac{q_1^+}{-q_1^+ k^- - q_1^+ k^- - (\mathbf{q}_1 - \mathbf{k})^2 + i\epsilon} C_\mu(q_1, q_2). \quad (4.58)$$

Note that the $i\epsilon$ -prescription of the above ' ω '-factors and of the poles in Eq. (4.56) coincides, as for the sum of the poles the dependence on q_1^+ is absent. The integral is easily evaluated and yields

$$(T^{b_1} T^{b_2})_{ac} \Gamma_{(A)}^\mu = -\frac{g^2}{2} (T^{b_1}, T^{b_2})_{ac} \frac{q_1^+}{|q_1^+|} \left| \frac{p_A^+}{q_1^+} \right|^{\omega_1} C_\mu(q_1, q_2), \quad (4.59)$$

where we already approximated $\Lambda_a \simeq (\mathbf{q}_1 - \mathbf{k})^2$ in accordance with the LLA. To obtain the complete RP2R-vertex, we add up our results Eq. (4.59) and Eq. (4.59) and complete them by supplementing their counterparts, obtained from exchanging color and momenta of the two lower reggeized gluons. Altogether we obtain

$$\Gamma_{RP2R}^{acb_1 b_2, \mu}(\omega_1; p_A^+, q_1^+, \mathbf{k}, \mathbf{q}_2 - \mathbf{k}) = -\frac{q_1^+}{|q_1^+|} \left| \frac{p_A^+}{q_1^+} \right|^{\omega_1} \tilde{\Gamma}_{RP2R}^{acb_1 b_2, \mu}(q_1, q_2, \mathbf{k}). \quad (4.60)$$

From the point of view of Reggeon-field theory, $\tilde{\Gamma}_{RP2R}$ constitutes the proper RP2R-vertex, as it does not contain any dependence on s -channel energy-variables. $\tilde{\Gamma}_{RP2R}$ can then be written as the sum of two terms, symmetric (Γ^S) and antisymmetric (Γ^A) under the exchange of the lower reggeized gluons,

$$\tilde{\Gamma}_{RP2R}^{acb_1 b_2, \mu}(q_1, q_2, \mathbf{k}) = \left[\{T^{b_1}, T^{b_2}\}_{ac} \tilde{\Gamma}^{S, \mu}(q_1, q_2, \mathbf{k}) + [T^{b_1}, T^{b_2}]_{ac_1} \tilde{\Gamma}^{A, \mu}(q_1, q_2, \mathbf{k}) \right], \quad (4.61)$$

where

$$\begin{aligned} \tilde{\Gamma}_{RP2R}^{S; \mu}(q_1, q_2, \mathbf{k}) = g^2 \left[C_\mu(q_1, q_2) - \frac{1}{2} \frac{\mathbf{q}_1^2}{(\mathbf{q}_1 - \mathbf{k})^2} C_\mu(q_1 - k, q_2 - k) \right. \\ \left. - \frac{1}{2} \frac{\mathbf{q}_1^2}{(\mathbf{q}_1 - \mathbf{q}_2 + \mathbf{k})^2} C_\mu(q_1 - q_2 + k, k) \right] \end{aligned} \quad (4.62)$$

and

$$\tilde{\Gamma}_{RP2R}^{A; \mu}(q_1, q_2, \mathbf{k}) = -g^2 \left[\frac{1}{2} \frac{\mathbf{q}_1^2}{(\mathbf{q}_1 - \mathbf{k})^2} C_\mu(q_1 - k, q_2 - k) - \frac{1}{2} \frac{\mathbf{q}_1^2}{(\mathbf{q}_1 - \mathbf{q}_2 + \mathbf{k})^2} C_\mu(q_1 - q_2 + k, k) \right]. \quad (4.63)$$

Note that the latter term gives a first example of a coupling of a QCD-particle to a state of two reggeized gluons, which is antisymmetric under the combined exchange of color and momenta.

4.3.2 Mixed and positive signature for the $2 \rightarrow 3$ amplitude

With the results of the previous paragraph, we have now all ingredients to construct the various $2 \rightarrow 3$ production amplitudes with mixed and positive signature of Fig.4.8. We start with the mixed signature case ($\tau_1 = -, \tau_2 = +$) whereas the case ($\tau_1 = +, \tau_2 = -$) follows by symmetry. Inserting Eq. (4.60) into Eq. (4.49) we obtain for the $2 \rightarrow 3$ production amplitude the following expression:

$$i\mathcal{M}_{2 \rightarrow 3}^{(-,+)} = 2\pi s \frac{s_2}{|s_2|} \int \frac{d\omega_1}{2\pi i} \int \frac{d\omega_2}{2\pi i} |s|^{\omega_1} |s_2|^{\omega_2 - \omega_1} \frac{1}{2} (e^{-i\pi\omega_2} + 1) V_{(-,+)}(\omega_1, \omega_2; \mathbf{q}_1, \mathbf{q}_2) \quad (4.64)$$

with

$$\begin{aligned} V_{(-,+)}(\omega_1, \omega_2; \mathbf{q}_1, \mathbf{q}_2) = g t^a \times \frac{1}{\omega_1 - \beta(\mathbf{q}_1^2)} \frac{1}{t_1} \times \tilde{\Gamma}_{RP2R}^{acb_1 b_2, \mu}(q_1, q_2, \mathbf{l}) \epsilon_\mu(q_1 - q_2) \\ \otimes_l G_{\text{BFKL}}^{b_1 b_2; b'_1 b'_2}(\omega_2; \mathbf{l}, \mathbf{q}_2 - \mathbf{l}; \mathbf{k}, \mathbf{q}_2 - \mathbf{k}) \otimes_{\mathbf{k}} A_{(2,0)}^{b'_1 b'_2}(\mathbf{k}, \mathbf{q}_2 - \mathbf{k}) \end{aligned} \quad (4.65)$$

For the partial wave³ $V_{(-,+)}$ we note that it can be obtained directly from Fig.4.11b, by applying a simple set of diagrammatic rules, which we present in the following. It should be noted that these

³Note that the partial waves appearing in the following all carry a signature dependence unlike the partial waves in the analytical representations. It is due to the fact that within the effective action sometimes two or more partial waves of the analytical representations are combined, which makes the final result different for every signature configuration

are *not* Feynman-rules of the effective action, but serve only to construct partial waves given the factorization Eq.(4.64) in energy-factors and partial wave. In the diagrammatic language, we have for the coupling of the external quarks to the single and the state of reggeized gluons respectively:

$$\begin{array}{c} A \rightarrow \bullet \rightarrow A' \\ \downarrow \\ q \\ \downarrow \\ a \end{array} = g^t_{AA'} \quad \begin{array}{c} A \rightarrow \bullet \rightarrow A' \\ \downarrow \\ k \\ \downarrow \\ a_1 \quad a_2 \\ \downarrow \\ q-k \end{array} = A^{a_1 a_2}_{(2,0)}(\mathbf{k}, \mathbf{q} - \mathbf{k}) \quad (4.66)$$

Propagation of the single reggeized gluon and the state of two reggeized gluon corresponds to

$$\begin{array}{c} c \\ \downarrow \\ q, \omega \\ \downarrow \\ c' \end{array} = \frac{1}{\omega - \beta(\mathbf{q}^2)} \frac{1}{-\mathbf{q}^2} \quad \begin{array}{c} a_1 \quad q-l \quad a_2 \\ \downarrow \\ \omega \\ \downarrow \\ b_1 \quad k \quad q-k \quad b_2 \end{array} = G^{a_1 a_2; b_1 b_2}_{\text{BFKL}}(\omega; \mathbf{l}, \mathbf{q} - \mathbf{l}; \mathbf{k}, \mathbf{q} - \mathbf{k}). \quad (4.67)$$

Further the RP2R-vertex is given by

$$\begin{array}{c} a \\ \downarrow \\ q_1 \\ \downarrow \\ k \\ \downarrow \\ b_1 \end{array} \begin{array}{c} \bullet \\ \downarrow \\ q_1 - q_2 \\ \downarrow \\ q_2 - k \\ \downarrow \\ b_2 \end{array} \begin{array}{c} c \\ \downarrow \\ \text{red wavy line} \\ \downarrow \\ c \end{array} = \tilde{\Gamma}_{RP2R}^{ac_1 b_1 b_2, \mu}(q_1, q_2, \mathbf{l}) \epsilon_\mu(q_1 - q_2) \quad (4.68)$$

and every loop of two reggeized gluons requires the following convolution symbol (already implicitly contained inside the BFKL-Green's function)

$$\otimes_{\mathbf{k}} = \int \frac{d^2 \mathbf{k}_1}{(2\pi)^3} \frac{1}{\mathbf{k}_1^2 \mathbf{k}_2^2} \quad (4.69)$$

which contains both transverse loop integration and transverse reggeized gluon propagators. As usually, transverse momenta obey the constraint $\mathbf{q}_i = \mathbf{k}_1 + \mathbf{k}_2$ with $t_i = \mathbf{q}_i^2$ the momentum transfer of the corresponding t -channel. Using these rules, construction of the partial wave Eq.(4.65) from diagram Fig.4.11b is straight-forward.

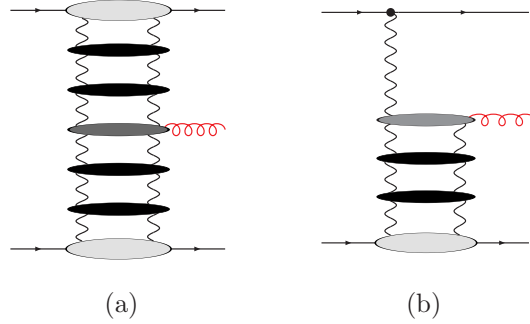


Figure 4.11: Diagrams corresponding to the $2 \rightarrow 3$ production amplitude with mixed ($\tau_1 = -1, \tau_2 = +1$) and positive ($\tau_1 = \tau_2 = +1$) signature. Making use of the diagrammatic rules described in the text, these diagrams allow for the derivation of the corresponding partial waves.

For $V_{(-,+)}$ we then only note that, due to the symmetry of the quark-impact factor $A_2^{b_1 b_2}(\omega_2)$ under exchange of transverse momenta and color of the reggeized gluons, the RP2R-vertex is projected on its symmetric part Eq.(4.62), whereas the anti-symmetric part Eq.(4.63) decouples in that case. Taking a closer look at the energy-dependence of the production amplitude Eq. (4.64), we observe at first the absence of singularities in overlapping production channels and conclude that the Steinmann-relations are fulfilled for Eq. (4.64). In a next step we confront Eq.(4.64) with the analytic representation of the $2 \rightarrow 3$ production amplitude, Eq. (4.6).

At first we note that Eq. (4.6) does not contain the partial wave V_1 : As outlined in [33], for the signature configuration ($\tau_1 = -, \tau_2 = +$), the energy-factors in front of V_1 are sub-leading in

comparison to those appearing in front of V_2 and consequently the partial wave V_1 is absent in our LLA-analysis.

For the second term we first observe that the behavior of Eq. (4.64) under substitutions $s \rightarrow -s$ and $s_2 \rightarrow -s_2$ is in full agreement with the signature structure of Eq. (4.6). As far the explicit form of the signature factors is concerned, we apply Eq. (3.82) to rewrite Eq. (4.64) into the following form

$$\mathcal{M}_{2 \rightarrow 3}^{(-,+)} = -2\pi s \int \frac{d\omega_1}{2\pi i} \int \frac{d\omega_2}{2\pi i} |s|^{\omega_1} |s_2|^{\omega_2 - \omega_1} \frac{e^{-i\pi\omega_2} - 1}{\sin(\pi\omega_2)} V_{(-,+)}(\omega_1, \omega_2; \mathbf{q}_1, \mathbf{q}_2). \quad (4.70)$$

Nevertheless, the signature factors of Eq. (4.70) coincides with those in Eq. (4.6) only in the limit $\omega_1 \rightarrow 0$. This means that within our accuracy, the upper reggeized gluon is completely real and

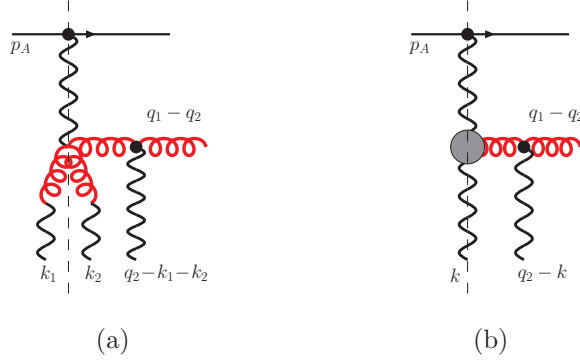


Figure 4.12: Higher contributions which yield a non-zero s -discontinuity for symmetric (a) and anti-symmetric (b) color in the t_2 -channel. While diagram (a) involves a coupling of the two lower reggeized gluons to the upper reggeized gluons, diagram (b) contains the production vertex at next-to-leading order, which allows for a s -channel cut.

contains no imaginary part. We note that also this observation coincides with the analysis of the mixed signature production amplitude by taking discontinuities: As outlined in [33], the signature configuration ($\tau_1 = -, \tau_2 = +$) is determined within the LLA by the s_2 -discontinuity, whereas the discontinuity in s is of higher order and does not occur at leading order and the LLA. We expect first corrections to the signature factor to occur from diagrams like Fig.4.12 which contain elements that allow for 'cutting' of the upper reggeized gluon.

The $2 \rightarrow 3$ production amplitude with positive signature, Fig. 4.11b is obtained within the LLA, by inserting the RPR-production vertex Eq. (4.11) either on the first Fig. 4.8a or on the second Fig. 4.8b reggeized gluon. Construction of the phase structure requires some care and we shall shortly outline the basic steps of the underlying analysis. To this end we start with the Born diagram, where only reggeized gluons are exchanged and no interaction kernel between the reggeized gluons is included. Leaving for simplicity all details about the transverse momentum structure of the diagram aside, we obtain, restricting only to the part dependent on Mellin-variables the following expression

$$\int \frac{d\tilde{\omega}}{2\pi i} \frac{s^{\tilde{\omega}} \xi^{(-)}(\tilde{\omega})}{\tilde{\omega} - \beta} \int \frac{d\tilde{\omega}_1}{2\pi i} \frac{s_1^{\tilde{\omega}_1} \xi^{(-)}(\tilde{\omega}_1)}{\tilde{\omega}_1 - \beta_1} \int \frac{d\tilde{\omega}_2}{2\pi i} \frac{s_2^{\tilde{\omega}_2} \xi^{(-)}(\tilde{\omega}_2)}{\tilde{\omega}_2 - \beta_2}, \quad (4.71)$$

where we further abbreviated the trajectory functions as

$$\beta \equiv \beta(\mathbf{k}), \quad \beta_1 \equiv \beta(\mathbf{q}_1 - \mathbf{k}), \quad \beta_2 \equiv \beta(\mathbf{q}_2 - \mathbf{k}). \quad (4.72)$$

Using

$$s_2 = \frac{s\kappa}{s_1} \quad (4.73)$$

and $\kappa^{-\tilde{\omega}_2} \simeq 1$ within the LLA and further introducing new Mellin-variables $\tilde{\omega} \rightarrow \omega_2 = \tilde{\omega} + \tilde{\omega}_2$, we arrive at

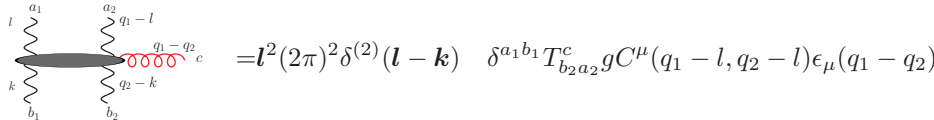
$$\int \frac{d\omega_2}{2\pi i} \int \frac{d\tilde{\omega}_1}{2\pi i} \int \frac{d\tilde{\omega}_2}{2\pi i} \frac{s^{\omega_2} \xi^{(-)}(\omega_2 - \tilde{\omega}_2) \xi^{(-)}(\tilde{\omega}_2) s_1^{\tilde{\omega}_1 - \tilde{\omega}_2} \xi^{(-)}(\tilde{\omega}_1)}{(\omega_2 - \tilde{\omega}_2 - \beta)(\tilde{\omega}_2 - \beta) \tilde{\omega}_1 - \beta_1}. \quad (4.74)$$

The Double-Regge-Kinematics allows now for the $\tilde{\omega}_2$ contour to be closed only to the right-hand-side, which corresponds to the Residue at $\tilde{\omega}_2 = \omega_1 - \beta$. Substituting furthermore $\tilde{\omega}_1 \rightarrow \omega_1 + \beta$ we finally arrive at

$$\int \frac{d\omega_1}{2\pi i} \int \frac{d\omega_2}{2\pi i} \frac{s^{\omega_2} \xi^{(-)}(\beta) \xi^{(-)}(\omega_2 - \beta) s_1^{\omega_1 - \omega_2} \xi^{(-)}(\omega_1 - \beta)}{(\omega_2 - \beta_2 - \beta) (\omega_1 - \beta_1 - \beta)}. \quad (4.75)$$

With Eq. (3.66) and Eq. (3.82) the product $\xi^{(-)}(\beta) \xi^{(-)}(\omega_2 - \beta)$ converts within the LLA into $\sim \xi^{(+)}(\omega_2) / \sin \pi \omega_2$. In particular allowing furthermore for interactions between the reggeized gluons, this allows then for a derivation of the BFKL-Green's function along the lines of Sec. 3.2.2 for the t_2 -channel. As far as the t_1 -channel is concerned we note that within the LLA $s^{\omega_2} s^{\omega_1 - \omega_2} = s^{\omega_1} s^{\omega_2 - \omega_1}$, making use of Eq. (4.73). With Eq. (3.66) and Eq. (3.82) the product $\xi^{(-)}(\beta) \xi^{(-)}(\omega_1 - \beta)$ can be converted into $\sim \xi^{(+)}(\omega_1) / \sin \pi \omega_1$, which then allows for the derivation of the BFKL-Green's function in the t_1 -channel.

For the formulation of the corresponding partial wave, we further require a new ingredient in our diagrammatic language, namely the RRPRR-vertex, which at this level of accuracy is built up of two disconnected contributions, mainly given by insertions of the production vertex Eq. (4.11). We have



$$= l^2 (2\pi)^2 \delta^{(2)}(\mathbf{l} - \mathbf{k}) \delta^{a_1 b_1} T_{b_2 a_2}^c g C^\mu(q_1 - l, q_2 - l) \epsilon_\mu(q_1 - q_2) \\ + (q_1 - l)^2 (2\pi)^2 \delta^{(2)}(\mathbf{l} - \mathbf{k} - \mathbf{q}_1 + \mathbf{q}_2) T_{b_1 a_1}^c \delta^{a_2 b_2} g C^\mu(l, l - q_1 + q_2) \epsilon_\mu(q_1 - q_2) \quad (4.76)$$

Note that the production vertices do not depend on the longitudinal momenta, in particular not on l^+ and l^- . The $2 \rightarrow 3$ production amplitude with positive signature in both t -channels is within the LLA given by

$$\mathcal{M}_{2 \rightarrow 3}^{(+,+)} = -2\pi s \int \frac{d\omega_1}{2\pi i} \int \frac{d\omega_2}{2\pi i} |s_1|^{\omega_1} |s_2|^{\omega_2 - \omega_1} \frac{e^{-i\pi\omega_1} - 1}{\sin \pi\omega_1} V_{(+,+)}(\omega_1, \omega_2; q_1, q_2) \\ \simeq -2\pi s \int \frac{d\omega_1}{2\pi i} \int \frac{d\omega_2}{2\pi i} |s_1|^{\omega_2} |s_2|^{\omega_1 - \omega_2} \frac{e^{-i\pi\omega_2} - 1}{\sin \pi\omega_2} V_{(+,+)}(\omega_1, \omega_2; q_1, q_2), \quad (4.77)$$

where the identity holds with LLA accuracy and the partial wave $V_{(+,+)}$ can be obtained making use of our diagrammatic rules. Further we note that the above expression is in accordance with the Steinmann-relations and within the considered accuracy also with the analytic representation of the $2 \rightarrow 3$ production amplitude, Eq. (4.6). As explained in detail in [33], the $2 \rightarrow 3$ production amplitude with positive signature in both t -channels is proportional to the s -discontinuity, whereas the discontinuity in s_1 and s_2 contributes only at higher orders, in accordance with the above findings. As a consequence the above partial wave cannot be associated with any of the partial waves in Eq. (4.6), but has to be understood as their combined sum.

4.3.3 Mixed and positive signature for the $2 \rightarrow 4$ amplitude

Next we turn to the various $2 \rightarrow 4$ production amplitudes with positive and mixed signature. As before, the individual partial waves can be obtained applying the diagrammatic rules given above to the graphs in Fig. 4.13. We start with the case, $(+, +, +)$ where signature in all three t -channels is positive, Fig. 4.13a. Within the LLA, this amplitude is found [33] to be proportional to the discontinuity in s . For the analytic representation this means that the amplitude is within the

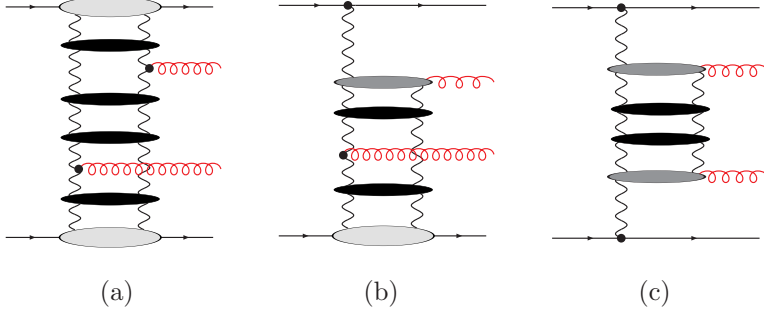


Figure 4.13: Contributions to the $2 \rightarrow 4$ production amplitude with positive (a) and mixed (b,c,d) signature. Explicitly we have the following signature configurations a: $(+, +, +)$, b: $(-, +, +)$, c: $(-, +, -)$, d: $(+, -, +)$.

LLA proportional to the sum of all five partial waves in Eq. (4.9). From the effective action we find within the LLA the following result

$$\mathcal{M}_{2 \rightarrow 4}^{(+,+,+)} = -2\pi s \int \frac{d\omega_1}{2\pi i} \int \frac{d\omega_2}{2\pi i} \int \frac{d\omega_3}{2\pi i} |s|^{\omega_3} |s_{012}|^{\omega_2 - \omega_3} |s_1|^{\omega_1 - \omega_2} \frac{e^{-i\pi\omega_3} - 1}{\sin \pi\omega_3} \times W_{(+,+,+)}(\omega_1, \omega_2, \omega_3; q_1, q_2, q_3) \quad (4.78)$$

where to leading accuracy the following identity can be shown to hold

$$\begin{aligned} |s|^{\omega_3} |s_{012}|^{\omega_2 - \omega_3} |s_1|^{\omega_1 - \omega_2} \frac{e^{-i\pi\omega_3} - 1}{\sin \pi\omega_3} &\simeq |s|^{\omega_2} |s_1|^{\omega_1 - \omega_2} |s_2|^{\omega_3 - \omega_2} \frac{e^{-i\pi\omega_2} - 1}{\sin \pi\omega_2} \\ &\simeq |s|^{\omega_1} |s_{123}|^{\omega_2 - \omega_1} |s_3|^{\omega_3 - \omega_2} \frac{e^{-i\pi\omega_1} - 1}{\sin \pi\omega_1}, \end{aligned} \quad (4.79)$$

and using further identities like

$$|s_{123}|^{\omega_2 - \omega_1} |s_3|^{\omega_3 - \omega_2} \simeq |s_{123}|^{\omega_3 - \omega_1} |s_2|^{\omega_2 - \omega_3}, \quad (4.80)$$

that equally hold with the LLA, it is easily shown that the energy dependence of Eq. (4.78) is in agreement with the leading terms of Eq. (4.9). The partial wave $W_{(+,+,+)}$ on the other hand can be obtained from Fig. 4.13, making use of the diagrammatic rules.

Next we turn to the signature configuration $(-, +, +)$, Fig. 4.13b. Within the LLA this amplitude is proportional to its discontinuity in s_{123} . For the analytic representation Eq. (4.9), it is hence to leading accuracy proportional to the sum of partial waves W_2 and W_4 . From the effective action we obtain

$$\mathcal{M}_{2 \rightarrow 4}^{(-,+,+)} = -2\pi s \int \frac{d\omega_1}{2\pi i} \int \frac{d\omega_2}{2\pi i} \int \frac{d\omega_3}{2\pi i} |s|^{\omega_1} |s_{123}|^{\omega_2 - \omega_1} |s_3|^{\omega_3 - \omega_1} \frac{e^{-i\pi\omega_2} - 1}{\sin \pi\omega_2} \times W_{(-,+,+)}(\omega_1, \omega_2, \omega_3; q_1, q_2, q_3), \quad (4.81)$$

where within the LLA

$$|s_{123}|^{\omega_2} |s_3|^{\omega_3 - \omega_1} \frac{e^{-i\pi\omega_2} - 1}{\sin \pi\omega_2} \simeq |s_{123}|^{\omega_3} |s_2|^{\omega_2 - \omega_3} \frac{e^{-i\pi\omega_3} - 1}{\sin \pi\omega_3}. \quad (4.82)$$

To the given level of accuracy, the energy dependence of the effective action is therefore found to be in accordance with the one of the analytic representation Eq. (4.9).

The signature configuration $(-, +, -)$, Fig. 4.13c, is proportional to its discontinuity in s_2 and therefore proportional to the sum of the partial waves W_3 and W_4 . From the effective action analysis we obtain

$$\mathcal{M}_{2 \rightarrow 4}^{(-,+,-)} = -2\pi s \int \frac{d\omega_1}{2\pi i} \int \frac{d\omega_2}{2\pi i} \int \frac{d\omega_3}{2\pi i} |s|^{\omega_1} |s_{123}|^{\omega_3 - \omega_1} |s_2|^{\omega_2 - \omega_3} \frac{e^{-i\pi\omega_2} - 1}{\sin \pi\omega_2} \times W_{(-,+,-)}(\omega_1, \omega_2, \omega_3; q_1, q_2, q_3), \quad (4.83)$$

while the LLA allows for the following manipulation

$$|s|^{\omega_1} |s_{123}|^{\omega_3 - \omega_1} |s_2|^{\omega_2 - \omega_3} \frac{e^{-i\pi\omega_2} - 1}{\sin \pi\omega_2} \simeq |s|^{\omega_3} |s_{012}|^{\omega_1 - \omega_3} |s_2|^{\omega_2 - \omega_1} \frac{e^{-i\pi\omega_2} - 1}{\sin \pi\omega_2}. \quad (4.84)$$

The partial wave $W_{(-,+,-)}$ is obtained with the help of the diagrammatic rules.

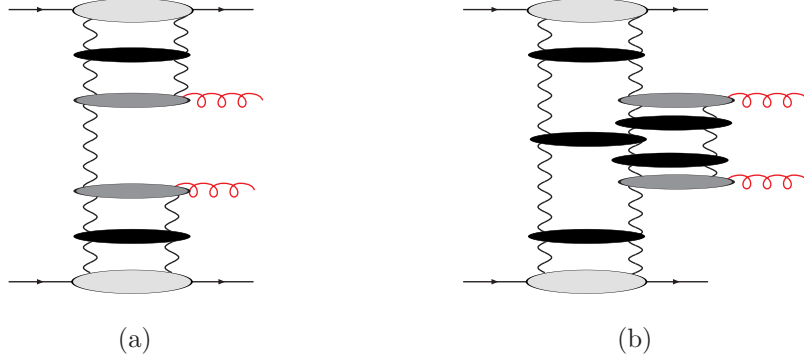


Figure 4.14: Graphs that contribute to the production amplitude with the signature configuration $(+,-,+)$

The production amplitude with the signature configuration $(+, -, +)$ on the other hand is of higher order. This appears from the analysis of both the effective action and the analytic representation. From latter we find that to leading accuracy the partial waves W_3 , W_4 and W_5 contribute, which can be obtained by taking the double-discontinuity in s_1 and s_3 (W_5) and in s and s_2 (W_3 , W_4). For the effective action, these contributions correspond to the diagrams in Fig. 4.14a and Fig. 4.14b respectively. Whereas Fig. 4.14a contains only states of two reggeized gluons and can in principle be constructed, Fig. 4.14b requires the exchange of a state of three reggeized gluons, which has not been addressed so far from the effective action. The description of these states within the effective will be addressed in the following chapter, where we however refer to the elastic amplitude as a reference process.

The same applies to the Regge-cut contributions for the signature configuration $(-, -, -)$, found in the analysis of [89], which has not been discovered in Sec. 4.2, as it is of higher order: Also this contribution requires within the effective action the state of three reggeized gluons.

4.4 Conclusion

In the present chapter the results of Cha.3 have been applied to the study of production amplitudes. The analysis of production amplitudes with negative signature revealed that the phase structure of the reggeized gluon, Eq.(3.29), must be taken with some care: The Reggeon-Particle-Reggeon vertex, which describes the production of a gluon, carries itself a inner phase structure. The phase structure of the complete amplitude is therefore only obtained correctly if simultaneously with the phase structure of the reggeized gluons, the inner phase structure of the production vertex is included. Within the LLA, only the leading part of the production vertex is included, which is real. Including then nevertheless the complete signature factor of the reggeized gluon, one finds simultaneous discontinuities in over-lapping channels which violate Steinmann-relations. For the final result, phases of the reggeized gluons should be therefore only trusted with the same amount of accuracy as the corresponding inner phases of production vertices are taken into account.

We then demonstrated by an explicit calculation that the 1-loop corrections to the production vertex yield the onset of the required corrections. In particular they could be shown to be in accordance with the analytic representation of the production amplitudes, which satisfy the Steinmann-relations by construction.

For the construction of production amplitudes with positive and mixed signature, the Reggeon-Particle-2Reggeon (RP2R) vertex has been determined. Together with the production vertex,

Eq.(4.12), the RP2R-vertex allowed for the construction of all signature configurations of the $2 \rightarrow 3$ and $2 \rightarrow 4$ production amplitude, apart from the configuration $(+, -, +)$ which requires information about the state of three-reggeized gluons. The basis for constructing amplitudes with states of more than two reggeized gluons will be laid in following chapter. There we will consider states of three and four reggeized gluons within the elastic scattering amplitude. The results can then be applied also to the construction of production amplitudes.

Chapter 5

Exchanges of $n > 2$ reggeized gluons in the elastic amplitude

In this chapter we aim to arrive on a description of states of $n > 2$ within the effective action. At the end of the previous chapter it turned out that in order to describe all signature configuration of n -particle production amplitudes within the effective action, knowledge about the states with more than two reggeized gluons is inevitable. Apart from the $(+, -, +)$ configuration of the $2 \rightarrow 4$ production amplitude, which requires the state of three reggeized gluons already at leading order, unitarity requires also the presence of the three-Reggeon-cut for the $(-, -, -)$ configuration. States with many reggeized gluons are generally connected with unitarity corrections and it is generally argued that inclusion of the exchange of an arbitrary high number of reggeized gluons yields unitarization of the BFKL-Pomeron.

The main goal of this chapter is to provide the necessary tools for the study of exchanges of more than two reggeized gluons within the effective action. As in the previous chapters, we will be mainly concerned with the issue of longitudinal integrations. In particular the subtraction mechanism for reggeized gluon loops, introduced in Cha. 3 is needed to be generalized and we determine the pole prescription for the higher induced vertices.

As a reference process we consider as in Cha. 3, elastic scattering of two quarks at high center of mass energies with exchange of three and four reggeized gluons. We then determine the coupling of three and four reggeized gluons to the quark. Apart from the interaction between the reggeized gluons themselves, the complete description of the state of three and four reggeized gluons requires vertices that describe transitions from one-to-three and two-to-four reggeized gluons respectively are included. Combining them with pairwise interactions between reggeized gluons, they can be shown to yield for the four reggeized gluon state in the overall color singlet the 2-4 reggeized gluon transition vertex of [35].

The outline of this chapter is the following: In Sec. 5.1 we determine the pole structure of induced vertices up to the third order. In Sec. 5.2 we discuss the quark-impact factor and propose a all order generalization of the subtraction scheme for the two reggeized gluon exchange in Sec. 3.2. In Sec. 5.3 we discuss the properties of transitions that change the number of reggeized gluons while in Sec.5.4 we compare our findings with the analysis of [35].

5.1 The pole prescription of induced vertices

In the following section we investigate more closely the pole structure of the induced vertices. In particular we will explicitly determine the pole structure for induced vertices up to the third order, while the formalism that is presented allows in principle also for the determination of the pole structure of induced vertices of arbitrary high order. For the exchange of up to four reggeized gluons, this pole structure is of two-fold need: It is needed for the proper definition of

the longitudinal integrations and for the higher induced vertices that occur as a building block of the reggeized gluon transition vertices.

5.1.1 The induced vertex of the first order

As preparation for the discussion of the pole structure of higher induced vertices, we briefly review the derivation of the pole structure of the induced vertex of the first order in Sec.3.1. There, the following pole prescription has been found by comparing the effective theory diagram with the underlying QCD-diagram and expanding the quark-propagators of the QCD-amplitude in the center of mass energy of the quark-2 gluon sub-amplitude $p_A^+ k^-$:

$$\frac{(t^{c_1} t^{c_2})_{AA'}}{-k^- + i\epsilon/p_A^+} + \frac{(t^{c_2} t^{c_1})_{AA'}}{k^- + i\epsilon/p_A^+}. \quad (5.1)$$

To arrive at the color structure of the induced vertex, Eq. (2.36), we further decomposed the products of $SU(N_c)$ generators, $t^{c_1} t^{c_2}$ and $t^{c_2} t^{c_1}$ into two terms, symmetric and anti-symmetric under exchange of the gluon color labels c_1 and c_2 , and identified the antisymmetric part with the induced vertex of the first order, Eq. (2.36). Note, that equally well we could have decided to decompose the color structure in a different way, as long as one of the elements would yield the commutator. It would have been this term that would have had determined the pole-prescription of the induced vertex instead. An alternative possible choice would have been for instance, to keep the combination $t^{c_1} t^{c_2}$, while the second term would have been rewritten as the first term plus the commutator. Such a choice has been used for instance in the analysis of QCD-amplitudes of [99, 100]. Since the pole structure of the subtraction terms changes simultaneously with the pole structure of the induced vertices, the overall result for the sum of all different contributions remains unchanged, while individual results alter. Taking a different choice for the decomposition of the color structure in Eq. (5.1) than the originally chosen symmetric/anti-symmetric decomposition, leads to a reggeized gluon without signature. The symmetric/anti-symmetric decomposition corresponds therefore at least at this level to the decomposition of the quark-2 gluon amplitude into positive and negative signature, where the part with negative signature is associated with the reggeized gluon.

For the effective action a different choice than the symmetric/anti-symmetric decomposition, has the further disadvantage that it leads to a dependence of the pole structure on the value of¹ p_A^+ , whereas with the symmetric/antisymmetric choice

$$f^{c_1 c_2 c} \frac{1}{-k^-} \equiv \frac{1}{2} \frac{f^{c_1 c_2 c}}{-k^- + i\epsilon/p_A^+} - \frac{1}{2} \frac{f^{c_1 c_2 c}}{k^- + i\epsilon/p_A^+} = f^{c_1 c_2 c} \frac{1}{2} \left(\frac{1}{k^- - i\epsilon} + \frac{1}{k^- + i\epsilon} \right), \quad (5.2)$$

the dependence on p_A^+ cancels. Such a dependence is unsatisfactory from a point of view of Regge-factorization. From a technical point of view, it would at least complicate the regularization proposed for the two reggeized gluon state in Sec. 3.2. Furthermore, with the $i\epsilon$ prescription of the pole independent of the particle to which the associated reggeized gluon couples, it is possible to determine the pole-prescription directly from the effective action.

To this end we recall that, in the effective action, induced vertices arise from the term

$$\mathcal{L}_{\text{ind}}^{\text{GR}} = A_{\pm}(v) \partial_{\sigma}^2 A_{\mp} \quad \text{with} \quad A_{\pm}(v) = v_{\pm} - g v_{\pm} \frac{1}{\partial_{\pm}} v_{\pm} + g^2 v_{\pm} \frac{1}{\partial_{\pm}} v_{\pm} \frac{1}{\partial_{\pm}} v_{\pm} + \dots \quad (5.3)$$

where $v_{\pm}(x) = -it^a v_{\pm}^a(x)$ and $A_{\pm}(x) = -it^a A_{\pm}^a(x)$ are matrices in color space. To give meaning to the operators $1/\partial_{\pm}$ at zero, it is necessary to introduce a prescription for these poles in the effective action. A possible choice is given by² $\partial_{\pm} \rightarrow \partial_{\pm} - \epsilon$, which agrees especially with Eq. (5.1)

¹The dependence of the individual terms in Eq. (5.1) corresponds to a special kind of a Mandelstam-Leibbrandt prescription [101–103], where the conjugated momentum is not as usually the plus-momentum of the gluon, k^+ , , but the plus-momentum of the quark, p_A^+ . Restricting to the planar part of scattering amplitudes, only the first term in Eq. (5.1) is present and a prescription of this kind is needed.

²Such choices can be also found in the literature, for instance in the context of soft-effective theories, see [64]

for $p_A^+ > 0$. In general, path-ordered exponents with such a pole-prescription are used to describe to leading accuracy the propagation of a highly energetic particle interacting in a soft-gluon field [104].

With the proposed prescription, we obtain from the effective action the following term for the first induced vertex

$$i\mathbf{q}^2 2 \left(\frac{\text{tr}(t^{a_1} t^{a_2} t^c)}{k_2^- + i\epsilon} + \frac{\text{tr}(t^{a_2} t^{a_1} t^c)}{k_1^- + i\epsilon} \right) n_{\nu_1}^- n_{\nu_2}^-, \quad (5.4)$$

with $k_2^- = -k_1^-$. In the above and also in the following we restrict for simplicity to $A_-(v)$. All results apply equally to $A_+(v)$ with the corresponding substitutions. As for Eq.(5.1), the color structure does not reduce to the commutator as long $\epsilon \neq 0$. It is therefore necessary to rewrite the color structure in a symmetric/anti-symmetric color basis and we find

$$q^2 \left[\frac{f^{a_1 a_2 c}}{2} \left(\frac{1}{k_1^- + i\epsilon} + \frac{1}{k_1^- - i\epsilon} \right) + \frac{d^{a_1 a_2 c}}{2} \text{sgn}(\epsilon) 2\pi \delta(k_1^-) \right] n_{\nu_1}^- n_{\nu_2}^-. \quad (5.5)$$

Due to the regularization of the pole, we therefore obtain a second color structure proportional to the symmetric structure constant $d^{a_1 a_2 c}$ for the induced vertex of the first order, which is not present in the original formulation, Eq. (2.36). At first it might seem plausible to include also the second, symmetric term into the definition of the induced vertices. It would describe a reggeized gluon with positive signature in addition to the reggeized gluon with negative signature. Furthermore, this term does not contribute for real-production amplitudes, as it is proportional to the delta-function. It therefore leads not to a contradiction with the derivation of the effective action. We shall nevertheless reject the possibility to include this term for the following four reasons:

- (i) Inclusion of such terms is physically not motivated: Starting from the quark-gluon amplitude as given for instance by Eq. (5.1), the physical idea behind induced vertices is to gather the most divergent part of the sub-amplitude that does not vanish for large values of the product $p_A^+ k^-$. This does not include contributions proportional to a delta-function.
- (ii) While the term proportional to the commutator is independent (up to normalization) of the precise representation of the gluon-fields, the symmetric part differs for different representations of the gluon-field. For the adjoint representation for instance, the symmetric term in Eq. (5.5) vanishes. Unlike the commutator it is therefore not always possible to extract such a term from an underlying QCD-amplitude³.
- (iii) The symmetric term depends on the sign of ϵ or, in terms of the underlying QCD amplitude Eq. (5.1), on the sign of the light-cone-momentum p_A^+ .
- (iv) Including symmetric terms, the effective action is no longer hermitian [105], while an hermitian action is required for a unitary S -matrix.

We therefore conclude that it is preferable to keep only terms with antisymmetric color structure while terms with symmetric color structure should be dropped for the effective action. With the substitution $\partial_\pm \rightarrow \partial_\pm - \epsilon$, the correct $i\epsilon$ -prescription arises therefore not immediately from the effective action, but it is necessary to add some further, external information. In particular, to obtain the correct pole prescription for the induced vertices, one should first use the pole prescription $\partial_\pm \rightarrow \partial_\pm - \epsilon$ for the poles in Eq. (5.3), then derive the induced vertices in momentum space, decompose the traces of generators in a suitable symmetric/anti-symmetric basis, drop all symmetric terms and identify the terms containing only commutators with the induced vertex.

It would be desirable to have a better prescription of the operators Eq. (5.3), that allows to obtain the correct pole-prescription directly from the effective action, without the need to drop any terms by hand. This can be obtained at least perturbatively by using the above recipe and then inserting

³That there exists indeed a dependence on the representation of the scattering particles has also been observed in [79]. There an additional contribution for scattering particles in the adjoint representation has been found, which is not present for the fundamental representation.

in the action the term that yields the obtained result. As far as the first induced vertex is concerned, it is straight-forward to give such a pole-prescription,

$$-gv_- \frac{1}{2} \left(\frac{1}{\partial_- - \epsilon} + \frac{1}{\partial_- + \epsilon} \right) v_- \partial_\sigma^2 A_\mp, \quad (5.6)$$

which yields immediately the correct induced vertex, without the need to drop any term. For future reference we then further introduce a function

$$g_1(k_1^-, k_2^-) = \frac{1}{2} \left(\frac{1}{k_1^- + i\epsilon} + \frac{1}{k_1^- - i\epsilon} \right) = \frac{1}{[k_1^-]} \quad \text{with} \quad k_1^- + k_2^- = 0, \quad (5.7)$$

where,

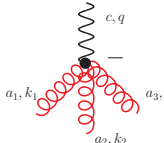
$$\frac{1}{[k^-]} = \frac{1}{2} \left(\frac{1}{k^- - i\epsilon} + \frac{1}{k^- + i\epsilon} \right), \quad (5.8)$$

is the Cauchy principal value, such that the induced vertex of the first order with pole-prescription is given by

$$\Delta_{\nu_1 \nu_2}^{a_1 a_2 c} = \mathbf{q}^2 g f^{a_1 a_2 c} g_1(k_1^-) n_{\nu_1}^- n_{\nu_2}^-. \quad (5.9)$$

5.1.2 The induced vertex of the second order

From the effective action without pole prescription the second induced vertex is given by



$$= \Delta_{a_1 a_2 a_3 c}^{\nu_1 \nu_2 \nu_3 +} = ig^2 \mathbf{q}^2 \left(\frac{f^{a_3 a_2 a} f^{a_1 a c}}{k_3^- k_1^-} + \frac{f^{a_3 a_1 a} f^{a_2 a c}}{k_3^- k_2^-} \right) (n^-)^{\nu_1} (n^-)^{\nu_2} (n^-)^{\nu_3}$$

$$k_1^- + k_2^- + k_3^- = 0. \quad (5.10)$$

As far the prescription of the poles is concerned, a first guess might be, that it is suitable to describe every single pole of the second induced vertex by a Cauchy principal value. However, such a choice needs to be rejected as it violates Bose-symmetry of the vertex. This is due to the fact the eikonal identity that applies for Cauchy principal values holds not in a purely algebraic sense, but yields an extra term proportional to two delta-functions (see also [103])

$$\frac{1}{[k_1^-][k_1^- + k_2^-]} + \frac{1}{[k_1^-][k_1^- + k_2^-]} = \frac{1}{[k_1^-][k_2^-]} + \pi^2 \delta(k_1^-) \delta(k_2^-). \quad (5.11)$$

It is therefore not possible to simple 'guess' the correct pole structure of the second induced vertex, but it needs to be derived explicitly, along the lines stated above. In particular, to derive the pole-prescription, we need to find an appropriate symmetry basis that generalizes the decomposition in commutator and anti-commutator of the previous paragraph. This basis needs to contain elements with a double-commutator, which then yield the color structure of the induced vertex Eq. (5.10). Furthermore to obtain a reggeized gluon with negative signature, it is desirable to find a prescription that is invariant under substitutions $\epsilon \rightarrow -\epsilon$. In the following we use a short-cut notation, which makes the underlying structure of the above expressions more apparent.

$$[1, 2] = [t^{a_1}, t^{a_2}] \quad (5.12)$$

represents the commutator of two generators with color indices a_1 and a_2 and

$$S_n(1 \dots n) = \frac{1}{n!} \sum_{i_1, \dots, i_n} t^{a_{i_1}} \dots t^{a_{i_n}} \quad (5.13)$$

with the sum over all permutations of the numbers $1, \dots, n$, yields symmetrization of n generators. In this notation, a suitable 'basis' is given by

$$[[3, 1], 2], \quad [[3, 2], 1], \quad S_2([1, 2]3), \quad S_2([1, 3]2), \quad S_2([2, 3]1), \quad S_3(123). \quad (5.14)$$

Here terms that do not contain commutators are maximally symmetrized. Note that Eq. (5.12) yields again a generator and therefore expressions like $S_2([1, 3]2)$ which contain symmetrization of commutators are well defined. In particular, in such a expressions, a commutator should be always dealt with like a single generator, for instance

$$S_2([1, 3]2) = \frac{1}{2} (t^{a_1} t^{a_3} t^{a_2} - t^{a_3} t^{a_1} t^{a_2} + t^{a_2} t^{a_1} t^{a_3} - t^{a_2} t^{a_3} t^{a_1}). \quad (5.15)$$

The set Eq. (5.14) contains then two double-anti-symmetric, three mixed-symmetric and one totally symmetric element. There exists also a third double-antisymmetric element $[[1, 2], 3]$, which can be expressed in terms of the other two by means of the Jacobi-identity. The above decomposition shares some properties with the usual Young-tableau decomposition, while the definition of anti-symmetrization differs in the present case.

To derive the pole prescription of the induced vertex of the second order, we start from the effective action with the following expression

$$g^2 v_- \frac{1}{\partial_- - \epsilon} v_- \frac{1}{\partial_- - \epsilon} v_- \partial_\sigma^2 A_+ \quad (5.16)$$

which yields

$$\begin{aligned} & -ig^2 2\mathbf{q}^2 n_{\nu_1}^- n_{\nu_2}^- n_{\nu_3}^- \\ & \left(\frac{\text{tr}(t^{a_1} t^{a_2} t^{a_3} t^c)}{(k_2^- + k_3^- + i\epsilon)(k_3^- + i\epsilon)} + \frac{\text{tr}(t^{a_2} t^{a_1} t^{a_3} t^c)}{(k_1^- + k_3^- + i\epsilon)(k_3^- + i\epsilon)} + \frac{\text{tr}(t^{a_1} t^{a_3} t^{a_2} t^c)}{(k_2^- + k_3^- + i\epsilon)(k_2^- + i\epsilon)} \right. \\ & \left. + \frac{\text{tr}(t^{a_3} t^{a_1} t^{a_2} t^c)}{(k_1^- + k_2^- + i\epsilon)(k_2^- + i\epsilon)} + \frac{\text{tr}(t^{a_3} t^{a_2} t^{a_1} t^c)}{(k_1^- + k_2^- + i\epsilon)(k_1^- + i\epsilon)} + \frac{\text{tr}(t^{a_2} t^{a_3} t^{a_1} t^c)}{(k_1^- + k_3^- + i\epsilon)(k_1^- + i\epsilon)} \right) \end{aligned} \quad (5.17)$$

with $k_1^- + k_2^- + k_3^- = 0$. Leaving aside for the moment the factor $-ig^2 2\mathbf{q}^2 n_{\nu_1}^- n_{\nu_2}^- n_{\nu_3}^-$ and also the projection on the color octet, $\text{tr}(\cdot t^c)$, where the dot represents any product of $SU(N_c)$ generators, we obtain for the basis Eq.(5.14) from Eq.(5.17)

$$\begin{aligned} & -\frac{1}{6} [[3, 1], 2] \left(\frac{2}{(k_3^- - i\epsilon)(k_1^- + i\epsilon)} + \frac{2}{(k_3^- + i\epsilon)(k_1^- - i\epsilon)} + \frac{1}{(k_2^- + i\epsilon)(k_3^- - i\epsilon)} \right. \\ & \left. + \frac{1}{(k_2^- - i\epsilon)(k_3^- + i\epsilon)} + \frac{1}{(k_1^- + i\epsilon)(k_2^- - i\epsilon)} + \frac{1}{(k_1^- - i\epsilon)(k_2^- + i\epsilon)} \right) \\ & -\frac{1}{6} [[3, 2], 1] \left(\frac{2}{(k_3^- - i\epsilon)(k_2^- + i\epsilon)} + \frac{2}{(k_3^- + i\epsilon)(k_2^- - i\epsilon)} + \frac{1}{(k_1^- + i\epsilon)(k_3^- - i\epsilon)} \right) \\ & \left. + \frac{1}{(k_1^- - i\epsilon)(k_3^- + i\epsilon)} + \frac{1}{(k_2^- + i\epsilon)(k_1^- - i\epsilon)} + \frac{1}{(k_2^- - i\epsilon)(k_1^- + i\epsilon)} \right) \\ & -\frac{1}{2} S_2([1, 2]3) \left(\frac{1}{(k_3^- - i\epsilon)(k_1^- + i\epsilon)} - \frac{1}{(k_3^- + i\epsilon)(k_1^- - i\epsilon)} + \frac{1}{(k_2^- - i\epsilon)(k_3^- + i\epsilon)} \right. \\ & \left. - \frac{1}{(k_2^- + i\epsilon)(k_3^- - i\epsilon)} + \frac{1}{(k_1^- + i\epsilon)(k_2^- - i\epsilon)} - \frac{1}{(k_1^- - i\epsilon)(k_2^- + i\epsilon)} \right) \\ & -\frac{1}{2} S_2([1, 3]2) \left(\frac{1}{(k_2^- - i\epsilon)(k_1^- + i\epsilon)} - \frac{1}{(k_2^- + i\epsilon)(k_1^- - i\epsilon)} + \frac{1}{(k_3^- - i\epsilon)(k_2^- + i\epsilon)} \right. \\ & \left. - \frac{1}{(k_3^- + i\epsilon)(k_2^- - i\epsilon)} + \frac{1}{(k_1^- + i\epsilon)(k_3^- - i\epsilon)} - \frac{1}{(k_1^- - i\epsilon)(k_3^- + i\epsilon)} \right) \end{aligned}$$

$$\begin{aligned}
& -\frac{1}{2}S_2([2,3]1) \left(\frac{1}{(k_3^- - i\epsilon)(k_1^- + i\epsilon)} - \frac{1}{(k_3^- + i\epsilon)(k_1^- - i\epsilon)} + \frac{1}{(k_2^- + i\epsilon)(k_3^- - i\epsilon)} \right. \\
& \quad \left. - \frac{1}{(k_2^- - i\epsilon)(k_3^- + i\epsilon)} + \frac{1}{(k_1^- - i\epsilon)(k_2^- + i\epsilon)} - \frac{1}{(k_1^- + i\epsilon)(k_2^- - i\epsilon)} \right) \\
& -S_3(123) \left(\frac{1}{(k_3^- - i\epsilon)(k_1^- + i\epsilon)} + \frac{1}{(k_3^- + i\epsilon)(k_1^- - i\epsilon)} + \frac{1}{(k_2^- - i\epsilon)(k_3^- + i\epsilon)} \right. \\
& \quad \left. + \frac{1}{(k_2^- + i\epsilon)(k_3^- - i\epsilon)} + \frac{1}{(k_1^- + i\epsilon)(k_2^- - i\epsilon)} + \frac{1}{(k_1^- - i\epsilon)(k_2^- + i\epsilon)} \right)
\end{aligned} \tag{5.18}$$

To obtain the induced vertices with pole-prescription, we drop all symmetric terms that come with an S_2 or an S_3 symbol and keep only the terms coming with double anti-symmetric structure, which yield the color structure of Eq.(5.10). Making use of the Jacobi-Identity, Bose-symmetry of the induced vertex is easily verified. The pole structure can further be simplified by means of the eikonal identity

$$\frac{1}{k_1^- + i\epsilon} \frac{1}{k_1^- + k_2^- + i\epsilon} + \frac{1}{k_2^- + i\epsilon} \frac{1}{k_1^- + k_2^- + i\epsilon} = \frac{1}{k_1^- + i\epsilon} \frac{1}{k_2^- + i\epsilon}, \tag{5.19}$$

which holds not only in a purely algebraic sense, but is with the above pole prescription also true in the sense of the theory of distributions [103], unlike the eikonal identity for poles with principal value prescription, Eq.(5.11). Evaluating commutators and adding the color-octet projection together with the common factor of Eq.(5.17), which altogether corresponds to the following substitution

$$\begin{aligned}
[[3, 1], 2] & \rightarrow -ig^2 \mathbf{q}^2 n_{\nu_1}^- n_{\nu_2}^- n_{\nu_3}^- f^{a_3 a_2 a} f^{a_1 a c}, \\
[[3, 2], 1] & \rightarrow -ig^2 \mathbf{q}^2 n_{\nu_1}^- n_{\nu_2}^- n_{\nu_3}^- f^{a_3 a_1 a} f^{a_2 a c},
\end{aligned} \tag{5.20}$$

we obtain for the second induced vertex from Eq. (5.18)

$$\Delta_{a_1 a_2 a_3 c}^{\nu_1 \nu_2 \nu_3 +} = -ig^2 \mathbf{q}^2 n_{\nu_1}^- n_{\nu_2}^- n_{\nu_3}^- [f^{a_3 a_2 a} f^{a_1 a c} g_2(k_3^-, k_2^-, k_1^-) + f^{a_3 a_1 a} f^{a_2 a c} g_2(k_3^-, k_1^-, k_2^-)], \tag{5.21}$$

where

$$g_2(k_3^-, k_1^-, k_2^-) = -\frac{1}{6} \left[\frac{1}{k_3^- - i\epsilon} \left(\frac{2}{k_2^- + i\epsilon} + \frac{1}{k_2^- - i\epsilon} \right) + \frac{1}{k_3^- + i\epsilon} \left(\frac{2}{k_2^- - i\epsilon} + \frac{1}{k_2^- + i\epsilon} \right) \right]. \tag{5.22}$$

It is then easily verified that Eq.(5.21) reduces to Eq. (2.37) in the limit $\epsilon = 0$. Eq.(5.21) can be further rewritten in a more symmetric way, making use of the identity,

$$\frac{1}{k^- + i\epsilon} - \frac{1}{k^- - i\epsilon} = -2\pi i \delta(k^-), \tag{5.23}$$

which leads to

$$g_2(k_3^-, k_1^-, k_2^-) = \left[\frac{-1}{[k_3^-][k_2^-]} - \frac{\pi^2}{3} \delta(k_2^-) \delta(k_3^-) \right]. \tag{5.24}$$

With Eq. (5.11), Bose-symmetry of Eq.(5.24) is easily proven. In particular, taking into account $k_1^- + k_2^- + k_3^- = 0$, we find

$$g_2(k_3^-, k_2^-, k_1^-) = -g_2(k_1^-, k_3^-, k_2^-) - g_2(k_3^-, k_1^-, k_2^-). \tag{5.25}$$

It is therefore possible to replace Eq.(5.16) in the effective action by

$$\begin{aligned}
& \frac{1}{6} \left[gv_- \left[\frac{1}{\partial_- - \epsilon} v_- \left(\frac{2}{\partial_- - \epsilon} + \frac{1}{\partial_- + \epsilon} \right) \right. \right. \\
& \quad \left. \left. + \frac{1}{\partial_- + \epsilon} v_- \left(\frac{2}{\partial_- + \epsilon} + \frac{1}{\partial_- - \epsilon} \right) \right] v_- \partial_\sigma^2 A_+ \right].
\end{aligned} \tag{5.26}$$

Every term proportional to a trace of four $SU(N_c)$ generators (as on the right hand side of Eq.(5.17)), will have the pole prescription of Eq.(5.21). This prescription on the other hand is equivalent to Eq.(5.24) and satisfies Eq.(5.25). Therefore, any symmetric term drops out, similar to the case, where the $i\epsilon$ -prescription is absent and we obtain Eq.(5.21) directly from the effective action.

5.1.3 The induced vertex of the third order

The derivation of the pole-prescription of the induced vertex of the third order follows the same lines: Again we will chose a symmetry basis built up of multiple commutators and symmetrization in the remaining color indices. However the number of terms increases rapidly with the number of gluons involved, and therefore the resulting expression become large. We therefore present in the following only the main results. In particular, the color basis now consists 24 terms and is given by

$$\begin{array}{l}
[[[4, 1], 2], 3] \\
[[[4, 1], 3], 2] \\
[[[4, 2], 1], 3] \\
[[[4, 2], 3], 1] \\
[[[4, 3], 1], 2] \\
[[[4, 3], 2], 1]
\end{array}
\left| \begin{array}{l}
S_2([1, 2], [3, 4]) \\
S_2([1, 3], [2, 4]) \\
S_2([1, 4], [2, 3])
\end{array} \right.
\left| \begin{array}{l}
S_2([[1, 2], 3]4) \\
S_2([[3, 2], 1]4) \\
S_2([[1, 2], 4]3) \\
S_2([[4, 2], 1]3) \\
S_2([[1, 3], 4]2) \\
S_2([[4, 3], 1]2) \\
S_2([[2, 3], 4]1) \\
S_2([[4, 3], 2]1)
\end{array} \right.
\left| \begin{array}{l}
S_3([1, 2]34) \\
S_3([1, 3]24) \\
S_3([1, 4]23) \\
S_3([2, 3]14) \\
S_3([2, 4]13) \\
S_3([3, 4]12)
\end{array} \right.
\left| S_4(1234) \right.
\tag{5.27}$$

As for the first and second induced vertex, we start from the effective action with the following expression

$$-g^3 v_- \frac{1}{\partial_- - \epsilon} v_- \frac{1}{\partial_- - \epsilon} v_- \frac{1}{\partial_- - \epsilon} v_- \partial_\sigma^2 A_+. \tag{5.28}$$

We obtain from this expression 24 terms that each come with four $SU(N_c)$ generators projected on the color octet by the projector $\text{tr}(.t^c)$ where every term corresponds to a specific ordering of the four generators. These products of generators can then be expressed in terms of the color basis Eq.(5.27), which similarly to Eq.(5.18), leads to certain combination of poles for every basis-element. In general, each of the 24 basis elements comes with 24 pole-terms. For the induced vertex of the third order, we then drop all symmetric terms, and keep only those proportional to a triple commutator, of the first column of Eq.(5.27). Making use of the eikonal identity, Eq.(5.19), we arrive at the following pole-prescription

$$\begin{aligned}
\Delta_{a_1 a_2 a_3 c}^{\nu_1 \nu_2 \nu_3 +} &= -g^3 \mathbf{q}^2 n_{\nu_1}^- n_{\nu_2}^- n_{\nu_3}^- n_{\nu_4}^- \times \\
&\left[f^{a_4 a_1 d_2} f^{d_2 a_3 d_1} f^{d_1 a_2 c} g_3(k_4^-, k_1^-, k_3^-, k_2^-) + f^{a_4 a_1 d_2} f^{d_2 a_2 d_1} f^{d_1 a_3 c} g_3(k_4^-, k_1^-, k_2^-, k_3^-) \right. \\
&+ f^{a_4 a_2 d_2} f^{d_2 a_1 d_1} f^{d_1 a_3 c} g_3(k_4^-, k_2^-, k_1^-, k_3^-) + f^{a_4 a_2 d_2} f^{d_2 a_3 d_1} f^{d_1 a_1 c} g_3(k_4^-, +k_2^-, k_3^-, k_1^-) \\
&\left. + f^{a_4 a_3 d_2} f^{d_2 a_1 d_1} f^{d_1 a_2 c} g_3(k_4^-, k_3^-, k_1^-, k_2^-) + f^{a_4 a_3 d_2} f^{d_2 a_2 d_1} f^{d_1 a_1 c} g_3(k_4^-, k_3^-, k_2^-, k_1^-) \right]
\end{aligned} \tag{5.29}$$

where the function $g_3(k_4^-, k_1^-, k_3^-, k_2^-)$ is defined as

$$\begin{aligned}
g_3(k_4^-, k_1^-, k_3^-, k_2^-) &= \\
&= -\frac{1}{12} \left\{ \frac{1}{k_4 + i\epsilon} \left[\frac{1}{k_2^- + i\epsilon} \left(\frac{1}{k_2^- + k_3^- + i\epsilon} + \frac{1}{k_2^- + k_3^- - i\epsilon} \right) + \frac{1}{k_2^- - i\epsilon} \left(\frac{3}{k_2^- + k_3^- - i\epsilon} + \frac{1}{k_2^- + k_3^- + i\epsilon} \right) \right] \right. \\
&\quad \left. \frac{1}{k_4 - i\epsilon} \left[\frac{1}{k_2^- - i\epsilon} \left(\frac{1}{k_2^- + k_3^- - i\epsilon} + \frac{1}{k_2^- + k_3^- + i\epsilon} \right) + \frac{1}{k_2^- + i\epsilon} \left(\frac{3}{k_2^- + k_3^- + i\epsilon} + \frac{1}{k_2^- + k_3^- - i\epsilon} \right) \right] \right\}
\end{aligned} \tag{5.30}$$

Similarly to Eq.(5.11), the function $g_3(k_2^-, k_2^- + k_3^-, k_2^-)$ can be written as combination of Cauchy-principal values and delta-functions:

$$g_3(k_4^-, k_1^-, k_3^-, k_2^-) = \left(\frac{-1}{[k_4^-][k_2^- + k_3^-][k_2^-]} - \frac{\pi^2}{3} \delta(k_2^-) \delta(k_3^-) \frac{-1}{[k_4^-]} \right. \\ \left. - \frac{\pi^2}{3} \delta(k_2^-) \delta(k_4^-) \frac{1}{[k_3^-]} - \frac{\pi^2}{3} \delta(k_2^- + k_3^-) \delta(k_4^-) \frac{1}{[k_2^-]} \right). \quad (5.31)$$

With Eq.(5.11) it can then be shown that identities like

$$g_3(k_4^-, k_1^-, k_3^-, k_2^-) = g_3(k_2^-, k_3^-, k_1^-, k_4^-) + g_3(k_2^-, k_3^-, k_4^-, k_1^-) + g_3(k_2^-, k_1^-, k_3^-, k_4^-) \quad (5.32)$$

hold, which allow to prove Bose-symmetry of the induced vertex with the above pole-prescription. Furthermore, due to those identities, we can state the pole-prescription for the induced vertex of the third order already at the action level, similar to the case of first and the second induced vertex; Eq.(5.28) is to replace by:

$$\frac{1}{12} \left[gv_- \left(\frac{1}{\partial_- - \epsilon} v_- \left[\frac{1}{\partial_- - \epsilon} v_- \left(\frac{1}{\partial_- - \epsilon} + \frac{1}{\partial_- + \epsilon} \right) \right. \right. \right. \\ \left. \left. \left. + \frac{1}{\partial_- + \epsilon} v_- \left(\frac{3}{\partial_- + \epsilon} + \frac{1}{\partial_- - \epsilon} \right) \right] \right) \right. \\ \left. \frac{1}{\partial_- + \epsilon} v_- \left[\frac{1}{\partial_- + \epsilon} v_- \left(\frac{1}{\partial_- + \epsilon} + \frac{1}{\partial_- - \epsilon} \right) \right. \right. \\ \left. \left. + \frac{1}{\partial_- - \epsilon} v_- \left(\frac{3}{\partial_- - \epsilon} + \frac{1}{\partial_- + \epsilon} \right) \right] v_- \partial_\sigma^2 A_+ \right]. \quad (5.33)$$

Obviously Eq.(5.30) and Eq.(5.31) follow a certain symmetry pattern and taking further into account Eq. Eq.(5.21) and Eq.(5.8) it seems plausible that there exists a general formula that fixes the poles of all induced vertices. This suggests that the poles of the induced vertex of the n th order with $n + 1$ gluons are described by the following function g

$$g(k_{n+1}^-, k_n^-, \dots, k_2^-) = \frac{1}{c_n} \left\{ \left(\frac{1}{k_{n+1} + i\epsilon} + \frac{1}{k_{n+1} - i\epsilon} \right) \left(\frac{1}{k_2^- + \dots + k_{n-1}^- + i\epsilon} + \frac{1}{k_2^- + \dots + k_{n-1}^- - i\epsilon} \right) \right. \\ \left. \times \dots \times \left(\frac{1}{k_2^- + i\epsilon} - \frac{1}{k_2^- - i\epsilon} \right) + \frac{n}{(k_{n+1} - i\epsilon)(k_2^- + \dots + k_{n-1}^- + i\epsilon)(k_2^- + \dots + k_{n-2}^- + i\epsilon) \dots (k_2^- + i\epsilon)} \right. \\ \left. \frac{n}{(k_{n+1} + i\epsilon)(k_2^- + \dots + k_{n-1}^- - i\epsilon)(k_2^- + \dots + k_{n-2}^- - i\epsilon) \dots (k_2^- - i\epsilon)} \right\}, \quad (5.34)$$

where

$$c_n = 2^n + 2(n - 1) \quad \text{with} \quad c_1 = 2, c_2 = 6, c_3 = 12. \quad (5.35)$$

The above formula is in accordance with the induced vertices of the first, second and third order. Whether this function really yields the correct pole structure for the induced vertex of the fifth order, for instance, and whether it yields for a general induced vertex Bose-symmetry remains however to be verified.

5.2 Quark-impact factors and subtraction terms

In the present section we begin our study of the elastic quark-quark scattering amplitude where the interaction of the quarks involves the exchange of three and four reggeized gluons in the t -channel.



Figure 5.1: Typical diagrams for the exchange of three (a) and four (b) reggeized gluons. In both cases, longitudinal integrations factorize, in analogy to the exchange of two reggeized gluons

5.2.1 The quark-impact factor with three gluons

To leading order in g , the state of three reggeized gluons appears for the first time with diagrams like Fig. 5.1a. Similar to the exchange of two reggeized gluons, the longitudinal integrals can be factorized between the two scattering quarks and it is therefore sufficient to consider for the longitudinal integral the impact factor of the quark alone. The Born-amplitudes with exchange of three reggeized gluons is therefore given by the following convolution

$$\mathcal{M}_{2 \rightarrow 2}^{\text{B|3R}} = \frac{2(2\pi)^2}{3!} p_A^+ p_B^- A_{(3;0)}^{a_1 a_2 a_3}(\mathbf{k}_1, \mathbf{k}_2, \mathbf{k}_3) A_{(3;0)}^{a_1 a_2 a_3}(\mathbf{k}_1, \mathbf{k}_2, \mathbf{k}_3). \quad (5.36)$$

The convolution symbol is defined to contain both transverse integrals and the transverse propagators of the reggeized gluons,

$$\otimes_{\mathbf{k}_{\{123\}}} = \int \frac{d^2 \mathbf{k}_1}{(2\pi)^3} \int \frac{d^2 \mathbf{k}_2}{(2\pi)^3} \frac{1}{\mathbf{k}_1^2 \mathbf{k}_2^2 \mathbf{k}_3^2}, \quad (5.37)$$

with the constraint $\mathbf{k}_1 + \mathbf{k}_2 + \mathbf{k}_3 = \mathbf{q}$ implied. The factor $1/3!$ is a symmetry factor, while the dependence of the impact factor on the external color labels of the quarks has been suppressed in our notation. As the impact factors can be shown not to depend on p_A^+ and p_B^- and are therefore independent of s , we note that the amplitude Eq. (5.52) is real and carries negative signature. This is expected, as we consider the exchange of a state of three reggeized gluons, which has negative signature itself. Signature of a Regge-cut is given by the product of signature of contributing Regge-poles. The 3-gluon quark impact factors is then obtained from the following integral:

$$\begin{aligned} iA_{AA',(3;0)}^{a_1 a_2 a_3}(\mathbf{k}_1, \mathbf{k}_2, \mathbf{k}_3) = & (ig)^3 \int \frac{d\mu_1}{(-2\pi i)} \int \frac{d\mu_2}{(-2\pi i)} \left[(t^{a_1} t^{a_2} t^{a_3})_{AA'} F_3(p_A, p'_A; k_1, k_2, k_3) \right. \\ & + (t^{a_2} t^{a_1} t^{a_3})_{AA'} F_3(p_A, p'_A; k_2, k_1, k_3) + (t^{a_1} t^{a_3} t^{a_2})_{AA'} F_3(p_A, p'_A; k_1, k_3, k_2) \\ & + (t^{a_3} t^{a_1} t^{a_2})_{AA'} F_3(p_A, p'_A; k_3, k_1, k_2) + (t^{a_2} t^{a_3} t^{a_1})_{AA'} F_3(p_A, p'_A; k_2, k_3, k_1) \\ & \left. + (t^{a_3} t^{a_2} t^{a_1})_{AA'} F_3(p_A, p'_A; k_3, k_2, k_1) \right], \end{aligned} \quad (5.38)$$

with

$$F_3(p_A, p'_A; k_1, k_2, k_3) = \frac{1}{(\mu_1 + p_A^+ p_A^- - (\mathbf{p}_A - \mathbf{k}_1)^2 - m_A^2 + i\epsilon)(\mu_1 + \mu_2 + p_A^+ p_A^- - (\mathbf{p}_A - \mathbf{k}_1 - \mathbf{k}_2)^2 - m_A^2 + i\epsilon)}. \quad (5.39)$$

In Eq. (5.39) we defined, similar to Sec.3.2. $\mu_i = -p_A^+ k_i^-$ with $i = 1, 2, 3$ with the constraint $\mu_1 + \mu_2 + \mu_3 = 0$. We want to note here that the statement concerning signature of the state of three reggeized gluons, can be immediately connected to the variable change $\mu_i = -p_A^+ k_i^-$. Whereas for the state of two reggeized gluons, with only one integral over k^- , the variable change yields a Jacobian factor $1/|p_A^+|$, for three reggeized gluons, the Jacobian is $1/(p_A^+)^2$ instead. While corresponding factors in the numerator lead always to an amplitude proportional to s , the precise

structure of the Jacobian factors in the denominator determines the behavior of the amplitude under the substitution $s \rightarrow -s$ and hence its signature. We further note that the above function F_3 is more general than needed for the determination of the quark-impact factor. For instance for the quark-impact factor the transverse quark-momentum is zero, $\mathbf{p}_A = 0$, and $p_A^+ p_A^- = m_A^2$ due to on-shellness of the quarks and cancels with the corresponding term. Later we shall encounter examples which require the general form of F_3 , while the integral over the μ_i can be treated in complete analogy to the present case. Actually, as far as the evaluation of the integral over μ_i is concerned, we are mainly interested in the μ_i -dependence and it is therefore convenient to define quantities

$$\begin{aligned} m_i^2 &= -p_A^+ p_A^- + (\mathbf{p}_A - \mathbf{k}_i)^2 - m_A^2 \\ m_{ij}^2 &= -p_A^+ p_A^- + (\mathbf{p}_A - \mathbf{k}_i - \mathbf{k}_j)^2 - m_A^2 \\ m_{ijk}^2 &= -p_A^+ p_A^- + (\mathbf{p}_A - \mathbf{k}_i - \mathbf{k}_j - \mathbf{k}_k)^2 - m_A^2 \quad \text{etc.} \end{aligned} \quad (5.40)$$

that gather the (for the moment) redundant information such that

$$F_3(p_A, p_A'; k_1, k_2, k_3) = \frac{1}{(\mu_1 - m_1^2 + i\epsilon)(\mu_1 + \mu_2 - m_{12}^2 + i\epsilon)} \quad (5.41)$$

We further note that F_3 contains only contributions due to the direct coupling of the reggeized gluons to the quark and no contributions due to subtraction terms are included at this stage. Attempting a straight forward integration of F_3 over μ_1 and μ_2 one realizes soon that this integrals are not well-defined: Starting with the integration over μ_1 , the integral is convergent and yields zero result, as all singularities lie on same side of the integration contour. Starting with μ_2 the integral turns out to be divergent and cannot be evaluated. Changing furthermore integrations variables from μ_2 to $\mu_3 = -\mu_1 - \mu_2$, also the first integral turns out to be divergent and can no longer be calculated. It is however well known that integrals like Eq. (5.38) can give nevertheless a meaningful result from the QED-limit, where all $SU(N_c)$ -generators are replaced by a unit matrix. This allows for cancellation of all singularities between individual terms. In QED, this is known as the 'eikonal formula'(see for instance [106] and references therein) and it can be demonstrated that the integral over the sum of all terms leads to a finite result.

In QCD, on the other hand, such a cancellation of divergences between individual terms is prohibited by the color structure of the individual terms. It is therefore necessary to find a different solution to the problem. An analogous problem was already present for the state of two reggeized gluons in Sec.3.2. In that case, the expression corresponding to the above F_3 is given by

$$F_2(k_1, k_2) = \frac{1}{\mu_1 - m_1^2 + i\epsilon}. \quad (5.42)$$

with m_1^2 defined by Eq. (5.40). It is then possible to decompose this function further,

$$F_2(k_1, k_2) = F_2^R(k_1, k_2) + g_1(\mu_1, \mu_2), \quad (5.43)$$

where

$$F_2^R(k_1, k_2) = \frac{1}{2} \left(\frac{1}{\mu_1 + i\epsilon} + \frac{1}{\mu_1 - i\epsilon} \right) \frac{m_1^2}{\mu_1 - m_1^2 + i\epsilon}, \quad (5.44)$$

yields a convergent integrand in μ_1 , while the divergent part is contained in the function $g_1(\mu_1)$, which is the pole part of the first induced vertex, Eq.(5.7). Making use of a subtraction graph, the function $g_1(\mu_1, \mu_2)$ in Eq. (5.43) is canceled and one is left with the convergent integral over F_2^R .

So far the subtraction terms have been obtained from the diagram, where the state of two reggeized gluons arises from a direct decay of a single reggeized gluon into two gluons, by means of an induced vertex (compare Fig. 3.12 and Fig. 4.10e). This term was then subtracted from the original expression. As we will see in short, also for F_3 the divergent parts of the integrand can be isolated and removed by means of corresponding subtraction terms. However in that case it becomes rather uncomfortable to first determine all possible direct couplings of reggeized gluons

to each other and then to subtract them in the appropriate way. It seems therefore advisable to supplement the effective Lagrangian by a subtraction term. It generates these subtraction diagrams automatically and the correct choice of sign is implemented automatically. Furthermore, this term also allows to remove the direct couplings of the reggeized gluons to each other by induced vertices, as they are now meaningless⁴. The term to be added to the Lagrangian is given by

$$\mathcal{L}_{\text{subtract}}(A_+, A_-) = -2\text{tr}(A_+(A_+) - A_+)\partial_\sigma^2 A_- - 2\text{tr}(A_-(A_-) - A_-)\partial_\sigma^2 A_+, \quad (5.45)$$

with

$$A_\pm(A_\pm) = -\frac{1}{g}\partial_\pm U(A_\pm) = -\text{tr}\frac{1}{g}\partial_\pm \mathcal{P} \exp\left(-\frac{1}{2}g \int_{-\infty}^{x^\pm} dx'^\pm A_\pm(x')\right). \quad (5.46)$$

The complete effective action then reads

$$S_{\text{eff}} = \int d^4x [\mathcal{L}_{\text{QCD}}(v_\mu, \psi) + \mathcal{L}_{\text{ind}}(v_\pm, A_\pm) + \mathcal{L}_{\text{subtract}}(A_+, A_-)]. \quad (5.47)$$

As this term only depends on the reggeized gluon fields, it does not contribute to the tree-diagrams of the production amplitudes in the Quasi-Multi-Regge-Kinematics and it is therefore not in conflict with the original formulation of the effective action. The resulting subtraction diagrams then



Figure 5.2: The two reggeized gluon impact factor is given as the sum of the direct couplings of the two reggeized gluons to the quark, minus the subtraction graph, integrated over $\mu_1 = -p_A^+ k_1^-$.

remove the direct couplings of reggeized gluons by induced vertices and parts of the particle- n -reggeized gluons amplitudes, that are already contained in the induced vertices and which would lead otherwise to a double-counting of parts of the underlying QCD-diagrams. We therefore remove with this term two different contribution which explains the overall factor of two in Eq.(5.45).

For the two-reggeized gluon impact factor, all contributing diagrams are then given in Fig.5.2. Note that Eq. (5.45) already contains the minus sign needed for the subtraction and therefore the subtraction graphs appear in Fig.5.2 with a relative plus. The diagram with direct coupling of three reggeized gluons denotes the subtraction term. Direct coupling of a reggeized gluon by an induced vertex on the other hand are from now understood to be removed from the effective action by the subtraction terms and appear no longer.

For the three-reggeized-gluon impact-factor, the relevant graphs, including subtraction diagrams are depicted in Fig. 5.3, where we used the two-reggeized gluon impact factor, Fig. 5.2, to compactify the representation.

To evaluate the integrations in Eq. (5.38) one can use for the function F_3 the following decomposition

$$F_3(k_1, k_2, k_3) = F_3^R(k_1, k_2, k_3) + g_2(\mu_1, \mu_2, \mu_3) F_2^R(k_1, k_2 + k_3)g_1(\mu_1 + \mu_2, \mu_3) + F_2^R(k_1 + k_2, k_3)g_1(\mu_1, \mu_2 + \mu_3), \quad (5.48)$$

with the regularized F_3 -function

$$F_3^R(k_1, k_2, k_3) = \frac{m_1^2 m_{12}^2}{(\mu_1 - m_1^2 + i\epsilon)(\mu_1 + \mu_2 - m_{12}^2 + i\epsilon)} \times \frac{1}{6} \left[\frac{1}{\mu_1 + i\epsilon} \left(\frac{2}{\mu_1 + \mu_2 - i\epsilon} + \frac{1}{\mu_1 + \mu_2 + i\epsilon} \right) + \frac{1}{\mu_1 - i\epsilon} \left(\frac{2}{\mu_1 + \mu_2 + i\epsilon} + \frac{1}{\mu_1 + \mu_2 - i\epsilon} \right) \right], \quad (5.49)$$

⁴It has been thought that those terms might be needed for more complicated processes, like the six-point-amplitude for instance. So far however we could not encounter any need for those transitions in any amplitude studied by us so far and we therefore suggest to remove these terms from the Lagrangian. Indeed we believe that those terms would instead lead to an over-counting which could be only cured by introducing another cut-off, which to our understanding is not necessary.

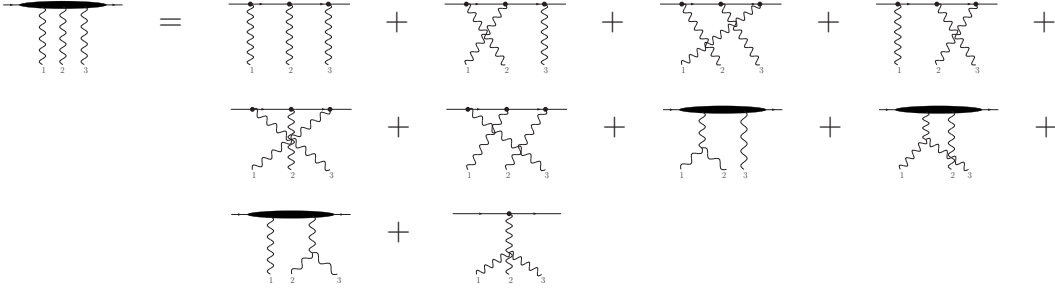


Figure 5.3: Diagrams that contribute to the three reggeized gluon quark-impact-factor. For the sum of the subtraction graphs, we used the two-reggeized gluon to compactify the presentation.

where we suppressed in our notation the dependence of F_3 on p_A, p'_A . For all terms in Eq. (5.48) that come with a function g_2 or g_3 , it can be demonstrated that the integral over μ_1 and μ_2 yields zero result if these terms are combined with the subtraction diagrams. The integral over F_3^R on the other hand is convergent,

$$\int \frac{d\mu_1}{(-2\pi i)} \int \frac{d\mu_2}{(-2\pi i)} F_3^R(k_1, k_2, k_3) = \frac{1}{6}. \quad (5.50)$$

We obtain hence for the quark-impact-factor

$$iA_{AA',(3;0)}^{a_1 a_2 a_3}(\mathbf{k}_1, \mathbf{k}_2, \mathbf{k}_3) = (ig)^3 \frac{1}{3!} \sum_{i_1 \dots i_3} t^{a_{i_1}} t^{a_{i_2}} t^{a_{i_3}}, \quad (5.51)$$

where the sum is over all permutations of numbers $1, \dots, 3$. An important check on the correctness of this result is given by the QED-limit, where all $SU(N_c)$ -generators are replaced by 1, which can easily be verified to be fulfilled.

5.2.2 The quark-impact factor with four gluons

The determination of the quark-impact factor follows a similar scheme: Starting from

$$\mathcal{M}_{2 \rightarrow 2}^{\text{B|4R}} = -i \frac{2(2\pi)^3}{4!} |p_A^+| |p_B^-| A_{(4;0)}^{a_1 a_2 a_3 a_4}(\mathbf{k}_1, \mathbf{k}_2, \mathbf{k}_3, \mathbf{k}_4) \otimes_{\mathbf{k}_{1234}} A_{(4;0)}^{a_1 a_2 a_3 a_4}(\mathbf{k}_1, \mathbf{k}_2, \mathbf{k}_3, \mathbf{k}_4), \quad (5.52)$$

where the convolution symbol is defined as

$$\otimes_{\mathbf{k}_{1234}} = \int \frac{d^2 \mathbf{k}_1}{(2\pi)^3} \int \frac{d^2 \mathbf{k}_2}{(2\pi)^3} \int \frac{d^2 \mathbf{k}_3}{(2\pi)^3} \frac{1}{\mathbf{k}_1^2 \mathbf{k}_2^2 \mathbf{k}_3^2 \mathbf{k}_4^2}, \quad (5.53)$$

with the constraint $\mathbf{k}_1 + \dots + \mathbf{k}_4 = \mathbf{q}$. As appropriate for the state of four reggeized gluons we observe that the above amplitude carries positive signature. The four gluon impact factor results from the following integral,

$$A_{AA',(3;0)}^{a_1 a_2 a_3}(\mathbf{k}_1, \mathbf{k}_2, \mathbf{k}_3) = (ig)^4 \int \frac{d\mu_1}{(-2\pi i)} \int \frac{d\mu_2}{(-2\pi i)} \int \frac{d\mu_3}{(-2\pi i)} \sum_{i_1, \dots, i_4} (t^{a_{i_1}} t^{a_{i_2}} t^{a_{i_3}} t^{a_{i_4}})_{AA'} [F_4(k_{i_1}, k_{i_2}, k_{i_3}, k_{i_4}) + F_4^S(k_{i_1}, k_{i_2}, k_{i_3}, k_{i_4})], \quad (5.54)$$

where the sum is over all permutations of the numbers $1, \dots, 4$. The function F_4 is defined as

$$F_4(p_A, p'_A; k_1, k_2, k_3, k_4) = \frac{1}{\mu_1 - m_1^2 + i\epsilon} \frac{1}{\mu_1 + \mu_2 - m_{12}^2 + i\epsilon} \frac{1}{\mu_1 + \mu_2 + \mu_3 - m_{123}^2 + i\epsilon}, \quad (5.55)$$

and contains all contributions due to the direct coupling of the reggeized gluon to the quark. F_4^S on the other hand contains all contributions that arise due to the presence of the subtraction diagrams and we defined as previously $\mu_i = -p_A^+ k_i^-$ with $i = 1, \dots, 4$ and $\sum_{i=1}^4 \mu_i = 0$.

Similarly to F_3 , the function F_4 can be decomposed into a convergent part F_4^R and parts in which the divergent contributions are gathered:

$$\begin{aligned}
F_4(k_1, k_2, k_3, k_4) &= F_4^R(1, 2, 3, 3) + g_4(1, 2, 3, 4) \\
&+ F_3^R(1, 2, 34)g_1(123, 4) + F_3^R(1, 23, 4)g_1(12, 34) + F_3^R(12, 3, 4)g_1(1, 234) \\
&+ F_2^R(123, 4)g_2(1, 2, 3) + F_2^R(1, 234)g_2(2, 3, 4) + F_2^R(12, 34)g_1(1, 234)g_1(123, 4).
\end{aligned} \tag{5.56}$$

where we introduced the following short-cut notation

$$F_3^R(12, 3, 4) = F_3^R(k_1 + k_2, k_3, k_4) \quad g(1, 234) = g_1(\mu_1, \mu_2 + \mu_3 + \mu_4) \tag{5.57}$$

where a string of numbers corresponds to the sum of the momenta with the corresponding indices. The convergent contribution is given by

$$\begin{aligned}
F_4^R(k_1, k_2, k_3, k_4) &= \frac{1}{24} \\
&\left[\left(\frac{4}{\mu_1 - m_1^2 + i\epsilon} - \frac{1}{\mu_1 - i\epsilon} - \frac{3}{\mu_1 + i\epsilon} \right) \left(\frac{1}{\mu_1 + \mu_2 - m_{12}^2 + i\epsilon} - \frac{1}{\mu_1 + \mu_2 - i\epsilon} \right) \right. \\
&\left(\frac{1}{-\mu_4 - m_{123}^2 + i\epsilon} + \frac{1}{\mu_4 + i\epsilon} \right) \\
&+ \left(\frac{4}{\mu_1 - m_1^2 + i\epsilon} - \frac{1}{\mu_1 + i\epsilon} - \frac{3}{\mu_1 - i\epsilon} \right) \left(\frac{1}{\mu_1 + \mu_2 - m_{12}^2 + i\epsilon} - \frac{1}{\mu_1 + \mu_2 + i\epsilon} \right) \\
&\left(\frac{1}{-\mu_4 - m_{123}^2 + i\epsilon} + \frac{1}{\mu_4 - i\epsilon} \right) \\
&+ \left(\frac{8}{\mu_1 - m_1^2 + i\epsilon} - \frac{5}{\mu_1 - i\epsilon} - \frac{3}{\mu_1 + i\epsilon} \right) \left(\frac{1}{\mu_1 + \mu_2 - m_{12}^2 + i\epsilon} - \frac{1}{\mu_1 + \mu_2 + i\epsilon} \right) \\
&\left(\frac{1}{-\mu_4 - m_{123}^2 + i\epsilon} + \frac{1}{\mu_4 + i\epsilon} \right) \\
&+ \left(\frac{8}{\mu_1 - m_1^2 + i\epsilon} - \frac{5}{\mu_1 + i\epsilon} - \frac{3}{\mu_1 - i\epsilon} \right) \left(\frac{1}{\mu_1 + \mu_2 - m_{12}^2 + i\epsilon} - \frac{1}{\mu_1 + \mu_2 - i\epsilon} \right) \\
&\left. \left(\frac{1}{-\mu_4 - m_{123}^2 + i\epsilon} + \frac{1}{\mu_4 - i\epsilon} \right) \right].
\end{aligned} \tag{5.58}$$

The integral over divergent parts of Eq.(5.56), which is contained in the functions g_i , $i = 1, 2, 3$, vanishes, when combined with the contributions from subtraction diagrams F_4^S . The integral over F_4^R yields on the other hand the following result

$$\int \frac{d\mu_1}{(-2\pi i)} \int \frac{d\mu_2}{(-2\pi i)} \int \frac{d\mu_3}{(-2\pi i)} F_4^R(k_1, k_2, k_3, k_4) = \frac{1}{24}, \tag{5.59}$$

and the four gluon quark-impact factor is given by

$$A_{AA',(4;0)}^{a_1 a_2 a_3}(\mathbf{k}_1, \mathbf{k}_2, \mathbf{k}_3) = g^4 \frac{1}{4!} \sum_{i_1 \dots i_4} t^{a_{i_1}} t^{a_{i_2}} t^{a_{i_3}} t^{a_{i_4}}, \tag{5.60}$$

where the sum is over all permutations of numbers $1, \dots, 4$. Again, taking the QED-limit, $t^{a_i} \rightarrow 1$, we find coincidence of the above result with the QED-'eikonal-formula'.

5.3 Number changing Reggeon transition kernels

Compared to the exchange of a single reggeized gluon, with negative signature, and the state of two-reggeized gluons, with positive signature, states of three and four reggeized gluons are suppressed by a relative factor of g^2 compared to the corresponding leading part. Resumming therefore loop corrections to the exchange of three and four reggeized gluons that are maximally enhanced by

logarithms in the center of mass energy \sqrt{s} , we are therefore strictly speaking working within Generalized LLA (GLLA) as defined in [33,38], where all loop-corrections are resummed that are enhanced by a maximal power of logarithms in s . One part of the corrections is given by the pairwise interaction of the reggeized gluons by a two-to-two kernel, as derived in Sec.3.2, which are known as BKP-corrections [33,34]. Apart from them, a complete description of the state of $n > 2$ reggeized gluons within the GLLA requires to include transition vertices. In the present case these are transitions from one-to-three and two-to-four reggeized gluons. Transitions from one-to-two and two-to-three are on the other hand not allowed by signature conservation [5]. In the following we will see that signature conservation is for the elastic amplitude satisfied automatically and is not needed to be imposed as an external constraint.

5.3.1 The transition of 1-2 and 1-3 reggeized gluons

As far as the description of the relevant longitudinal integrations is concerned, transitions from one to two and one to three reggeized gluons share many features. In the following we restrict then to the case where a single reggeized gluon, coming from the quark A, couples to two and three reggeized gluons respectively, which connected to the quark B, see also Fig.5.4 and Fig.5.5. All other cases can then be easily obtained from this expression.

Both for the one-to-two and the one-to-three transitions, the reggeized gluons couple to each other by a gluon loop, similar to the central rapidity diagram of Sec. 3.1 that yields the gluon trajectory function. Apart from the coupling of the 'upper' to the 'lower' reggeized gluons by a gluon-loop, there occur also various subtraction diagrams. As far as integrations over longitudinal momenta

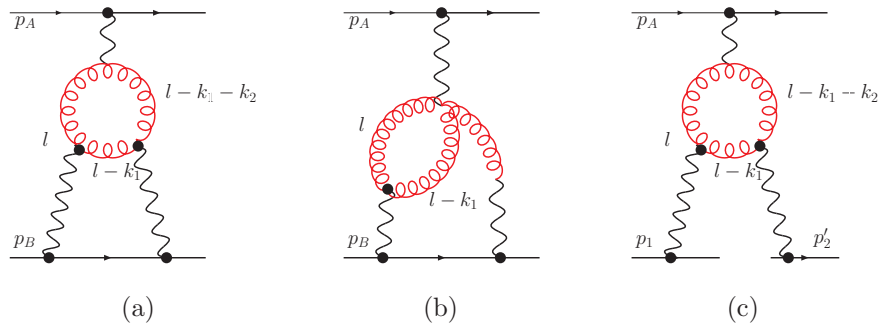


Figure 5.4: Diagrams with an induced vertex of the first (a) and the second (b) order that contribute to the 1-2 transition. While the 1-2 transition has to vanish within the elastic amplitude, it might contribute to the triple-Regge-limit of the 6-point amplitude (c).

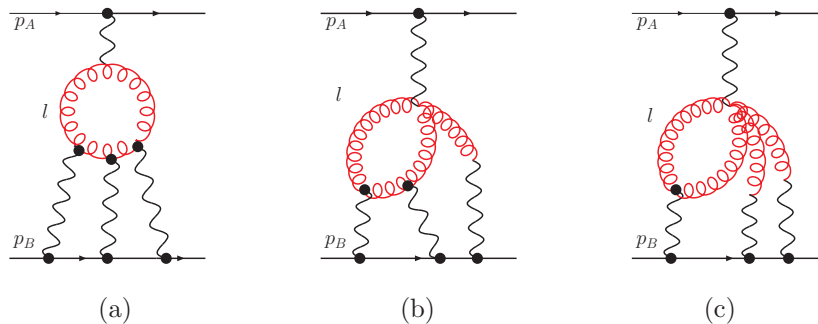


Figure 5.5: Diagrams with an induced vertex of the first (a), the second (b) and the third order (c) that contribute to the 1-3 transition.

are concerned, we have as usual the constraint, that every 4-point sub-amplitude, where the interaction is mediated by a reggeized gluon, requires a large center of mass energy. This constraint

is imposed by the usual Mellin integrals. They further allow to include due to reggeization of the gluon and corrections to the state of two and three reggeized gluon respectively in an easy and straight-forward way LLA-corrections. As far as the upper reggeized gluon is concerned, the description is identical to the case of the gluon trajectory function in Sec. 3.1. The case, where the reggeized gluon couples to the gluon loop by an induced vertex of higher order, as in Fig. 5.4b and Fig. 5.5b-c, requires however special care. There, the reggeized gluon is seemingly part of a 5- or a 6-point sub-amplitude and not of a 4-point amplitude. We follow also in the following the solution proposed in Sec.4.2, where a similar problem occurred. The natural choice to define the relevant 4-point-amplitude is given by imposing the constraint on the gluon momenta that enter the gluon-loop: In the essential region of integration of the gluon-loop, loop momenta are close to the mass-shell and in this sense, the constraint on the center-of-mass energy can be related to a corresponding constraint on the rapidity-variable. The gluons that do not enter the gluon loop, on the other hand, couple directly to reggeized gluons and are therefore generally off-shell and do not impose any constraint on rapidity. As far as the correct choice of the momenta inside the loop is concerned, we recall from Sec.4.2 that it is always possible to state higher induced vertices in a form, that there is always only one pole that contains the loop momenta and it is then this pole-momentum that should be used to construct the corresponding center-of-mass energy.

For the lower reggeized gluons, one has to distinguish between the case where only one reggeized gluon couples to the gluon-loop from below, as in Fig. 5.4b and Fig. 5.5c, and the case where a state of two or three reggeized gluons couples to the gluon-loop as in Fig. 5.4a and Fig. 5.5a-b. While in the former case we proceed in the same way as for the gluon trajectory, Sec. 3.1, in the latter case we combine the phases of the individual reggeized gluons, making repeatedly use of Eq. (3.66).

For the general evaluation of the diagrams we note that there occurs a large amount of cancellations between individual diagrams, which we partly trace back to identities between the induced vertices like Eq. (2.26). In particular it seems to be possible to find a general argument related to gauge invariance, that allows to exclude certain contributions from the very beginning which would facilitate the calculations considerably. Unfortunately, such a general rule has not been found yet. Nevertheless it seems advisable to achieve as many cancellations as possible between the individual diagrams, which in particular cancels certain divergent parts and to start only after-wards the evaluation of the integrals.

As a next step we evaluate the longitudinal part of the reggeized-gluon-loop-integral, which can be attributed to the transition vertex: With the loop momenta of the gluon loop denoted by l and the loop momenta of the reggeized gluon loop by k_i where $i = 1$ for the one-to-two transition and $i = 1, 2$ for the one-to-three transition (see Fig. 5.4 and Fig. 5.5), we substitute the minus momenta of the reggeized gluon loops, k_i^- , by $k_i^- \rightarrow \mu_i = -l^+ k_i^-$. This yields Jacobian factors $1/|l^+|$ and $1/(l^+)^2$ for the one-to-two and the one-to-three transition respectively. As we will see in short, these Jacobian factors connect again directly to the signature of the states of reggeized gluons. The integrals over the μ_i are then easily evaluated, taking into account contributions due to subtraction diagrams and following closely the procedure described in Sec. 5.2 for the evaluation of the impact factors. For the the one-to-two transition we then arrive typically at integrals of the following form

$$\int \frac{d^4 l}{(2\pi)^4} \left[\left(\frac{-p_A^+ l^- - i\epsilon}{\Lambda_a} \right)^{\omega_1} + \left(\frac{p_A^+ l^- - i\epsilon}{\Lambda_a} \right)^{\omega_1} \right] \left[\left(\frac{-p_B^+ l^+ - i\epsilon}{\Lambda_b} \right)^{\omega_2} + \left(\frac{p_B^+ l^+ - i\epsilon}{\Lambda_b} \right)^{\omega_2} \right] \frac{1}{|l^+|} \frac{1}{l^-} \frac{1}{l^+ l^- - l^2 + i\epsilon} \frac{1}{l^+ l^- - (l - \mathbf{k}_1 + \mathbf{k}_2)^2 + i\epsilon} \quad (5.61)$$

where the precise structure of transverse momenta differs for different diagrams. Furthermore there exists a contribution that comes with an additional factor $l^+ l^-$ in the numerator. In any case the integrals over l^+ and l^- are convergent and substituting simultaneously $l^+ \rightarrow -l^+$ and $l^- \rightarrow -l^-$, the above integral changes sign and therefore yields zero and as a consequence, the transition from one to two reggeized gluons inside the elastic amplitude vanishes. We however note, that the reason for vanishing of this integral is given by the Jacobian factor $|l^+|$ that occurs as a consequence of the longitudinal loop integral of the reggeized gluon loop. Note that the above result allows for the

one-to-two transition to occur inside a 6-point amplitude, Fig. 5.4c, for instance, where an integral over the relative momenta of the reggeized gluons is not present.

For the transition of one to three reggeized gluons we arrive after evaluating integrals over μ_1 and μ_2 at integrals of the following form

$$\int \frac{d^4 l}{(2\pi)^4} \left[\left(\frac{-p_A^+ l^- - i\epsilon}{\Lambda_a} \right)^{\omega_1} + \left(\frac{p_A^+ l^- - i\epsilon}{\Lambda_a} \right)^{\omega_1} \right] \left[\left(\frac{-p_B^+ l^+ - i\epsilon}{\Lambda_b} \right)^{\omega_2} + \left(\frac{p_B^+ l^+ - i\epsilon}{\Lambda_b} \right)^{\omega_2} \right] \frac{1}{l^+ l^-} \frac{1}{l^+ l^- - l^2 + i\epsilon} \frac{1}{l^+ l^- - (l - \mathbf{k}_1 + \mathbf{k}_2)^2 + i\epsilon} \quad (5.62)$$

Due to the different Jacobian factors, the integral does not vanish but can be evaluated in analogy to the central rapidity diagram of Sec. 3.1. Taking into account simplifications due to the LLA, we arrive at the following result for elastic quark-quark scattering amplitude with a transition from one to three reggeized gluons:

$$\mathcal{M}_{2 \rightarrow 2} = \frac{(2\pi)^2}{3!} p_A^+ p_B^- \int \frac{d\omega}{2\pi i} \left[\left(\frac{-p_A^+ p_B^-}{m_A^+ m_B^-} \right)^\omega + \left(\frac{p_A^+ p_B^-}{m_A^+ m_B^-} \right)^\omega \right] \phi_{1 \rightarrow 3}^{\text{NC}}(\omega, t) \quad (5.63)$$

where

$$\phi_{1 \rightarrow 3}^{\text{NC}}(\omega, t) = g t^a \frac{1}{q^2} \frac{1}{\omega - \beta(q^2)} \int \frac{d^2 \mathbf{k}_1}{(2\pi)^3} \int \frac{d^2 \mathbf{k}_2}{(2\pi)^3} U_{1 \rightarrow 3}^{a; b_1 b_2 b_3}(\mathbf{q}; \mathbf{k}_1, \mathbf{k}_2, \mathbf{k}_3) \frac{1}{\mathbf{k}_1^2 \mathbf{k}_2^2 \mathbf{k}_3^2} A_{(3;0)}^{b_1 b_2 b_3}(\omega | \mathbf{k}_1, \mathbf{k}_2, \mathbf{k}_3) \quad (5.64)$$

with $U_{1 \rightarrow 3}$ to 1-to-3 reggeized gluon transition vertex. To display the transverse momentum structure of the vertex, we make use of so-called Reggeon-momentum diagrams (for an detailed introduction to these diagrams see for instance [38]), which allow to illustrate the transverse momentum structure in a diagrammatic way. In every diagram there is a lowest vertex, which determines the resulting expression. While the sum of momenta that leaves the vertex below determines the numerator, the two lines that enter this vertex from above determine the two denominators. Further, closed loop imply an integration over the transverse loop momentum. For the 1-to-3 reggeized gluon transition vertex, the following diagrams occur, which correspond to the following expression in momentum space:

$$\begin{array}{c} \circ \\ | \\ 1 \quad 2 \quad 3 \end{array} = \int \frac{d^2 l}{(2\pi)^3} \frac{(\mathbf{k}_1 + \mathbf{k}_2 + \mathbf{k}_3)^2}{l^2 (\mathbf{k}_1 + \mathbf{k}_2 + \mathbf{k}_3 - l)^2}, \quad (5.65)$$

$$\begin{array}{c} | \\ \circ \\ | \quad | \\ 1 \quad 2 \quad 3 \end{array} = \int \frac{d^2 l}{(2\pi)^3} \frac{(\mathbf{k}_1 + \mathbf{k}_2)^2}{l^2 (\mathbf{k}_1 + \mathbf{k}_2 - l)^2}, \quad (5.66)$$

$$\begin{array}{c} | \\ | \\ \circ \\ | \quad | \\ 1 \quad 2 \quad 3 \end{array} = \int \frac{d^2 l}{(2\pi)^3} \frac{\mathbf{k}_1^2}{l^2 (\mathbf{k}_1 - l)^2}. \quad (5.67)$$

The complete transition vertex is then given by

$$U_{1 \rightarrow 3}^{a; b_1 b_2 b_3}(\mathbf{q}; \mathbf{k}_1, \mathbf{k}_2, \mathbf{k}_3) = \text{tr} (T^a T^{b_1} T^{b_2} T^{b_3}) U(\mathbf{q}; \mathbf{k}_1, \mathbf{k}_2, \mathbf{k}_3) + \text{tr} (T^a T^{b_2} T^{b_1} T^{b_3}) U(\mathbf{q}; \mathbf{k}_2, \mathbf{k}_1, \mathbf{k}_3) + \text{tr} (T^a T^{b_1} T^{b_3} T^{b_2}) U(\mathbf{q}; \mathbf{k}_1, \mathbf{k}_3, \mathbf{k}_2), \quad (5.68)$$

where the sum is over all permutations of numbers $1, \dots, 3$ with the trace and generators in the adjoint representation of $SU(N_c)$ and

$$U(\mathbf{q}; \mathbf{k}_1, \mathbf{k}_2, \mathbf{k}_3) = g^4 \frac{q^2}{6} \left[\begin{array}{c} \circ \\ | \\ 1 \quad 2 \quad 3 \end{array} - \begin{array}{c} | \\ \circ \\ | \quad | \\ 1 \quad 2 \quad 3 \end{array} + \begin{array}{c} | \\ | \\ \circ \\ | \quad | \\ 1 \quad 2 \quad 3 \end{array} \right]. \quad (5.69)$$

5.3.2 The transition of 2-3 and 2-4 reggeized gluons

In accordance with the discussion of the two-to-two transition in Sec.3.2 and the Reggeon-Particle-2-Reggeon vertex in Sec.4.3, it is also in the present case advisable to consider for the discussion of longitudinal integrations not individual diagrams, but to group the sum of all diagrams first according to their color- and then according to their transverse momentum structure. In this way cancellation of certain divergent parts between individual diagrams is achieved, which is otherwise difficult to be obtained. Diagrams that contribute to the two-to-three reggeized gluons transitions are shown in Fig.5.6a-b, while a typical contribution to the two-to-four reggeized gluon transition can be found in Fig.5.6c.

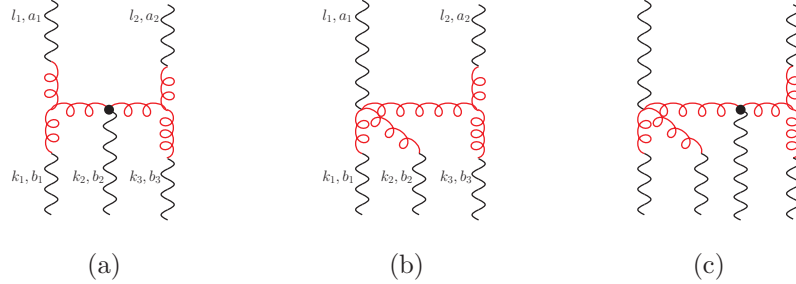


Figure 5.6: Diagrams that contribute to the transition from two-to-three (a,b) and two-to-four reggeized gluons.

In the case of the 2 – 3 transition, the obtained unintegrated transition vertex is for *one* ordering of color and momenta indices given by

$$\begin{aligned}
 & i l^+ 16 (T^{b_1} T^{b_2} T^{b_3})_{a_1 a_2} \left[\left(\mathbf{q}^2 - \mathbf{l}_1^2 (\mathbf{q} - \mathbf{k}_1)^2 g_1(\mu_1, -\mu_2 - \mu_3) - \mathbf{l}_2^2 (\mathbf{q} - \mathbf{k}_3)^2 g_1(\mu_1 + \mu_2, -\mu_3) \right. \right. \\
 & \quad \left. \left. + \mathbf{l}_1^2 \mathbf{k}_2^2 \mathbf{l}_2^2 g_1(\mu_1, -\mu_2 - \mu_3) g_1(\mu_1 + \mu_2, -\mu_3) \right) F_3(l_1, l_2; k_1, k_2, k_3) \right. \\
 & \quad \left. + \mathbf{l}_1^2 \mathbf{k}_3^2 g_2(\mu_3, \mu_2, \mu_1) F_2(l_1, l_2; k_1 + k_2, k_3) + \mathbf{l}_2^2 \mathbf{k}_1^2 g_2(\mu_1, \mu_2, \mu_3) F_2(l_1, l_2; k_1, k_2 + k_3) \right] \quad (5.70)
 \end{aligned}$$

where $\mu_i = -l^+ k_i^-$, $i = 1, 2, 3$ with $\mu_1 + \mu_2 + \mu_3 = 0$. Further $\mathbf{k}_1 + \mathbf{k}_2 + \mathbf{k}_3 = \mathbf{q} = \mathbf{l}_1 + \mathbf{l}_2$, while $l_1^+ = -l_2^+ \equiv l^+$ and $l_1^- = 0 = l_2^-$. The appearance of the functions g_i $i = 1, 2$ in Eq.(5.70) is directly associated with the occurrence of induced vertices in the underlying Feynman-diagrams. For instance the first term in the first line of Eq.(5.70) comes from a combination with no induced vertex, while the term in the second line of Eq.(5.70) comes due to a combination of two induced vertices of the first order. Terms in third line on the other hand come from a combination of an induced vertex of the second order with a reggeized gluon that couples without an induced vertex to the gluon. In the case of the two-to-four transition a very similar expression can be derived, which contains as a new element also the function g_3 , corresponding to an induced vertex of the third order.

Also in the present case, every 4-point amplitude where the interaction is mediated by a reggeized gluon, requires a large center of mass energy, and a corresponding lower bound is imposed making use of the Mellin-integral. For the graphs Fig.5.7a-b, where the reggeized gluon couples to the gluon by a three-gluon-vertex or an induced vertex of the first order, the situation is similar to the 2-2 transition and the squared center-of-mass energy is given by $p_A^+ k_1^-$. However, unlike the case of the 2-2 transition, it is generally no longer possible to combine the two Mellin-integrals that belong to the two upper reggeized gluons into a single one for the whole sub-amplitude. Instead, every reggeized gluon is treated separately and are only combined into a single Mellin-integral, after the longitudinal integrations have been carried out. For graphs like Fig.5.7c-d, which contain induced vertices of higher order, a problem similar to the one in Sec. 5.3.1 arises: The reggeized gluon is seemingly part of a 5- or a 6-point sub-amplitude and not a 4-point amplitude. In analogy with the

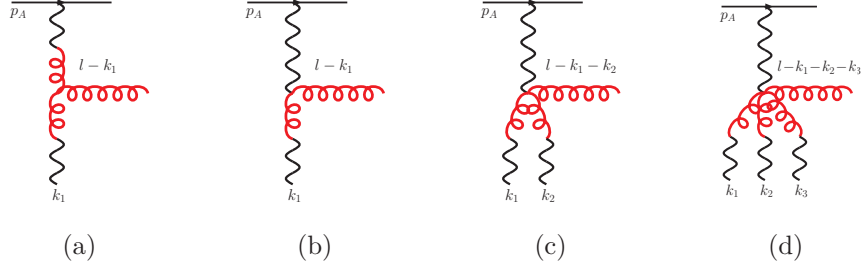


Figure 5.7: Different kind of center of mass energies that need to be large, in order for the interaction to be correctly described by a reggeized gluon.

procedure in Sec. 5.3.1 we will use in the following the momentum of the 'produced' QCD gluon to construct the center-of-mass energy, on which the lower bound is imposed and which enters the Mellin integral. In particular for Fig. 5.7c and Fig. 5.7d, this results into the center-of-mass energies $s_A^{(c)} = p_A^+(k_1^- + k_2^-)$ and $s_A^{(d)} = p_A^+(k_1^- + k_2^- + k_3^-)$ respectively. Anticipating that all longitudinal integrals are convergent, once subtraction graphs are included, this then implies that the transition is fixed at central rapidities, as required.

Taking into account further subtraction diagrams, longitudinal integrals turn out to be convergent and can be evaluated similarly to the two-to-two transition in Sec. 3.2, with the methods described in Sec. 5.2. Especially, using the methods of Sec. 5.2, we arrive in the course of the analysis on the 'regularized' integrands F_2^R , F_3^R and F_4^R which all come with certain poles in light-cone momenta, and for a correct evaluation of the integral it is mandatory that the $i\epsilon$ prescription of these poles coincides with the one of the branch-cuts appearing due to the Mellin-integral. In the case of the 2-3 transition, after including subtraction diagrams, the first term in the first line of Eq.(5.70) will be proportional to the function F_3^R of Eq. (5.49), plus terms with vanishing integral. The integral is then given by

$$\int \frac{dl^+}{l^+} [(-p_B^- l^+ - i\epsilon)^\omega + (p_B^- l^+ - i\epsilon)^{\omega_2}] \int \frac{d\mu_1}{(-2\pi i)} \int \frac{d\mu_2}{(-2\pi i)} \frac{m_1^2 m_{12}^2}{(\mu_1 - m_1^2 + i\epsilon)(\mu_1 + \mu_2 - m_{12}^2 + i\epsilon)} \times \frac{1}{6} \left[\left(\frac{p_A^+ \mu_1}{l^+} - i\epsilon \right)^{\omega_1 - 1} \left[\left(\frac{p_A^+(\mu_1 + \mu_2)}{l^+} - i\epsilon \right)^{\omega_2 - 1} - 2 \left(\frac{-p_A^+(\mu_1 + \mu_2)}{l^+} - i\epsilon \right)^{\omega_2 - 1} \right] - \left(\frac{-p_A^+ \mu_1}{l^+} - i\epsilon \right)^{\omega_1 - 1} \left[2 \left(\frac{p_A^+(\mu_1 + \mu_2)}{l^+} - i\epsilon \right)^{\omega_2 - 1} - \left(\frac{-p_A^+(\mu_1 + \mu_2)}{l^+} - i\epsilon \right)^{\omega_2 - 1} \right] \right], \quad (5.71)$$

where we note that the factor $1/l^+$ arises due to a Jacobian factor from the transition $k_i^- \rightarrow \mu_i = -l^+ k_i^-$, $i = 1, 2$ and $m_1^2 = (l - k_1)^2$ and $m_{12}^2 = (l - k_1 - k_2)^2$. With the substitutions $l^+ \rightarrow -l^+$ the integral changes sign and correspondingly the integral vanishes. A similar observation can be made for all integrals connected with the transition from two to three reggeized gluons. The two-to-three transition vanishes therefore, if inserted into the elastic amplitude. On the other hand, if it would occur inside in a 6-point amplitude for instance, it is generally possible to obtain a non-zero result for this transition.

Integrals occurring for the two-to-four transition are very similar to Eq. (5.71), the main difference being that they contain three integrations over μ_i , $i = 1, \dots, 4$ and that the corresponding Jacobian yields therefore a factor of $1/|l^+|$, instead. As a consequence, the integrals do not vanish in that case, in accordance with signature conservation.

For the elastic scattering amplitude with one transition from two to four reggeized gluons we then find the following expression:

$$\mathcal{M}_{2 \rightarrow 2} = \frac{(2\pi)^3}{4!} s \int \frac{d\omega}{2\pi i} \left(\frac{s}{s_R} \right)^\omega \frac{\xi^{(+)}}{\sin \pi \omega} \phi_4^{\text{NC}}(\omega, t), \quad (5.72)$$

with

$$\begin{aligned} \phi_4^{\text{NC}}(\omega, t) = & A_{(2;0)}^{a_1 a_2}(\mathbf{l}_1, \mathbf{l}_2) \frac{1}{\omega - \sum_i^2 \beta(\mathbf{l}_i^2)} \otimes_{l_{12}} U_{2 \rightarrow 4}^{a_1 a_2; b_1 b_2 b_3 b_4}(\mathbf{l}_1, \mathbf{l}_2; \mathbf{k}_1, \mathbf{k}_2, \mathbf{k}_3, \mathbf{k}_4) \\ & \frac{1}{\omega - \sum_i^4 \beta(\mathbf{k}_i^2)} \otimes_{\mathbf{k}_{\{1234\}}} A_{(4;0)}^{a_1 a_2 a_3 a_4}(\mathbf{k}_1, \mathbf{k}_2, \mathbf{k}_3, \mathbf{k}_4). \end{aligned} \quad (5.73)$$

The transition is given as the sum of a connected and a disconnected part

$$\begin{aligned} U_{2 \rightarrow 4}^{a_1 a_2; b_1 b_2 b_3 b_4}(\mathbf{l}_1, \mathbf{l}_2; \mathbf{k}_1, \mathbf{k}_2, \mathbf{k}_3, \mathbf{k}_4) = & U_{\text{connect}}^{a_1 a_2; b_1 b_2 b_3 b_4}(\mathbf{l}_1, \mathbf{l}_2; \mathbf{k}_1, \mathbf{k}_2, \mathbf{k}_3, \mathbf{k}_4) \\ & + U_{\text{disconnect}}^{a_1 a_2; b_1 b_2 b_3 b_4}(\mathbf{l}_1, \mathbf{l}_2; \mathbf{k}_1, \mathbf{k}_2, \mathbf{k}_3, \mathbf{k}_4) \end{aligned} \quad (5.74)$$

where the latter arises as all possible combinations of the 1-3 transition Eq.(5.68) of the previous section:

$$\begin{aligned} U_{\text{disconnect}}^{a_1 a_2; b_1 b_2 b_3 b_4}(\mathbf{l}_1, \mathbf{l}_2; \mathbf{k}_1, \mathbf{k}_2, \mathbf{k}_3, \mathbf{k}_4) = & \\ = \frac{1}{2} \sum_{i_1, i_2} \left[& \delta^{a_{i_1} b_4} (2\pi)^3 \delta^{(2)}(\mathbf{l}_{i_2} - \mathbf{k}_4) U_{1 \rightarrow 3}^{a_{i_2}; b_1 b_2 b_3}(\mathbf{l}_{i_1}; \mathbf{k}_1, \mathbf{k}_2, \mathbf{k}_3) \right. \\ & + \delta^{a_{i_1} b_3} (2\pi)^3 \delta^{(2)}(\mathbf{l}_{i_2} - \mathbf{k}_3) U_{1 \rightarrow 3}^{a_{i_2}; b_1 b_2 b_4}(\mathbf{l}_{i_1}; \mathbf{k}_1, \mathbf{k}_2, \mathbf{k}_4) \\ & + \delta^{a_{i_1} b_2} (2\pi)^3 \delta^{(2)}(\mathbf{l}_{i_2} - \mathbf{k}_2) U_{1 \rightarrow 3}^{a_{i_2}; b_1 b_3 b_4}(\mathbf{l}_{i_1}; \mathbf{k}_1, \mathbf{k}_3, \mathbf{k}_4) \\ & \left. + \delta^{a_{i_1} b_1} (2\pi)^3 \delta^{(2)}(\mathbf{l}_{i_2} - \mathbf{k}_1) U_{1 \rightarrow 3}^{a_{i_2}; b_2 b_3 b_4}(\mathbf{l}_{i_1}; \mathbf{k}_2, \mathbf{k}_3, \mathbf{k}_4) \right] \end{aligned} \quad (5.75)$$

where the sum is over permutations of the numbers 1, 2. To state the connected part, we again make use of a diagrammatic notation in terms of Reggeon momentum diagrams. For the connected part, the following types of expressions are needed:

$$\begin{aligned} \begin{array}{c} 1 \quad 2 \\ \diagdown \quad \diagup \\ \diagup \quad \diagdown \\ 1 \quad 2 \quad 3 \quad 4 \end{array} &= \frac{(\mathbf{k}_1 + \mathbf{k}_2 + \mathbf{k}_3 + \mathbf{k}_4)^2}{l_1^2 l_2^2} & \begin{array}{c} 1 \quad 2 \\ | \quad | \\ \diagdown \quad \diagup \\ 1 \quad 2 \quad 3 \quad 4 \end{array} &= \frac{(\mathbf{k}_1 + \mathbf{k}_2 + \mathbf{k}_3)^2}{l_1^2 (l_2 - \mathbf{k}_4)^2} \\ \begin{array}{c} 1 \quad 2 \\ | \quad | \\ \diagdown \quad \diagup \\ 1 \quad 2 \quad 3 \quad 4 \end{array} &= \frac{(\mathbf{k}_2 + \mathbf{k}_3)^2}{(l_1 - \mathbf{k}_1)^2 (l_2 - \mathbf{k}_4)^2} & \begin{array}{c} 1 \quad 2 \\ | \quad | \\ \diagup \quad \diagdown \\ 1 \quad 2 \quad 3 \quad 4 \end{array} &= \frac{(\mathbf{k}_1 + \mathbf{k}_2)^2}{l_1^2 (l_2 - \mathbf{k}_3 - \mathbf{k}_4)^2} \\ \begin{array}{c} 1 \quad 2 \\ | \quad | \\ \diagup \quad \diagdown \\ 1 \quad 2 \quad 3 \quad 4 \end{array} &= \frac{\mathbf{k}_3^2}{(l_1 - \mathbf{k}_1 - \mathbf{k}_2)^2 (l_2 - \mathbf{k}_4)^2} \end{aligned} \quad (5.76)$$

The transition vertex is then given by

$$U_{\text{connect}}^{a_1 a_2; b_1 b_2 b_3 b_4}(\mathbf{l}_1, \mathbf{l}_2; \mathbf{k}_1, \mathbf{k}_2, \mathbf{k}_3, \mathbf{k}_4) = \sum_{j_1, \dots, j_4} (T^{b_{j_1}} T^{b_{j_2}} T^{b_{j_3}} T^{b_{j_4}})_{a_1 a_2} U_C(\mathbf{l}_{i_1}, \mathbf{l}_{i_2}; \mathbf{k}_{j_1}, \mathbf{k}_{j_2}, \mathbf{k}_{j_3}, \mathbf{k}_{j_4}) \quad (5.77)$$

where the sum is over all permutations of numbers 1, ..., 4 and generators are in the adjoint representation of $SU(N_c)$. The function U_C is given by

$$\begin{aligned} U_C(\mathbf{l}_1, \mathbf{l}_2; \mathbf{k}_1, \mathbf{k}_2, \mathbf{k}_3, \mathbf{k}_4) = & \\ g^4 l_1^2 l_2^2 \left[& \frac{1}{24} \begin{array}{c} 1 \quad 2 \\ \diagdown \quad \diagup \\ \diagup \quad \diagdown \\ 1 \quad 2 \quad 3 \quad 4 \end{array} - \frac{1}{12} \begin{array}{c} 1 \quad 2 \\ | \quad | \\ \diagdown \quad \diagup \\ 1 \quad 2 \quad 3 \quad 4 \end{array} - \frac{1}{12} \begin{array}{c} 1 \quad 2 \\ | \quad | \\ \diagup \quad \diagdown \\ 1 \quad 2 \quad 3 \quad 4 \end{array} + \frac{1}{8} \begin{array}{c} 1 \quad 2 \\ | \quad | \\ \diagdown \quad \diagup \\ 1 \quad 2 \quad 3 \quad 4 \end{array} \right. \\ & \left. + \frac{1}{24} \begin{array}{c} 1 \quad 2 \\ | \quad | \\ \diagup \quad \diagdown \\ 1 \quad 2 \quad 3 \quad 4 \end{array} - \frac{1}{24} \begin{array}{c} 1 \quad 2 \\ | \quad | \\ \diagup \quad \diagdown \\ 1 \quad 2 \quad 3 \quad 4 \end{array} + \frac{1}{24} \begin{array}{c} 1 \quad 2 \\ | \quad | \\ \diagdown \quad \diagup \\ 1 \quad 2 \quad 3 \quad 4 \end{array} - \frac{1}{24} \begin{array}{c} 1 \quad 2 \\ | \quad | \\ \diagup \quad \diagdown \\ 1 \quad 2 \quad 3 \quad 4 \end{array} \right] \end{aligned} \quad (5.78)$$

5.4 The state of three and four reggeized gluons

For a description of the complete state of three and four reggeized gluons, the above derived transition vertices need to be combined with the pairwise interactions by two-to-two transition kernels between the individual reggeized gluons.

5.4.1 Integral equations

For three reggeized gluons, the relevant contributions within the GLLA are depicted in Fig.5.8, with all other corrections suppressed at least by an additional factor of g^2 .

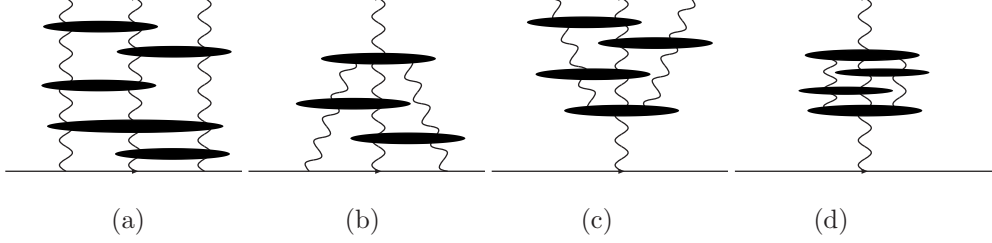


Figure 5.8: Different types of loop corrections to the state of three reggeized gluons (a) three reggeized gluons coupling to both quarks and diagrams containing one (b)(c) and two (d) transition(s) between the one and three reggeized gluon state.

For every diagram it is possible to identify at a certain stage a state of three reggeized gluons. We then factorize the amplitude at this point into two quark-three reggeized gluon amplitudes. Expressing the complete amplitude within the GLLA as the following Mellin-transform

$$\mathcal{M}_{2 \rightarrow 2}^{\text{LLA}|3\text{R}} = \frac{(2\pi)^2}{3!} s \int \frac{d\omega}{2\pi i} \left(\frac{s}{s_R} \right)^\omega \xi^{(-)}(\omega) \phi_3(\omega, t), \quad (5.79)$$

we write the partial wave $\phi_3(\omega, t)$ the following convolution:

$$\phi_3(\omega, t) = A_3^{a_1 a_2 a_3}(\omega | \mathbf{k}_1, \mathbf{k}_2, \mathbf{k}_3) \left(\omega - \sum_i^3 \beta(\mathbf{k}_i^2) \right) \otimes_{\mathbf{k}_{123}} A_3^{a_1 a_2 a_3}(\mathbf{k}_1, \mathbf{k}_2, \mathbf{k}_3) \quad (5.80)$$

where $A_3^{a_1 a_2 a_3}(\omega)$ denote the corresponding quark-3reggeized gluon amplitudes which is defined to contain a factor $1/(\omega - \sum_i^3 \beta(\mathbf{k}_i^2))$ for the external reggeized gluons. The state of three reggeized gluons can both arise from a direct coupling to the quark and by a transition from a 1-3 transition. It is therefore within the GLLA resummed by the following integral equation

$$\left(\omega - \sum_{i=1}^3 \beta(\mathbf{k}_i^2) \right) A_3^{b_1 b_2 b_3}(\omega | \mathbf{k}_1, \mathbf{k}_2, \mathbf{k}_3) = A_{(3;0)}^{a_1 a_2 a_3} + U_{1 \rightarrow 3}^{a; b_1 b_2 b_3} A_1^a(\omega) + \sum \mathcal{K}_{2 \rightarrow 2}^{\{b\} \rightarrow \{a\}} \otimes A_3^{a_1 a_2 a_3}, \quad (5.81)$$

where the sum on the right-hand-side contains all possible insertions of the 2-2 kernel and

$$A_1^a(\omega | \mathbf{q}) = g t^a \frac{1}{\omega - \beta(\mathbf{q}^2)} \frac{1}{\mathbf{q}^2} \quad (5.82)$$

is the amplitude describing coupling of a single reggeized gluon to the quark.

The partial wave that describes the exchange of four reggeized gluons can be factorized in an analogous way. The different contributions are depicted in Fig.5.9: The state of four reggeized gluons may either arise from a direct coupling of the four reggeized gluon to the upper quark (in

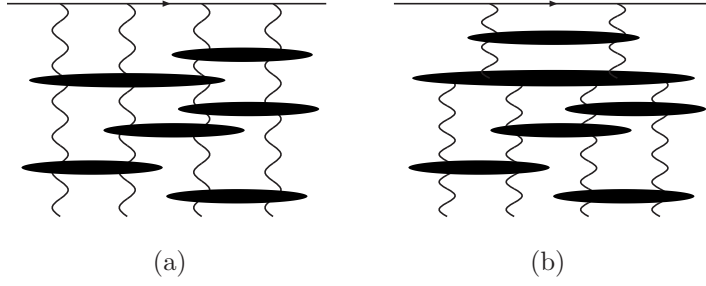


Figure 5.9: Different contributions to the state of four reggeized gluons: (a) : direct coupling of the four reggeized gluons to the quark (b): transition from the two to the four reggeized gluon state

the case of Fig.5.9) or by a transition between the state of two and four reggeized gluons. The elastic scattering amplitude with exchange of four reggeized gluons within the GLLA given by

$$\mathcal{M}_{2 \rightarrow 2}^{\text{LLA|4R}} = \frac{(2\pi)^3}{4!} s \int \frac{d\omega}{2\pi i} \left(\frac{s}{s_R} \right)^\omega \frac{\xi^{(+)}}{\sin \pi \omega} \phi_4(\omega, t). \quad (5.83)$$

The partial wave $\phi_4(\omega, t)$ is then factorized into two quark-four-reggeized gluons amplitudes in the following way:

$$\phi_4(\omega, t) = A_4^{a_1 a_2 a_3 a_4}(\omega | \mathbf{k}_1, \mathbf{k}_2, \mathbf{k}_3, \mathbf{k}_4) (\omega - \sum_{i=1}^4 \beta(\mathbf{k}_i^2)) \otimes_{\mathbf{k}_{1234}} A_4^{a_1 a_2 a_3 a_4}(\omega | \mathbf{k}_1, \mathbf{k}_2, \mathbf{k}_3, \mathbf{k}_4). \quad (5.84)$$

As for the state of three reggeized gluons, also the quark-four-reggeized gluons amplitude is non-amputated and contains a factor $1/(\omega - \sum_{i=1}^4 \beta(\mathbf{k}_i^2))$ for its external reggeized gluons. It satisfies the following integral equation

$$\begin{aligned} (\omega - \sum_{i=1}^4 \beta(\mathbf{k}_i^2)) A_4^{b_1 b_2 b_3 b_4}(\omega | \mathbf{k}_1, \mathbf{k}_2, \mathbf{k}_3, \mathbf{k}_4) &= A_{(4;0)}^{b_1 b_2 b_3 b_4} + U_{2 \rightarrow 4}^{a_1 a_2; b_1 b_2 b_3 b_4} \otimes A_2^{a_1 a_2}(\omega) \\ &+ \sum \mathcal{K}_{2 \rightarrow 2}^{\{a\} \rightarrow \{b\}} \otimes A_4^{a_1 a_2 a_3 a_4}(\omega). \end{aligned} \quad (5.85)$$

Compared to existing results in the literature (to which we compare in the following paragraph) the above integral equations have the special feature that they are not restricted to the overall color singlet. In particular they allow for a search of further Regge-poles in the color-octet channel. In the following we shall however not do so, but compare instead our results with the yet existing results for the color singlet channel.

5.4.2 The four reggeized gluon state in the color singlet

In the following section, we compare the above obtained result with existing results in the literature. In particular the question arises in which sense the integral equations describing the state of four reggeized gluons are related to the analysis of [35–37]. While the analysis presented there was carried out for $N_c = 3$, the result was reproduced for arbitrary, finite N_c in [38] and we will refer if we compare the exact form of results.

To compare with [35] we consider quark-reggeized gluons amplitudes, as shown in Fig.5.9. In [35] the analysis has been carried out for state of four reggeized gluons coupling to a virtual photon, and not to a quark. In particular this restricts the four reggeized gluon state to the overall color singlet. In turn, we shall therefore only take the color-singlet part of the scattering quark A into account.

5.4.3 The Born-result

To lowest order in the coupling constant, the contribution due to the transition of two-to-four reggeized gluons is absent and we encounter only the contribution due to the quark impact factor with four reggeized gluons, Eq. (5.60). To compare with the presentation in [35, 38] we project the scattering quark onto the color singlet and write the four gluon impact-factor Eq.(5.60) as a superposition of the two-reggeized gluon quark-impact factor Eq. (3.47), in analogy with the analysis of [35, 38]. Projected onto the color-singlet, the two-gluon impact factor reads

$$B_{(2;0)}^{a_1 a_2}(\mathbf{k}_1, \mathbf{k}_2) = \delta^{a_1 a_2} B_{(2;0)}(\mathbf{k}_1, \mathbf{k}_2) = \frac{-g^2}{2N_c} \delta^{a_1 a_2}. \quad (5.86)$$

where we denote here impact factors and partial waves by a letter 'B' in order stress that in the following case the quarks are explicitly projected on their color singlet. The transverse momenta dependence of the above function is of course trivial. We however attempt to stay as close as possible to the analysis of [35] and that is why it is convenient for us to introduce formally such a function. Furthermore, let us define color tensors,

$$d^{a_1 a_2 a_3 a_4} = \text{tr}(t^{a_1} t^{a_2} t^{a_3} t^{a_4}) + \text{tr}(t^{a_4} t^{a_3} t^{a_2} t^{a_1}), \quad (5.87)$$

following [35, 38]. In the present case, it is then furthermore useful to introduce analogous color tensors, one which is symmetric under the exchange of the first two and the last two pairs of indices

$$d_2^{a_1 a_2 a_3 a_4} = \frac{1}{2} [d^{a_1 a_2 a_3 a_4} + d^{a_2 a_1 a_3 a_4}], \quad (5.88)$$

and one which is symmetric under exchange of any pair of color indices

$$d_S^{a_1 a_2 a_3 a_4} = \frac{1}{3} [d^{a_1 a_2 a_3 a_4} + d^{a_2 a_1 a_3 a_4} + d^{a_1 a_3 a_2 a_4}]. \quad (5.89)$$

The impact factor for four reggeized gluons coupling to the quark, as derived from the effective action, can then be expressed, for the overall color singlet, in terms of the two reggeized gluon impact factor in the following way:

$$\begin{aligned} B_{(4;0)}^{a_1 a_2 a_3 a_4}(\mathbf{k}_1, \mathbf{k}_2, \mathbf{k}_3, \mathbf{k}_4) = & \\ & -g^2 d_S^{a_1 a_2 a_3 a_4} [B_{(2;0)}(123, 4) + B_{(2;0)}(124, 3) + B_{(2;0)}(134, 2) + B_{(2;0)}(234, 1)] \\ & + g^2 d_2^{a_1 a_2 a_3 a_4} B_{(2;0)}(12, 34) + g^2 d_2^{a_1 a_3 a_2 a_4} B_{(2;0)}(13, 24) + g^2 d_2^{a_1 a_4 a_2 a_3} B_{(2;0)}(14, 23), \end{aligned} \quad (5.90)$$

where we introduced the following short-hand notation

$$B_{(2;0)}(12, 34) = B_{(2;0)}(\mathbf{k}_1 + \mathbf{k}_2, \mathbf{k}_3 + \mathbf{k}_4), \quad (5.91)$$

where a string of numbers represent a sum of transverse momenta with the corresponding indices. In [35], the corresponding result was obtained from taking the triple discontinuity of the six-point amplitude, as outlined in the first part of this thesis. With $D_{(2;0)}$ and $D_{(4;0)}$ denoting the virtual photon impact factor with two and four reggeized gluons, the result for the four gluon impact factor is given by

$$\begin{aligned} D_{(4;0)}^{a_1 a_2 a_3 a_4}(\mathbf{k}_1, \mathbf{k}_2, \mathbf{k}_3, \mathbf{k}_4) = & \\ & -g^2 d^{a_1 a_2 a_3 a_4} [D_{(2;0)}(123, 4) + D_{(2;0)}(234, 1) + D_{(2;0)}(14, 23)] \\ & -g^2 d^{a_2 a_1 a_3 a_4} [D_{(2;0)}(134, 2) + D_{(2;0)}(124, 3) - D_{(2;0)}(12, 34) + D_{(2;0)}(13, 24)]. \end{aligned} \quad (5.92)$$

Comparing the two results, one observes, apart from the different impact factors, the following difference compared to Eq.(5.92): Eq.(5.90) lacks a certain antisymmetric color structure. While, for example, the term $D_{(2;0)}(12, 34)$ comes with a color tensor

$$d^{a_2 a_1 a_3 a_4} = d_2^{a_1 a_2 a_3 a_4} + \frac{1}{4} f^{a_1 a_2 k} f^{a_3 a_4 k}, \quad (5.93)$$

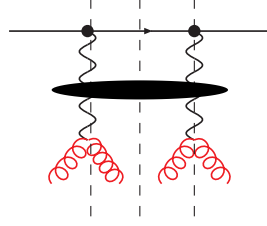


Figure 5.10: A contribution of the effective action that can yield a contribution to the triple discontinuity with antisymmetric color.

the analogous term $B_{(2;0)}(12, 34)$ in Eq.(5.90) lacks the second color antisymmetric structure on the left hand side of Eq.(5.93). The reason lies in the different definitions of the two quantities: Whereas Eq.(5.92) arises from the triple-discontinuity of a six-point amplitude, which naturally includes both symmetric and anti-symmetric color structure, Eq.(5.90) constitutes an impact factor of the effective theory. In Sec.3.2 and Sec.5.2 it has been shown that for the effective action the configurations with antisymmetric color are completely contained in the reggeized gluons, due, in particular, to the presence of the induced vertices. The state of two and four reggeized gluons coupling to the quark is on the other hand restricted to completely symmetric color configurations. In particular, reggeized gluons in the effective action carry phase factors and therefore have a non-zero discontinuity themselves. The triple energy discontinuity for the antisymmetric color configuration should therefore arise in the effective action form graphs like Fig.5.9c. Indeed, obtaining in Eq.(5.90) also the antisymmetric color states, would have been a strong hint for a possible over-counting in the effective action.

5.4.4 The four reggeized gluons and the triple Pomeron vertex

To resum the state of four reggeized gluons, Fig.5.9, we then use the integral equation Eq.(5.85)

$$\begin{aligned}
 (\omega - \sum_{i=1}^4 \beta(\mathbf{k}_i^2)) B_4^{b_1 b_2 b_3 b_4}(\omega | \mathbf{k}_1, \mathbf{k}_2, \mathbf{k}_3, \mathbf{k}_4) = & B_{(4;0)}^{b_1 b_2 b_3 b_4} + U_{2 \rightarrow 4}^{a_1 a_2; b_1 b_2 b_3 b_4} \otimes B_2^{a_1 a_2}(\omega) \\
 & + \sum \mathcal{K}_{2 \rightarrow 2}^{\{a\} \rightarrow \{b\}} \otimes B_4^{a_1 a_2 a_3 a_4}(\omega). \quad (5.94)
 \end{aligned}$$

In the following analysis we then follow closely the approach taken in [35] and split up the four-reggeized-gluon amplitude into a reggeizing part B_4^R and into an irreducible part B_4^I ,

$$B_4 = B_4^R + B_4^I. \quad (5.95)$$

The reggeizing part is then given as the superposition of two-reggeized gluon amplitudes $B_2(\omega)$

$$\begin{aligned}
 B_4^{R; a_1 a_2 a_3 a_4}(\omega | \mathbf{k}_1, \mathbf{k}_2, \mathbf{k}_3, \mathbf{k}_4) = & \\
 -g^2 d_S^{a_1 a_2 a_3 a_4} [B_2(\omega | 123, 4) + B_2(\omega | 124, 3) + B_2(\omega | 134, 2) + B_2(\omega | 234, 1)] & \\
 +g^2 d_2^{a_1 a_2 a_3 a_4} B_2(\omega | 12, 34) + g^2 d_2^{a_1 a_3 a_2 a_4} B_2(\omega | 13, 24) + g^2 d_2^{a_1 a_4 a_2 a_3} B_2(\omega | 14, 23) & \quad (5.96)
 \end{aligned}$$

where the particular form is obtained by replacing all two-reggeized gluon impact-factors $B_{(2;0)}$ in the four-reggeized gluon impact factor Eq.(5.90) by their corresponding quark-2 reggeized gluon amplitudes, following [35]. We then insert the ansatz Eq.(5.95) into the integral equation Eq.(5.94) and obtain as such a new integral equation for B_4^I . Using the BFKL-equation for $B_2(\omega)$,

$$(\omega - \sum_{i=1}^2 \beta(\mathbf{k}_i^2)) B_2(\omega | \mathbf{k}_1, \mathbf{k}_2) = B_{(2;0)}^{b_1 b_2} + (-N_c) \mathcal{K}_{2 \rightarrow 2}^{\{a\} \rightarrow \{b\}} \otimes B_2^{a_1 a_2}(\omega) \quad (5.97)$$

and employing various color identities (see for instance [38] for a suitable collection), we finally arrive at the following integral equation for B_4^I ,

$$\begin{aligned}
(\omega - \sum_{i=1}^4 \beta(\mathbf{k}_i^2)) B_4^{I;b_1 b_2 b_3 b_4}(\omega | \mathbf{k}_1, \mathbf{k}_2, \mathbf{k}_3, \mathbf{k}_4) = & V_{2 \rightarrow 4}^{a_1 a_2; b_1 b_2 b_3 b_4} \otimes B_2^{a_1 a_2}(\omega) \\
& + \sum \mathcal{K}_{2 \rightarrow 2}^{\{a\} \rightarrow \{b\}} \otimes B_4^{I;a_1 a_2 a_3 a_4}(\omega) \quad (5.98)
\end{aligned}$$

where the kernel $V_{2 \rightarrow 4}$ agrees with the arbitrary N_c version [38] of the two-to-four reggeized gluon vertex of [35].

5.5 Conclusion

In the present chapter we extended our study of the effective action to the exchange of states of $n > 2$ reggeized gluons in the t -channel of the elastic scattering amplitude. As a particular example, the state of three and four reggeized gluons has been considered. While the former has negative signature and provides a correction to the exchange of a single reggeized gluon, the latter can be shown to have positive signature and gives a correction to the state of two reggeized gluons.

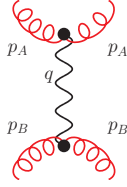
A first step to arrive at these results requires to determine the pole prescription of higher induced vertices. They can be obtained by the following recipe: Starting from a simple pole prescription $1/\partial \rightarrow 1/\partial - \epsilon$ in the effective action, one decomposes the color structure into a basis of color tensors, which is constructed from multiple entangled commutators of generators and symmetrization in the remaining parts. The most antisymmetric terms, given in terms of multiple entangled commutators alone, coincide in their color structure with induced vertices without pole-prescription. We then identified the momentum structure proportional to these maximal antisymmetric color structure as the induced vertex with pole-prescription, while we drop all other terms. The resulting vertices turns out to be Bose-symmetric.

For the longitudinal loop integrals of loops containing more than two reggeized gluons we found that, also in that case bad convergence properties of the occurring integrals ask for suitable subtraction diagrams. We proposed to add a subtraction term to the effective Lagrangian that generates the subtraction diagrams. Including these diagrams, a derivation of quark impact-factors with three and four reggeized gluons and of vertices which describe the transition from one to three and two to four reggeized gluons becomes possible. Transition vertices from one-to-two and two-to-three reggeized gluons on the other hand, are not allowed due to signature conservation: Their vanishing is obtained as a result from the effective action and is not needed to be imposed as an external constraint.

In a next step we presented integral equations for the state of three and four reggeized gluons, which resum corrections within the generalized LLA. Apart from the derived non-zero transition vertices, they resum pairwise interactions between reggeized gluons by two-to-two transition kernels. We then investigate more closely the integral equation for the quark-four-reggeized-gluons amplitude with the quark projected onto the color singlet. Following a similar analysis by Bartels and Wüsthoff in [35], the four-reggeized gluon amplitude was split up into a reggeizing and an irreducible part. While the former takes the form of a state of two reggeized gluons that finally decays with various symmetric color tensors, the latter arises from the two-to-four Reggeon transition vertex derived by Bartels and Wüsthoff in [35]. The symmetric color tensors of the reggeizing contributions reflect the choice of the color basis of the induced vertices in Sec.5.1. Contributions with antisymmetric color tensors are contained inside higher order corrections to the reggeized gluon and occur therefore not as a part of the state of four reggeized gluons.

With the above discussion of the state of three and four reggeized gluons we finish our discussion of longitudinal integrations within the effective action. Let us therefore shortly summarize our central results: The effective action [55, 56] factorizes high-energy-QCD amplitudes into sub-amplitudes which are local in rapidity. Non-local interaction between these sub-amplitudes is mediated by the exchange of reggeized gluons. This statement implies a non-trivial constraint on the longitudinal

momenta of QCD-particles inside the local sub-amplitudes. In practice, this can be achieved by imposing a lower bound on the 'center-of-mass' energy of the reggeized gluons that connects the local sub-amplitudes. To give a proper definition of the center-of-mass energy of a reggeized gluon, it is necessary to consider the latter always as an object embedded into a minimal sub-amplitude that can be associated with its exchange. The prime example is the case where the reggeized gluon couples on both ends to a Particle-Particle-Reggeon vertex, which allows for a straight-forward definition of the center-of-mass energy of the reggeized gluon. The lower bound on the center of mass energy can be then imposed through an (inverse) Mellin-integral. It has the advantage that it allows to include easily both higher order corrections due to reggeization of the gluon and signature of the reggeized gluon. In the following we state the example where the reggeized gluon couples on both ends to a gluon by a Gluon-Gluon-Reggeon vertices Γ_{GGR} :



$$= \int \frac{d\omega}{4\pi i} \Gamma_{GGR}^+(p_A, q) \frac{i/2}{\mathbf{q}^2} \frac{1}{\omega - \beta(\mathbf{q}^2)} \left[\left(\frac{-s - i\epsilon}{s_R} \right)^\omega + \left(\frac{s - i\epsilon}{s_R} \right)^\omega \right] \Gamma_{GGR}^-(p_B, q). \quad (5.99)$$

The squared center-of-mass energy s is always defined as the product of the large light-cone-momenta of the scattering particles, in the present case $s = p_A^+ p_B^-$, also if transverse or other light-cone momenta of the scattering particles are non-zero. This is particularly suitable as it preserves Bose-symmetry of the external gluons: Due to the general property of the reggeized gluon fields

$$\partial_- A_+ = 0 = \partial_+ A_-, \quad (5.100)$$

we have $p_A^+ = -p_{A'}^+$ and $p_B^- = -p_{B'}^-$. s_R is the lower bound that is imposed on s : With the contour of integration of the ω -integral parallel to the imaginary axis, to the right of the singularity at $\omega = \beta(\mathbf{q}^2)$, the integral yields zero, unless $s > s_R$. $\beta(\mathbf{q}^2)$ is the gluon trajectory function, which for the bare reggeized gluon needs to be replaced by a parameter $-\nu$, $\nu > 0$, which is taken in the limit $\nu \rightarrow 0$. Other couplings of the reggeized gluon to particles and further reggeized gluons involve the four-gluon-vertex and higher induced vertices. In these cases s is no longer uniquely determined. Implementations for these cases can be found in Sec. 4.2 and Sec. 5.3.

For states of two or more reggeized gluons the above regularization applies equally. Sometimes it is however useful to combine phases of individual reggeized gluons to a single phase, see Sec. 3.2 for instance. For the evaluation of longitudinal integrals of loops containing reggeized gluons we propose to introduce so-called subtraction-diagrams. They remove an over-counting inside the diagrams of the effective action and provide well-defined convergent integrals for states of $n \geq 2$ reggeized gluons. They can be derived directly from the Lagrangian of the effective theory, by supplementing it by a subtraction term,

$$\mathcal{L}_{\text{subtract}}(A_+, A_-) = -2\text{tr}(A_+(A_+) - A_+) \partial_\sigma^2 A_- - 2\text{tr}(A_-(A_-) - A_-) \partial_\sigma^2 A_+, \quad (5.101)$$

with

$$A_\pm(A_\pm) = -\frac{1}{g} \partial_\pm U(A_\pm) = -\text{tr} \frac{1}{g} \partial_\pm \mathcal{P} \exp \left(-\frac{1}{2} g \int_{-\infty}^{x^\pm} dx'^\pm A_\pm(x') \right). \quad (5.102)$$

The complete effective action then reads

$$S_{\text{eff}} = \int d^4x [\mathcal{L}_{\text{QCD}}(v_\mu, \psi) + \mathcal{L}_{\text{ind}}(v_\pm, A_\pm) + \mathcal{L}_{\text{subtract}}(A_+, A_-)]. \quad (5.103)$$

A last point concerns the pole-prescription of the induced vertices of \mathcal{L}_{ind} , which also enters the subtraction terms: A suitable pole-prescription has been determined in Sec. 5.1 and explicit expressions can be found there, see Eqs. (5.9), (5.21) and (5.29). The presented choice of the

pole prescription yields induced vertices that coincide in their color structure with the originally proposed induced vertices without pole-prescription. Apart from that, they can be shown to obey Bose-symmetry and to agree with negative signature of the reggeized gluon. As a final rule we want to emphasize that, whenever a pole-momenta coincides with a momenta inside the Reggeon-factor in Eq. (5.99), it is mandatory that the $i\epsilon$ -prescription of the pole and the branch-cut coincide with each other.

With this short summary of results concerning longitudinal integrals, we conclude the discussion of the effective action. In the following chapter we turn to the study high-energy amplitudes in the context of the large N_c expansion in terms of topologies. In particular we will consider color factors with the topology of the pair-of-pants for the six-point-amplitude in the triple-Regge-limit.

Chapter 6

The triple Pomeron vertex and the pair-of-pants topology

6.1 Introduction

Starting from the classical paper by 't Hooft [73] the large N_c limit of gauge theories has remained in the center of attention for more than 25 years. In high energy QCD-phenomenology for instance, the large- N_c expansion proves its usefulness as a simplifying tool, if one attempts to resum higher order contributions, enhanced by large logarithms. With the general structure of the color factors being often too complex, the large N_c limit allows for resummation with an acceptable reduction of accuracy.

A new attraction of the large N_c expansion results nowadays from the fact that it organizes the color structure of Feynman diagrams in terms of topologies of two-dimensional surfaces which resemble the loop expansion of a closed string theory. With the advance of the AdS/CFT correspondence [52–54] which, in the limit of large N_c , connects $N = 4$ Super-Yang-Mills theory with a closed string theory in Anti-de-Sitter space and with string coupling proportional to N_c^{-1} this idea is more prevailing than ever.

The leading term of the large N_c expansion is given by color factors that have the topology of the sphere or equivalently the plane, and one usually refers to these leading contributions as 'planar' diagrams. Planar diagrams contribute, for example, to gluon-gluon scattering amplitudes or to multi-gluon production amplitudes. On the other hand, there exist also processes where the N_c leading color factor has not the topology of the plane. This is, for instance, the case for the scattering of two electromagnetic currents or virtual photons at high energies where the center of mass energy squared s is far bigger than the momentum transfer squared and the virtualities of the photons. In this case, the interaction between the scattering currents is mediated by the exchange of gluons between two quark loops, and, with quarks in QCD in the fundamental representation of the gauge group $SU(N_c)$, the leading color factor has the topology of a sphere with two boundaries, a cylinder. Within perturbative QCD such processes, at leading [7–11] and next-to-leading order accuracy [12, 13], are described by the BFKL-Pomeron, which is a bound state of two reggeized gluons. Higher order unitarity corrections are expected to involve bound states of more than 2 reggeized gluons, so called BKP-states [33, 34], which for the cylinder topology have been found to be integrable [39–41].

In the present study we go one step further and consider the class of process whose leading color factor has the topology of a sphere with three boundaries. Such a surface is depicted in Fig.6.1 and it is usually referred to as the topology of a 'pair of pants'. As a suitable example we consider the three-to-three process which describes the scattering of a highly virtual photon on two virtual photons in the triple Regge limit. Similar to the BFKL-Pomeron on the cylinder, we resum all contributions which are maximally enhanced by logarithms of energies. The class of diagrams selected in this way is illustrated in Fig.6.2: the three photon impact factors introduce three

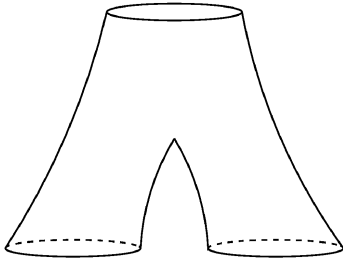


Figure 6.1: The 'pair of pants' topology

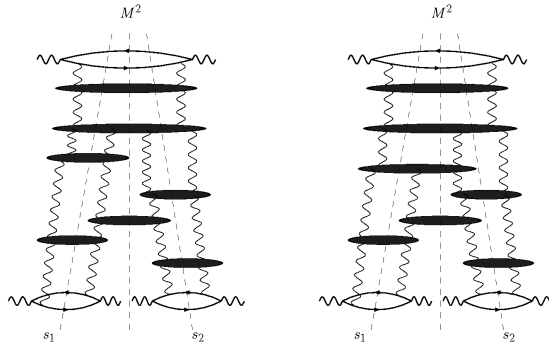


Figure 6.2: Typical contributions to the triple energy discontinuity for scattering of three virtual photons

boundaries, and thus belong to the topology depicted in Fig.6.1. Compared to the simple BFKL cylinder, the new feature is the splitting of one cylinder into two cylinders which is related to the 'triple Pomeron vertex' [35]. Within the AdS/CFT correspondence, the electromagnetic current corresponds to the R-current, and the high energy behavior of the 6-point amplitude, on the string side, is expected to exhibit the triple graviton vertex.

In QCD this $3 \rightarrow 3$ process has been investigated before for $N_c = 3$ in [35], the triple Pomeron vertex has been derived, and it has been shown to be invariant under two-dimensional Möbius transformations [107]. It is straightforward to repeat the analysis for arbitrary N_c and to take the large- N_c limit of these calculations. The system of four reggeized gluons and the triple Pomeron vertex have been further investigated particularly for the limit $N_c \rightarrow \infty$ in [74, 108, 109]. However the connection of these results with the expansion in terms of topologies of two-dimensional surfaces is not apparent. Instead of the pair-of-pants, the color factor rather seems to correspond to three disconnected cylinders. In the present chapter, we therefore demonstrate that by summing only diagrams with the topology of the pair-of-pants, Fig.6.1, one obtains the result of the large- N_c limit of [35]. In particular we find that the 'reggeizing' and 'irreducible' terms of [35] can be attributed to distinct classes of diagrams on the surface of the pair-of-pants.

This chapter is organized as follows. In section 6.2 we briefly review the planar and cylinder topologies. In the high energy limit, the planar diagrams satisfy the bootstrap condition of the reggeized gluon, whereas the cylinder diagrams lead to the famous BFKL amplitude. In section 3 we turn to the analytic form of the $3 \rightarrow 3$ scattering amplitude and give a general description of the diagrams which need to be summed. In Section 4 we study the color lines on the surface of the pants, arriving at the definition of two distinct classes of diagrams in color space (named 'planar' and 'non-planar'). We also review the different momentum space kernels which describe the interactions of reggeized gluons. In section 5 we sum the 'planar' diagrams and arrive at the 'reggeized' amplitudes introduced in [35], whereas in the section 6 we investigate the 'non-planar' diagrams and re-derive the triple Pomeron vertex of [35]. In section 7 we briefly summarize our results, and the final section 8 contains a few conclusions.

6.2 Elastic amplitudes

In this section we begin by recalling the definition of the large N_c expansion, following the classical paper by 't Hooft [73]. As a preparation for the study of the pair-of-pants topology, we then reconsider the simplest examples of diagrams, whose color factor have the topology of the plane and of the cylinder. In the Regge-limit they yield the reggeized gluon and the BFKL-Pomeron, respectively.

6.2.1 The large N_c expansion

To study the large N_c limit as an expansion of topologies of the color factor, one is asked to translate the color factors of a scattering amplitude into the so-called double line notation. To this end we use the $SU(N_c)$ generators in the fundamental representation, $(g^a)_j^i$, in the normalization¹ $\text{tr}(g^a g^b) = \delta^{ab}$, and we make use of the identity

$$f^{abc} = \frac{1}{i\sqrt{2}} [\text{tr}(g^a g^b g^c) - \text{tr}(g^c g^b g^a)]. \quad (6.1)$$

For all inner gluon lines in the adjoint representation, the indices can then be expressed in terms of (anti-)fundamental indices by means of the Fierz identity

$$(g^a)_j^i (g^a)_l^k = \delta_l^i \delta_j^k - \frac{1}{N_c} \delta_j^i \delta_l^k. \quad (6.2)$$

Making use of a diagrammatic notation, where a Kronecker-delta is represented by a single line with an arrow, indicating the flow from the upper to the lower index,

$$\delta_j^i = i \longrightarrow j, \quad (6.3)$$

the structure constants f^{abc} are expressed as

$$f^{a_1 a_2 a_3} (g^{a_1})_{j_1}^{i_1} (g^{a_2})_{j_2}^{i_2} (g^{a_3})_{j_3}^{i_3} = \frac{1}{i\sqrt{2}} \left(\begin{array}{c} i_1 \quad j_1 \\ \downarrow \quad \downarrow \\ \longleftarrow i_3 \quad \longrightarrow j_3 \\ \downarrow \quad \downarrow \\ j_2 \quad i_2 \end{array} - \begin{array}{c} i_1 \quad j_1 \\ \downarrow \quad \downarrow \\ \longrightarrow i_3 \quad \longleftarrow j_3 \\ \downarrow \quad \downarrow \\ j_2 \quad i_2 \end{array} \right). \quad (6.4)$$

In order to arrive at the large N_c expansion, one drops, in the Fierz-identity Eq.(7.1), the second term. As a consequence, the gluon is represented by a double line

$$\delta_l^i \delta_j^k = \begin{array}{c} i \longrightarrow l \\ j \longleftarrow k \end{array}. \quad (6.5)$$

The neglect of second term of the Fierz-identity Eq.(7.1) which serves to subtract the trace of the $SU(N_c)$ gluon implies that we consider an $U(N_c)$ gluon rather than an $SU(N_c)$ gluon. While this term is suppressed for large N_c , dropping this term is only correct as long as we stay within the leading term of the expansion. Tracelessness of the $SU(N_c)$ gluon can be taken into account by introducing an additional $U(1)$ ghost field [110–112], which subtracts the trace of the $U(N_c)$ -gluon. Since the $U(1)$ ghost-field commutes with the $U(N_c)$ gluon-field, it couples only to quarks, but not to gluons. Within the Leading Logarithmic Approximation, which we will use in the following, the interaction between scattering objects is mediated only by gluons, while quarks occur in the coupling of the gluons to the scattering objects. Corrections due to the $U(1)$ ghost in this approximation therefore appear only in low orders of the strong coupling and are taken into account easily.

Using the double line representation for gluons, Eq.(7.4), and representing quarks in the fundamental representation by single lines, the color factor of a vacuum Feynman diagram turns into a network of double and single lines, which can be drawn on a two-dimensional surface with Euler number $\chi = 2 - 2h - b$, where h is the number of handles of the surface, and b the number of boundaries or holes. A closed color-loop always delivers a factor N_c . With quarks being represented by single lines, a closed quark-loop, compared to a corresponding gluon-loop, is $1/N_c$ suppressed and leads always to a boundary. For an arbitrary vacuum graph T one arrives at the following expansion in N_c

$$T = \sum_{h,b}^{\infty} N_c^{2-2h-b} T_{h,b}(\lambda). \quad (6.6)$$

¹Note that this deviates by a factor 2 from the standard normalization $\text{tr}(t^a t^b) = \delta^{ab}/2$.

where

$$\lambda = g^2 N_c \tag{6.7}$$

is the 't Hooft-coupling which is held fixed, while N_c is taken to infinity. The expansion Eq.(7.6) matches the loop expansion of a closed string theory with the string coupling $1/N_c$. For $N_c \rightarrow \infty$, the leading diagrams are those that have the topology of a sphere: zero handles and zero boundaries, $h = b = 0$. If quarks are included, the leading diagrams have the topology of a disk, i.e. the surface with zero handle and one boundary, $h = 0, b = 1$. The disk fits on the plane, with the boundary as the outermost edge. Diagrams with two boundaries and zero handles can be drawn on the surface of a cylinder, those with three boundaries on the surface of a pair-of-pants. Boundaries are also be obtained by removing, from the sphere, one or more points: removing one point, one obtains the disk, which can be drawn on the plane, and by identifying the removed point with infinity, the graphs can be drawn on the (infinite) plane. Removing two points we obtain the cylinder and so on. By definition, the expansion Eq.(7.6) is defined for vacuum graphs. However, from the earliest days on [113], the large N_c -limit has been also applied to the scattering of colored objects. In order to consider the topological expansion of an amplitude with colored external legs, one needs to embed it into a vacuum graph which then defines the topological expansion of an amplitude with colored external legs.

In the following it will be convenient to define modified couplings

$$\bar{g} = \frac{g}{\sqrt{2}}, \quad \bar{\lambda} = \bar{g}^2 N_c = \frac{g^2 N_c}{2}, \tag{6.8}$$

which absorb the factor $1/\sqrt{2}$. Due to our normalization of $SU(N_c)$ generators which differs from the more standard one, $\text{tr}(t^a t^b) = \delta^{ab}/2$, such a factor $1/\sqrt{2}$ arises for each quark-gluon coupling and, because of Eq.(6.4), also for each gluon-gluon coupling.

6.2.2 Planar amplitudes: Reggeization of the gluon

In the present paragraph, we shall discuss the Regge-limit of planar amplitudes (first addressed in [75]) which satisfy the bootstrap condition of the reggeized gluon, the basic ingredient for the further studies. In order to study reggeization of the gluon, one considers the scattering of colored objects. To be definite, we consider the scattering of a quark on an anti-quark. The disk-topology of the color factors becomes apparent, if we connect color lines of the incoming quark and antiquark with each other and of the outgoing quark and antiquark (note that, if instead we would connect the color lines of the ingoing and outgoing quark with each other and of the incoming and outgoing antiquark, we would discover the cylinder topology). As far as the momentum part of the diagrams is concerned, our method is the following: We consider the Regge limit $s \gg -t$ of the elastic amplitude and make use of the Leading Logarithmic Approximation (LLA), where we select all diagrams that are maximally enhanced by a logarithm in s , i.e. that are proportional to $\frac{\lambda}{N_c} (\lambda \ln s)^n$, and sum them up to all orders in λ . Furthermore, in this approximation, all t -channel particles are gluons (quark exchanges are power suppressed).

We start by considering tree- and one-loop-level diagrams within the LLA, and convince ourselves that these leading order result, for planar color graphs, satisfy the bootstrap condition and are thus in agreement with the reggeization of the gluon. At tree level, the (anti-)quarks interact by exchange of a single gluon. In the standard adjoint notation, the color factor of the diagram is given by $(g^a)_j^i (g^a)_k^l$, which in the double-line notation turns into $\delta_k^i \delta_j^l$, while the $U(1)$ -ghost can be disregarded for the plane. We therefore have



$$\text{Diagram} = \text{Diagram} \times T_{qq}^{\text{tree}}(s, t), \quad T_{qq}^{\text{tree}}(s, t) = 2\bar{g} \frac{-s}{t} \bar{g}. \tag{6.9}$$

From now on we adopt the following notation: in a Feynman diagram gluons are usually denoted by curly lines, and in this notation the diagram is understood to represent both the color factors

and the momentum part. Alternatively, when drawing a diagram with the double line notation for each gluon, this diagram represents only the color part, and the momentum part has to be written separately.

Turning to higher order graphs, we have the restriction that, with every insertion of an additional internal loop coming with a factor g^2 , we have to produce a closed color loop, yielding a factor N_c which then combines to the 't Hooft coupling $\lambda = g^2 N_c$. Only such higher order term will be included into the planar approximation discussed in this section. This restriction holds also for other topologies in the expansion Eq.(7.6): every insertion of an additional gluon into the Born diagram provides automatically a factor g^2 and must be compensated by a closed color loop in order to stay within the considered coefficient $T_{h,b}$ of the expansion. For our planar loop, for each higher order graph the tensorial structure of the color factor will be proportional to the one of the Born term. As far as the momentum part is concerned, the 1-loop diagrams for quark-antiquark scattering that contribute within the LLA are shown in Fig.6.3. For both diagrams,

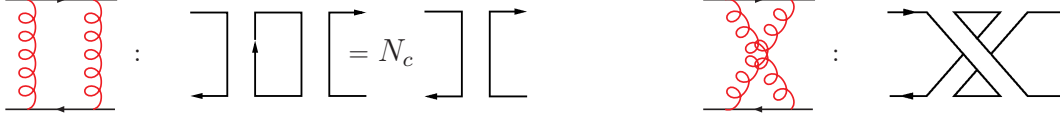


Figure 6.3: One-loop corrections to quark-antiquark scattering. On the left hand side, the color factor of the planar Feynman diagram is N_c times the Born color factor. On the right hand side, the non-planar diagram does not fit onto the plane and is N_c suppressed.

the momentum part is of the same order of magnitude, i.e. it is proportional to $g^2 s \ln(-s)$ and $g^2 u \ln(-u)$, respectively, with $u \simeq -s$ in the Regge limit. However, when counting closed color loops, one sees that only the first diagram is leading in N_c . Also, when closing the color lines of the incoming quark and antiquark and of the outgoing particles, we observe that for the first diagram the 'closed' color factor, indeed, fits on the disk with $h = 0, b = 1$, while the second 'closed' color factor has an additional handle $h = 1, b = 1$. We therefore find for the quark-antiquark scattering amplitude at 1-loop:

$$T_{q\bar{q}}^{1\text{-loop}}(s, t) = \ln(-s)\beta(t)T_{q\bar{q}}^{\text{tree}}(s, t) \quad \text{with} \quad \beta(-\mathbf{q}^2) = \bar{\lambda} \int \frac{d^2\mathbf{k}}{(2\pi)^3} \frac{-\mathbf{q}^2}{\mathbf{k}^2(\mathbf{q}-\mathbf{k})^2}, \quad (6.10)$$

where the color factor N_c has already been included into the gluon trajectory function, and bold letters denote Euclidean momenta perpendicular to the light-like momenta p_1 and p_2 of the scattering quark and antiquark; in particular $t = -\mathbf{q}^2$. Eq.(6.10) can be understood as the order $\mathcal{O}(g^4)$ term of the expansion of the exchange of a planar reggeized gluon:

$$T_{q\bar{q}}(s, t) = 2\bar{g}(-s)^{1+\beta(t)} \frac{1}{t} \bar{g}. \quad (6.11)$$

For our further analysis we use the following analytic representation of the planar elastic amplitude in the Regge limit:

$$T_{2 \rightarrow 2}(s, t) = s \int_{\sigma-i\infty}^{\sigma+i\infty} \frac{d\omega}{2\pi i} s^\omega \xi(\omega) \phi(\omega, t). \quad (6.12)$$

The partial wave amplitude $\phi(\omega, t)$ is a real-valued function, and phases are contained in the signature factor $\xi(\omega)$:

$$\xi(\omega) = -\pi \frac{e^{-i\pi\omega}}{\sin(\pi\omega)}. \quad (6.13)$$

Note the difference from the 'usual' signature factor $\xi \sim e^{-i\pi\omega} \pm 1$ which contains both right and left hand energy cuts: at one loop we have shown that only the Feynman diagram with the s -channel discontinuity belongs to the planar approximation whereas the u discontinuity is

absent. For quark-antiquark-scattering, this also holds for higher order terms. We then take the discontinuity in s

$$\Im m_s T_{2 \rightarrow 2}(s, t) = \text{disc}_s T_{2 \rightarrow 2}(s, t) = \pi s \int \frac{d\omega}{2\pi i} s^\omega \phi(\omega, t), \quad (6.14)$$

which, by unitarity

$$2\Im m_s T_{2 \rightarrow 2}(s, t) = \sum \int T_{2 \rightarrow n} T_{2 \rightarrow n}^* \quad (6.15)$$

relates the Mellin transform of the partial wave amplitude $\phi(\omega, t)$ to the sum of production processes. To leading order in g , the partial wave has the form

$$\phi^{(0)}(\omega, t) = \frac{2}{\omega} \phi_{(2;0)} \otimes \phi_{(2;0)} = \frac{2\bar{g}^2}{\omega t} \beta(t) \quad (6.16)$$

where $\phi_{(2;0)} = \bar{g}^2 N_c^{1/2}$ denotes the non-singlet two gluon impact factor for quark and antiquark, and the convolution symbol is defined as

$$\otimes = \int \frac{d^2 \mathbf{k}}{(2\pi)^3 \mathbf{k}_1^2 \mathbf{k}_2^2} \quad (6.17)$$

with $\mathbf{q} = \mathbf{k}_1 + \mathbf{k}_2$ and $t = -\mathbf{q}^2$. Higher order corrections involve diagrams where additionally real gluons are produced. To leading logarithmic accuracy, real particle production takes place within the Multi-Regge-Kinematics (MRK), where the produced particles are widely separated in rapidity. The leading order diagram, with one additional s -channel gluon, is illustrated in Fig.6.4: Here the particle production vertex (depicted by a dot) is an effective vertex for the production of

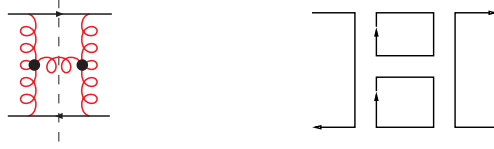


Figure 6.4: s -channel discontinuity with three real particles. To the right the corresponding planar color factor.

one real gluon. This production vertex is build by the following Feynman diagrams:

$$\begin{aligned} & \text{Diagram with dot} = \text{Diagram 1} + \text{Diagram 2} + \text{Diagram 3} + \text{Diagram 4} + \text{Diagram 5} \\ & \frac{1}{i} \left(\text{Color Factor 1} - \text{Color Factor 2} \right) \quad \frac{-1}{i} \text{Color Factor 3} \quad \frac{1}{i} \text{Color Factor 4} \quad \frac{1}{i} \text{Color Factor 5} \quad \frac{-1}{i} \text{Color Factor 6} \quad (6.18) \end{aligned}$$

In the second line we show, for each of the five different Feynman-diagrams, the corresponding color factor in the double-line notation. For the last four diagrams on the right hand side, where the real gluon is emitted from the quark and the antiquark respectively, we have shifted factors i and $(-i)$ from the momentum part to the color factor. With such a shift, the (remaining) momentum parts of the second and the third diagram and the momentum parts of the fourth and the fifth diagram coincide in the considered kinematical regime with each other. Color factors and momentum parts of the production vertex can therefore be written in a factorized form, and we obtain

$$\begin{aligned} & \text{Diagram with dot} = \frac{\bar{g}}{i} \left(\text{Color Factor 1} - \text{Color Factor 2} \right) \times C(l, k) \cdot \epsilon_{(\lambda)}, \quad (6.19) \end{aligned}$$

where λ denotes the helicity of the produced gluon. With the light-like momenta of the quark and the antiquark given by p_1 and p_2 respectively we have with $s \simeq 2p_1 \cdot p_2$,

$$C^\mu(l, k) = \left(\alpha_l + 2 \frac{l^2}{\beta_k s} \right) p_1^\mu + \left(\beta_k + 2 \frac{k^2}{\alpha_l s} \right) p_2^\mu - (l_\perp^\mu + k_\perp^\mu), \quad (6.20)$$

where $\alpha_l s = 2p_2 \cdot l$ and $\beta_k s = 2p_1 \cdot k$. When squaring the production amplitude, we find for the color part that only one of the four possible combinations fits on the plane, namely the one shown on the right hand side of Fig.6.4. From the point of view of Feynman-diagrams, the planar approximation includes only a sub-set of the diagrams in Eq.(6.18), namely those with the color structure

$$\begin{array}{c} \text{---} \\ \text{---} \\ \text{---} \end{array} + \begin{array}{c} \text{---} \\ \text{---} \\ \text{---} \end{array} + \begin{array}{c} \text{---} \\ \text{---} \\ \text{---} \end{array} \quad (6.21)$$

However due to the factorization of momentum and color parts in the MRK, Eq.(6.19), we still recover the complete production vertex C_μ and therefore the BFKL kernel. Making use of our re-defined couplings \bar{g} and $\bar{\lambda}$, and including the factors $1/i$ of Eq.(6.19), we find, for the plane, the $2 \rightarrow 2$ Reggeon transition kernel $K_{2 \rightarrow 2}$ as:

$$\begin{array}{c} l_1 \\ \text{---} \\ k_1 \end{array} \begin{array}{c} l_2 \\ \text{---} \\ k_2 \end{array} = \bar{\lambda} K_{2 \rightarrow 2}(l_1, l_2; \mathbf{k}_1, \mathbf{k}_2) = -\bar{\lambda} \left[(\mathbf{k}_1 + \mathbf{k}_2)^2 - \frac{l_1^2 k_2^2}{(\mathbf{k}_1 - \mathbf{l}_1)^2} - \frac{l_2^2 k_1^2}{(\mathbf{k}_1 - \mathbf{l}_1)^2} \right] \quad (6.22)$$

with the constraint $\mathbf{l}_1 + \mathbf{l}_2 = \mathbf{k}_1 + \mathbf{k}_2 = \mathbf{q}$.

Higher order terms with the production of n -gluons within the MRK are taken into account in a similar way. Making use of Regge-factorization of the production amplitudes, it can be shown that each emission of an additional real gluon is taken into account by insertion of the effective production vertex Eq.(6.19), as illustrated in Fig.6.5 for the squared production amplitude. Similar to the production of one-gluon, for each of the inserted production vertices only one of the four possible combinations of color factors fits onto the plane, and the resulting color factor can be found on the right-hand-side of Fig.6.5.

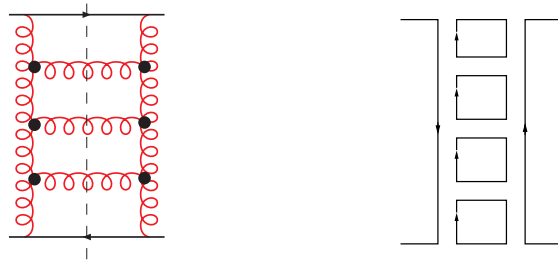


Figure 6.5: The s-channel discontinuity of the elastic quark-antiquark scattering amplitude for three gluon production. On the right, the color structure of the planar diagrams.

In order to obtain the complete expression of order λ^n of the partial wave ϕ , we need to include the reggeization of the gluon. This is done in the same way as in the finite- N_c case, except that at each step we have to restrict ourselves to the planar approximation. In lowest order we return, on the rhs of the unitarity equation (6.15), to the elastic intermediate state and include, in one of the two factors $T_{2 \rightarrow 2}$, the one loop result (6.10). Together with the real one-gluon production discussed above, this provides, in (6.11), the complete imaginary part to order g^6 (or λ^3). Compared to the tree diagram expression (6.9), (6.11) replaces the exchange of an elementary t -channel gluon by a reggeized gluon. In higher order g , the analogous replacement has to be done, on the rhs of (6.15), for all t -channel exchanges in the production amplitudes $T_{2 \rightarrow n}$.

In order to prove the self-consistency of this procedure, one has to show that the BFKL bootstrap condition is satisfied in the planar approximation. For the partial wave in Mellin-space, reggeization of the t -channel gluons within the LLA requires to introduce, for every t -channel state of two gluons, a Reggeon-propagator $1/(\omega - \beta(\mathbf{k}) - \beta(\mathbf{q} - \mathbf{k}))$. In order to perform the resummation of all production processes in Fig.6.5, it is most convenient to formulate the BFKL integral-equation in the planar approximation. To this end we first factorize off, at the lower end of the ladder, the antiquark-impact factor $\phi_{(2;0)}$. We then define, for the scattering of a quark on a reggeized gluon, the amplitude $\phi_2(\omega|\mathbf{k}_1, \mathbf{k}_2)$, which contains the Reggeon propagator $1/(\omega - \beta(\mathbf{k}_1) - \beta(\mathbf{k}_2))$ of the two reggeized gluons at the lower end. The BFKL-equation for this amplitude reads:

$$\left(\omega - \sum_i^2 \beta(\mathbf{k}_i)\right) \phi_2(\omega|\mathbf{k}_1, \mathbf{k}_2) = \phi_{(2;0)}(\mathbf{k}_1 + \mathbf{k}_2) + \bar{\lambda} K_{2 \rightarrow 2} \otimes \phi_2(\omega|\mathbf{k}_1, \mathbf{k}_2), \quad (6.23)$$

where the kernel coincides with the finite N_c case. With our impact factor $\phi_{(2;0)}$ which depends only on the sum of the transverse momenta of the t -channel gluons we find for Eq. (6.23) the familiar pole solution

$$\phi_2(\omega|\mathbf{k}_1 + \mathbf{k}_2) = \frac{\phi_{(2;0)}}{\omega - \beta(-(\mathbf{k}_1 + \mathbf{k}_2)^2)}. \quad (6.24)$$

The partial wave for quark-antiquark scattering becomes

$$\phi(\omega, t) = 2 \int \frac{d^2 \mathbf{l}}{(2\pi)^3} \frac{1}{\mathbf{l}_1^2 \mathbf{l}_2^2} \frac{\phi_{(2;0)} \phi_{(2;0)}}{\omega - \beta(t)} = \frac{1}{t} \frac{2\bar{g}^2 \beta(t)}{\omega - \beta(t)}. \quad (6.25)$$

Inserting this into Eq.(6.12) and using that in LLA $\sin \pi\omega \simeq \pi\omega$, we find the reggeized gluon, as proposed in Eq.(6.11). This proves that, in the planar approximation, the bootstrap property is satisfied.

6.2.3 Cylinder topology: The BFKL-Pomeron

Next we turn to the cylinder topology which, in the Regge-limit, leads to the BFKL-Pomeron. In the expansion Eq.(7.6), this corresponds to the term with two boundaries and zero handles, $b = 2, h = 0$. Even though it would be possible to carry out this analysis for quark-antiquark scattering, it is more natural to do so for scattering of two highly virtual photons, which provides an IR-finite and gauge-invariant amplitude. Reggeization of the gluon will be an important ingredient in this analysis, as we will see in short. As a physical process with such a topology we consider

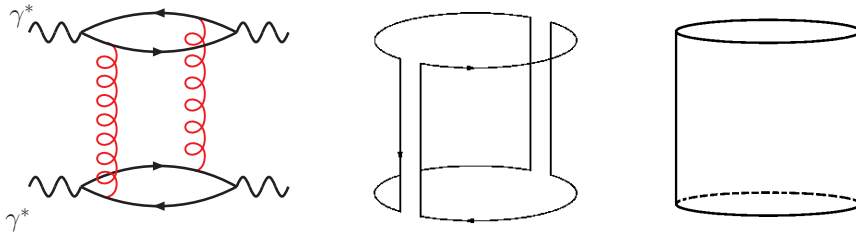


Figure 6.6: To the left, a typical leading order diagram with its double-line color line factor in the middle. The color factor fits on the cylinder surface, depicted to the right.

the scattering of two highly virtual photons in the Regge limit $s \gg |t|$, and again we use the LLA to sum to all orders those diagrams which have one power of $\ln s$ for each loop. In particular, the interaction between the two photons is mediated by gluons in the t -channel, and to lowest order in the electromagnetic coupling, each photon couples to a quark-loop. The quark-loops provide the two boundaries of the cylinder. To leading order, the two photons interact by the exchange of two t -channel gluons. A typical leading order diagram is shown in Fig.6.6, together with its color factor. Unlike the planar case, color factors of diagrams with both discontinuities in the s - and

in the u -channel fit on the cylinder. The t -channel-interaction has therefore positive signature, similar to the N_c finite case,

To resum higher order terms we use again the analytic representation Eq.(6.12) of the elastic amplitude in the Regge limit. Now the signature factor includes both right and left hand cuts:

$$\xi(\omega) = -\pi \frac{e^{-i\pi\omega} - 1}{\sin(\pi\omega)} \quad (6.26)$$

and belongs to positive signature in the t -channel. As in the previous paragraph, we take the discontinuity in s which allows to determine the partial wave amplitude by considering real particle production processes. Coupling of the two gluon state to the virtual photon is described by the two gluon impact factor of the virtual photon which is given by the sum of the following four Feynman diagrams:

$$D_{(2;0)}(\mathbf{k}_1, \mathbf{k}_2) = \text{[Four Feynman diagrams]} \quad (6.27)$$

with the constraint $\mathbf{k}_1 + \mathbf{k}_2 = \mathbf{q}$. It has the important properties to be symmetric under exchange of its transverse momenta arguments, and to vanish whenever one of the transverse momenta goes to zero². For the large N_c treatment it is convenient to absorb a factor N_c into the impact factor by defining $\mathcal{D}_{(2;0)}(\mathbf{k}_1, \mathbf{k}_2) := N_c D_{(2;0)}(\mathbf{k}_1, \mathbf{k}_2)$ which is proportional to the 't Hooft coupling λ . To leading order in λ , the partial wave is given by

$$\phi^{(0)}(\omega, t) = \frac{2}{\omega} \mathcal{D}_{(2;0)} \otimes \mathcal{D}_{(2;0)}. \quad (6.28)$$

Higher order corrections to the s -discontinuity are taken into account by considering real gluon production in the Multi-Regge-kinematics. Production of real gluons is described, in the same way as in the previous section, by the particle production vertex in Eq.(6.19). To study the color factor on the cylinder, we start with the Born term, Fig.6.6 and insert one additional s -channel gluon which leads us to the diagram Fig.6.7. For the color factors on the cylinder we find, compared to

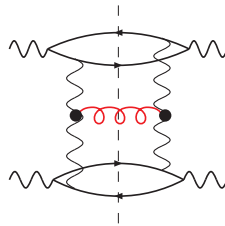


Figure 6.7: s -discontinuity for the scattering of two virtual photons with one additional real s -channel gluon. Wavy lines for t -channel gluons denote reggeized gluons.

the plane an important difference: in addition to the combinations that fits on the plane,

$$\text{[Diagram showing a transition from a planar diagram to a cylindrical diagram]} \quad (6.29)$$

²An analytic form of $D_{(2;0)}$ for the forward case can be found in [35]. In particular, the above $D_{(2;0)}$ is $1/\sqrt{8}$ times Eq.(2.4) of [35], where the factor $\sqrt{8}$ originates from $\sqrt{N_c^2 - 1}$ with $N_c = 3$.

on the cylinder also the following combination contributes:

(6.30)

For the two-to-two Reggeon transition on the cylinder we therefore obtain a factor two compared to the plane. This counting generalizes to diagrams with more than one real gluon: For each produced real gluon the two combinations of color factors Eq.(6.29) and Eq.(6.30) need to be added. An example with three produced gluons is shown in Fig.6.8: For each rung, we have two

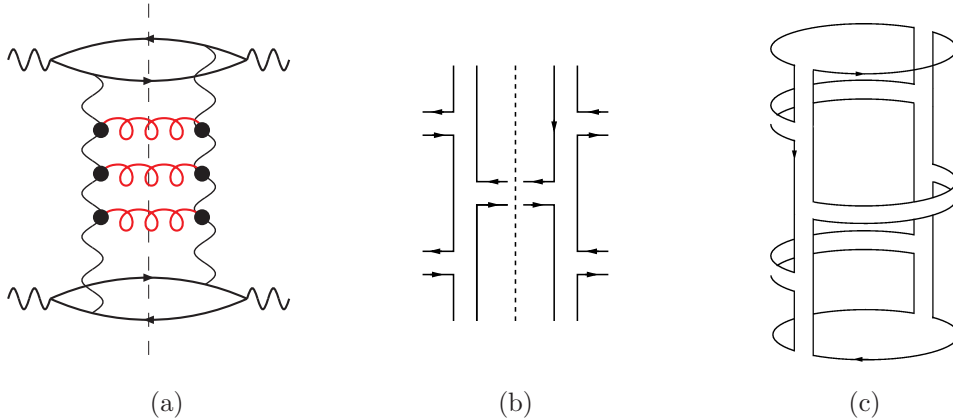


Figure 6.8: Multi-gluon emission within the MRK. (a) The cut Feynman diagram (b) Combination of relevant color diagrams of the production vertex. (c) The combination of (b) on the cylinder.

possibilities of connecting the t -channel lines of the ladder, either on the forefront and or on the backside of the cylinder³ Similar to the planar case discussed before, the summation over all production processes is done by formulating the BFKL equation on the cylinder. This integral equation coincides with Eq.(6.23), except for the factor 2 in front of $K_{2 \rightarrow 2}$, which results from the cylinder topology. Technically, we again split off the impact factor of the lower virtual photon and consider the partial wave amplitude $\mathcal{D}_2(\omega|\mathbf{k}_1, \mathbf{k}_2)$ for the scattering of a virtual photon on two reggeized gluons, which as before we define to contain the Reggeon propagator of the external reggeized gluons. We find

$$\left(\omega - \sum_i^2 \beta(\mathbf{k}_i)\right) \mathcal{D}_2(\omega|\mathbf{k}_1, \mathbf{k}_2) = \mathcal{D}_{2,0}(\mathbf{k}_1, \mathbf{k}_2) + 2\bar{\lambda} K_{2 \rightarrow 2} \otimes \mathcal{D}_2(\omega|\mathbf{k}_1, \mathbf{k}_2). \quad (6.31)$$

The kernel coincides with the BFKL kernel. Unlike the planar BFKL-equation Eq.(6.23), Eq.(6.31) has no pole solution, but the solution is known to have a cut in the complex ω -plane. The solution is known both for the forward ($t = 0$) [7–11] and the non-forward ($t \neq 0$) case [116]. Furthermore, the BFKL-Green's function, which is obtained from $\mathcal{D}_2(\omega)$ by splitting up the impact factor of the above virtual photon, is invariant under Möbius transformations.

6.3 Six-point amplitudes and the pair-of-pants -topology

Returning to the expansion Eq.(7.6), we finally address the term with three boundaries and zero handles $b = 3, h = 0$. It is proportional to $1/N_c$ and leads to color factors that fit on the pair-of-pants, as illustrated in Fig.6.9. As we did for scattering amplitudes on the plane and on the

³The fact that, on the cylinder, each emission has two possibilities, one on the forefront and another one on the backside of the cylinder, has been realized also in [114, 115]. However, the approach pursued in this paper is quite different from ours: it starts from Park-Taylor amplitudes.

cylinder, also for the pair-of-pants we identify a QCD-amplitude which, using the LLA, will be determined in a certain kinematical high energy limit. As it was the case for the elastic amplitude,

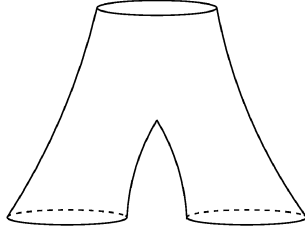


Figure 6.9: The sphere with three boundaries $b = 3$ and no handles $h = 0$ which yields the pair-of-pants.

within the LLA, quark loops occur only inside the coupling to external states. In order to arrive at a surface with three boundaries, we are thus led to a six-point amplitude, which we will study in the triple-Regge limit, to be specified in the following.

Within QCD, scattering amplitudes with more than 4 external particles arise naturally in the context of deep inelastic scattering on a weakly bound nucleus, see Fig.6.10a. To be definite, let us consider deep inelastic electron scattering on deuterium. The total cross section of this scattering process is obtained from the elastic scattering amplitude, $T_{\gamma^*(pn) \rightarrow \gamma^*(pn)}$, which describes a $3 \rightarrow 3$ process,

$$\sigma_{\gamma^*(pn) \rightarrow \gamma^*(pn)}^{tot} = \frac{1}{s} \Im T_{\gamma^*(pn) \rightarrow \gamma^*(pn)}, \quad (6.32)$$

where s denotes the square of the total center of mass energy of the scattering process. To study the pair-of-pants topology, we replace the two nucleons by virtual photons which furthermore provides us with a clean perturbative environment for the study of the six-point amplitude. The kinematics is illustrated in Fig.6.10. Large energy variables are $s_1 = (q + p_1)^2$, $s_2 = (q' + p_2')^2$, and $M^2 = (q + p_1 - p_1')^2$ which gives the squared mass of the diffractive system in which the upper virtual photon dissociates. The total energy square is given by $s = (q + p_1 + p_2)^2$. Furthermore, we have the momentum transfer variables $t = (q - q')^2$, $t_1 = (p_1 - p_1')^2$, and $t_2 = (p_2 - p_2')^2$. The triple Regge-limit is given by $s_1 = s_2 \gg M^2 \gg t, t_1, t_2$. The investigation of such a process, for finite N_c , has been started in [35], in the context of diffractive dissociation in deep inelastic scattering, and in the following we will stay close to the methods used there.

Let us begin with finite N_c . The $3 \rightarrow 3$ amplitude in the triple Regge limit has the following analytic representation

$$T_{3 \rightarrow 3}(s_1, s_2, M^2 | t_1, t_2, t) = \frac{s_1 s_2}{M^2} \int \frac{d\omega_1 d\omega_2 d\omega}{(2\pi i)^3} s_1^{\omega_1} s_2^{\omega_2} (M^2)^{\omega - \omega_1 - \omega_2} \xi(\omega_1) \xi(\omega_2) \xi(\omega, \omega_1, \omega_2) \cdot F(\omega, \omega_1, \omega_2 | t, t_1, t_2). \quad (6.33)$$

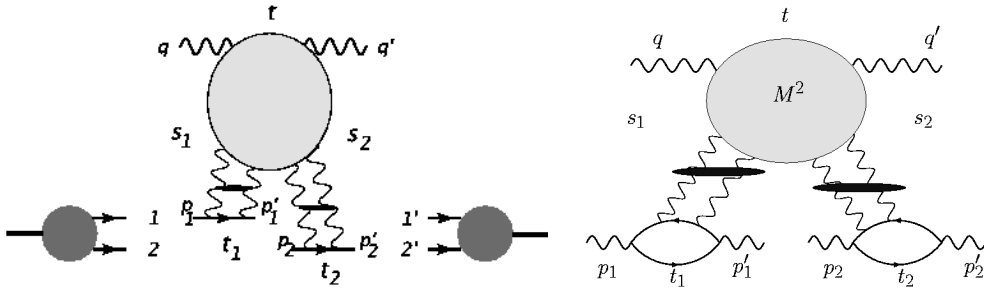


Figure 6.10: Scattering of a virtual photon on a weakly bound nucleus and the corresponding process where the lower nuclei are replaced by two highly virtual photons to the right.

All three t -channels carry positive signature, and the signature factors are given by

$$\xi(\omega) = -\pi \frac{e^{-i\pi\omega} - 1}{\sin(\pi\omega)} \quad \text{and} \quad \xi(\omega, \omega_1, \omega_2) = -\pi \frac{e^{-i\pi(\omega - \omega_1 - \omega_2)} - 1}{\sin \pi(\omega - \omega_1 - \omega_2)}. \quad (6.34)$$

The partial wave $F(\omega_1, \omega_2, \omega | t_1, t_2, t)$ has no phases and is real valued. In analogy to the treatment of $T_{2 \rightarrow 2}$, we take the triple energy discontinuity in s_1 , M^2 , and s_2 ,

$$\text{disc}_{s_1} \text{disc}_{s_2} \text{disc}_{M^2} T_{3 \rightarrow 3} = \pi^3 \frac{s_1 s_2}{M^2} \int \frac{d\omega_1 d\omega_2 d\omega}{(2\pi i)^3} s_1^{\omega_1} s_2^{\omega_2} (M^2)^{\omega - \omega_1 - \omega_2} \cdot F(\omega_1, \omega_2, \omega | t_1, t_2, t), \quad (6.35)$$

which via a triple Mellin transform relates the partial wave $F(\omega_1, \omega_2, \omega | t_1, t_2, t)$ to the real valued triple energy discontinuity.

Within the LLA, each of the three virtual photons couples to the t -channel gluons by a quark-loop (which in the topological expansion provides the three boundaries of the pair-of-pants). To leading order in g^2 , four t channel gluons couple to the upper quark-loop, and two gluons to each of the two lower quark-loops, which yields diagrams like the one shown in Fig.6.11. When taking the

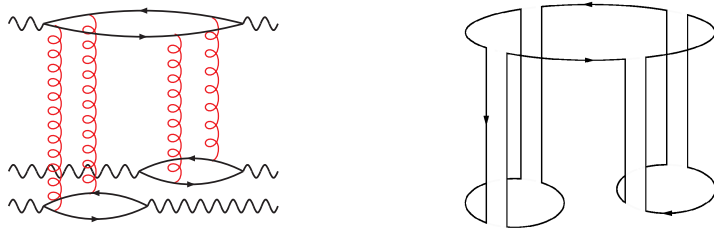


Figure 6.11: An example of a leading order diagram for the six-point amplitude with its color factor depicted to the right. The diagram is proportional to $g^8 N_c^3 = \lambda^4 N_c^{-1}$ as required for the pair-of-pants.

triple energy discontinuity, all intermediate states between the t channel gluons are on mass-shell. For higher order corrections to these diagrams, we make extensive use of unitarity and compute sums over products of production processes. Some examples are shown in Fig.6.12. Due to the

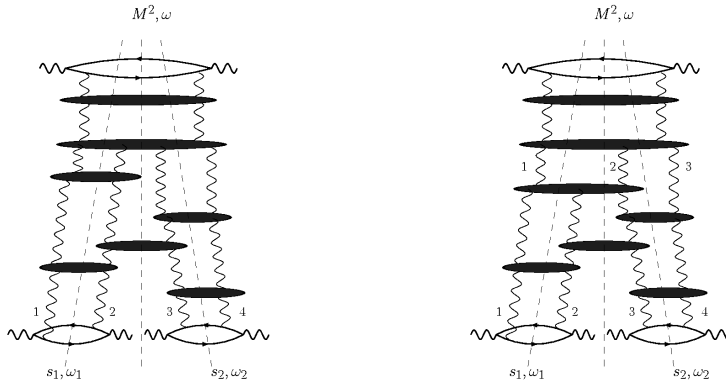


Figure 6.12: A few contributions to the triple energy discontinuity of Eq.(6.33)

triple discontinuity, t -channel gluons do not intersect, and it is therefore useful to enumerate them from the left to right, with the most left gluon carrying the index 1. In order to form, within the LLA, color singlet states which at the top couple to the virtual photon and at the bottom to two virtual photons, we are lead to QCD diagrams with four t -channel gluons at the lower and two, three or four t -channel gluons at the upper end. In contrast to our previous discussion of scattering processes on the plane and on the cylinder, the number of t -channel gluons can change, i.e. a t channel gluon can emerge also from a s channel produced gluon. However, in LLA there is the restriction that, when moving downwards, the number of reggeized t channel gluons never decreases.

A special role in our analysis is taken by the diffractive mass M^2 as it defines the size of the upper 'cylinder' of the pair-of-pants. In particular, the lowest intermediate state inside the M^2 -discontinuity (descending from the top to the bottom of the diagram) defines the last interaction between the two 'legs' of the pants, i.e. the branching point of the upper into the two lower cylinders. We use this branching point to factorize the partial wave $F(\omega, \omega_1, \omega_2)$ into a convolution of three different amplitudes. With $s_1, s_2 \gg M^2 \gg t, t_1, t_2$, the diagrams below the branching point, within the LLA, do not depend on the details of the dissociation of the upper virtual photon, and are therefore described by two independent amplitudes $\mathcal{D}_2(\omega_1)$ and $\mathcal{D}_2(\omega_2)$ which describe scattering of two t -channel gluons and their coupling to the lower photons. The functions $\mathcal{D}_2(\omega_1)$ and $\mathcal{D}_2(\omega_2)$ are given by BFKL-Pomeron Green's functions, convoluted with the impact factors of the corresponding lower virtual photon. In the following we will confirm that, in our topological approach, on the pair-of-pants the required color factors work out correctly. The part above the the branching point is resummed by the amplitude $\mathcal{D}_4(\omega)$, which describes the scattering of the upper virtual photon on the four t -channel gluons. In the following, our interest will mainly concentrate on this part of our scattering amplitude.

6.4 Color factors with pair-of-pants topology

After our general outline of which QCD diagrams contribute to the leading log approximation of the $3 \rightarrow 3$ process we have to select now the contributions which belong to the large- N_c limit on the pair-of-pants. This will be done by attributing to each QCD diagram a 'color diagram' on the pair-of pants surface, where each gluon is drawn by a pair of color lines with opposite directions, as done for the plane and the cylinder in Sec.6.2.

6.4.1 Color factors at Born-level

All diagrams that contribute to the Born approximation of the triple-discontinuity have the form of Fig.6.11, with t -channel gluons coupling to the the quark-loop in all possible ways. Overall, one finds sixteen different diagrams. Because of the triple energy discontinuity t -channel gluons never intersect and hence can be labeled from the left to the right. A closer look then shows that, inside the quark loop, we have the four different orderings of color matrices: (1234), (2134), (1243), and (2143) (not distinguishing between cyclic permutations). These four structures are illustrated in Fig.7.5 and are all of the order

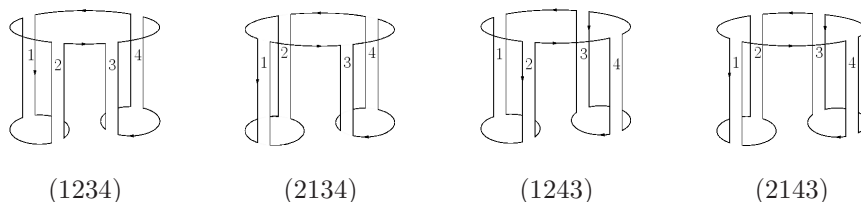


Figure 6.13: The four different orderings of color factors of the Born-term.

$$g^8 N_c^3 = N_c^{-1} \lambda^4. \quad (6.36)$$

6.4.2 Gluon production on the pair-of-pants surface

In order to study corrections to these Born-amplitudes, we consider real gluon production processes on the pair-of-pants surface (t -channel gluons are always reggeized). As to the selection of diagrams, we are searching the maximal power of color factors N_c . With (6.36) the diagrams we are going to collect will come with the weight

$$g^8 N_c^3 (g^2 N_c)^k = N_c^{-1} \lambda^{4+k}, \quad (6.37)$$

with k being some positive integer number. This leads to the requirement that, for each gluon, the pair of color lines has to be planar, i.e. it never intersects.

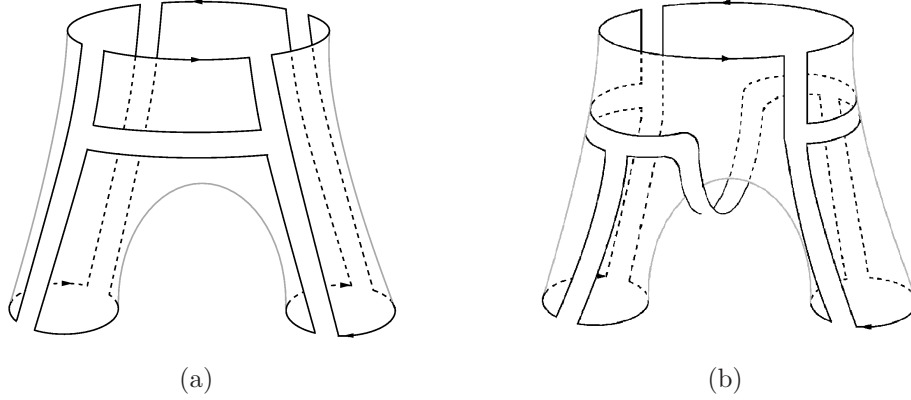


Figure 6.14: (a) A typical color factor of the planar class (A). (b) A typical color factor of the non-planar class (B) which has the interpretation of the Mandelstam diagram.

As a result we find two classes of color diagrams. The first class (A) consists of all diagrams which, by contracting closed color loops, coincide with one of the lowest order diagrams in Fig.7.5. An example for such a diagram is given in Fig.6.14.a. In the following we will refer to these diagrams as 'planar' diagrams. The second class (B) consists of those diagrams where the 'last' vertex before the separation into the two lower cylinders is of the form illustrated in Fig.6.14.b: one easily verifies that the power of color factors is $g^8 N_c^3 (g^2 N_c) = N_c^{-1} \lambda^{4+1}$, as required by condition Eq.(6.37). Also, there is no intersection of color lines on the pair-of-pants surface. These diagrams cannot be redrawn, by contracting closed color loops in a straightforward way, such that they coincide with one of the lowest order diagrams of Fig.7.5. The structure shown in Fig.6.14.b is reminiscent of the Mandelstam diagram ('Mandelstam cross') which, when integrated over the diffractive mass M , couples to the two Pomeron cut; we will therefore call it 'non-planar' (although it fits onto the surface of the pair-of-pants). Note that this non-planar structure appears only once, namely at the point where the upper cylinder splits into the two lower ones.

In the remainder of this section, we describe these two sets of diagrams in more detail. In particular, we list the momentum space expressions which belong to the gluon transition kernels. In the following section, we derive integral equations which sum all diagrams of set (A). For set (B) we re-derive the triple Pomeron vertex.

6.4.3 Two-to-two Reggeon transitions

We start with the case, where all four t -channel gluons couple to the upper quark-loop. We therefore consider only insertions of the two-to-two transition kernel,

$$\begin{aligned}
 \text{Diagram} &= \bar{g}^2 \left(\left| \begin{array}{c} \text{---} \\ \text{---} \\ \text{---} \end{array} \right| - \left| \begin{array}{c} \text{---} \\ \text{---} \\ \text{---} \end{array} \right| \right) \cdot \left(\left| \begin{array}{c} \text{---} \\ \text{---} \\ \text{---} \end{array} \right| - \left| \begin{array}{c} \text{---} \\ \text{---} \\ \text{---} \end{array} \right| \right) K_{2 \rightarrow 2}(\mathbf{l}_1, \mathbf{l}_2; \mathbf{k}_1, \mathbf{k}_2), \quad (6.38)
 \end{aligned}$$

into the Born diagrams of Fig.7.5, with $K_{2 \rightarrow 2}$ given by Eq.(6.22). To be definite, we consider corrections to the first diagram of Fig.7.5; the other Born diagrams are treated in the same way. We start with the case where the interaction is between gluons which end up in the same lower quark-loop, i.e. the interaction is inside the gluon pairs (12) or (34). In the case of the gluon pair (12), the two combinations of color factors of Fig.6.15 fit on the pair-of-pants, similar to the cylinder discussed before. An analogous result holds for the gluon pair (34). If the interacting t -channel gluons end up in different quark-loops we need to distinguish between two different cases. In the first case, shown in Fig.6.16, the interaction is between gluons '2' and '3'; on the surface of

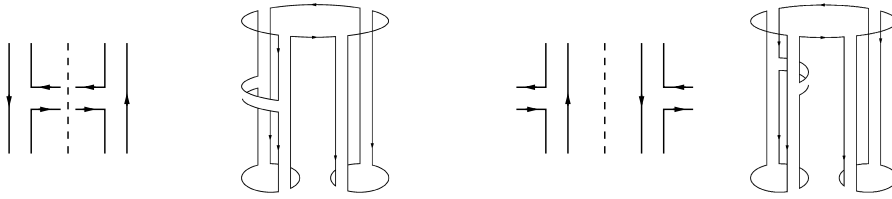


Figure 6.15: Two combination of color-factors for the interaction between gluons '1' and '2'.

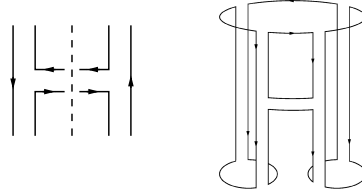


Figure 6.16: Color-factors of an interacting between two neighboring t -channel gluons.

the upper cylinder the two gluons are neighboring. We call this interaction planar: by contracting the color loop above the rung between gluon '2' and '3', we are back to the first Born diagram in Fig.7.5. In the second case, shown in Fig.6.17, the interaction is between gluon '2' and '4', These two gluons are not neighboring, and although the color diagram fits onto the surface of the pair-of-pants without any intersection of color lines, it will be referred to as 'non-planar'. It cannot be reduced to the Born diagram in Fig.7.5. Counting closed color loops, it is of the same order as that of Fig.6.16. Note, however, that compared to the planar one it has a relative minus sign. The

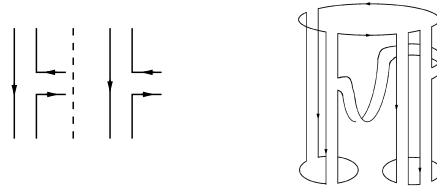


Figure 6.17: Color factors of an interaction between two non-neighboring t -channel gluons.

same discussion applies if the interaction is between gluon '1' and '3'.

We summarize the four possibilities in Fig.6.18. Apart from the last diagram, all diagrams belong to the class of 'planar' graphs. Note, however, that while in the first graph we can contract the closed color loop either above or below, in the second graph we can contract only the lower loop on the lower cylinder: it is planar w.r.t. the lower left cylinder.

When inserting more two-to-two interactions, it is useful to descend from the top to the bottom of the diagram: we start by inserting s -channel gluons between t -channel gluons which, on the upper cylinder, are neighboring (Figs.6.18a and c). This generates planar graphs. Moving further down, these planar insertions come to a stop as soon as one of the following interactions is included:

- (i) either an interaction of the type Fig.6.18b which is still planar but belongs to the lower left cylinder. Below such an interactions, further interactions lie on the surface of one of the two lower cylinders, i.e. they are inside the pairs (12) or (34). An interaction between the two cylinders, e.g., between gluon '1' and '3', loses a color factor N_c and does not contribute on the pair-of-pants.
- (ii) alternatively, a non-planar interaction of the type Fig.6.18: This interaction occurs at most once, and any further interaction below, again, lies on the surface of one of the two lower cylinders and hence is inside the pairs (12) or (34).

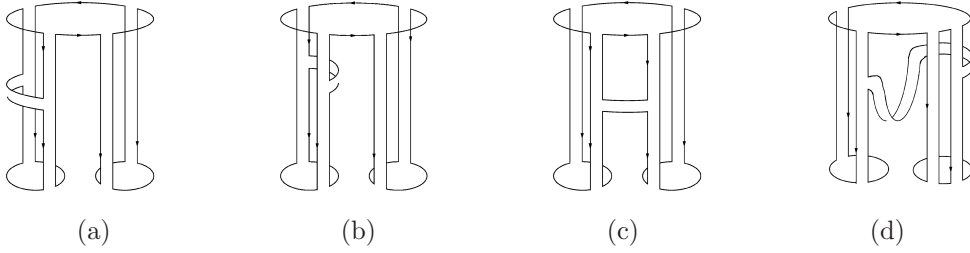


Figure 6.18: Different structures due to insertion of a two-to-two kernel on the pair-of-pants.

6.4.4 Two-to-four Reggeon transition

Apart from the above examples we have further the possibility that some of the t -channel gluons do not start at the upper quark loop but emerge from produced s -channel gluons. We start with the transition from two to four t -channel gluons. In this case we start, at the upper quark loop, with two t -channel gluons which end at a two-to-four transition. Leaving for the moment details on the momentum structure of the transition kernel $K_{2 \rightarrow 4}$ aside, the transition from two to four reggeized gluons is given by

$$\left. \begin{array}{c} \text{---} \\ \text{---} \\ \text{---} \\ \text{---} \end{array} \right\} = \bar{g}^4 \left(\left| \begin{array}{c} \text{---} \\ \text{---} \end{array} \right| - \left| \begin{array}{c} \text{---} \\ \text{---} \end{array} \right| \right) \left(\begin{array}{c} \text{---} \\ \text{---} \end{array} - \begin{array}{c} \text{---} \\ \text{---} \end{array} \right) \left(\begin{array}{c} \text{---} \\ \text{---} \end{array} - \begin{array}{c} \text{---} \\ \text{---} \end{array} \right) \left(\begin{array}{c} \text{---} \\ \text{---} \end{array} \left| \begin{array}{c} \text{---} \\ \text{---} \end{array} \right| \right) K_{2 \rightarrow 4}. \quad (6.39)$$

Of the 16 possible combinations of color factors, only a subset fits on the pair-of-pants, of which two examples are shown in Figs.6.19 and 6.20. Again, we have two distinct structures: Fig.6.19,

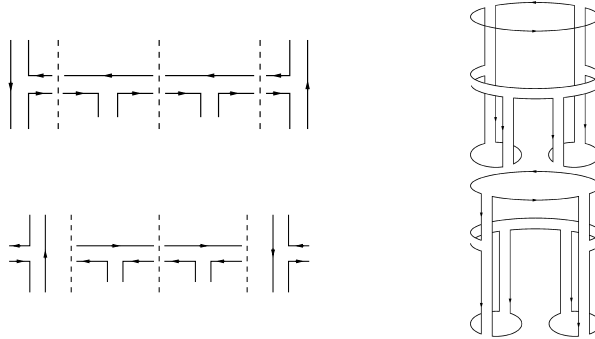


Figure 6.19: The planar two-to-four Reggeon transition.

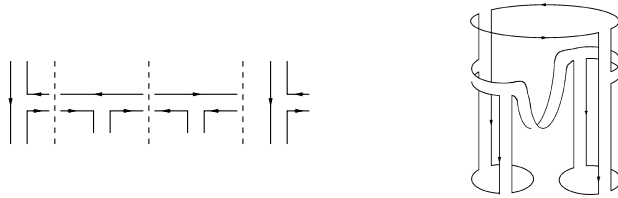


Figure 6.20: The non-planar two-to-four Reggeon transition.

by contracting the closed color loop on the upper cylinder, can be reduced to one of the Born diagrams, and thus belongs to class of planar diagrams. In contrast, Fig.6.20 cannot be contracted and is non-planar.

Further rungs above the $2 \rightarrow 4$ transition vertex can always be contracted to either Figs.6.19 or 6.20. As to the interactions below the $2 \rightarrow 4$ transition, we have to distinguish between the

two classes. For the planar class in Figs.6.19, we can continue by inserting $2 \rightarrow 2$ interactions as described in the previous subsection. For the non-planar class in Fig.6.20 any further $2 \rightarrow 2$ interaction is either inside the pair (12) or (34) and can always be reduced to Fig.6.20.

For the momentum structure of the $2 \rightarrow 4$ transition vertex we need, apart from the real gluon production vertex in Eq.(6.19), the vertex which describes coupling of a t -channel gluon to a real s -channel gluon, which is known as the Reggeon-Particle-Particle (RPP)-vertex. Similar to the production vertex, the RPP-vertex is an effective vertex. To lowest order, for the scattering of a gluon on an antiquark at high center of mass energies, this RPP-vertex is built up from the following diagrams:

$$\text{Diagram} = \text{Diagram}_1 + \text{Diagram}_2 + \text{Diagram}_3 \quad (6.40)$$

Similar to the production vertex, at high center of mass energies the last two diagrams coincide with each other up to a sign, and color factor and momentum part of the RPP-vertex can be written in the factorized form

$$-i\bar{g} \left[\begin{array}{c} \overrightarrow{\quad} \\ \overleftarrow{\quad} \\ \overrightarrow{\quad} \\ \overleftarrow{\quad} \end{array} - \begin{array}{c} \overrightarrow{\quad} \\ \overleftarrow{\quad} \\ \overleftarrow{\quad} \\ \overrightarrow{\quad} \end{array} \right] \epsilon_{(\lambda')}^* \cdot \Gamma \cdot \epsilon_{(\lambda)} \quad (6.41)$$

Sandwiching one or two RPP vertices between two production vertices then leads to two-to-three and two-to-four Reggeon transition kernels. They have been constructed in [33] and for details we refer to this reference. The momentum part of the $2 \rightarrow 4$ transition is then given by

$$K_{2 \rightarrow 4} = \mathbf{q}^2 - \frac{l_1^2(\mathbf{q} - \mathbf{k}_1)^2}{(l_1 - \mathbf{k}_1)^2} - \frac{l_2^2(\mathbf{k}_1 + \mathbf{k}_2 + \mathbf{k}_3)^2}{(l_2 - \mathbf{k}_4)^2} + \frac{l_1^2(\mathbf{q} - \mathbf{k}_1)^2 l_2^2}{(l_1 - \mathbf{k}_1)^2 (l_2 - \mathbf{k}_4)^2} \quad (6.42)$$

6.4.5 Two-to-three Reggeon transition

Last we need to consider diagrams that contain, at least, one transition from two to three gluons. Beginning with the momentum structure, we remind that the coupling of an additional 'new' t -channel to an s -channel gluon takes place by the RPP-vertex in Eq.(6.41). The result for two-to-three Reggeon transition is described by

$$\text{Diagram} = i\bar{g}^3 \left(\begin{array}{c} \overrightarrow{\quad} \\ \overleftarrow{\quad} \end{array} - \begin{array}{c} \overleftarrow{\quad} \\ \overrightarrow{\quad} \end{array} \right) \left(\begin{array}{c} \overrightarrow{\quad} \\ \overleftarrow{\quad} \end{array} - \begin{array}{c} \overleftarrow{\quad} \\ \overrightarrow{\quad} \end{array} \right) \left(\begin{array}{c} \overrightarrow{\quad} \\ \overleftarrow{\quad} \end{array} - \begin{array}{c} \overleftarrow{\quad} \\ \overrightarrow{\quad} \end{array} \right) K_{2 \rightarrow 3} \quad (6.43)$$

with

$$K_{2 \rightarrow 3}^{\{\{12\} \rightarrow \{123\}\}} = (\mathbf{k}_1 + \mathbf{k}_2 + \mathbf{k}_3)^2 - \frac{l_1^2(\mathbf{k}_2 + \mathbf{k}_3)^2}{(l_1 - \mathbf{k}_1)^2} - \frac{l_2^2(\mathbf{k}_1 + \mathbf{k}_2)^2}{(l_2 - \mathbf{k}_3)^2} + \frac{l_1^2 l_2^2}{(l_1 - \mathbf{k}_1)^2 (l_2 - \mathbf{k}_3)^2} \quad (6.44)$$

where the superscripts on the kernel refer to the ingoing and outgoing t -channel gluons respectively. As to the general structure of diagrams with $2 \rightarrow 3$ transitions, we have two possibilities: either we start, at the upper quark loop, with three gluons. In this case we need, somewhere further below, only one $2 \rightarrow 3$ transition. Alternatively, we could start with two gluons and then need two $2 \rightarrow 3$ transition vertices.

For the discussion of the color diagrams we start with the former case. As before we encounter planar and non-planar graphs. An example of a planar graph is shown in Fig.6.21, a non-planar graph in Fig.6.22. In both cases, the planar class, Fig.6.21, and the non-planar class, Fig.6.22, above the vertex any further $2 \rightarrow 2$ interaction is between lines which are neighbored on the surface of the upper cylinder. Below the $2 \rightarrow 3$ vertex we have the same situation as for the $2 \rightarrow 4$ vertex: for the planar graph in Fig.6.21 we proceed as described in Sec.6.4.3, whereas for the non-planar graph there is no further communication between the two lower cylinders.

For the graphs which, at the top, start with two t -channel gluons the two classes arise in the following way. Beginning at the top, the first $2 \rightarrow 3$ transition always lies on the surface of the upper cylinder. Below this vertex we have the same situation which we have described a moment ago, i.e. the same as for the case where at the fermion quark loop we start with three gluons: the second $2 \rightarrow 3$ transition decides whether the graph is planar or non-planar. Planar examples are shown in Fig.6.23.

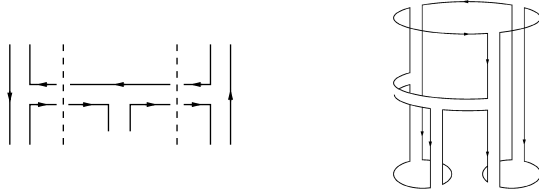


Figure 6.21: Planar graph with one two-to-three transition.

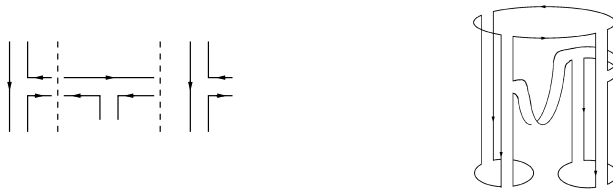


Figure 6.22: Non-planar graph with one two-to-three transition.

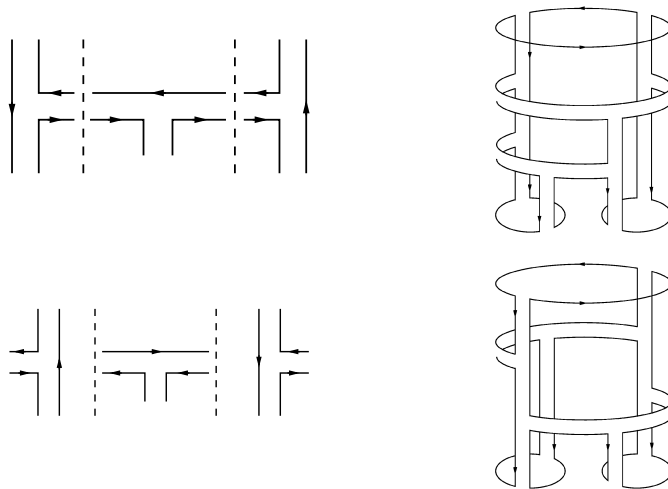


Figure 6.23: Combination of two transitions of two to three t -channel gluons. From Eq.(6.43) one finds a relative minus sign for the second combination.

6.4.6 Planar and non-planar partial waves

In this final subsection we collect the results and prepare the summation of all diagrams on the pair-of-pants surface. At the end of Sec.6.3 we proposed to factorize at the branching point, i.e. at the last interaction between the two 'legs' of the pair-of-pants, the partial wave $F(\omega, \omega_1, \omega_2)$ into a convolution of three amplitudes $\mathcal{D}_4(\omega)$, $\mathcal{D}_2(\omega_1)$, and $\mathcal{D}_2(\omega_2)$, depending on ω , ω_1 , or ω_2 , resp.. In order to find closed expressions for these amplitudes we shall, similar to our treatment of the diagrams in the plane and on the surface of the cylinder, formulate integral equations which sum up the different classes of diagrams.

The situation is easiest for the two amplitudes that start from the two lower virtual photons, $\mathcal{D}_2(\omega_1)$, and $\mathcal{D}_2(\omega_2)$. For these amplitudes we need to resum, for both legs, contributions like those in Fig.6.15. Their resummation yields the BFKL-equation on the cylinder Eq.(6.31).

The upper amplitude, $\mathcal{D}_4(\omega)$ is defined to include the branching vertex, which by definition is the lowest interaction that connects the gluon pair (12) with the pair (34). Below this vertex, there are only interactions inside the pair (12) or (34). The branching vertex can be either a $2 \rightarrow 2$, a $2 \rightarrow 3$, or a $2 \rightarrow 4$ transition vertex. From this definition it follows that the upper amplitude always has four reggeized gluons at its lower end.

From now on it becomes important to distinguish between 'planar' and 'non-planar' graphs. For

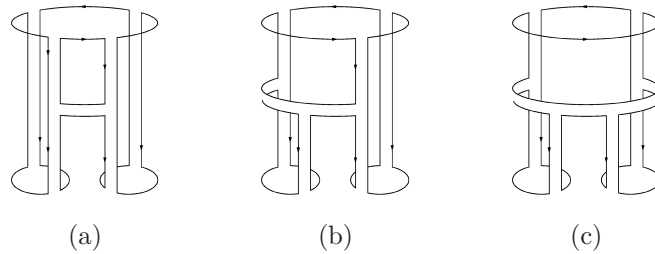


Figure 6.24: 'Planar' color factors on the pair-of-pants which reduce in an apparent way to the color structure of the Born-term by extracting a closed color loop with the *upper* quark-loop.

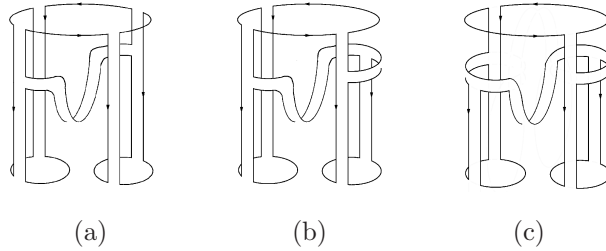


Figure 6.25: 'Non-planar' color factors that cannot be reduced trivially to the color structure of the Born-term by extracting a closed color loop with the *upper* quark-loop.

convenience we list, once more, three examples of planar and non-planar graphs: Fig.6.24 contains the planar example, and Fig.6.25 the non-planar ones. They are of the order $g^8 N_c^3 (g^2 N_c)$.

Beginning with the planar diagrams in Fig.6.24 one easily verifies that we always can contract one closed color loop to arrive at the first diagram of Fig.7.5. For the other diagrams in Fig.7.5 we have analogous sets of graphs. Next, the figures Fig.6.24a-c differ from each other in that, at the fermion loop at the top, in (a) we start with four gluons, in (b) with only three gluons, and in (c) with two gluons. Correspondingly, in (a) the branching vertex consists of a two-to-two kernel, in (b) a two-to-three kernel, and in (c) a two-to-four kernel. At the branching vertex, all diagrams have four t -channel gluon lines. Higher order diagrams are obtained by inserting, above the branching vertex, pairwise interactions between neighboring t -channel gluons. Also, in Fig.6.24b and d we could insert a $2 \rightarrow 2$ interaction between gluons '2' and '3' or '1' and '4': in this case, the branching

vertex consists of a two-to-two kernel. In all cases, by drawing a horizontal cutting line just below the branching vertex, we arrive at amplitudes with four t -channel gluons. We will denote the sum of all graphs by $\mathcal{D}_4^{(1234)}(\omega)$, $\mathcal{D}_4^{(2134)}(\omega)$, $\mathcal{D}_4^{(2143)}(\omega)$, and $\mathcal{D}_4^{(2134)}(\omega)$ where the upper label refers to the four terms in Fig.7.5, i.e. it indicates to which of the four Born terms the diagrams can be contracted (a more precise definition will be given further below in section 6.5).

For the task of summing of all diagrams it will be convenient to define also auxiliary amplitudes with two and three gluons in the t -channel. In Fig.6.24c one sees that, starting at the upper quark loop, we begin with two gluons which, when higher order corrections are included, interact through two-to-two kernels. The sum of these diagrams leads to the BFKL cylinder and therefore coincides with $\mathcal{D}_2(\omega)$ of Sec.6.2.3. For the three gluon amplitude above the branching vertex in Fig.6.24b

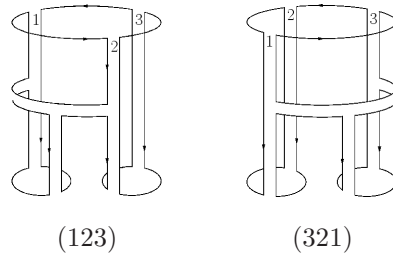


Figure 6.26: The two possible orderings of three gluons along the quark-loop which leads to the definition of $\mathcal{D}_3^{(123)}(\omega)$ and $\mathcal{D}_3^{(321)}(\omega)$.

we have two inequivalent couplings to the quark loops, as illustrated in Fig.6.26. We denote them by $\mathcal{D}_3^{(123)}(\omega)$ and $\mathcal{D}_3^{(132)}(\omega)$.

When writing down integral equations for the amplitudes \mathcal{D}_3 and \mathcal{D}_4 , we observe that they will be coupled. The three gluon state at the lower end of \mathcal{D}_3 can start as a two gluons at the quark loop, then undergo a two-to-three transition. Similarly, the four gluon state can start from two or three gluons and then make transitions to the final four gluon state. The formulation of these coupled integral equations will be carried out in the subsequent section.

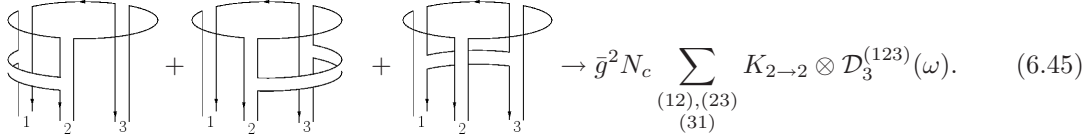
Next we turn to the non-planar diagrams of Fig.6.25. They cannot be reduced to the color structure of the Born diagrams, and we therefore define an additional partial wave that sums up these terms. They all have in common that the non-planar structure at the lower end of the upper cylinder is always the branching vertex: below this vertex, there is no further communication between the two lower cylinders. As an example, an interaction between gluon '2' and '3' would be subleading in powers N_c . Similar to the planar diagrams in Fig.6.24, we see three different structures: above the branching vertex we have four (Fig.6.24a), three (Fig.6.24b), or two (Fig.6.24c) t -channel gluons. This suggests that above the branching vertex the structure is the same as for the planar graphs, and we simply have to convolute the non-planar branching vertex with the planar amplitudes \mathcal{D}_2 , \mathcal{D}_3 , and \mathcal{D}_4 . The resulting expression will be denoted by $\mathcal{D}_4^{(\text{NP})}(\omega)$. Its derivation will be the content of Sec.6.6.

6.5 Integral equations: gluon amplitudes with planar color structure

In the following we will formulate integral equations for amplitudes of the planar class with two, three and four t -channel gluons. The amplitude with four t -channel gluons that belongs to the non-planar class will be addressed in Sec.6.6.

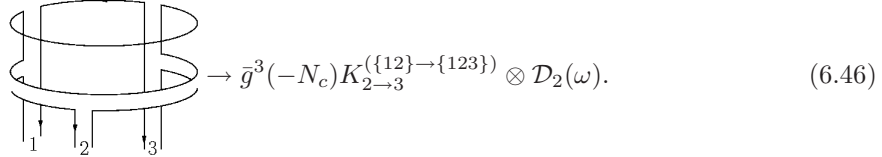
6.5.1 Integral equations for the three gluon amplitude

The evolution of the three gluon state is described by the sum of pairwise interactions, i.e. the two-to-two transition kernels acting on the three gluon state



$$\text{Diagram 1} + \text{Diagram 2} + \text{Diagram 3} \rightarrow \bar{g}^2 N_c \sum_{\substack{(12),(23) \\ (31)}} K_{2 \rightarrow 2} \otimes \mathcal{D}_3^{(123)}(\omega). \quad (6.45)$$

The transition from the two gluon state to the three gluon state is mediated by the two-to-three transition kernels acting on the two-gluon state,

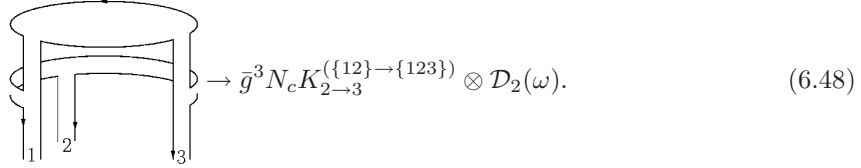


$$\text{Diagram} \rightarrow \bar{g}^3 (-N_c) K_{2 \rightarrow 3}^{\{\{12\} \rightarrow \{123\}\}} \otimes \mathcal{D}_2(\omega). \quad (6.46)$$

Similar to $\mathcal{D}_2(\omega)$, also the amplitude $\mathcal{D}_3(\omega)$ is defined to contain the Reggeon propagator of the external reggeized gluons, $1/(\omega - \sum_i^3 \beta(\mathbf{k}_i))$. With these ingredients, the integral equation for $\mathcal{D}_3^{(123)}(\omega)$ is given by

$$\begin{aligned} (\omega - \sum_i^3 \beta(\mathbf{k}_i)) \mathcal{D}_3^{(123)}(\omega | \mathbf{k}_1, \mathbf{k}_2, \mathbf{k}_3) = & \mathcal{D}_{(3,0)}^{(123)} + \bar{g}^3 (-N_c) K_{2 \rightarrow 3}^{\{\{12\} \rightarrow \{123\}\}} \otimes \mathcal{D}_2(\omega) \\ & + \bar{g}^2 N_c \sum K_{2 \rightarrow 2} \otimes \mathcal{D}_3^{(123)}(\omega). \end{aligned} \quad (6.47)$$

In complete analogy the equation for $\mathcal{D}_3^{(321)}(\omega)$ contains the two-to-three transition kernel



$$\text{Diagram} \rightarrow \bar{g}^3 N_c K_{2 \rightarrow 3}^{\{\{12\} \rightarrow \{123\}\}} \otimes \mathcal{D}_2(\omega). \quad (6.48)$$

The integral equation is given by:

$$\begin{aligned} ((\omega - \sum_i^3 \beta(\mathbf{k}_i)) \mathcal{D}_3^{(321)}(\omega | \mathbf{k}_1, \mathbf{k}_2, \mathbf{k}_3) = & \mathcal{D}_{(3,0)}^{(321)} + \bar{g}^3 N_c K_{2 \rightarrow 3}^{\{\{12\} \rightarrow \{123\}\}} \otimes \mathcal{D}_2(\omega) \\ & + \bar{g}^2 N_c \sum_{\substack{(13),(32) \\ (21)}} K_{2 \rightarrow 2} \otimes \mathcal{D}_3^{(321)}(\omega). \end{aligned} \quad (6.49)$$

6.5.2 Reggeization of the three-gluon amplitude

To study the integral equations Eq.(6.47) and Eq.(6.49) we need the impact factors $\mathcal{D}_{(3,0)}^{(123)}$ and $\mathcal{D}_{(3,0)}^{(321)}$. Both impact factors have the same properties as in the N_c finite case [35], and they can be written as a superposition of two-gluon impact factors $\mathcal{D}_{(2;0)}$:

$$\mathcal{D}_{(3;0)}^{(123)}(\mathbf{k}_1, \mathbf{k}_2, \mathbf{k}_3) = +\frac{\bar{g}}{2} [\mathcal{D}_{(2;0)}(12, 3) - \mathcal{D}_{(2;0)}(13, 2) + \mathcal{D}_{(2;0)}(1, 23)] \quad (6.50)$$

$$\mathcal{D}_{(3;0)}^{(321)}(\mathbf{k}_1, \mathbf{k}_2, \mathbf{k}_3) = -\frac{\bar{g}}{2} [\mathcal{D}_{(2;0)}(12, 3) - \mathcal{D}_{(2;0)}(13, 2) + \mathcal{D}_{(2;0)}(1, 23)]. \quad (6.51)$$

On the right hand side we introduced a short-hand notation: a string of numbers stands for the sum of the corresponding transverse momenta, for instance

$$\mathcal{D}_{(2;0)}(12, 3) \equiv \mathcal{D}_{(2;0)}(\mathbf{k}_1 + \mathbf{k}_2, \mathbf{k}_3). \quad (6.52)$$

We will make use of this notation in the following, whenever it proves useful to clarify the underlying structure of complex expressions. It can be now demonstrated that the structure on the rhs of Eqs.(6.50) and Eqs.(6.51) also holds for the solutions of the integral equations Eq.(6.47) and Eq.(6.49):

$$\mathcal{D}_3^{(123)}(\omega|\mathbf{k}_1, \mathbf{k}_2, \mathbf{k}_3) = +\frac{\bar{g}}{2}[\mathcal{D}_2(\omega|12, 3) - \mathcal{D}_2(\omega|13, 2) + \mathcal{D}_2(\omega|1, 23)] \quad (6.53)$$

$$\mathcal{D}_3^{(321)}(\omega|\mathbf{k}_1, \mathbf{k}_2, \mathbf{k}_3) = -\frac{\bar{g}}{2}[\mathcal{D}_2(\omega|12, 3) - \mathcal{D}_2(\omega|13, 2) + \mathcal{D}_2(\omega|1, 23)]. \quad (6.54)$$

Obviously this solution shares important properties with the reggeization of the planar gluon discussed in Sec.6.2.2: in each term on the rhs, two gluons 'collapse' into a single gluon which, at the end, decays into two gluons. This allows also to deform the color factor as shown in Fig.6.27:

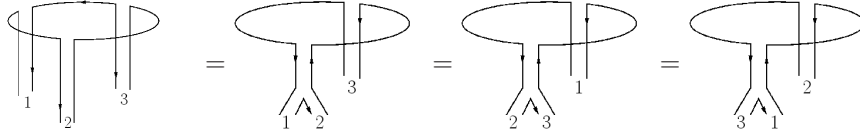


Figure 6.27: The color factor associated with $\mathcal{D}_3^{(123)}(\omega)$ can be deformed such that the form of the color factor coincides with the momentum structure of the solution in terms of \mathcal{D}_2 . A similar observation holds for $\mathcal{D}_3^{(321)}(\omega)$.

6.5.3 The integral equations for the four gluon amplitude with planar color structure

For the four gluon amplitude, $\mathcal{D}_4^{(1234)}(\omega)$, the evolution of the four gluon state is describes by the sum of pairwise interactions between neighboring gluons. For the amplitude $\mathcal{D}_4^{(1234)}(\omega)$ the sum of the two-to-two transition is given by

$$\begin{aligned} & \text{Four diagrams showing pairwise interactions between neighboring gluons} \rightarrow \bar{g}^2 N_c \sum_{\substack{(12),(23) \\ (34),(41)}} K_{2 \rightarrow 2} \otimes \mathcal{D}_4^{(1234)}(\omega). \end{aligned} \quad (6.55)$$

The corresponding expressions for $\mathcal{D}_4^{(2134)}(\omega)$, $\mathcal{D}_4^{(2143)}(\omega)$ and $\mathcal{D}_4^{(1243)}(\omega)$ are easily obtained by simply exchanging the corresponding labels on the t -channel gluons. For $\mathcal{D}_4^{(1234)}(\omega)$, the two-to-three transitions are

$$\begin{aligned} & \text{Two diagrams showing two-to-three transitions} \rightarrow \bar{g}^3 N_c K_{2 \rightarrow 3}^{\{\{12\} \rightarrow \{123\}\}} \otimes \mathcal{D}_3^{(123)}(\omega) \\ & \quad + \bar{g}^3 N_c K_{2 \rightarrow 3}^{\{\{23\} \rightarrow \{234\}\}} \otimes \mathcal{D}_3^{(123)}(\omega), \end{aligned} \quad (6.56)$$

while the two-to-four transition is

$$\text{Diagram showing two-to-four transition} \rightarrow \bar{g}^4 N_c K_{2 \rightarrow 4}^{\{\{12\} \rightarrow \{1234\}\}} \otimes \mathcal{D}_2(\omega). \quad (6.57)$$

Also $\mathcal{D}_4^{(1234)}(\omega)$ is defined to contain the Reggeon-propagator of the external reggeized gluons. Including this contribution together with the four gluon impact factor, $\mathcal{D}_{(4;0)}^{(1234)}$, the integral equation for $\mathcal{D}_4^{(1234)}(\omega)$ is given by

$$\begin{aligned} (\omega - \sum_i^4 \beta(\mathbf{k}_i)) \mathcal{D}_4^{(1234)}(\omega) &= \mathcal{D}_{(4;0)}^{(1234)} + \bar{g}^3 N_c \left[K_{2 \rightarrow 3}^{\{\{12\} \rightarrow \{123\}\}} \otimes \mathcal{D}_3^{(123)}(\omega) + K_{2 \rightarrow 3}^{\{\{23\} \rightarrow \{234\}\}} \otimes \mathcal{D}_3^{(123)}(\omega) \right] \\ &\quad + \bar{g}^4 N_c^2 K_{2 \rightarrow 4}^{\{\{12\} \rightarrow \{1234\}\}} \otimes \mathcal{D}_2(\omega) + \bar{g}^2 N_c \sum_{\substack{(12), (23) \\ (34), (41)}} K_{2 \rightarrow 2} \otimes \mathcal{D}_4^{(1234)}(\omega). \end{aligned} \quad (6.58)$$

For $\mathcal{D}_4^{(2143)}(\omega)$ the two-to-three transition arises from

$$\begin{aligned} \text{Diagram 1} + \text{Diagram 2} &\rightarrow \bar{g}^3 (-N_c) K_{2 \rightarrow 3}^{\{\{12\} \rightarrow \{123\}\}} \otimes \mathcal{D}_3^{(321)}(\omega) \\ &\quad + \bar{g}^3 (-N_c) K_{2 \rightarrow 3}^{\{\{23\} \rightarrow \{234\}\}} \otimes \mathcal{D}_3^{(321)}(\omega), \end{aligned} \quad (6.59)$$

and the two-to-four transition comes from

$$\text{Diagram 3} \rightarrow \bar{g}^4 N_c K_{2 \rightarrow 4}^{\{\{12\} \rightarrow \{1234\}\}} \otimes \mathcal{D}_2(\omega). \quad (6.60)$$

We obtain the integral equation

$$\begin{aligned} (\omega - \sum_i^4 \beta(\mathbf{k}_i)) \mathcal{D}_4^{(2143)}(\omega) &= \mathcal{D}_{(4;0)}^{(2143)} + \bar{g}^3 (-N_c) \left[K_{2 \rightarrow 3}^{\{\{12\} \rightarrow \{123\}\}} \otimes \mathcal{D}_3^{(321)}(\omega) + K_{2 \rightarrow 3}^{\{\{23\} \rightarrow \{234\}\}} \otimes \mathcal{D}_3^{(321)}(\omega) \right] \\ &\quad + \bar{g}^4 N_c^2 K_{2 \rightarrow 4}^{\{\{12\} \rightarrow \{1234\}\}} \otimes \mathcal{D}_2(\omega) + \bar{g}^2 \sum_{\substack{(21), (14) \\ (43), (32)}} K_{2 \rightarrow 2} \otimes \mathcal{D}_4^{(2143)}(\omega) \end{aligned} \quad (6.61)$$

Finally, for $\mathcal{D}_4^{(2134)}(\omega)$ and $\mathcal{D}_4^{(1243)}(\omega)$ the two-to-three transition are

$$\begin{aligned} \text{Diagram 4} + \text{Diagram 5} &\rightarrow \bar{g}^3 (-N_c) K_{2 \rightarrow 3}^{\{\{13\} \rightarrow \{124\}\}} \otimes \mathcal{D}_3^{(123)}(\omega) \\ &\quad + \bar{g}^3 N_c K_{2 \rightarrow 3}^{\{\{13\} \rightarrow \{134\}\}} \otimes \mathcal{D}_3^{(321)}(\omega) \end{aligned} \quad (6.62)$$

and

$$\begin{aligned} \text{Diagram 6} + \text{Diagram 7} &\rightarrow \bar{g}^3 N_c K_{2 \rightarrow 3}^{\{\{13\} \rightarrow \{124\}\}} \otimes \mathcal{D}_3^{(321)}(\omega) \\ &\quad + \bar{g}^3 (-N_c) K_{2 \rightarrow 3}^{\{\{13\} \rightarrow \{134\}\}} \otimes \mathcal{D}_3^{(123)}(\omega) \end{aligned} \quad (6.63)$$

respectively, while two-to-four transition are absent in that case. The integral equations are given by

$$\begin{aligned}
(\omega - \sum_i^4 \beta(\mathbf{k}_i)) \mathcal{D}_4^{(2134)}(\omega) &= \mathcal{D}_{(4;0)}^{(2134)} + \bar{g}^3 (-N_c) K_{2 \rightarrow 3}^{\{\{13\} \rightarrow \{124\}\}} \otimes \mathcal{D}_3^{(123)}(\omega) \\
&\quad + \bar{g}^3 N_c K_{2 \rightarrow 3}^{\{\{13\} \rightarrow \{134\}\}} \otimes \mathcal{D}_3^{(321)}(\omega) + \bar{g}^2 N_c \sum_{\substack{(21), (13) \\ (34), (42)}} K_{2 \rightarrow 2} \otimes \mathcal{D}_4^{(2134)}(\omega)
\end{aligned} \tag{6.64}$$

$$\begin{aligned}
(\omega - \sum_i^4 \beta(\mathbf{k}_i)) \mathcal{D}_4^{(1243)}(\omega) &= \mathcal{D}_{(4;0)}^{(1243)} + \bar{g}^3 (-N_c) K_{2 \rightarrow 3}^{\{\{13\} \rightarrow \{134\}\}} \otimes \mathcal{D}_3^{(123)}(\omega) \\
&\quad + \bar{g}^3 N_c K_{2 \rightarrow 3}^{\{\{13\} \rightarrow \{124\}\}} \otimes \mathcal{D}_3^{(321)}(\omega) + \bar{g}^2 N_c \sum_{\substack{(12), (24) \\ (43), (31)}} K_{2 \rightarrow 2} \otimes \mathcal{D}_4^{(1243)}(\omega).
\end{aligned} \tag{6.65}$$

6.5.4 Reggeization of four-gluon-amplitudes with planar color structure

Similar to the three-gluon amplitude, the four independent integral equations for the four-gluon-amplitudes with planar color structure are solved by a reggeization ansatz. Again the starting point is given by the virtual photon impact factors which, similar to the three-gluon case, can be expressed in terms of the two-gluon impact factor:

$$\mathcal{D}_{(4;0)}^{(1234)}(\mathbf{k}_1, \mathbf{k}_2, \mathbf{k}_3, \mathbf{k}_4) = -\frac{\bar{\lambda}}{2N_c} [\mathcal{D}_{(2;0)}(123, 4) + \mathcal{D}_{(2;0)}(1, 234) - \mathcal{D}_{(2;0)}(14, 23)] \tag{6.66}$$

$$\mathcal{D}_{(4;0)}^{(2143)}(\mathbf{k}_1, \mathbf{k}_2, \mathbf{k}_3, \mathbf{k}_4) = -\frac{\bar{\lambda}}{2N_c} [\mathcal{D}_{(2;0)}(123, 4) + \mathcal{D}_{(2;0)}(1, 234) - \mathcal{D}_{(2;0)}(14, 23)] \tag{6.67}$$

$$\mathcal{D}_{(4;0)}^{(2134)}(\mathbf{k}_1, \mathbf{k}_2, \mathbf{k}_3, \mathbf{k}_4) = -\frac{\bar{\lambda}}{2N_c} [\mathcal{D}_{(2;0)}(134, 2) + \mathcal{D}_{(2;0)}(124, 3) - \mathcal{D}_{(2;0)}(12, 34) - \mathcal{D}_{(2;0)}(13, 24)] \tag{6.68}$$

$$\mathcal{D}_{(4;0)}^{(1243)}(\mathbf{k}_1, \mathbf{k}_2, \mathbf{k}_3, \mathbf{k}_4) = -\frac{\bar{\lambda}}{2N_c} [\mathcal{D}_{(2;0)}(134, 2) + \mathcal{D}_{(2;0)}(124, 3) - \mathcal{D}_{(2;0)}(12, 34) - \mathcal{D}_{(2;0)}(13, 24)]. \tag{6.69}$$

This decomposition also holds for the solutions of the integral equations, Eq.(6.58), Eq.(6.61), Eq.(6.64) and Eq.(6.65):

$$\mathcal{D}_4^{(1234)}(\omega | \mathbf{k}_1, \mathbf{k}_2, \mathbf{k}_3, \mathbf{k}_4) = -\frac{\bar{\lambda}}{2N_c} [\mathcal{D}_2(\omega | 123, 4) + \mathcal{D}_2(\omega | 1, 234) - \mathcal{D}_2(\omega | 14, 23)] \tag{6.70}$$

$$\mathcal{D}_4^{(2143)}(\omega | \mathbf{k}_1, \mathbf{k}_2, \mathbf{k}_3, \mathbf{k}_4) = -\frac{\bar{\lambda}}{2N_c} [\mathcal{D}_2(\omega | 123, 4) + \mathcal{D}_2(\omega | 1, 234) - \mathcal{D}_2(\omega | 14, 23)] \tag{6.71}$$

$$\mathcal{D}_4^{(2134)}(\omega | \mathbf{k}_1, \mathbf{k}_2, \mathbf{k}_3, \mathbf{k}_4) = -\frac{\bar{\lambda}}{2N_c} [\mathcal{D}_2(\omega | 134, 2) + \mathcal{D}_2(\omega | 124, 3) - \mathcal{D}_2(\omega | 12, 34) - \mathcal{D}_2(\omega | 13, 24)] \tag{6.72}$$

$$\mathcal{D}_4^{(1243)}(\omega | \mathbf{k}_1, \mathbf{k}_2, \mathbf{k}_3, \mathbf{k}_4) = -\frac{\bar{\lambda}}{2N_c} [\mathcal{D}_2(\omega | 134, 2) + \mathcal{D}_2(\omega | 124, 3) - \mathcal{D}_2(\omega | 12, 34) - \mathcal{D}_2(\omega | 13, 24)]. \tag{6.73}$$

Similar to the the three gluon case, each term on the rhs consists of a two gluon state where at the end one (or both) gluons decay: this again generalizes the reggeization discussed in the context of planar amplitudes. It allows to redraw the color factors as shown in Fig.6.28.

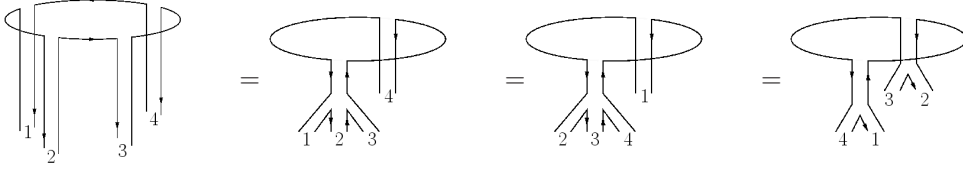


Figure 6.28: Color factors associated with the four gluon amplitude with planar color structure can be deformed to coincide with the momentum structure of the solution in terms of \mathcal{D}_2 . Above we show the ordering (1234).

For the sum of these planar four gluon amplitudes, it is convenient to define, following [35], an effective $2 \rightarrow 4$ vertex V^R , which sums the various decay-channels of the two reggeized gluons,

$$\begin{aligned}
 V^R(\mathbf{l}_1, \mathbf{l}_2; \mathbf{k}_1, \mathbf{k}_2, \mathbf{k}_3, \mathbf{k}_4) = & -l_1^2 l_2^2 \left[\delta^{(2)}(\mathbf{l}_1 - \mathbf{k}_1 - \mathbf{k}_2 - \mathbf{k}_3) + \delta^{(2)}(\mathbf{l}_1 - \mathbf{k}_1 - \mathbf{k}_2 - \mathbf{k}_4) \right. \\
 & + \delta^{(2)}(\mathbf{l}_1 - \mathbf{k}_1 - \mathbf{k}_3 - \mathbf{k}_4) + \delta^{(2)}(\mathbf{l}_1 - \mathbf{k}_2 - \mathbf{k}_3 - \mathbf{k}_4) \\
 & \left. - \delta^{(2)}(\mathbf{l}_1 - \mathbf{k}_1 - \mathbf{k}_2) - \delta^{(2)}(\mathbf{l}_1 - \mathbf{k}_1 - \mathbf{k}_3) - \delta^{(2)}(\mathbf{l}_1 - \mathbf{k}_1 - \mathbf{k}_4) \right], \tag{6.74}
 \end{aligned}$$

such that

$$\sum_{(ijkl)=\substack{(1234), (2143), \\ (2134), (1243)}} \mathcal{D}_4^{(ijkl)}(\omega | \mathbf{k}_1, \mathbf{k}_2, \mathbf{k}_3, \mathbf{k}_4) = \frac{\bar{\lambda}}{N_c} V^{(R)} \otimes \mathcal{D}_2(\omega). \tag{6.75}$$

It is instructive to compare the results of this section with the finite N_c results of [35]. For finite N_c it was found that the four gluon amplitude D_4 can be written as a sum of two terms, the reggeizing term and the triple Pomeron vertex:

$$D_4 = D_4^R + D_4^I \tag{6.76}$$

This decomposition was motivated by t -channel requirements: the reggeizing pieces contained in D_4^R are antisymmetric under the exchange of the pair of gluons which forms the reggeized gluon, whereas the remainder D_4^I (which contains the triple Pomeron vertex), is completely symmetric. In the present approach which is based upon the expansion in topologies, this decomposition into reggeizing and non-reggeizing pieces comes automatically, as a consequence of different classes of color structures. This suggests that the reggeization is deeply linked to the planar structure of scattering amplitudes.

6.6 The triple Pomeron vertex on the pair-of-pants

In this section we turn now to the partial wave amplitude associated with the non-planar class, $\mathcal{D}_4^{(\text{NP})}(\omega)$. As we have outlined at the end of Sec.6.4.6, we have to convolute, in Fig.6.25a - c, the branching vertices with \mathcal{D}_4 , \mathcal{D}_3 , and \mathcal{D}_2 . Let us go through these convolutions in more detail.

We begin with those contributions where the branching vertex consists of a two-to-two transition (Fig.6.25a). They are to be combined with one of the four planar amplitudes discussed before. Contributions involving $\mathcal{D}_4^{(1234)}(\omega)$ are

$$\begin{aligned}
 & \text{Four diagrams showing the convolution of a two-to-two transition with } \mathcal{D}_4^{(1234)} \text{ in different topologies.} \\
 & \rightarrow \bar{g}^2 N_c \sum_{\substack{(12), (13), \\ (24), (34)}} K_{2 \rightarrow 2} \otimes \mathcal{D}_4^{(1234)}(\omega), \tag{6.77}
 \end{aligned}$$

where, on the rhs, the subscripts under the sum indicate which pairings of gluons should be included. A comment on the first and the last terms is in place. These interactions are inside the gluon pairs (12) or (34) and thus do not belong to the production of an s -channel gluon inside the M^2 discontinuity. Hence, these interactions are not part of the branching vertex. It is only for our convenience that we, nevertheless, include them into our definition of $\mathcal{D}_4^{(\text{NP})}(\omega)$ (later on, when defining the partial waves, we will have to subtract them again). In (6.77), the second and third term (the interactions (13) and (24)) carry an additional minus sign, due to the color structure (see Sec.6.4.3). Similarly one has

$$\begin{aligned}
 & \text{Four diagrams with external lines 1, 2, 3, 4 and internal gluon lines} \rightarrow \bar{g}^2 N_c \sum_{\substack{(12),(23), \\ (14),(34)}} K_{2 \rightarrow 2} \otimes \mathcal{D}_4^{(2134)}(\omega), \\
 & \hspace{15em} (6.78)
 \end{aligned}$$

while the contributions containing $\mathcal{D}_4^{(2143)}(\omega)$ and $\mathcal{D}_4^{(1243)}(\omega)$ are

$$\bar{g}^2 N_c \sum_{\substack{(12),(13), \\ (24),(34)}} K_{2 \rightarrow 2} \otimes \mathcal{D}_4^{(2143)}(\omega) + \bar{g}^2 N_c \sum_{\substack{(12),(23), \\ (14),(34)}} K_{2 \rightarrow 2} \otimes \mathcal{D}_4^{(1243)}(\omega). \quad (6.79)$$

In all three sums, the second and third terms carry minus signs, and the first and last terms are kept for convenience and will have to be removed later on.

For the two-to-three transition (Fig.6.25b) we have two contributions: terms that originate from $\mathcal{D}_3^{(123)}(\omega)$ are given by

$$\begin{aligned}
 & \text{Four diagrams with external lines 1, 2, 3, 4 and internal gluon lines} \rightarrow \bar{g}^3 N_c \sum K_{2 \rightarrow 3} \otimes \mathcal{D}_3^{(123)}(\omega), \\
 & \hspace{15em} (6.80)
 \end{aligned}$$

where, on the rhs, the sum is over the four possible two-to-three transitions, allowed by the triple discontinuity. Again, in the second and the third terms a minus sign originating from the color factor has to be included. Contributions with $\mathcal{D}_3^{(321)}(\omega)$ are

$$\begin{aligned}
 & \text{Four diagrams with external lines 1, 2, 3, 4 and internal gluon lines} \rightarrow \bar{g}^3 (-N_c) \sum K_{2 \rightarrow 3} \otimes \mathcal{D}_3^{(321)}(\omega), \\
 & \hspace{15em} (6.81)
 \end{aligned}$$

where the sum is again over all four possible two-to-three transitions and for the second and third term a relative minus sign has to be included. Finally, from the two-to-four transition (Fig.6.25c) we have two contributions. They are given by

$$\begin{aligned}
 & \text{Two diagrams with external lines 1, 2, 3, 4 and internal gluon lines} \rightarrow 2\bar{g}^4 N_c K_{2 \rightarrow 4} \otimes \mathcal{D}_2(\omega). \\
 & \hspace{15em} (6.82)
 \end{aligned}$$

Combining these three groups and including the Reggeon-propagators we obtain for the amplitude

$\mathcal{D}_4^{\text{NP}}$:

$$\begin{aligned}
(\omega - \sum_i^4 \beta(\mathbf{k}_i) \mathcal{D}_4^{\text{NP}}(\omega|\mathbf{k}_1, \mathbf{k}_2, \mathbf{k}_3, \mathbf{k}_4)) &= \bar{g}^3 N_c \sum K_{2 \rightarrow 3} \otimes \mathcal{D}_3^{(123)}(\omega) + \bar{g}^3 (-N_c) \sum K_{2 \rightarrow 3} \otimes \mathcal{D}_3^{(321)}(\omega) \\
&+ 2\bar{g}^4 N_c K_{2 \rightarrow 4} \otimes \mathcal{D}_2(\omega) + \bar{g}^2 N_c \left[\sum_{\substack{(12),(13), \\ (24),(34)}} K_{2 \rightarrow 2} \otimes \mathcal{D}_4^{(1234)}(\omega) + \sum_{\substack{(12),(13), \\ (24),(34)}} K_{2 \rightarrow 2} \otimes \mathcal{D}_4^{(2143)}(\omega) \right. \\
&\quad \left. + \sum_{\substack{(12),(23), \\ (14),(34)}} K_{2 \rightarrow 2} \otimes \mathcal{D}_4^{(2134)}(\omega) + \sum_{\substack{(12),(23), \\ (14),(34)}} K_{2 \rightarrow 2} \otimes \mathcal{D}_4^{(1243)}(\omega) \right].
\end{aligned} \tag{6.83}$$

In the next step we make use of the fact that, according to the results of Sec.6.5.2 and Sec.6.5.4, all planar three and four gluon partial amplitudes on the rhs, \mathcal{D}_3 and \mathcal{D}_4 , can be written as superpositions of two gluon amplitudes $\mathcal{D}_2(\omega)$. As a result, the right hand side of Eq.(6.83) depends only on $\mathcal{D}_2(\omega)$, convoluted with the sum of transition kernels:

$$(\omega - \sum_{i=1}^4 \beta(\mathbf{k}_i) \mathcal{D}_4^{\text{NP}}(\omega|\mathbf{k}_1, \mathbf{k}_2, \mathbf{k}_3, \mathbf{k}_4)) = \frac{\bar{\lambda}^2}{N_c} V_{\text{TPV}} \otimes \mathcal{D}_2(\omega). \tag{6.84}$$

The right hand side of Eq.(6.84) defines the Triple-Pomeron-Vertex V_{TPV} on the pairs-of-pants. It describes the coupling of the upper BFKL Pomeron, $\mathcal{D}_2(\omega)$, to the lower ones, $\mathcal{D}_2(\omega_1)$ and $\mathcal{D}_2(\omega_2)$. The function V_{TPV} coincides with the V function found in [35]. In this paper, a finite N_c calculation with $N_c = 3$ has been carried out, and the following result for the $2 \rightarrow 4$ gluon vertex has been obtained:

$$\begin{aligned}
V_{2 \rightarrow 4}^{a_1 a_2 a_3 a_4}(\mathbf{l}_1, \mathbf{l}_2|\mathbf{k}_1, \mathbf{k}_2, \mathbf{k}_3, \mathbf{k}_4) &= \delta^{a_1 a_2} \delta^{a_3 a_4} V(\mathbf{l}_1, \mathbf{l}_2|\mathbf{k}_1, \mathbf{k}_2; \mathbf{k}_3, \mathbf{k}_4) \\
&+ \delta^{a_1 a_3} \delta^{a_2 a_4} V(\mathbf{l}_1, \mathbf{l}_2|\mathbf{k}_1, \mathbf{k}_3; \mathbf{k}_2, \mathbf{k}_4) + \delta^{a_1 a_4} \delta^{a_2 a_3} V(\mathbf{l}_1, \mathbf{l}_2|\mathbf{k}_1, \mathbf{k}_4; \mathbf{k}_2, \mathbf{k}_3).
\end{aligned} \tag{6.85}$$

Here a_i , $i = 1, \dots, 4$ denote color indices in the adjoint representation of the t -channel gluons. To compare with our result, we use the finite N_c version of Eq.(6.85) in [38] which has been obtained for arbitrary N_c and we find

$$\frac{\bar{\lambda}^2}{N_c} V_{\text{TPV}}(\mathbf{l}_1, \mathbf{l}_2|\mathbf{k}_1, \mathbf{k}_2; \mathbf{k}_3, \mathbf{k}_4) = N_c V(\mathbf{l}_1, \mathbf{l}_2|\mathbf{k}_1, \mathbf{k}_2; \mathbf{k}_3, \mathbf{k}_4). \tag{6.86}$$

It is easy to verify that this result is in complete agreement with the large large- N_c limit of [35,38]. Namely, if we project, in Eq.(6.85), on the color single state of the gluon-pairs (12) and (34) and then consider the limit of large N_c , only the first term on the right hand side of Eq.(6.85) contributes, and we indeed obtain agreement of the two results as required. In [107] it has been shown that the vertex V is invariant under Möbius transformations. Furthermore, V can be expressed in terms of another function $G(\mathbf{k}_1, \mathbf{k}_2, \mathbf{k}_3)$:

$$\begin{aligned}
V(\mathbf{k}_1, \mathbf{k}_2, \mathbf{k}_3, \mathbf{k}_4) &= \bar{\lambda} [G(1, 23, 4) + G(2, 13, 4) + G(1, 24, 3) + G(2, 14, 3) - G(12, 3, 4) \\
&\quad - G(12, 4, 3) - G(1, 2, 34) - G(2, 1, 34) + G(12, -, 34)],
\end{aligned} \tag{6.87}$$

where we suppressed the dependence on the momenta \mathbf{l}_1 and \mathbf{l}_2 . This function G has been first introduced for the forward case and $N_c = 3$ in [35], whereas the above version was introduced in [74]. It has the nice property that it is not only infra-red finite but also by itself invariant under Möbius transformations [74].

6.7 The six-point amplitude on the pair-of-pants surface

With the results of the previous sections, we have almost all constituents that are needed to build the triple Regge limit of the six-point amplitude with the pair-of-pants topology. However before

we add together the amplitudes of the foregoing sections, we need to take care of a peculiarity inside the planar piece of the upper amplitude. To leading order in λ , the two lower Pomerons couple directly to the upper quark-loop, as depicted in Fig.6.29 and the branching vertex is not given by a real gluon, but by the quark-loop itself. As long as we have, in addition to the $q\bar{q}$ pair, one (or more) s -channel gluons that contribute to the M^2 discontinuity, the mass of the $q\bar{q}$ -system is integrated over, and this integration enters into the definition of the impact factors $\mathcal{D}_{4;0}^{(ijkl)}$. Without such gluons, the mass of the $q\bar{q}$ pair coincides with the diffractive mass M which is a fixed external parameter. In this case, the coupling of the t -channel four gluon system to the quark-loop is hence given by the triple discontinuity of the quark loop without the integration over the diffractive mass of the $q\bar{q}$ -system, and defines an 'unintegrated' four gluon impact factor, $\bar{\mathcal{D}}_{(4;0)}(M^2)$. Its precise analytic form can be obtained from Eq.(2.8) of [35]. Correspondingly, its Mellin transform, which enters the partial wave $F(\omega, \omega_1, \omega_2)$ will be denoted by $\bar{\mathcal{D}}_{(4;0)}(\omega)$. When $\bar{\mathcal{D}}_{(4;0)}(M^2)$ is integrated over the squared diffractive mass M^2 , it coincides with sum over the impact factors $\mathcal{D}_{4;0}^{(ijkl)}$.

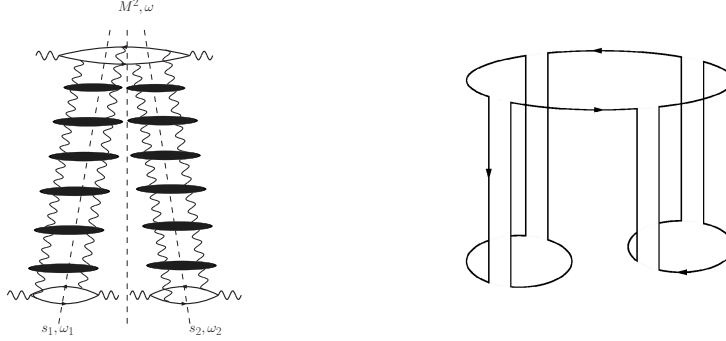


Figure 6.29: Diagrams where the two Pomerons couple directly to the upper quark-loop. They contain the lowest order diagram in Fig.6.11. The color factors can be reduced to the color factor to the right and therefore belong to the planar class.

After this remark we write the final result as the sum of two terms:

$$F(\omega, \omega_1, \omega_2) = F^{(P)}(\omega, \omega_1, \omega_2) + F^{(NP)}(\omega, \omega_1, \omega_2), \quad (6.88)$$

where the first term sums the planar diagrams (including the 'unintegrated' impact factors), the second term the non-planar ones. When doing the convolution of the three amplitudes, special care has to be taken of the counting of interactions inside the gluon pairs (12) and (34) just below the branching point where the upper cylinder splits into two cylinders (c.f. the discussion given in Sec.6.4.6). This issue has been addressed, for the ' N_c -finite' case, in Sec.4 of [35] (see, in particular Eqs.(4.14) and Eq.(4.15)), and in the following we shall apply the same line of arguments. We identify, for the M^2 discontinuity, the lowest s -channel intermediate state which leads to the 'last' interaction between the two gluon pairs (12) and (34): below this interaction, the upper cylinder has split into two separate cylinders. In particular, this last interaction cannot consist of a two-to-two kernel acting on the gluon pairs (12) or (34). Since, in Secs.6.5.3 and 6.6, we have defined the functions $\mathcal{D}_4^{(ijkl)}$ and $\mathcal{D}_4^{(NP)}$ in such a way that the last interaction includes these contributions, we first have to remove them. Furthermore, as explained above, the coupling of the $\mathcal{D}_2^{(12)}(\omega_1)$ and $\mathcal{D}_2^{(34)}(\omega_2)$ directly to the upper quark-loop is described by $\bar{\mathcal{D}}_{4;0}(\omega)$, and we write this term separately. We therefore arrive at the full partial wave in the following form:

$$\begin{aligned} F(\omega, \omega_1, \omega_2) &= 4\mathcal{D}_2^{(12)}(\omega_1) \otimes_{12} \mathcal{D}_2^{(34)}(\omega_2) \otimes_{34} \\ &\left(\bar{\mathcal{D}}_{(4;0)}(\omega) + \left[\omega - \sum_{i=1}^4 \beta(\mathbf{k}_i) \right] \sum_{(ijkl)=\substack{(1234),(2143), \\ (2134),(1243)}} \mathcal{D}_4^{(ijkl)}(\omega) + \frac{\bar{\lambda}^2}{N_c} V_{TPV} \otimes \mathcal{D}_2(\omega) \right. \\ &\left. - 2\bar{\lambda}(K_{2 \rightarrow 2}^{(12)} + K_{2 \rightarrow 2}^{(34)}) \otimes \sum_{(ijkl)=\substack{(1234),(2143), \\ (2134),(1243)}} \mathcal{D}_4^{(ijkl)}(\omega) \right) \end{aligned} \quad (6.89)$$

In the first line, the indices of the convolution symbols indicate that $\mathcal{D}_2^{(12)}(\omega_1)$ and $\mathcal{D}_2^{(34)}(\omega_2)$ are to be contracted with the gluons (12) and (34), resp. The last line subtracts the two-to-two kernels acting on gluon pairs (12) and (34). Using the BFKL-equation

$$2\bar{\lambda}K_{2\rightarrow 2}^{(12)}\mathcal{D}_2^{(12)}(\omega_1) = (\omega_1 - \beta(\mathbf{k}_1) - \beta(\mathbf{k}_2))\mathcal{D}_2^{(12)}(\omega_1) - \mathcal{D}_{(2;0)}^{(12)}$$

(and a similar expression for the gluon pair (34)), and making further use of Eq.(6.75), we arrive at

$$F(\omega, \omega_1, \omega_2) = 4 \left\{ \mathcal{D}_2^{(12)}(\omega_1) \otimes_{12} \mathcal{D}_2^{(34)}(\omega_2) \otimes_{34} \left(\bar{\mathcal{D}}_{(4;0)}(\omega) + [\omega - \omega_1 - \omega_2] V^R \otimes \mathcal{D}_2(\omega) + \frac{\bar{\lambda}^2}{N_c} V_{\text{TPV}} \otimes \mathcal{D}_2(\omega) \right) + \mathcal{D}_2^{(12)}(\omega_1) \otimes_{12} \mathcal{D}_{(2;0)}^{(34)} \otimes_{34} V^R \otimes \mathcal{D}_2(\omega) + \mathcal{D}_{(2;0)}^{(12)} \otimes_{12} \mathcal{D}_2^{(34)}(\omega_2) \otimes_{34} V^R \otimes \mathcal{D}_2(\omega) \right\}. \quad (6.90)$$

The terms in the last line are either independent of ω_2 or ω_1 and the integrals over ω_2 or ω_1 vanish in Eq.(6.33). We therefore drop these terms and obtain for the two partial waves $F^{(P)}(\omega, \omega_1, \omega_2)$ and $F^{(NP)}(\omega, \omega_1, \omega_2)$ the following results:

$$F^{(P)}(\omega, \omega_1, \omega_2) = 4\mathcal{D}_2^{(12)}(\omega_1) \otimes_{12} \mathcal{D}_2^{(34)}(\omega_2) \otimes_{34} \left(\bar{\mathcal{D}}_{(4;0)}(\omega) + [\omega - \omega_1 - \omega_2] \frac{\bar{\lambda}}{N_c} V^R \otimes \mathcal{D}_2(\omega) \right) \quad (6.91)$$

and

$$F^{(NP)}(\omega, \omega_1, \omega_2) = 4\mathcal{D}_2^{(12)}(\omega_1) \otimes_{12} \mathcal{D}_2^{(34)}(\omega_2) \otimes_{34} \frac{\bar{\lambda}^2}{N_c} V_{(\text{TPV})} \otimes \mathcal{D}_2(\omega). \quad (6.92)$$

Both terms are illustrated in Figs.6.30a and 6.30b.

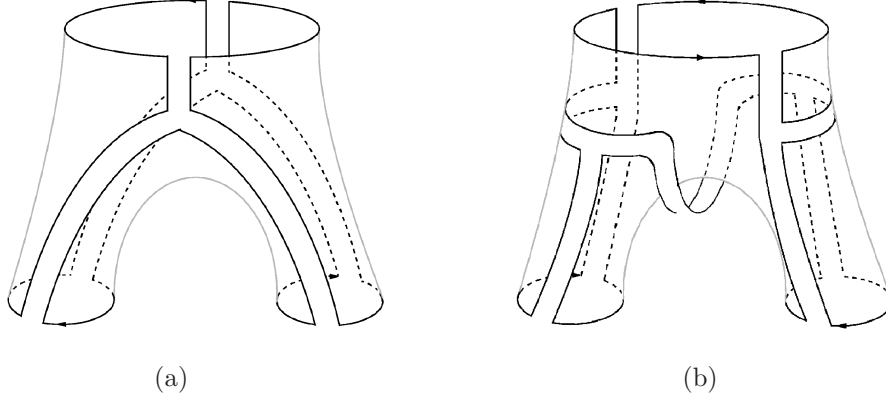


Figure 6.30: (a) Planar color graphs associated with the decay of two reggeized gluons and (b) non-planar color graphs which lead to the Triple-Pomeron-Vertex. In both cases a two gluon state decays into a four gluon state.

6.8 Conclusion

In the present analysis we have considered, in the large- N_c limit, the triple Regge-limit of the scattering of three virtual photons. Our emphasis has been on the topology of color factors: we have summed, in the generalized leading-log approximation, only those diagrams which fit onto the pair-of-pants surfaces. These diagrams group themselves naturally into two classes (Fig.6.30). The first class consists of all diagrams which, by contracting closed color loops, coincide with one

of the lowest order graphs (of order $g^8 N_c^3$) illustrated in Fig.13. Making use of the bootstrap conditions, the sum of these graphs is shown to reduce to reggeized gluons with a simple splitting vertex. In addition, starting at the order $g^8 N_c^3 (g^2 N_c)$, a second class of diagrams appears which, by contracting closed color loops, cannot be drawn as one of the lowest order graphs shown in Fig.13. The sum of these graphs can be written as a convolution of three BFKL amplitudes, connected by the triple Pomeron vertex found in earlier papers. This triple Pomeron vertex has been shown to be invariant under Möbius transformation [107].

The analytic expression for the six-point amplitude derived in this chapter coincides with the large- N_c limit of the QCD result in [35]. However, the analysis of the present chapter provides another interpretation of gluon reggeization and the appearance of the Möbius invariant triple Pomeron vertex: on the pair-of-pant surface, the reggeizing pieces are completely planar, whereas the triple Pomeron vertex belongs to a distinct class of color diagrams which reflect the non-planar Mandelstam cross.

We believe that the topological approach pursued in this chapter is well-suited for studying the Regge limit of N=4 Super Yang Mills Theory within the AdS/CFT correspondence. On the string side, amplitudes are naturally expanded in terms of topologies. In particular, the pair-of-pants topology studied in this chapter is the same as that of the vertex which describes the coupling of three closed strings.

For a systematic study of the AdS/CFT correspondence it is convenient to make use of R -currents: they allow to formulate current correlators which are well-defined both on the gauge theory side and on the string side. As a first step of investigating, in the Regge limit, the duality between N=4 Super Yang Mills Theory and AdS_5 string theory, the 4-point function for such currents has been studied on the gauge theory side in [78]. This study confirms that the interaction between two R -currents in the Regge-limit is, indeed, mediated by a BFKL-Pomeron, and it contains the two gluon impact factors in N=4 SYM. On the string side, the scattering of two R -currents has been shown to involve, in lowest order, the one-graviton exchange [117]. In the present chapter we have addressed, on the gauge theory side, the next term in the topological expansion. As a start, we have restricted ourselves to nonsupersymmetric QCD(N_c). The generalization to the supersymmetric case where, inside the impact factors, fermions and scalar particles in the adjoint representation have to be considered, will be presented elsewhere [79]. On the string side, the analogous 6-point R -current correlator is expected to contain the triple graviton vertex. This project is currently being studied.

Chapter 7

The topology of the triple Pomeron vertex in $\mathcal{N} = 4$ SYM

Within the AdS/CFT correspondence which relates $\mathcal{N} = 4$ supersymmetric Yang Mills quantum field theory (SYM) in four dimensions to a string theory in a $AdS_5 \otimes S_5$ space correlators of R -currents provide a useful tool for investigating the Regge limit, in particular the correspondence between the BFKL Pomeron in $\mathcal{N} = 4$ SYM and the graviton on the string side.

In the simplest case, the elastic scattering of two R -currents, both ends of the correspondence have been investigated in leading order. On the gauge theory side, the supersymmetric impact factors consisting of the sum of a fermion and of a scalar loop in the adjoint representation of the gauge group have been computed, and it has been verified that the high energy behavior is described by the BFKL Pomeron [78]. On the string side, the leading contribution in the zero slope limit is given by the Witten diagram with graviton exchange [117]. Beyond the zero slope limit, the graviton is believed to reggeize.

A next step along this line is the six point function of R -currents in the triple Regge limit. In this kinematic limit one expects to see the triple Pomeron vertex which represents, besides the BFKL kernel, another fundamental element of high energy QCD: it describes the splitting of a BFKL Pomeron into two BFKL Pomerons. On the string side, one expects the graviton self interaction to play the analogous role. For QCD - with fermions in the fundamental representation and with the electromagnetic current in place of the R -current - the six point function at finite N_c has first been studied in [35]. As the main result, the triple Pomeron vertex has been calculated, which by now has been derived in several other approaches. In [79] the case of the six point function of R -currents in $\mathcal{N} = 4$ SYM has been studied for finite N_c : whereas the triple Pomeron vertex remains the same as in the nonsupersymmetric case, a new contribution to the six point correlator appears which results from the adjoint color representation of the particles and has no counterpart in QCD.

Another line of interest is the integrability of the BKP equation: since in the leading logarithmic approximation there is no difference between QCD and its supersymmetric generalization, $\mathcal{N} = 4$ SYM, one expects that the integrability which has been discovered for the large- N_c limit of QCD in fact is 'inherited' from $\mathcal{N} = 4$ SYM. The environment where the large- N_c limit of BKP states can be studied are higher order current correlators, e.g. the eight point function in a suitable Multi-Regge limit. Within the AdS/CFT correspondence, the counterpart of the BKP states has not been addressed at all.

Recently, an attempt has been started to investigate these high energy limits within a topological approach: in the large- N_c limit, the color structure of scattering amplitudes can be attributed to surfaces: spheres, planes, cylinders, pairs-of-pants, etc. The simplest examples include, in QCD with fermions in the fundamental representation, multigluon scattering amplitudes in the plane and the BFKL Pomeron on the cylinder. Recently [118] also the six point correlator of electromagnetic currents has been studied in the large- N_c limit by summing diagrams whose color structure lies

on the surface of a pair-of-pants. The study of these color diagrams provides a new view on the reggeization of the gluon and on the triple Pomeron vertex: whereas the reggeization can be understood as a feature of planar QCD, the triple Pomeron vertex requires a non-planar structure, reminiscent of the non-planar Mandelstam cross diagram.

When turning, from QCD with fundamental fermions, to $\mathcal{N} = 4$ SYM with fermions and scalars in the adjoint representation, one encounters changes in the topology of the surfaces and in the structure of color graphs. The first example is the BFKL Pomeron which lies on the surface of a sphere with zero boundaries. Apart from this the form of the impact factor stays the same. In the present paper we address in the large- N_c limit a six point correlator of R -currents in $\mathcal{N} = 4$ SYM in the topological approach. We sum graphs whose color structure belongs to a specific deformation of a sphere, corresponding to the pair-of-pants investigated in [118].

We first review the color structure of Feynman diagrams in the large- N_c limit and define the classes of graphs which we are going to sum. We then formulate integral equations which sum these graphs and discuss their solutions. Our final result for the large- N_c limit consists of three terms which represent three distinct classes of color diagrams on the surface of the deformed sphere.

7.1 Topology of graphs in $\mathcal{N} = 4$ SYM

It may be useful to recapitulate the large- N_c limit of QCD with fermions in the fundamental representation, and to recall a few features of the classical paper of 't Hooft [73]. Starting from the Fierz identity

$$(g^a)_j^i (g^a)_l^k = \delta_l^i \delta_j^k - \frac{1}{N_c} \delta_j^i \delta_l^k, \quad (7.1)$$

where $(g^a)_j^i$ denoted the $SU(N_c)$ generators in the fundamental representation (with the normalization $\text{tr}(g^a g^b) = \delta^{ab}$), and from the identity

$$f^{abc} = \frac{1}{i\sqrt{2}} [\text{tr}(g^a g^b g^c) - \text{tr}(g^c g^b g^a)], \quad (7.2)$$

one is lead to draw, in the large- N_c limit, color diagrams with the following elements:

(i) for each quark in the fundamental representation, a single line with an arrow, indicating the flow from the upper to the lower index,

$$\delta_j^i = i \longrightarrow j; \quad (7.3)$$

(ii) for each inner gluon a double line

$$\delta_l^i \delta_j^k = \begin{array}{c} i \longrightarrow l \\ j \longleftarrow k \end{array}; \quad (7.4)$$

(iii) for each triple gluon vertex

$$f^{abc} = \frac{1}{i\sqrt{2}} [\text{tr}(g^a g^b g^c) - \text{tr}(g^c g^b g^a)]. \quad (7.5)$$

As a result, each graph turns into a network of double and single lines. The resulting diagrams represent only the color factors. A usual Feynman diagram represents both the color factors and the momentum part. In the double line notation the momentum part has to be written separately.

The double line diagrams can be drawn on a two-dimensional surface with Euler number $\chi = 2 - 2h - b$, where h is the number of handles of the surface, and b the number of boundaries or holes. A closed color-loop always delivers a factor N_c , and a closed quark-loop, compared to a corresponding gluon-loop, is $1/N_c$ suppressed and leads to a boundary. For an arbitrary vacuum graph T one arrives at the following expansion in N_c

$$T = \sum_{h,b}^{\infty} N_c^{2-2h-b} T_{h,b}(\lambda) \quad (7.6)$$

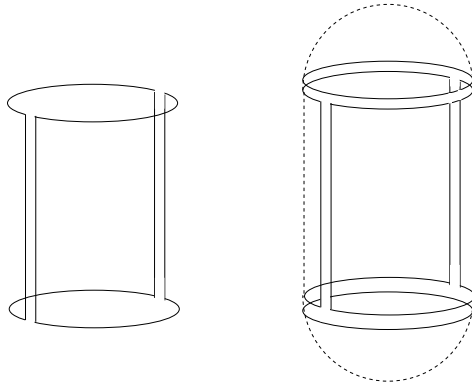


Figure 7.1: Cylinder topology for the $2 \rightarrow 2$ scattering in QCD (left) and in $\mathcal{N} = 4$ SYM (right)

where

$$\lambda = g^2 N_c \tag{7.7}$$

is the 't Hooft-coupling which is held fixed, while N_c is taken to infinity.

In the expansion Eq.(7.6) which matches the loop expansion of a closed string theory with the string coupling $1/N_c$, the leading- N_c diagrams are those that have the topology of a sphere: zero handles and zero boundaries, $h = b = 0$. If quarks are included, the leading diagrams have the topology of a disk, i.e. the surface with zero handle and one boundary, $h = 0, b = 1$, fits on the plane, with the boundary as the outermost edge. Diagrams with two boundaries and zero handles can be drawn on the surface of a cylinder, those with three boundaries on the surface of a pair-of-pants. Boundaries are also be obtained by removing, from the sphere, one or more points. Removing one point, one obtains the disk, which can be drawn on the plane, and by identifying the removed point with infinity, the graphs can be drawn on the (infinite) plane. Removing two points we obtain the cylinder and so on. By definition, the expansion Eq.(7.6) is defined for vacuum graphs. However, from the earliest days on [113], the large- N_c limit has been also applied to the scattering of colored objects. In order to consider the topological expansion of an amplitude with colored external legs, one needs to embed it into a vacuum graph which then defines the topological expansion of an amplitude with colored external legs.

In the large- N_c limit of high energy QCD, quark scattering amplitudes are drawn on a plane; in particular, one can show that the BFKL bootstrap condition is satisfied on the plane (zero handles, one boundary). Next, for the BFKL Pomeron the color diagrams lie on the surface of a cylinder (zero handles, two boundaries), (Fig.7.1, left), and the triple Pomeron vertex is obtained from diagrams which fit on the pair-of-pants surface (zero handles, three boundaries), (Fig.7.2).

Let us now turn to $\mathcal{N} = 4$ SYM where fermions and scalars belong to the adjoint representation and therefore are represented by double lines, in the same way as the gauge bosons. Now fermion loops no longer define sections and therefore cannot be used define separate topologies. As an example, in QCD with fundamental quarks the diagrams of the BFKL Pomeron fit onto the surface of a cylinder (Fig.7.1, left): the closed quark loops at the top and at the bottom define the two sections. In $\mathcal{N} = 4$ SYM with adjoint fermions and scalars, the top and the bottom obtain double lines (Fig.7.1, right) and turn into caps, as a results of which the cylinder turns into a (stretched) sphere (zero handles, zero boundaries).

An analogous result holds for the six point function of external currents in the triple Regge limit. For QCD with fundamental quarks the sphere has three sections (for each impact factor, the closed fermion loop defines a section), (Fig.7.3, left) and it has been shown in [118] that the color diagrams fit on the surface of a pair-of-pants (Fig.7.2). When switching to $\mathcal{N} = 4$ SYM where fermions and scalars belong to the adjoint representation, the closed lines of the upper and lower impact factors turn into double lines, and the sections of the pair-of-pants are replaced by caps, (Fig.7.3, right).

As a result, we again arrive at a sphere, shaped as a pair of pants, and we are asked to sum, for the triple Regge limit, diagrams which lie on the surface of this body. As we shall see in the following,

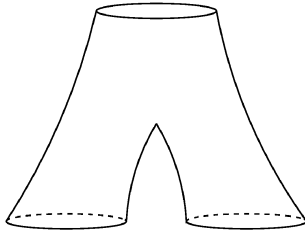


Figure 7.2: Pair-of-pants topology for the $3 \rightarrow 3$ amplitude in the triple Regge limit

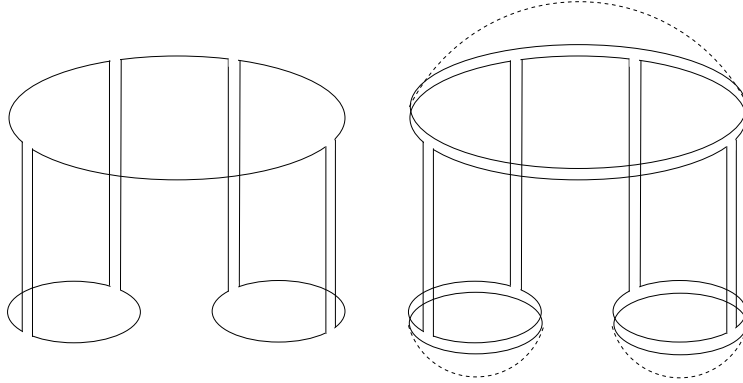


Figure 7.3: Pair-of-pants topology for the $3 \rightarrow 3$ amplitude in QCD (left) and in $\mathcal{N} = 4$ SYM (right)

there are three distinct classes of diagrams: two of them are the same as in (nonsupersymmetric) QCD, whereas the third one is new and has no analogue in QCD.

7.2 Selection of diagrams

Six point amplitudes depend on three energy variables, $s_1 = (q + p_1)^2$, $s_2 = (q' + p_2')^2$ and $M^2 = (q + p_1 - p_1')^2$. The momentum transfer variables are $t = (q - q')^2$, $t_1 = (p_1 - p_1')^2$ and $t_2 = (p_2 - p_2')^2$. The kinematics of a six point amplitude with external R -currents are illustrated in Fig.7.4. Then the triple Regge limit is given by

$$s_1 = s_2 \gg M^2 \gg t, t_1, t_2. \quad (7.8)$$

In the Regge limit there is an easy way of computing six point amplitudes of R -currents, namely we take the triple energy discontinuity in s_1 , s_2 and M^2 . In lowest order the main ingredients

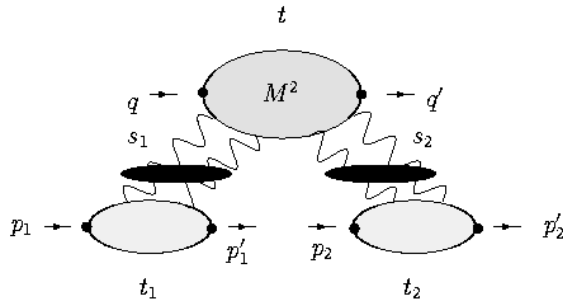


Figure 7.4: Kinematics of a six point amplitude

of a diagram are three impact factors and four t -channel gluons. The impact factors consisting of a fermion and a scalar loop represent the coupling of the t -channel gluons to the external R -currents. The insertion of the R -currents is symbolized by the small black dots in Fig.7.4. Higher order corrections are taken into account by the production of real gluons in the Regge kinematics.

We now discuss in the double line notation the relevant diagrams which contribute to the triple Regge limit of the six point correlators of R -currents. We will closely follow the discussion of [118], and we will use the same notation. In the following double line diagrams we do not show the attached R -currents, we only consider the gluons and adjoint particle loops.

We begin with a comment on the cylinder in QCD, (Fig.7.1, left). When replacing, at the top of the cylinder, the fermion in the fundamental representation by an adjoint fermion, we simply draw, above the already existing color line of the fermion, an additional closed color loop which generates an additional factor N_c . The double line notation now also includes scalar loops. The two t -channel gluons are attached to the same color line of the closed loop, either to the lower line or to the upper one as shown in Fig.7.1, right. Diagrams where the two t -channel lines are attached to different lines lose this additional factor N_c and are suppressed. As a result of this simple observation, the contribution of the adjoint fermions to the impact factors is proportional to N_c times that of a fundamental one¹. In $\mathcal{N} = 4$ SYM, the four point correlator is of the form $N_c^2 A_{2 \rightarrow 2}(\lambda)$, whereas in nonsupersymmetric QCD it is of the form $N_c^0 A_{2 \rightarrow 2}(\lambda)$.

Let us now turn to the six point function. In QCD in lowest order the four t -channel gluons couple to the upper loop in all possible ways, all together there a 16 different diagrams. A closer look shows that we have inside the 16 diagrams four different orderings of color matrices. For the lowest order diagrams in the nonsupersymmetric QCD case, the four different structures are illustrated in Fig.7.5. Switching to $\mathcal{N} = 4$ SYM, we simply perform, for each of the three impact factors, the

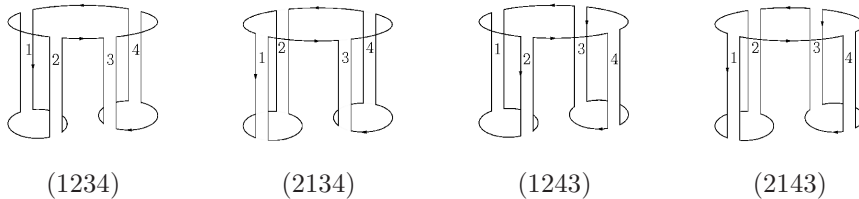


Figure 7.5: The four different orderings of color factors of the Born-term

substitution we have just described for the BFKL cylinder, and we obtain the additional factor N_c^3 , leading to a result of the order $N_c^2 \lambda^4$. Whereas in QCD the analogous lowest order graphs fit on the surface of a pair-of-pants in Fig.7.2, the diagrams now have the shape of a deformed sphere as shown once again in Fig.7.6(a). Here both gluons cylinders are coupled to the same line of the upper loop.

A closer inspection shows that, in addition to Fig.7.6(a), another configuration is possible: without losing a factor N_c , we can attach one of the cylinders to the outer loop, the other one to the inner loop (Fig.7.6(b)). This additional piece in the four gluon impact factor which has no counterpart in the fundamental representation, has first been found in [79]. An alternative way of drawing this graph is shown in Fig.7.7.

Moving on to the next order, we first note that for the diagram in Fig.7.6(b), one can only start to 'dress' the two cylinders: an example is shown in Fig.7.8. In particular, any rung connecting the two cylinders loses a power of N_c . As a result, this class of diagrams simply consists of two BFKL Pomerons coupled to the four gluon impact factor, and the resulting amplitude is of the form $N_c^2 A_{3 \rightarrow 3}(\lambda)$. This class of diagrams will be named 'direct': the two BFKL Pomerons couple directly to the impact factor. As discussed in [118], on the cylinder each gluon rung comes in two

¹This is nothing else but the consequence of the different normalizations of generators. In the fundamental representation we use $\text{tr}(t^a t^b) = \delta_{ab}$, whereas in the adjoint representation we have $\text{tr}(T^a T^b) = N_c \delta_{ab}$. Note that our normalization of the fundamental generators deviates by a factor 2 from the standard normalization $\text{tr}(\tau^a \tau^b) = \delta^{ab}/2$.

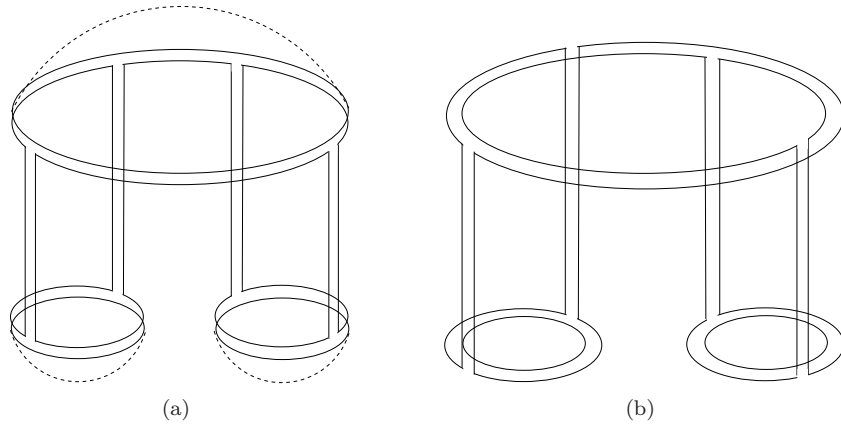


Figure 7.6: Pair-of-pants topology for the $3 \rightarrow 3$ amplitude in $\mathcal{N} = 4$ SYM: (a) a color configuration already present in QCD, and (b) a new one which exists only for adjoint particles

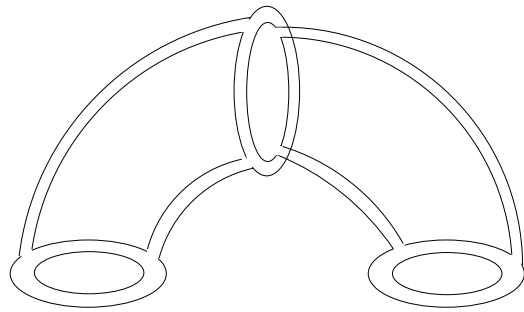


Figure 7.7: An alternative way of drawing Fig.7.6(b)

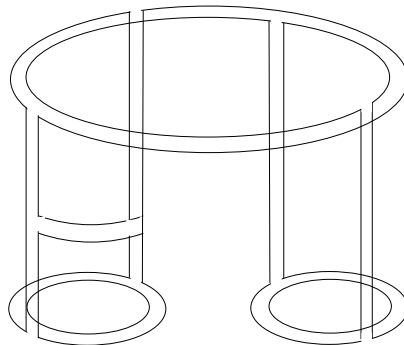


Figure 7.8: Example of a next-to-leading order diagram of Fig.7.6(b)

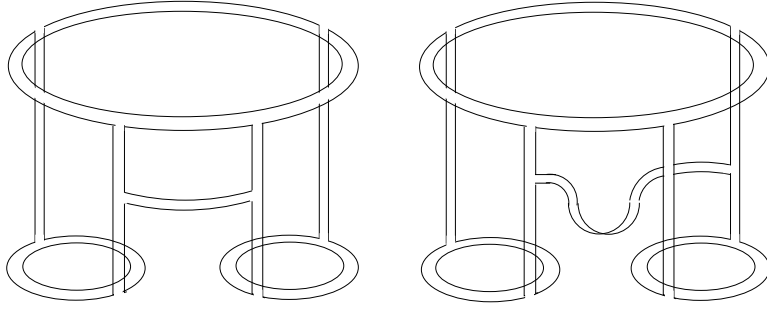


Figure 7.9: Two classes of diagrams: planar graphs (left) and non-planar graphs (right)

different ways, one in front of the cylinder, the other one on the backside. This observation also applies to our $\mathcal{N} = 4$ SYM case.

Returning to the other diagrams in Fig.7.6, that are already present in nonsupersymmetric QCD, insertion of one more rung opens two distinct classes of graphs: examples are given in Fig.7.9, and it is suggestive to name them as 'planar' and 'nonplanar', respectively. By definition, planar graphs have the property that, by contracting closed color loops, they can be reduced to the $\mathcal{N} = 4$ SYM version of the graphs in Fig.7.5. For the non-planar ones, this is not possible, beginning with the graph shown in Fig.7.9, right, there is a new class of diagrams which cannot be deformed into planar graphs.

In higher order λ , several possibilities arise. We briefly summarize the discussion given in [79]. The general structure of the diagrams is the following: At the upper impact factor we start with a t -channel state with two, three or four gluons. The propagation of the t -channel gluons is described by the BKP equations and transition between different states by vertices. We can have $2 \rightarrow 2$, $2 \rightarrow 3$, or $2 \rightarrow 4$ vertices. There is always a lowest interaction between the gluons defined by the M^2 -discontinuity below which the upper cylinder breaks up into two disconnected ones. After this branching vertex the gluons interact only pairwise according to the BFKL equation and are coupled to the two impact factors of the R -currents at the bottom.

We have to distinguish three different types of diagrams: the direct, the planar, and the nonplanar diagrams. In the first case, the direct diagrams, the lowest interaction between the two cylinders is the upper impact factor itself. The four gluons couple directly the upper loop without interaction between the two disconnected BFKL Pomerons.

Planar diagrams, the second type of diagrams, are reggeizing pieces. At the upper loop they start with two, three, or four t -channel gluons. These gluons undergo transitions by $2 \rightarrow 2$, $2 \rightarrow 3$, or $2 \rightarrow 4$ vertices, respectively. One of these transitions is the branching vertex below which we always have four gluons but each two gluons only interact pairwise after the branching vertex. They form once again the two noninteracting BFKL Pomerons.

The last possibility are nonplanar diagrams. At the upper loop they can also start with two, three, or four t -channel gluons and the structure above the branching vertex is the same as for planar diagrams. But the branching vertex itself now provides a nonplanar structure. Below this nonplanar vertex the known disconnected BFKL cylinders show up.

7.3 Analytic expressions

Let us now turn to analytic expressions. It is convenient to use the analytic representations of multiparticle amplitudes. A detailed discussion can be found in [93]. We restrict ourselves to those contributions which have a nonvanishing discontinuity in M^2 . In the triple Regge limit, Eq.(7.8),

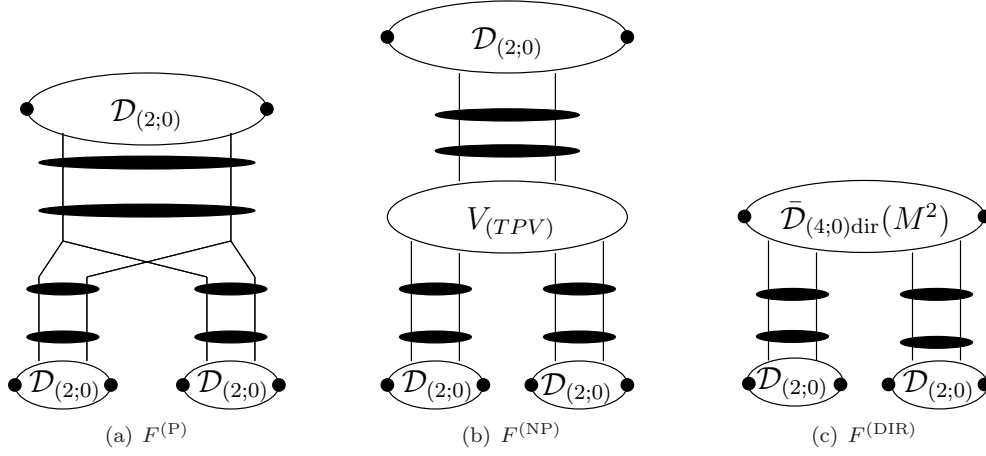


Figure 7.10: The three different parts of the six point function $T_{3 \rightarrow 3}$

we have for the $3 \rightarrow 3$ amplitude:

$$T_{3 \rightarrow 3}(s_1, s_2, M^2 | t_1, t_2, t) = \frac{s_1 s_2}{M^2} \int \frac{d\omega_1 d\omega_2 d\omega}{(2\pi i)^3} s_1^{\omega_1} s_2^{\omega_2} (M^2)^{\omega - \omega_1 - \omega_2} \xi(\omega_1) \xi(\omega_2) \xi(\omega, \omega_1, \omega_2) \cdot F(\omega, \omega_1, \omega_2 | t, t_1, t_2) + \dots \quad (7.9)$$

The dots represent three further terms that appear in the triple Regge limit: they do not contribute to the M^2 -discontinuity. The signature factors are given by

$$\xi(\omega) = -\pi \frac{e^{-i\pi\omega} - 1}{\sin(\pi\omega)} \quad \text{and} \quad \xi(\omega, \omega_1, \omega_2) = -\pi \frac{e^{-i\pi(\omega - \omega_1 - \omega_2)} - 1}{\sin \pi(\omega - \omega_1 - \omega_2)}. \quad (7.10)$$

As discussed in the previous section, for the computation we have taken the triple energy discontinuity of the amplitude in s_1 , s_2 , and M^2 :

$$\text{disc}_{s_1} \text{disc}_{s_2} \text{disc}_{M^2} T_{3 \rightarrow 3} = \pi^3 \frac{s_1 s_2}{M^2} \int \frac{d\omega_1 d\omega_2 d\omega}{(2\pi i)^3} s_1^{\omega_1} s_2^{\omega_2} (M^2)^{\omega - \omega_1 - \omega_2} \cdot F(\omega, \omega_1, \omega_2 | t_1, t_2, t), \quad (7.11)$$

which, via a triple Mellin transform, is related to the partial wave $F(\omega, \omega_1, \omega_2 | t_1, t_2, t)$. For the calculation of the triple discontinuity we have used unitarity integrals, and the summation of the diagrams has been performed by means of integral equations. Details can be found in [118], and we only describe the results.

Our result for the sum of the diagrams which fit on the surface of the deformed sphere (Fig.7.6) is given by the sum of three terms which sum different classes of diagrams: planar diagrams, non-planar diagrams, and direct diagrams:

$$T_{3 \rightarrow 3} = T_{3 \rightarrow 3}^{(P)} + T_{3 \rightarrow 3}^{(NP)} + T_{3 \rightarrow 3}^{(DIR)} \quad (7.12)$$

The three different parts are illustrated in Fig.7.10. In the triple Regge limit, Eq.(7.8), the partial waves factorize and consist of several building blocks. In our case we encounter two-gluon impact factors, BFKL Green's functions, and a triple vertex which connects them. The two-gluon impact factors, $D_{2,0}$, describe the coupling to the external R -currents. For $\mathcal{N} = 4$ SYM they have been computed in [78]. They contain both fermions and scalar in the adjoint representation.

Let us go into some detail. For the sum of the first two terms we use the representation (7.9) and write

$$F(\omega, \omega_1, \omega_2) = F^{(P)}(\omega, \omega_1, \omega_2) + F^{(NP)}(\omega, \omega_1, \omega_2). \quad (7.13)$$

As seen in Fig.7.10, the impact factors appear at the three different ends of the diagrams, and they are connected by BFKL Green's functions and a triple vertex in the center. The two terms differ from each other by the form of the triple vertex: in the second term, the vertex is due to the

non-planar diagrams and coincides with the triple Pomeron vertex found in QCD. The first term which results from the planar diagrams is a direct consequence of the reggeization of the gauge boson. The partial wave has the form:

$$F^{(P)}(\omega, \omega_1, \omega_2) = 4\mathcal{D}_2^{(12)}(\omega_1) \otimes_{12} \mathcal{D}_2^{(34)}(\omega_2) \otimes_{34} [\omega - \omega_1 - \omega_2] \frac{\bar{\lambda}}{N_c} V^R \otimes \mathcal{D}_2(\omega) \quad (7.14)$$

with

$$\bar{\lambda} = \bar{g}^2 N_c = \frac{g^2 N_c}{2}. \quad (7.15)$$

The convolution symbol is defined as

$$\otimes_{12} = \int \frac{d^2 \mathbf{k}_1}{(2\pi)^3 \mathbf{k}_1^2 \mathbf{k}_2^2}, \quad (7.16)$$

where \mathbf{k}_1 and \mathbf{k}_2 are the transverse momenta of the gluons 1 and 2. In (7.14) we have introduced the three functions $\mathcal{D}_2(\omega)$, $\mathcal{D}_2(\omega_1)$, $\mathcal{D}_2(\omega_2)$ which combine the three impact factors $D_{2;0}$ with their adjacent BFKL Green's functions. The subscript 12 at the convolution symbol indicates that the two gluon amplitude $\mathcal{D}_2^{(12)}(\omega_1)$ has to be contracted with the t -channel gluons 1 and 2. Similarly, \otimes_{34} belongs to the gluons 3 and 4. Analytic expressions for the triple vertex V^R can be found in [118].

The second part of the partial wave takes the form

$$F^{(NP)}(\omega, \omega_1, \omega_2) = 4\mathcal{D}_2^{(12)}(\omega_1) \otimes_{12} \mathcal{D}_2^{(34)}(\omega_2) \otimes_{34} \frac{\bar{\lambda}^2}{N_c} V_{(\text{TPV})} \otimes \mathcal{D}_2(\omega). \quad (7.17)$$

The new ingredient here is the triple Pomeron vertex $V_{(\text{TPV})}$, described in [118], Eq.(87).

Interesting enough, the first term, $F^{(P)}$, is present only in the triple Regge limit with fixed M^2 . As explained in [79, 118], after integration over M^2 and t_1 and t_2 , our six-point function can be viewed as a part of the scattering of the upper R current on a loosely bound state of the two lower R currents: in this case this part of the triple vertex disappears and turns into a special contribution to the initial conditions of the evolution of a BFKL Green's function, and only the triple Pomeron vertex remains (for a detailed discussion see [35]).

Finally, we have the third part in Fig.7.10, $T_{3 \rightarrow 3}^{\text{dir}}$, where the two BFKL Green's functions couple directly to the upper 'unintegrated' impact factor, $D_{(4;0)\text{DIR}}(M^2)$. Here the dependence upon M^2 is contained inside $D_{(4;0)\text{DIR}}$, and instead of (7.9) we use

$$T_{3 \rightarrow 3}^{\text{DIR}}(s_1, s_2, M^2 | t_1, t_2, t) = s_1 s_2 \int \frac{d\omega_1 d\omega_2}{(2\pi i)^2} \left(\frac{s_1}{M^2}\right)^{\omega_1} \left(\frac{s_2}{M^2}\right)^{\omega_2} \xi(\omega_1) \xi(\omega_2) F^{(\text{DIR})}(M^2, \omega_1, \omega_2 | t, t_1, t_2). \quad (7.18)$$

The partial wave is given by

$$F^{(\text{DIR})}(M^2, \omega_1, \omega_2) = 4 \mathcal{D}_2^{(12)}(\omega_1) \otimes_{12} \mathcal{D}_2^{(34)}(\omega_2) \otimes_{34} \bar{\mathcal{D}}_{(4;0)\text{DIR}}(M^2). \quad (7.19)$$

The direct coupling of the amplitudes $\mathcal{D}_2^{(12)}(\omega_1)$ and $\mathcal{D}_2^{(34)}(\omega_2)$ to the upper loop is described by the 'unintegrated' impact factor $\bar{\mathcal{D}}_{(4;0)\text{DIR}}(M^2)$ which has both right hand and left hand cuts in M^2 . In contrast to the 'normal' impact factors which are integrated over the mass M^2 , in this case the coupling to the upper R -current is with fixed M^2 . Restricting ourselves to the case of zero momentum transfers $t = t_1 = t_2 = 0$, we have the expressions (see also [79]):

$$\bar{\mathcal{D}}_{(4;0)\text{DIR}}^{hh'}(\mathbf{k}^2, \mathbf{k}'^2, M^2) = \frac{g^4}{32} \frac{1}{M^2} \delta_{hh'} \int_0^1 d\alpha I_v(\alpha, \mathbf{k}^2, M^2) I_v(\alpha, \mathbf{k}'^2, M^2) \quad (7.20)$$

and

$$\bar{\mathcal{D}}_{(4;0)\text{DIR}}^{LL}(\mathbf{k}^2, \mathbf{k}'^2, M^2) = \frac{g^4}{32} Q^2 \int_0^1 d\alpha \alpha(1-\alpha) I_s(\alpha, \mathbf{k}^2, M^2) I_s(\alpha, \mathbf{k}'^2, M^2). \quad (7.21)$$

Here the dependence on M^2 is explicit. L and h denote the different polarizations of the incoming and outgoing R -currents. After integration over the angle φ of the vector \mathbf{k} , the use of δ -functions to set the upper loop momentum $l^2 = \alpha(1 - \alpha)Q^2$, we have defined

$$\frac{l}{l^2} I_v(\alpha, \mathbf{k}^2, M^2) = \frac{l}{l^2} \left(\frac{Q^2 - M^2}{Q^2 + M^2} - \frac{\mathbf{k}^2 + \alpha(1 - \alpha)(Q^2 - M^2)}{\sqrt{(\mathbf{k}^2 + \alpha(1 - \alpha)(Q^2 - M^2))^2 + 4\alpha^2(1 - \alpha)^2 M^2 Q^2}} \right) \quad (7.22)$$

and

$$I_s(\alpha, \mathbf{k}^2, M^2) = 2 \left(\frac{1}{\sqrt{(\mathbf{k}^2 + \alpha(1 - \alpha)(Q^2 - M^2))^2 + 4\alpha^2(1 - \alpha)^2 M^2 Q^2}} - \frac{1}{\alpha(1 - \alpha)(Q^2 + M^2)} \right) \quad (7.23)$$

Compared to the first two terms, this term is sub-leading for large M^2 . Also, this term is present only in supersymmetric theories where the fermions are in the adjoint representation.

The expressions listed in this section can directly be compared with results obtained from the analysis of Witten diagrams in the strong coupling regime [119].

7.4 Conclusions

In this chapter we have presented results for the six point R -current correlator in $\mathcal{N} = 4$ SYM in the triple Regge limit. In view of the AdS/CFT correspondence, which relates the large- N_c limit of $\mathcal{N} = 4$ SYM to a string theory in AdS_5 , we have concentrated on those diagrams which fit on the surface of a sphere. This generalizes an earlier calculation in nonsupersymmetric QCD, where the leading diagrams fit on the surface of a pair-of-pants.

Our result consists of three terms which correspond to different classes of color diagrams. Each term is composed of several building blocks: impact factors, triple vertex, and BFKL Green's functions. They should be compared with corresponding parts of the Witten diagrams in the strong coupling region. Further work along these lines is in progress [119].

Chapter 8

Summary and outlook

In this last chapter we summarize our results and present possible lines which future research may follow. Our goal has been the study of the high energy behavior of QCD. In this attempt we followed two different lines:

The object of the first part was given by the gauge invariant effective action of high-energy QCD. The reformulation of QCD at high energies in terms of an effective field theory provides a systematic approach for the determination of high-energy QCD amplitudes. It factorizes high-energy QCD amplitudes into sub-amplitudes that are local in rapidity, while non-local interaction between them is mediated by the exchange of reggeized gluons. To separate local from non-local interactions, a factorization parameter η was furthermore introduced. However, even though the need for such a regularizing parameter is outlined in the original formulation of the effective action, a precise implementation that can be used by a practitioner is missing. In the first part of this thesis a proposal has been given for such a regularization that implements the requirements posed by the effective action. It is stated in form of a Mellin-integral and resembles in its precise formulation commonly used expressions in the analysis of high-energy QCD. However its role is special in the present context: We make use of its property to implicitly impose a lower bound on the squared center-of-mass energy that can be associated with the exchange of a single reggeized gluon. At least within the Leading-Logarithmic-Approximation (LLA) this constraint provides the required locality in rapidity of the interaction of usual gluons and quarks. An extension of the method to calculations within the Next-to-Leading-Logarithmic-Approximation (NLLA) has been proposed as well, and it could be successfully applied to extract particularly needed parts of these corrections. However no complete NLLA-result has been derived so far and at present it is not clear whether the proposed regularization is in that case adequate or not. In particular, at NLLA the necessity to consider renormalization of the effective action arises which has not been addressed at all so far.

Apart from above regularization, the study of states of $n \geq 2$ reggeized gluon revealed the need to introduce so-called subtraction diagrams. At first a certain term, which is contained both in the induced vertex and in the coupling of two reggeized gluons to a particle, needs to be removed from the latter to avoid an over-counting, which is achieved by the subtraction terms. From a practical point of view, subtraction terms make the integral over the longitudinal loop momenta of loops containing reggeized gluons finite, and allow for their evaluation. The subtraction diagrams can be systematically obtained by supplementing the Lagrangian of the effective action by a subtraction term, which yields the required subtraction diagrams. This method is particularly suitable, if entangled loops with $n > 2$ reggeized gluons are considered.

The proposed regularization methods allows to reproduce a number of various well-known results, ranging from reggeization of the gluon and the BFKL-equation, over production amplitudes to the analysis of the states of the three and four reggeized gluons state. The most non-trivial one is certainly the transition vertex from two-to-four reggeized gluons, originally derived by Bartels and Wüsthoff. In that case, the obtained result further allows for the study of the two-to-four transition in the color octet, which has not been determined so far. The results are however not

yet in a suitable form for an analysis of the properties of such a transition in the color octet, and doing so remains as a task for the future.

In a second part, an element of Reggeon-field-theory has been studied from the perspective of the large N_c expansion in terms of topologies of the color factor. Within the AdS/CFT-correspondence, the string coupling on the gravity side is proportional to $1/N_c$ and such analysis seems to provide a suitable basis for the search of a gravity dual of Reggeon-field-theory on the string side of the correspondence. Starting from a QCD-analysis of the scattering of three virtual photons in the triple-Regge-limit, only diagrams with the topology of the pair-of-pants surface have been resummed. Color graphs have then be found to group themselves naturally into two classes. While planar graphs reggeize, non-planar graphs yield the triple-Pomeron-vertex, where the non-planar structure, which reminds of the non-planar Mandelstam cross-diagram. Extending the study to the triple-Regge-limit of the six-point-correlator of R -currents in $\mathcal{N} = 4$ SYM, the color graphs have at first no longer the topology of a pair-of-pants, but of a sphere, as all particles are now in the adjoint representation of $SU(N_c)$. Nevertheless it is possible to group color factors into planar and non-planar graphs, which appear as pair-of-pants-like deformations of the sphere. Apart from these two contributions, a new group of color factors arises, which is not present in QCD. In contrast to the pair-of-pants-like structures, reggeizing contributions and triple-Pomeron-vertex, the new piece particularly contributes for low diffractive masses.

For future work it seems suggestive to combine the results obtained from the the two parts: The expansion of color factors in terms of two-dimensional surfaces provides a new view on reggeization. For the pair-of-pants, color graphs group diagrams into planar and non-planar sets, which yield reggeization and the triple-Pomeron-vertex, respectively. The question arises if this classification can be extended to the general case at finite N_c . If so, it would be natural to use such a classification in the formulation of the effective action to separate reggeizing and not-reggeizing parts.

Appendix A

The Rapidity scheme

In most of the calculations of the effective action in this thesis, a certain regularization scheme has been used, that imposed a certain lower cut-offs Λ_a and Λ_b on the squared center-of-mass energies of the corresponding quark-gluon or gluon-gluon sub-amplitudes.

This regularization scheme seems very plausible, as it exactly imposes the requirements that are needed to obtain the effective theory diagram out of the underlying QCD-diagram. Furthermore, also imaginary parts, leading to negative signature of the reggeized gluon are mapped one-to-one from the QCD-diagram to the effective theory amplitude. Nevertheless the method has some back-draws: To obtain the correct gluon trajectory function for instance, it has been necessary to drop a certain part (see the discussion after Eq. (3.14)). The dropped part does not contribute within the LLA and therefore everything is consistent within the desired accuracy. However at the present stage it is not clear, whether this dropped term can be combined in a meaningful way with the other corrections at NLLA or not. There exist also an alternative possibility to regularize the above expression, which imposes the lower bound on the rapidity of the gluon loop, rather than the (sub)-center-of-mass-energies.

Also this 'rapidity scheme' relies on the Mellin transform, but instead of Eq. (3.9) we use

$$\lim_{\nu \rightarrow 0} \int_{0-i\infty}^{0+i\infty} \frac{d\omega}{2\pi i} \frac{1}{\omega + \nu} e^{\omega Y_{ak} - \eta_a} = \begin{cases} 1 & Y_{ak} = \frac{1}{2} \ln \frac{p_A^+ k^-}{p_A^- k^+} > \eta_a = \ln \lambda_a \\ 0 & \text{otherwise} \end{cases} \quad (\text{A.1})$$

and the central-rapidity diagram CR takes the following form

$$\text{CR}^{(Y)} = i\mathcal{M}_{2 \rightarrow 2}^{\text{tree}}(s, t) \int \frac{d\omega_1}{4\pi i} \int \frac{d\omega_2}{4\pi i} \frac{1}{\omega_1 + \nu} \frac{1}{\omega_2 + \nu} \left[\left(\frac{-p_A^+}{m_A \lambda_a} \right)^{\omega_1} + \left(\frac{p_A^+}{m_A \lambda_a} \right)^{\omega_1} \right] A^{(Y)}(\omega_1, \omega_2) \left[\left(\frac{-p_B^-}{m_B \lambda_b} \right)^{\omega_2} + \left(\frac{p_B^-}{m_B \lambda_b} \right)^{\omega_2} \right] \quad (\text{A.2})$$

with

$$A^{(Y)}(\omega_1, \omega_2) = \int \frac{dk^+ dk^-}{2\pi i} \frac{1}{2} \left[\frac{(k^- + i\epsilon)^{(\omega_1 - \omega_2)/2}}{k^- + i\epsilon} + \frac{(k^- - i\epsilon)^{(\omega_1 - \omega_2)/2}}{k^- - i\epsilon} \right] \frac{1}{2} \left[\frac{(k^+ + i\epsilon)^{(\omega_2 - \omega_1)/2}}{k^+ + i\epsilon} + \frac{(k^+ - i\epsilon)^{(\omega_2 - \omega_1)/2}}{k^+ - i\epsilon} \right] \frac{(-g^2 N_c)}{2} \int \frac{d^2 \mathbf{k}}{(2\pi)^3} \frac{\mathbf{q}^2}{(k^2 + i\epsilon)((q - k)^2 + i\epsilon)}. \quad (\text{A.3})$$

Substituting $k^- \rightarrow \mu = k^+ k^-$ we obtain

$$A^{(Y)}(\omega_1, \omega_2) = \frac{1}{2} \int \frac{dk^+}{|k^+|} (k^+)^{\omega_2 - \omega_1} \int \frac{d\mu}{2\pi i} \left[\frac{(\mu + i\epsilon)^{(\omega_1 - \omega_2)/2}}{\mu + i\epsilon} + \frac{(\mu - i\epsilon)^{(\omega_1 - \omega_2)/2}}{\mu - i\epsilon} \right] \frac{(-g^2 N_c)}{2} \int \frac{d^2 \mathbf{k}}{(2\pi)^3} \frac{\mathbf{q}^2}{(\mu - \mathbf{k}^2 + i\epsilon)(\mu - (\mathbf{q} - \mathbf{k})^2 + i\epsilon)} = 2\pi i \delta(\omega_1 - \omega_2) \beta(\mathbf{q}). \quad (\text{A.4})$$

without the need to dropping any sub-leading term. Also for the calculation of reggeized gluon transition vertices, this kind of regularization can be used and prevents any dependence on transverse logarithms, which are then disregarded at LLA. On the other hand it is at the present stage not clear how to apply this method to loop-corrections to reggeized gluon-particle vertices. The proposed alternative scheme used throughout this thesis allows for such a treatment, while to verify whether it leads also to correct results at NLLA, it is necessary to carry out a full NLLA analysis, which remains as a task for the future.

Appendix B

Integrals

In the following appendix we present the explicit evaluation of two integrals that occurred in Sec.4.2, in the discussion of one-loop corrections to the production vertex.

B.1 The integral I_1

We consider

$$\begin{aligned}
 I_1 &= \frac{i}{2} \int \frac{dk^+}{k^+} \frac{dk^-}{k^-} \frac{1}{k^2 + i\epsilon} \frac{1}{(q_1 - k)^2 + i\epsilon} \frac{1}{(q_2 - k)^2 + i\epsilon} \\
 &\quad \left[\left(\frac{-p_A^+ k^- - i\epsilon}{s_1/\lambda_{12}} \right)^{\omega_1} + \left(\frac{p_A^+ k^- - i\epsilon}{s_1/\lambda_{12}} \right)^{\omega_1} \right] \left[\left(\frac{-p_B^- k^+ - i\epsilon}{s_2/\lambda_{21}} \right)^{\omega_2} + \left(\frac{p_B^- k^+ - i\epsilon}{s_2/\lambda_{21}} \right)^{\omega_2} \right] \\
 &= \frac{i}{2} \int \frac{dk^+}{k^+} \frac{dk^-}{k^-} \frac{1}{k^+ k^- - \mathbf{k}^2 + i\epsilon} \frac{1}{(k^+ - q_1^+) k^- - (\mathbf{q}_1 - \mathbf{k})^2 + i\epsilon} \frac{1}{k^+ (k^- - q_2^-) - (\mathbf{q}_2 - \mathbf{k}^2) + i\epsilon} \\
 &\quad \left[\left(\frac{-p_A^+ k^- - i\epsilon}{s_1/\lambda_{12}} \right)^{\omega_1} + \left(\frac{p_A^+ k^- - i\epsilon}{s_1/\lambda_{12}} \right)^{\omega_1} \right] \left[\left(\frac{-p_B^- k^+ - i\epsilon}{s_2/\lambda_{21}} \right)^{\omega_2} + \left(\frac{p_B^- k^+ - i\epsilon}{s_2/\lambda_{21}} \right)^{\omega_2} \right]. \quad (\text{B.1})
 \end{aligned}$$

The evaluation of the integral

The following calculation follows closely [91]. Using a Schwinger parametrisation of the propagators

$$\frac{1}{A + i\epsilon} = -i \int d\lambda \exp(i\lambda(A + i\epsilon)), \quad (\text{B.2})$$

extracting phase factors, substituting $k^- \rightarrow -k^-$ and defining rescaled integration variables $x = k^- q_1^+ / p_A^+$ and $y = -k^+ q_2^- / p_B^-$, we arrive at

$$\begin{aligned}
 I_1 &= \frac{i}{2} \kappa^{-\omega_1 - \omega_2} \lambda_{12}^{\omega_1} \lambda_{21}^{\omega_2} (-i) \int_0^\infty d\lambda_1 d\lambda_2 d\lambda_3 \exp[-i\lambda_1 \mathbf{k}^2 + i\epsilon] \exp[-i\lambda_2 (\mathbf{q}_1 - \mathbf{k})^2 + i\epsilon] \\
 &\quad \exp[-i\lambda_3 (\mathbf{q}_2 - \mathbf{k})^2 + i\epsilon] \\
 &\quad \int dx dy [e^{-i\pi\omega_1} (x + i\epsilon)^{\omega_1 - 1} + (x - i\epsilon)^{\omega_1 - 1}] [e^{-i\pi\omega_2} (y + i\epsilon)^{\omega_2 - 1} + (y - i\epsilon)^{\omega_2 - 1}] \\
 &\quad \exp[i(-\lambda xy/\kappa + \lambda_2 x + \lambda_3 y)] \\
 &= \frac{-1}{2} \kappa^{-\omega_1 - \omega_2} \lambda_{12}^{\omega_1} \lambda_{21}^{\omega_2} \int_0^\infty d\lambda_1 d\lambda_2 d\lambda_3 \exp[-i\lambda_1 \mathbf{k}^2 + i\epsilon] \exp[-i\lambda_2 (\mathbf{q}_1 - \mathbf{k})^2 + i\epsilon] \\
 &\quad \exp[-i\lambda_3 (\mathbf{q}_2 - \mathbf{k})^2 + i\epsilon] \\
 &\quad [e^{-i\pi\omega_1} e^{-i\pi\omega_2} J_1(+, +) + e^{-i\pi\omega_2} J_1(-, +) + e^{-i\pi\omega_1} J_1(+, -) + J_1(-, -)], \quad (\text{B.3})
 \end{aligned}$$

where $\lambda = \lambda_1 + \lambda_2 + \lambda_3$ and $\kappa = -q_1^+ q_2^-$. To carry out the integration over longitudinal variables, it is therefore needed to determine

$$J_1(\pm, \pm) = \int dx dy (x \pm i\epsilon)^{\omega_1-1} (y \pm i\epsilon)^{\omega_2-1} \exp[i(-\lambda xy/\kappa + \lambda_2 x + \lambda_3 y)]. \quad (\text{B.4})$$

Let us start with the case, where one of the $i\epsilon$ comes with a plus sign, for definitness we chose the one associated with the x -variable. We begin the evaluation by a rescaling $x \rightarrow x\lambda_2$ and $y \rightarrow y\lambda_3$. Furthermore we introduce $\alpha_i = \omega_i - 1$ $i = 1, 2$ and define $G := \kappa\lambda_2\lambda_3/\lambda > 0$. The integral is then given by

$$\begin{aligned} J_1(+, \pm) &= \lambda_2^{-\alpha_1-1} \lambda_3^{-\alpha_2-1} \exp[iG] \int_{-\infty}^{\infty} dx dy (x + i\epsilon)^{\alpha_1} (y \pm i\epsilon)^{\alpha_2} \exp[-i(x/G - 1)(y - G)] \\ &= \lambda_2^{-\alpha_1-1} \lambda_3^{-\alpha_2-1} \exp[iG] \int_{-\infty}^{\infty} dx dy (x + i\epsilon)^{\alpha_1} (y + G \pm i\epsilon)^{\alpha_2} e^{-ixy/G} e^{iy}. \end{aligned} \quad (\text{B.5})$$

The contour of the x -integration lies above the cut on the negative x -axis. For $y < 0$, the exponential function guarantees convergence in the upper semi-plane and the x -integral leads to a zero result. For $y > 0$ convergence is given for the lower semi-plane and we can enclose the contour around the cut. We obtain

$$J_1(+, \pm) = e^{iG} \lambda_2^{-\alpha_1-1} \lambda_3^{-\alpha_2-1} \int_0^{-\infty} dx [(x - i\epsilon)^{\alpha_1} - (x + i\epsilon)^{\alpha_1}] \int_0^{\infty} dy (y + G \pm i\epsilon)^{\alpha_2} e^{-ixy/G} e^{iy}. \quad (\text{B.6})$$

We are therefore lead to evaluate the discontinuity of the function $(x)^{\alpha_1}$ over the cut on the negative real axis. We find:

$$\begin{aligned} (x - i\epsilon)^{\alpha_1} - (x + i\epsilon)^{\alpha_1} &= (e^{-i\pi\alpha_1} - e^{i\pi\alpha_1})(-x)^{\alpha_1} \\ &= -2i \sin(\pi\alpha_1)(-x)^{\alpha_1} = \frac{2\pi i}{\Gamma(-\alpha_1)\Gamma(1 + \alpha_1)}(-x)^{\alpha_1}. \end{aligned} \quad (\text{B.7})$$

We then further substitute $x \rightarrow -x$ and obtain

$$J_1(+, \pm) = e^{iG} \lambda_2^{-\alpha_1-1} \lambda_3^{-\alpha_2-1} \frac{-2\pi i}{\Gamma(-\alpha_1)\Gamma(1 - \alpha_1)} \int_0^{\infty} dy (y + G \pm i\epsilon)^{\alpha_2} e^{iy} \int_0^{\infty} dx x^{\alpha_1} e^{ixy/G}. \quad (\text{B.8})$$

We rotate now the x -integral to the positive imaginary axis and substitute $x \rightarrow is$. We perform the integral which yields (together with the Jacobian factor from changing from x to s) $\Gamma(1 + \alpha_1)(iG/y)^{\alpha_1+1}$. The complete expression then reads:

$$J_1(+, \pm) = e^{iG} \lambda_2^{-\alpha_1-1} \lambda_3^{-\alpha_2-1} \frac{2\pi i \alpha_1 G^{1+\alpha_1+\alpha_2}}{\Gamma(-\alpha_1)} \int_0^{\infty} \frac{dy}{y} y^{-\alpha_1} \left(\frac{y}{G} + 1\right)^{\alpha_2} e^{iy}. \quad (\text{B.9})$$

Note that we are allowed to drop the $i\epsilon$ prescription for the y integral as the integrand is in the considered region single valued. Next we rotate the y -contour to the positive, imaginary axis and substitute $y = e^{i\pi/2}u$ which leads us to

$$J_1(+, \pm) = e^{iG} \lambda_2^{-\alpha_1-1} \lambda_3^{-\alpha_2-1} \frac{2\pi G^{1+\alpha_1+\alpha_2}}{\Gamma(-\alpha_1)} \int_0^{\infty} \frac{du}{u} u^{-\alpha_1} \left(\frac{u}{e^{-i\pi/2}G} + 1\right)^{\alpha_2} e^{-u}, \quad (\text{B.10})$$

with [120, 121]

$$\begin{aligned} \int_0^{\infty} du \left(1 + \frac{u}{z}\right)^{\alpha_2} u^{-\alpha_1-1} e^u &= \Gamma(-\alpha_1) \left[z^{-\alpha_1} \frac{\Gamma(\alpha_1 - \alpha_2)}{\Gamma(-\alpha_2)} M(-\alpha_1 | \alpha_2 - \alpha_1 + 1 | z) \right. \\ &\quad \left. + z^{-\alpha_2} \frac{\Gamma(\alpha_2 - \alpha_1)}{\Gamma(-\alpha_1)} M(-\alpha_2 | \alpha_1 - \alpha_2 + 1 | z) \right], \end{aligned} \quad (\text{B.11})$$

where $M(a|b|z) = {}_1F_1(a|b|z)$ is a confluent hypergeometric function (Kummer's function [96]). We obtain

$$\begin{aligned} J_1(+, \pm) &= 2\pi G^{\alpha_1+\alpha_2+1} \lambda_2^{-\alpha_1-1} \lambda_3^{-\alpha_2-1} e^{iG} [(e^{-i\pi/2}G)^{-\alpha_1} \frac{\Gamma(\alpha_1 - \alpha_2)}{\Gamma(-\alpha_2)} M(-\alpha_1|\alpha_2 - \alpha_1 + 1|e^{-i\pi/2}G) \\ &\quad + (e^{-i\pi/2}G)^{-\alpha_2} \frac{\Gamma(\alpha_2 - \alpha_1)}{\Gamma(-\alpha_1)} M(-\alpha_2|\alpha_1 - \alpha_2 + 1|e^{-i\pi/2}G)]. \end{aligned} \quad (\text{B.12})$$

Reinserting $G = \kappa\lambda_2\lambda_3/\lambda$ and $\alpha_i = \omega_i - 1$ we have for (B.4) in the case where at least one of the $i\epsilon$ comes with a plus sign [91]

$$\begin{aligned} J_1(+, \pm) &= 2\pi i \lambda_2^{\omega_2-1} \lambda_3^{\omega_1-1} \lambda^{1-\omega_1-\omega_2} \kappa^{\omega_1+\omega_2-1} e^{i\lambda_2\lambda_3\kappa/\lambda} \\ &\quad \left[\left(e^{i\pi} \frac{\lambda}{\lambda_2\lambda_3\kappa} \right)^{\omega_1-1} e^{-i\pi\omega_1/2} \frac{\Gamma(\omega_1 - \omega_2)}{\Gamma(1 - \omega_2)} M(1 - \omega_1|\omega_2 - \omega_1 + 1| - i\kappa\lambda_2\lambda_3/\lambda) + (\omega_1 \leftrightarrow \omega_2) \right], \end{aligned} \quad (\text{B.13})$$

which, applying a Kummer transformation $M(a|b|z) = \exp(z)M(b-a|b|-z)$, can be rewritten as

$$\begin{aligned} J_1(+, \pm) &= 2\pi i \lambda_2^{\omega_2-1} \lambda_3^{\omega_1-1} \lambda^{1-\omega_1-\omega_2} \kappa^{\omega_1+\omega_2-1} \\ &\quad \left[\left(e^{i\pi} \frac{\lambda}{\lambda_2\lambda_3\kappa} \right)^{\omega_1-1} e^{-i\pi\omega_1/2} \frac{\Gamma(\omega_1 - \omega_2)}{\Gamma(1 - \omega_2)} M(\omega_2|\omega_2 - \omega_1 + 1|i\kappa\lambda_2\lambda_3/\lambda) + (\omega_1 \leftrightarrow \omega_2) \right] \\ &= e^{i\omega_1\pi} \kappa^{\omega_2} V(\omega_1, \omega_2, \kappa, \lambda_1, \lambda_2, \lambda_3) + e^{i\omega_2\pi} \kappa^{\omega_1} V(\omega_2, \omega_1, \kappa, \lambda_1, \lambda_3, \lambda_2), \end{aligned} \quad (\text{B.14})$$

where we introduced the function $V(\omega_1, \omega_2, \kappa, \lambda_1, \lambda_2, \lambda_3)$ in order to compactify our expressions

$$V(\omega_1, \omega_2, \kappa, \lambda_1, \lambda_2, \lambda_3) := -2\pi i \frac{\lambda_2^{\omega_2-\omega_1} e^{-i\pi\omega_1/2} \Gamma(\omega_1 - \omega_2)}{\lambda^{\omega_2} \Gamma(1 - \omega_2)} M(\omega_2|\omega_2 - \omega_1 + 1|i\kappa\lambda_2\lambda_3/\lambda). \quad (\text{B.15})$$

We come now to the case where both $i\epsilon$ occur with a minus sign. After a rescaling and a shift $y \rightarrow y - G$, the integral is given by

$$J_1(-, -) = e^{iG} \lambda_2^{\alpha_1-1} \lambda_3^{\alpha_2-1} \int dx \int dy (x - i\epsilon)^{\alpha_1} (y + G - i\epsilon)^{\alpha_2} e^{-ixy/G} e^{iy}. \quad (\text{B.16})$$

In contrast to the above case, the contour of the x -integration is now enclosed round the cut for negative y :

$$J_1(-, -) = e^{iG} \lambda_2^{\alpha_1-1} \lambda_3^{\alpha_2-1} \int_0^{-\infty} dx [(x - i\epsilon)^{\alpha_1} - (x + i\epsilon)^{\alpha_1}] \int_0^{-\infty} dy (y + G - i\epsilon)^{\alpha_2} e^{-ixy/G} e^{iy}. \quad (\text{B.17})$$

We make now use again of Eq.(B.7) and substitute x to $-x$ and $y \rightarrow -y$, which gives us

$$J_1(-, -) = e^{iG} \lambda_2^{\alpha_1-1} \lambda_3^{\alpha_2-1} \frac{2i\pi}{\Gamma(-\alpha_1)\Gamma(1+\alpha_1)} \int_0^{\infty} dy (-y + G - i\epsilon)^{\alpha_2} e^{-iy} \int_0^{\infty} dx x^{\alpha_1} e^{-ixy/G}. \quad (\text{B.18})$$

We rotate now the x -integral to the negative imaginary axis and substitute $x = -is$ and we obtain the for the integral over x a factor $\Gamma(1 + \alpha_1)(-iG/y)^{1+\alpha_1}$. The complete expression reads:

$$J_1(-, -) = e^{iG} \lambda_2^{\alpha_1-1} \lambda_3^{\alpha_2-1} \frac{2\pi(-i)^{\alpha_1} G^{1+\alpha_1}}{\Gamma(-\alpha_1)} \int_0^{\infty} \frac{dy}{y} y^{-\alpha_1} (-y + G - i\epsilon)^{\alpha_2} e^{-iy}. \quad (\text{B.19})$$

We use now

$$\begin{aligned} (-y + G - i\epsilon)^{\alpha_2} &= G^{\alpha_2} \left(\frac{-y}{G} + 1 - i\epsilon \right)^{\alpha_2} = G^{\alpha_2} \left(\frac{-y - i\epsilon}{G} + 1 \right)^{\alpha_2} \\ &= G^{\alpha_2} \left(\frac{e^{-i\pi} y}{G} + 1 \right)^{\alpha_2} = G^{\alpha_2} \left(\frac{y}{e^{i\pi} G} + 1 \right)^{\alpha_2}, \end{aligned} \quad (\text{B.20})$$

and rotate the y -contour to the negative, imaginary axis and substitute $y = e^{-i\pi/2}u$ which leads to

$$\begin{aligned}
J_1(-, -) &= e^{iG} \lambda_2^{\alpha_1-1} \lambda_3^{\alpha_2-1} \frac{2\pi G^{1+\alpha_1+\alpha_2}}{\Gamma(-\alpha_1)} \int_0^\infty \frac{du}{u} u^{-\alpha_1} \left(\frac{u}{e^{i\pi/2}G} + 1 \right)^{\alpha_2} e^{-u} \\
&= 2\pi G^{1+\alpha_1+\alpha_2} e^{iG} \lambda_2^{\alpha_1-1} \lambda_3^{\alpha_2-1} \left[(e^{i\pi/2}G)^{-\alpha_1} \frac{\Gamma(\alpha_1 - \alpha_2)}{\Gamma(-\alpha_2)} M(-\alpha_1 | \alpha_2 - \alpha_1 + 1 | e^{i\pi/2}G) \right. \\
&\quad \left. + (e^{i\pi/2}G)^{-\alpha_2} \frac{\Gamma(\alpha_2 - \alpha_1)}{\Gamma(-\alpha_1)} M(-\alpha_2 | \alpha_1 - \alpha_2 + 1 | e^{i\pi/2}G) \right]. \tag{B.21}
\end{aligned}$$

In the case where both $i\epsilon$ come with a minus sign, (B.4) is then given by

$$\begin{aligned}
J_1(-, -) &= 2\pi i \lambda_2^{\omega_2-1} \lambda_3^{\omega_1-1} \lambda^{1-\omega_1-\omega_2} \kappa^{\omega_1+\omega_2-1} \\
&\quad \left[\left(e^{-\pi i} \frac{\lambda}{\lambda_2 \lambda_3 \kappa} \right)^{\omega_1-1} e^{-i\pi\omega_1/2} \frac{\Gamma(\omega_1 - \omega_2)}{\Gamma(1 - \omega_2)} M(\omega_2 | \omega_2 - \omega_1 + 1 | i\kappa\lambda_2\lambda_3/\lambda) + (\omega_1 \leftrightarrow \omega_2) \right] \\
&= e^{-i\omega_1\pi} \kappa^{\omega_2} V(\omega_1, \omega_2, \kappa, \lambda_1, \lambda_2, \lambda_3) + e^{-i\omega_2\pi} \kappa^{\omega_1} V(\omega_2, \omega_1, \kappa, \lambda_1, \lambda_2, \lambda_3), \tag{B.22}
\end{aligned}$$

where we used that $M(a|b|z)$ is an entire function of z . We obtain therefore for the last two lines of (B.3)

$$\begin{aligned}
&\int dx dy [e^{-i\pi\omega_1}(x+i\epsilon)^{\omega_1-1} + (x-i\epsilon)^{\omega_1-1}] [e^{-i\pi\omega_2}(y+i\epsilon)^{\omega_2-1} + (y-i\epsilon)^{\omega_2-1}] \\
&\quad \exp[i(-\lambda xy/\kappa + \lambda_2 x + \lambda_3 y)] \\
&= \xi_{\omega_1}^{(-)} \xi_{\omega_2}^{(-)} [\phi^{\omega_1} \kappa^{\omega_2} V(\omega_1, \omega_2, \kappa, \lambda_1, \lambda_2, \lambda_3) + \phi^{\omega_2} \kappa^{\omega_1} V(\omega_2, \omega_1, \kappa, \lambda_1, \lambda_2, \lambda_3)], \tag{B.23}
\end{aligned}$$

where we introduced, following closely [97], factors

$$\phi_{\omega_1\omega_2}^{\omega_i} = e^{i\pi\omega_i} - \frac{1}{\xi_{\omega_1}^{(-)} \xi_{\omega_2}^{(-)}} (e^{-i\pi\omega_i} - e^{i\pi\omega_i}), \tag{B.24}$$

with

$$\phi_{\omega_1\omega_2}^{\omega_1} = \frac{1}{\xi_{\omega_1}^{(-)} \xi_{\omega_2}^{(-)}} \xi_{\omega_1}^{(-)} \xi_{\omega_2\omega_1}^{(-,-)} \quad \phi_{\omega_1\omega_2}^{\omega_2} = \frac{1}{\xi_{\omega_1}^{(-)} \xi_{\omega_2}^{(-)}} \xi_{\omega_2}^{(-)} \xi_{\omega_1\omega_2}^{(-,-)} \tag{B.25}$$

and signature factors

$$\xi_{\omega}^{(-)} = e^{-i\pi\omega} + 1 \quad \xi_{\omega_1\omega_2}^{(-,-)} = e^{-i\pi(\omega_1-\omega_2)} + 1, \tag{B.26}$$

which results for (B.23) into

$$(\text{B.23}) = [\xi_{\omega_1}^{(-)} \xi_{\omega_2\omega_1}^{(-,-)} \kappa^{\omega_2} V(\omega_1, \omega_2, \kappa, \lambda_1, \lambda_2, \lambda_3) + \xi_{\omega_2}^{(-)} \xi_{\omega_1\omega_2}^{(-,-)} \kappa^{\omega_1} V(\omega_2, \omega_1, \kappa, \lambda_1, \lambda_3, \lambda_2)]. \tag{B.27}$$

The complete integral (B.31) is then given by

$$\begin{aligned}
I_1 &= -\lambda_{12}^{\omega_1} \lambda_{21}^{\omega_2} \int_0^\infty d\lambda_1 d\lambda_2 d\lambda_3 e^{-i\lambda_1 \mathbf{k}^2 + i\epsilon} e^{-i\lambda_2 (\mathbf{q}_1 - \mathbf{k})^2 + i\epsilon} e^{-i\lambda_3 (\mathbf{q}_2 - \mathbf{k})^2 + i\epsilon} [\xi_{\omega_1}^{(-)} \xi_{\omega_2\omega_1}^{(-,-)} \kappa^{-\omega_1} \\
&\quad \times V(\omega_1, \omega_2, \kappa, \lambda_1, \lambda_2, \lambda_3) + \xi_{\omega_2}^{(-)} \xi_{\omega_1\omega_2}^{(-,-)} \kappa^{-\omega_2} V(\omega_2, \omega_1, \kappa, \lambda_1, \lambda_3, \lambda_2)]. \tag{B.28}
\end{aligned}$$

In a next step we switch from Schwinger to Feynman-parameters $\lambda_i = x_i \lambda$ with $i = 1, 2, 3$ and $x_i \in [0, 1]$ and obtain

$$I_1 = \lambda_{12}^{\omega_1} \lambda_{21}^{\omega_2} \left[\kappa_1^{-\omega_1} \xi_{\omega_1}^{(-)} \xi_{\omega_2\omega_1}^{(-,-)} \frac{F_1(\omega_1', \omega_2', t_1, t_2, \kappa_1)}{\sin \pi(\omega_2' - \omega_1')} + \kappa_1^{-\omega_2'} \xi_{\omega_2}^{(-)} \xi_{\omega_1\omega_2}^{(-,-)} \frac{F_1(\omega_2', \omega_1', t_1, t_2, \kappa_1)}{\sin \pi(\omega_1' - \omega_2')} \right], \tag{B.29}$$

with signature factors defined as in Eqs. (4.5) and (4.8) and

$$\begin{aligned}
F_1(\omega_1, \omega_2, t_1, t_2, \kappa) &= \frac{-i\pi}{2} \int \frac{d^2 \mathbf{k}}{(2\pi)^3} \int_0^\infty d\lambda \lambda^{2-\omega_1} e^{-i\pi\omega_1/2} \int \prod_{i=1}^3 dx_i \delta(1 - \sum_{i=1}^3 x_i) x_2^{\omega_2-\omega_1} \\
&\quad e^{-i\lambda(x_1 \mathbf{k}^2 + x_2 (\mathbf{q}_1 - \mathbf{k})^2 + x_3 (\mathbf{q}_2 - \mathbf{k})^2)} \frac{M(\omega_2 | \omega_2 - \omega_1 + 1 | i\kappa_1 \lambda x_2 x_3)}{\Gamma(\omega_2 - \omega_1 + 1) \Gamma(1 - \omega_2)}. \tag{B.30}
\end{aligned}$$

B.2 The integral I_2

We consider

$$\begin{aligned}
I_2 &= \frac{i}{2} \int \frac{dk^+ dk^-}{k^+ k^-} \frac{1}{k^2 + i\epsilon} \frac{1}{(q_2 - k)^2 + i\epsilon} \\
&\quad \left[\left(\frac{-p_A^+ k^- - i\epsilon}{s_1/\lambda_{12}} \right)^{\omega_1} + \left(\frac{p_A^+ k^- - i\epsilon}{s_1/\lambda_{12}} \right)^{\omega_1} \right] \left[\left(\frac{-p_B^- k^+ - i\epsilon}{s_2/\lambda_{21}} \right)^{\omega_2} + \left(\frac{p_B^- k^+ - i\epsilon}{s_2/\lambda_{21}} \right)^{\omega_2} \right] \\
&= \frac{i}{2} \int \frac{dk^+ dk^-}{k^+ k^-} \frac{1}{k^+ k^- - \mathbf{k}^2 + i\epsilon} \frac{1}{k^+(k^- - q_2^-) - (q_2 - \mathbf{k}^2) + i\epsilon} \\
&\quad \left[\left(\frac{-p_A^+ k^- - i\epsilon}{s_1/\lambda_{12}} \right)^{\omega_1} + \left(\frac{p_A^+ k^- - i\epsilon}{s_1/\lambda_{12}} \right)^{\omega_1} \right] \left[\left(\frac{-p_B^- k^+ - i\epsilon}{s_2/\lambda_{21}} \right)^{\omega_2} + \left(\frac{p_B^- k^+ - i\epsilon}{s_2/\lambda_{21}} \right)^{\omega_2} \right]. \tag{B.31}
\end{aligned}$$

Using Schwinger parametrisation we arrive at

$$\begin{aligned}
I_2 &= \frac{i}{2} \kappa^{-\omega_1 - \omega_2} \lambda_{12}^{\omega_1} \lambda_{21}^{\omega_2} (-i)^2 \int_0^\infty d\lambda_1 d\lambda_2 e^{-i\lambda_1 \mathbf{k}^2} e^{-i\lambda_2 (q_2 - \mathbf{k})^2} \\
&\quad \int dx dy [e^{-i\pi\omega_1 (x + i\epsilon)^{\omega_1 - 1}} + (x - i\epsilon)^{\omega_1 - 1}] \\
&\quad [e^{-i\pi\omega_2 (y + i\epsilon)^{\omega_2 - 1}} + (y - i\epsilon)^{\omega_2 - 1}] e^{i(-\lambda xy/\kappa + \lambda_2 y)}, \tag{B.32}
\end{aligned}$$

and we define

$$J_2(\pm, \pm) = \int dx dy (x \pm i\epsilon)^{\omega_1 - 1} (y \pm i\epsilon)^{\omega_2 - 1} e^{i(-\lambda xy/\kappa + \lambda_2 y)}. \tag{B.33}$$

We then obtain

$$\begin{aligned}
J_2(+, \pm) &= e^{i\pi(\omega_1 + 1)} \lambda_2^{-\omega_2} 2 \sin(\pi\omega_1) \int_0^\infty dx dy x^{\omega_1 - 1} (y \pm i\epsilon)^{\omega_2 - 1} e^{i(-\lambda xy/\kappa + y)} \\
&= \lambda_2^{-\omega_2} 2 \sin(\pi\omega_1) e^{i\pi(\omega_1 + 1)} (e^{-i\pi/2} \frac{\lambda_2 \kappa}{\lambda})^{\omega_1} \Gamma(\omega_1) \int_0^\infty \frac{dy}{y} y^{\omega_2 - \omega_1} e^{iy} \\
&= -2i\pi e^{i\pi\omega_2/2} \kappa^{\omega_1} \lambda_2^{\omega_1 - \omega_2} \lambda^{-\omega_1} \frac{\Gamma(\omega_2 - \omega_1)}{\Gamma(1 - \omega_1)}. \tag{B.34}
\end{aligned}$$

For the the last integral to be convergent it is necessary that $\omega_2 > \omega_1$, according to the definition of the Gamma-function [96]. Similar

$$\begin{aligned}
J_2(-, \pm) &= -e^{i\pi\omega_1} \lambda_2^{-\omega_2} \int_0^\infty dx \int_{-\infty}^0 dy (-2 \sin(\pi\omega_1)) x^{\omega_1 - 1} (y \pm i\epsilon)^{\omega_2 - 1} e^{i(-\lambda xy/\kappa + \lambda_2 y)} \\
&= \frac{2i\pi}{\Gamma(\omega_1)\Gamma(1 - \omega_1)} \kappa^{\omega_1} e^{-i\pi\omega_1/2} \lambda_2^{\omega_1 - \omega_2} \lambda^{-\omega_1} \Gamma(\omega_1) \int_{-\infty}^0 dy (y \pm i\epsilon)^{\omega_2 - 1} y^{-\omega_1} e^{iy}. \tag{B.35}
\end{aligned}$$

We have to distinguish now different signs of the $i\epsilon$. We find

$$J_2(-, +) = -2i\pi e^{i\pi\omega_2/2} \kappa^{\omega_1} \lambda_2^{\omega_1 - \omega_2} \lambda^{-\omega_1} \frac{\Gamma(\omega_2 - \omega_1)}{\Gamma(1 - \omega_1)} = J_2(+, \pm), \tag{B.36}$$

and with

$$(y - i\epsilon)^{\omega_2} = (y + i\epsilon)^{\omega_2} e^{-2\pi i\omega_2}, \tag{B.37}$$

one has

$$J_2(-, -) = e^{-i2\pi\omega_2} J_2(+, \pm). \tag{B.38}$$

We therefore find

$$I_2 = \lambda_{12}^{\omega_1} \lambda_{21}^{\omega_2} \kappa_1^{-\omega_2} \xi_{\omega_2}^{(-)} \xi_{\omega_1 \omega_2}^{(-,-)} \frac{F_2(\omega_2, \omega_1, t_2, \kappa_1)}{\sin \pi(\omega_1 - \omega_2)} \Big|_{\Re \omega_2 > \Re \omega_1}. \quad (\text{B.39})$$

and F_2 is given by

$$F_2(\omega_1, \omega_2, t_2, \kappa) = \frac{-\pi}{2} \int \frac{d^2 \mathbf{k}}{(2\pi)^3} \int_0^\infty d\lambda \lambda^{1-\omega_1} e^{-i\pi\omega_2/2} \int \prod_{i=1}^2 dx_i \delta(1 - \sum_{i=1}^2 x_i) x_2^{\omega_1 - \omega_2} e^{-i\lambda(x_1 \mathbf{k}^2 + x_2(\mathbf{q}_2 - \mathbf{k})^2)} \frac{1}{\Gamma(\omega_2 - \omega_1 + 1) \Gamma(1 - \omega_2)}, \quad (\text{B.40})$$

Bibliography

- [1] H. D. Politzer, *Reliable perturbative results for strong interactions?*, *Phys. Rev. Lett.* **30** (1973) 1346–1349.
- [2] D. J. Gross and F. Wilczek, *Ultraviolet behavior of non-abelian gauge theories*, *Phys. Rev. Lett.* **30** (1973) 1343–1346.
- [3] P. D. B. Collins, *An Introduction to Regge Theory and High-Energy Physics*, . Cambridge 1977, 445p.
- [4] H. D. I. Abarbanel, J. B. Bronzan, R. L. Sugar and A. R. White, *Reggeon Field Theory: Formulation and Use*, *Phys. Rept.* **21** (1975) 119–182.
- [5] V. N. Gribov, *A reggeon diagram technique*, *Sov. Phys. JETP* **26** (1968) 414–422.
- [6] M. Baker and K. A. Ter-Martirosian, *Gribov's Reggeon Calculus: Its Physical Basis and Implications*, *Phys. Rept.* **28** (1976) 1–143.
- [7] L. N. Lipatov, *Reggeization of the Vector Meson and the Vacuum Singularity in Nonabelian Gauge Theories*, *Sov. J. Nucl. Phys.* **23** (1976) 338–345.
- [8] E. A. Kuraev, L. N. Lipatov and V. S. Fadin, *Multi - Reggeon Processes in the Yang-Mills Theory*, *Sov. Phys. JETP* **44** (1976) 443–450.
- [9] V. S. Fadin, E. A. Kuraev and L. N. Lipatov, *On the Pomeron Singularity in Asymptotically Free Theories*, *Phys. Lett.* **B60** (1975) 50–52.
- [10] E. A. Kuraev, L. N. Lipatov and V. S. Fadin, *The Pomeron Singularity in Nonabelian Gauge Theories*, *Sov. Phys. JETP* **45** (1977) 199–204.
- [11] I. I. Balitsky and L. N. Lipatov, *The Pomeron Singularity in Quantum Chromodynamics*, *Sov. J. Nucl. Phys.* **28** (1978) 822–829.
- [12] V. S. Fadin and L. N. Lipatov, *BFKL pomeron in the next-to-leading approximation*, *Phys. Lett.* **B429** (1998) 127–134 [[hep-ph/9802290](#)].
- [13] M. Ciafaloni and G. Camici, *Energy scale(s) and next-to-leading BFKL equation*, *Phys. Lett.* **B430** (1998) 349–354 [[hep-ph/9803389](#)].
- [14] V. S. Fadin, R. Fiore, M. G. Kozlov and A. V. Reznichenko, *Proof of the multi-Regge form of QCD amplitudes with gluon exchanges in the NLA*, *Phys. Lett.* **B639** (2006) 74–81 [[hep-ph/0602006](#)].
- [15] N. N. Nikolaev and B. G. Zakharov, *Colour transparency and scaling properties of nuclear shadowing in deep inelastic scattering*, *Z. Phys.* **C49** (1991) 607–618.
- [16] N. Nikolaev and B. G. Zakharov, *Pomeron structure function and diffraction dissociation of virtual photons in perturbative QCD*, *Z. Phys.* **C53** (1992) 331–346.
- [17] A. H. Mueller, *Soft gluons in the infinite momentum wave function and the BFKL pomeron*, *Nucl. Phys.* **B415** (1994) 373–385.

- [18] A. H. Mueller, *Unitarity and the BFKL pomeron*, *Nucl. Phys.* **B437** (1995) 107–126 [hep-ph/9408245].
- [19] I. Balitsky, *Operator expansion for high-energy scattering*, *Nucl. Phys.* **B463** (1996) 99–160 [hep-ph/9509348].
- [20] Y. V. Kovchegov, *Non-Abelian Weizsaecker-Williams field and a two-dimensional effective color charge density for a very large nucleus*, *Phys. Rev.* **D54** (1996) 5463–5469 [hep-ph/9605446].
- [21] Y. V. Kovchegov, *Quantum structure of the non-Abelian Weizsaecker-Williams field for a very large nucleus*, *Phys. Rev.* **D55** (1997) 5445–5455 [hep-ph/9701229].
- [22] I. Balitsky, *Factorization and high-energy effective action*, *Phys. Rev.* **D60** (1999) 014020 [hep-ph/9812311].
- [23] I. Balitsky, *High-energy QCD and Wilson lines*, hep-ph/0101042.
- [24] J. Jalilian-Marian, A. Kovner, L. D. McLerran and H. Weigert, *The intrinsic glue distribution at very small x* , *Phys. Rev.* **D55** (1997) 5414–5428 [hep-ph/9606337].
- [25] J. Jalilian-Marian, A. Kovner, A. Leonidov and H. Weigert, *The BFKL equation from the Wilson renormalization group*, *Nucl. Phys.* **B504** (1997) 415–431 [hep-ph/9701284].
- [26] J. Jalilian-Marian, A. Kovner, A. Leonidov and H. Weigert, *The wilson renormalization group for low x physics: Towards the high density regime*, *Phys. Rev.* **D59** (1999) 014014 [hep-ph/9706377].
- [27] J. Jalilian-Marian, A. Kovner and H. Weigert, *The Wilson renormalization group for low x physics: Gluon evolution at finite parton density*, *Phys. Rev.* **D59** (1999) 014015 [hep-ph/9709432].
- [28] J. Jalilian-Marian, A. Kovner, A. Leonidov and H. Weigert, *Unitarization of gluon distribution in the doubly logarithmic regime at high density*, *Phys. Rev.* **D59** (1999) 034007 [hep-ph/9807462].
- [29] A. Kovner, J. G. Milhano and H. Weigert, *Relating different approaches to nonlinear QCD evolution at finite gluon density*, *Phys. Rev.* **D62** (2000) 114005 [hep-ph/0004014].
- [30] H. Weigert, *Unitarity at small bjorken x* , *Nucl. Phys.* **A703** (2002) 823–860 [hep-ph/0004044].
- [31] E. Iancu, A. Leonidov and L. D. McLerran, *Nonlinear gluon evolution in the color glass condensate. I*, *Nucl. Phys.* **A692** (2001) 583–645 [hep-ph/0011241].
- [32] E. Ferreiro, E. Iancu, A. Leonidov and L. McLerran, *Nonlinear gluon evolution in the color glass condensate. II*, *Nucl. Phys.* **A703** (2002) 489–538 [hep-ph/0109115].
- [33] J. Bartels, *High-energy behavior in a nonabelian gauge theory. 2. first corrections to $t(n \rightarrow m)$ beyond the leading lns approximation*, *Nucl. Phys.* **B175** (1980) 365.
- [34] J. Kwiecinski and M. Praszalowicz, *Three Gluon Integral Equation and Odd c Singlet Regge Singularities in QCD*, *Phys. Lett.* **B94** (1980) 413.
- [35] J. Bartels and M. Wusthoff, *The Triple Regge limit of diffractive dissociation in deep inelastic scattering*, *Z. Phys.* **C66** (1995) 157–180.
- [36] J. Bartels, *Unitarity corrections to the Lipatov pomeron and the four gluon operator in deep inelastic scattering in QCD*, *Z. Phys.* **C60** (1993) 471–488.
- [37] J. Bartels, *Unitarity corrections to the Lipatov pomeron and the small x region in deep inelastic scattering in QCD*, *Phys. Lett.* **B298** (1993) 204–210.

- [38] J. Bartels and C. Ewerz, *Unitarity corrections in high-energy QCD*, *JHEP* **09** (1999) 026 [[hep-ph/9908454](#)].
- [39] L. N. Lipatov, *High-energy asymptotics of multicolor QCD and exactly solvable lattice models*, [hep-th/9311037](#).
- [40] L. N. Lipatov, *Asymptotic behavior of multicolor QCD at high energies in connection with exactly solvable spin models*, *JETP Lett.* **59** (1994) 596–599.
- [41] L. D. Faddeev and G. P. Korchemsky, *High-energy QCD as a completely integrable model*, *Phys. Lett.* **B342** (1995) 311–322 [[hep-th/9404173](#)].
- [42] L. N. Lipatov, *Evolution equations in QCD*, . Prepared for ICTP Conference on Perspectives in Hadronic Physics, Trieste, Italy, 12-16 May 1997.
- [43] A. V. Kotikov, L. N. Lipatov and V. N. Velizhanin, *Anomalous dimensions of Wilson operators in $N = 4$ SYM theory*, *Phys. Lett.* **B557** (2003) 114–120 [[hep-ph/0301021](#)].
- [44] A. V. Kotikov, L. N. Lipatov, A. I. Onishchenko and V. N. Velizhanin, *Three-loop universal anomalous dimension of the Wilson operators in $N = 4$ SUSY Yang-Mills model*, *Phys. Lett.* **B595** (2004) 521–529 [[hep-th/0404092](#)].
- [45] J. A. Minahan and K. Zarembo, *The Bethe-ansatz for $N = 4$ super Yang-Mills*, *JHEP* **03** (2003) 013 [[hep-th/0212208](#)].
- [46] N. Beisert and M. Staudacher, *The $N=4$ SYM Integrable Super Spin Chain*, *Nucl. Phys.* **B670** (2003) 439–463 [[hep-th/0307042](#)].
- [47] A. V. Kotikov, L. N. Lipatov, A. Rej, M. Staudacher and V. N. Velizhanin, *Dressing and Wrapping*, *J. Stat. Mech.* **0710** (2007) P10003 [[0704.3586](#)].
- [48] B. Eden and M. Staudacher, *Integrability and transcendentality*, *J. Stat. Mech.* **0611** (2006) P014 [[hep-th/0603157](#)].
- [49] N. Beisert, B. Eden and M. Staudacher, *Transcendentality and crossing*, *J. Stat. Mech.* **0701** (2007) P021 [[hep-th/0610251](#)].
- [50] Z. Bajnok, R. A. Janik and T. Lukowski, *Four loop twist two, BFKL, wrapping and strings*, *Nucl. Phys.* **B816** (2009) 376–398 [[0811.4448](#)].
- [51] L. N. Lipatov, *Integrability of scattering amplitudes in $N=4$ SUSY*, [0902.1444](#).
- [52] J. M. Maldacena, *The large N limit of superconformal field theories and supergravity*, *Adv. Theor. Math. Phys.* **2** (1998) 231–252 [[hep-th/9711200](#)].
- [53] S. S. Gubser, I. R. Klebanov and A. M. Polyakov, *Gauge theory correlators from non-critical string theory*, *Phys. Lett.* **B428** (1998) 105–114 [[hep-th/9802109](#)].
- [54] E. Witten, *Anti-de Sitter space and holography*, *Adv. Theor. Math. Phys.* **2** (1998) 253–291 [[hep-th/9802150](#)].
- [55] L. N. Lipatov, *Gauge invariant effective action for high-energy processes in QCD*, *Nucl. Phys.* **B452** (1995) 369–400 [[hep-ph/9502308](#)].
- [56] L. N. Lipatov, *Small- x physics in perturbative QCD*, *Phys. Rept.* **286** (1997) 131–198 [[hep-ph/9610276](#)].
- [57] M. Neubert, *Effective field theory and heavy quark physics*, [hep-ph/0512222](#).
- [58] J. Polchinski, *Effective field theory and the Fermi surface*, [hep-th/9210046](#).
- [59] S. Weinberg, *Phenomenological Lagrangians*, *Physica* **A96** (1979) 327.

- [60] C. W. Bauer, S. Fleming, D. Pirjol and I. W. Stewart, *An effective field theory for collinear and soft gluons: Heavy to light decays*, *Phys. Rev.* **D63** (2001) 114020 [[hep-ph/0011336](#)].
- [61] C. W. Bauer and I. W. Stewart, *Invariant operators in collinear effective theory*, *Phys. Lett.* **B516** (2001) 134–142 [[hep-ph/0107001](#)].
- [62] C. W. Bauer, D. Pirjol and I. W. Stewart, *Soft-Collinear Factorization in Effective Field Theory*, *Phys. Rev.* **D65** (2002) 054022 [[hep-ph/0109045](#)].
- [63] J. Chay and C. Kim, *Collinear effective theory at subleading order and its application to heavy-light currents*, *Phys. Rev.* **D65** (2002) 114016 [[hep-ph/0201197](#)].
- [64] M. Beneke, A. P. Chapovsky, M. Diehl and T. Feldmann, *Soft-collinear effective theory and heavy-to-light currents beyond leading power*, *Nucl. Phys.* **B643** (2002) 431–476 [[hep-ph/0206152](#)].
- [65] R. J. Hill and M. Neubert, *Spectator interactions in soft-collinear effective theory. ((U))*, *Nucl. Phys.* **B657** (2003) 229–256 [[hep-ph/0211018](#)].
- [66] H. Georgi, *An effective field theory for heavy quarks at low-energies*, *Phys. Lett.* **B240** (1990) 447–450.
- [67] W. E. Caswell and G. P. Lepage, *Effective Lagrangians for Bound State Problems in QED, QCD, and Other Field Theories*, *Phys. Lett.* **B167** (1986) 437.
- [68] G. T. Bodwin, E. Braaten and G. P. Lepage, *Rigorous QCD analysis of inclusive annihilation and production of heavy quarkonium*, *Phys. Rev.* **D51** (1995) 1125–1171 [[hep-ph/9407339](#)].
- [69] L. N. Lipatov, *High-energy scattering in QCD and in quantum gravity and two-dimensional field theories*, *Nucl. Phys.* **B365** (1991) 614–632.
- [70] R. Kirschner, L. N. Lipatov and L. Szymanowski, *Effective action for multi-Regge processes in QCD*, *Nucl. Phys.* **B425** (1994) 579–594 [[hep-th/9402010](#)].
- [71] R. Kirschner, L. N. Lipatov and L. Szymanowski, *Symmetry properties of the effective action for high-energy scattering in QCD*, *Phys. Rev.* **D51** (1995) 838–855 [[hep-th/9403082](#)].
- [72] O. Steinmann, *Über den Zusammenhang zwischen den Wightmanfunktionen und den retardierten Kommutatoren*, *Helv. Physica Acta* **33** (1960) 257–298.
- [73] G. 't Hooft, *A planar diagram theory for strong interactions*, *Nucl. Phys.* **B72** (1974) 461.
- [74] M. A. Braun and G. P. Vacca, *Triple pomeron vertex in the limit $N(c) \rightarrow \infty$* , *Eur. Phys. J.* **C6** (1999) 147–157 [[hep-ph/9711486](#)].
- [75] M. Braun, *On the multipomeron exchange and the BKP equation in the high colour limit*, *Z. Phys.* **C73** (1997) 517–525.
- [76] M. A. Braun, *The system of four reggeized gluons and the three-pomeron vertex in the high colour limit*, . Given at Madrid Workshop on Low x Physics, Madrid, Spain, 18-21 Jun 1997.
- [77] S. Mandelstam, *Cuts in the angular momentum plane. 2*, *Nuovo Cim.* **30** (1963) 1148–1162.
- [78] J. Bartels, A. M. Mischler and M. Salvadore, *Four point function of R-currents in $N=4$ SYM in the Regge limit at weak coupling*, *Phys. Rev.* **D78** (2008) 016004 [[0803.1423](#)].
- [79] J. Bartels, C. Ewerz, M. Hentschinski and A.-M. Mischler, *High Energy Behavior of a Six Point R-Current Correlator in $N=4$ SYM*, to be published.
- [80] V. S. Fadin and L. N. Lipatov, *High-Energy Production of Gluons in a QuasimultiRegge Kinematics*, *JETP Lett.* **49** (1989) 352.

- [81] E. N. Antonov, L. N. Lipatov, E. A. Kuraev and I. O. Cherednikov, *Feynman rules for effective Regge action*, *Nucl. Phys.* **B721** (2005) 111–135 [[hep-ph/0411185](#)].
- [82] M. E. Peskin and D. V. Schroeder, *An Introduction to quantum field theory*, . Reading, USA: Addison-Wesley (1995) 842 p.
- [83] J. Bartels, L. N. Lipatov and A. S. Vera, *BFKL Pomeron, Reggeized gluons and Bern-Dixon-Smirnov amplitudes*, 0802.2065.
- [84] M. Hentschinski, *Unitarity corrections from the high energy QCD effective action*, *Acta Phys. Polon.* **B39** (2008) 2567–2570 [[0808.3082](#)].
- [85] V. N. Gribov, *The theory of complex angular momenta: Gribov lectures on theoretical physics*, . Cambridge, UK: Univ. Pr. (2003) 297 p.
- [86] R. Kirschner and L. n. Lipatov, *Double Logarithmic Asymptotics and Regge Singularities of Quark Amplitudes with Flavor Exchange*, *Nucl. Phys.* **B213** (1983) 122–148.
- [87] I. Balitsky and G. A. Chirilli, *Next-to-leading order evolution of color dipoles*, *Phys. Rev.* **D77** (2008) 014019 [[0710.4330](#)].
- [88] J. R. Forshaw and D. A. Ross, *Quantum chromodynamics and the pomeron*, *Cambridge Lect. Notes Phys.* **9** (1997) 1–248.
- [89] J. Bartels, *High-energy behavior in a nonabelian gauge theory. 1. $t(n \rightarrow m)$ in the leading log normal s approximation*, *Nucl. Phys.* **B151** (1979) 293.
- [90] J. Bartels, *High-energy behavior in a nonAbelian gauge theory. 3. Multiple discontinuities and particle \rightarrow multi - reggeon vertices*, . DESY-91-074.
- [91] I. T. Drummond, P. V. Landshoff and W. J. Zakrzewski, *The two-reggeon/particle coupling*, *Nucl. Phys.* **B11** (1969) 383–405.
- [92] J. H. Weis, *Factorization of multi-regge amplitudes*, *Phys. Rev.* **D4** (1971) 1777–1787.
- [93] R. C. Brower, C. E. DeTar and J. H. Weis, *Regge Theory for Multiparticle Amplitudes*, *Phys. Rept.* **14** (1974) 257.
- [94] A. R. White, *Signature, factorization and unitarity in multi-regge theory - the five-point function*, *Nucl. Phys.* **B67** (1973) 189–231.
- [95] Z. Bern, L. J. Dixon and V. A. Smirnov, *Iteration of planar amplitudes in maximally supersymmetric Yang-Mills theory at three loops and beyond*, *Phys. Rev.* **D72** (2005) 085001 [[hep-th/0505205](#)].
- [96] M. Abramowitz and I. A. Stegun, *Handbook of Mathematical Functions with Formulas, Graphs, and Mathematical Tables, fifth printing*, . New York: Dover, 1966.
- [97] J. Bartels, *A Reggeon Calculus for the Production Amplitude. 1*, *Phys. Rev.* **D11** (1975) 2977.
- [98] M. A. Braun and M. I. Vyazovsky, *The reggeon \rightarrow 2 reggeons + particle vertex in the Lipatov effective action formalism*, *Eur. Phys. J.* **C51** (2007) 103–111 [[hep-ph/0612323](#)].
- [99] D. Treleani, *AGK cutting rules and perturbative QCD*, *Int. J. Mod. Phys.* **A11** (1996) 613–654.
- [100] H. Cheng, J. A. Dickinson, C. Y. Lo and K. Olausson, *Diagrammatic derivation of the eikonal formula for high- energy scattering in yang-mills theory*, *Phys. Rev.* **D23** (1981) 534.
- [101] S. Mandelstam, *Light Cone Superspace and the Ultraviolet Finiteness of the $N=4$ Model*, *Nucl. Phys.* **B213** (1983) 149–168.

- [102] G. Leibbrandt, *The Light Cone Gauge in Yang-Mills Theory*, *Phys. Rev.* **D29** (1984) 1699.
- [103] A. Bassetto, G. Nardelli and R. Soldati, *Yang-Mills theories in algebraic noncovariant gauges: Canonical quantization and renormalization*, . Singapore, Singapore: World Scientific (1991) 227 p.
- [104] I. Balitsky, *Operator expansion for high-energy scattering*, *Nucl. Phys.* **B463** (1996) 99–160 [[hep-ph/9509348](#)].
- [105] L. N. Lipatov, *Private conversation*.
- [106] H. Cheng and T. T. Wu, *Expanding protons: Scattering at high-energies*, . CAMBRIDGE, USA: MIT-PR. (1987) 285p.
- [107] J. Bartels, L. N. Lipatov and M. Wusthoff, *Conformal Invariance of the Transition Vertex $2 \rightarrow 4$ gluons*, *Nucl. Phys.* **B464** (1996) 298–318 [[hep-ph/9509303](#)].
- [108] M. Braun, *The Bootstrap condition for many Reggeized gluons and the photon structure function at low x and $N(c) \rightarrow$ infinity*, *Z. Phys.* **C71** (1996) 601–612 [[hep-ph/9502403](#)].
- [109] M. Braun, *The system of four reggeized gluons and the three-pomeron vertex in the high colour limit*, *Eur. Phys. J.* **C6** (1999) 321–330 [[hep-ph/9706373](#)].
- [110] S. R. Coleman, *"1/N" in Aspects of Symmetry*, . Cambridge University Press, Cambridge, 1985.
- [111] A. V. Manohar, *Large N QCD*, [hep-ph/9802419](#).
- [112] H. H. Matevosyan and A. W. Thomas, *Role of the $U(1)$ ghost beyond leading order in a large- $N(c)$ expansion*, *J. Phys.* **G35** (2008) 115006.
- [113] G. 't Hooft, *A Two-Dimensional Model for Mesons*, *Nucl. Phys.* **B75** (1974) 461.
- [114] V. Del Duca, *Parke-Taylor amplitudes in the multi - Regge kinematics*, *Phys. Rev.* **D48** (1993) 5133–5139 [[hep-ph/9304259](#)].
- [115] V. Del Duca, *Equivalence of the Parke-Taylor and the Fadin-Kuraev- Lipatov amplitudes in the high-energy limit*, *Phys. Rev.* **D52** (1995) 1527–1534 [[hep-ph/9503340](#)].
- [116] L. N. Lipatov, *The Bare Pomeron in Quantum Chromodynamics*, *Sov. Phys. JETP* **63** (1986) 904–912.
- [117] J. Bartels, J. Kotanski, A.-M. Mischler and V. Schomerus, *to be published*, .
- [118] J. Bartels and M. Hentschinski, *The triple Pomeron vertex in large- N QCD and the pair-of-pants topology*, 0903.5464.
- [119] J. Bartels, J. Kotanski, A.-M. Mischler and V. Schomerus, *in preparation*, .
- [120] M. Vaughn, *Introduction to Mathematical Physics*, . WILEY-VCH Verlag, Weinheim, 2007.
- [121] E. Whittaker and G. Watson, *A course of modern analysis, fourth edition*, . Cambridge, 1927.

Acknowledgements

First of all I want to thank my supervisor Prof. Jochen Bartels for his advice and guidance, for support and interest in my work. I am also particularly grateful to Prof. Lev N. Lipatov for very helpful discussions and explanations that deepened my understanding of high-energy QCD. I also wish to thank Prof. Mikhail Braun and Carlo Ewerz for useful conversations.

Diverse conversations broadened and deepened my physical knowledge. For discussions on various topics concerned with high-energy-limit of QCD, I want to thank particularly Florian Schwennsen, Leszek Motyka, Agustin Sabio-Vera, Salvadore Michele, Gian Paolo Vacca, Anna-Maria Mischler, Alexander Prygarin, Krzysztof Kutak and Jan Kotanski. For discussion on more general grounds I am grateful to Falk Neugebohrn, Michael Olschewsky, Mathias Butenschön, Thomas Danckaert, Hagen Triendl, Christian Hambrock, Sebastian Mendizabal, Marco Drewes, Torben Kneesch, Frank Fugel and Seyed Mohammad Moosavi Nejad. Moreover I want to thank to the members of the II. Institut für Theoretische Physik and the DESY Theory group for creating a very pleasant and stimulating working atmosphere.

Financial support from the Graduiertenkolleg "Zukünftige Entwicklungen in der Teilchenphysik" and from DESY is gratefully acknowledged.

I want to thank my family, my parents Rosmarie and Gottfried, my brother Stefan and my sister Monika for their emotional support during the preparation of this thesis.

Finally I want to express my gratitude to my wife Mary for her continuous support, understanding and love during the preparation of this thesis.